Lawrence Berkeley Laboratory
UNIVERSITY OF CALIFORNIA

EARTH SCIENCES DIVISION

MASS TRANSFER AND TRANSPORT IN A GEOLOGIC ENVIRONMENT

P.L. Chambré, T.H. Pigford, W.W.-L. Lee, J. Ahn, S. Kajiwara, C.L. Kim, H. Kimura, H. Lung, W.J. Williams, and S.J. Zavoshy

April 1985

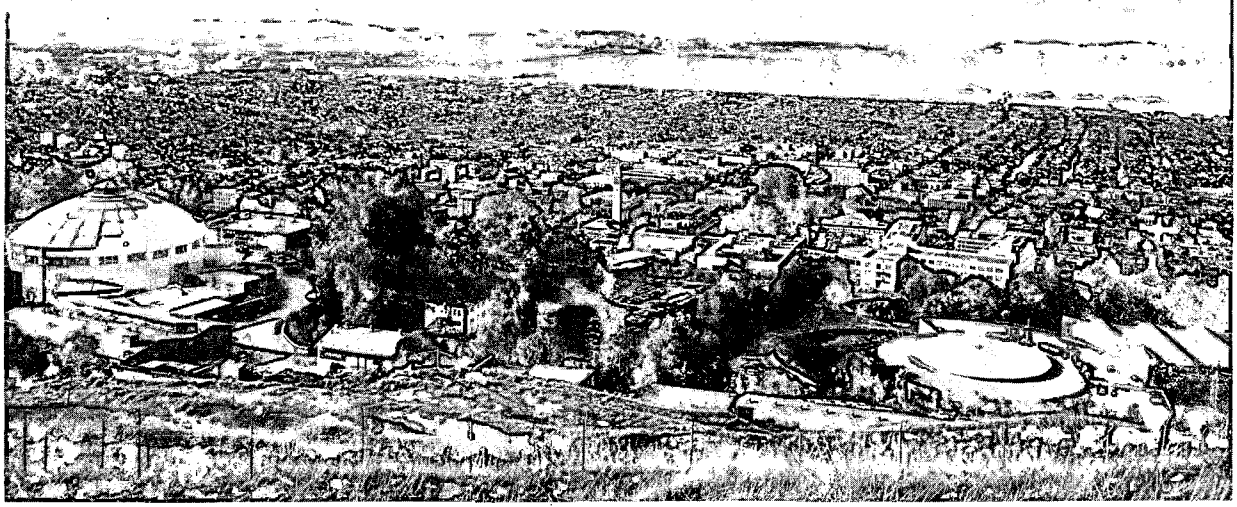

Prepared for the U.S. Department of Energy under Contract DE-AC03-76SF00098

DISCLAIMER

LBL-19430
UCB-NE-4057

MASS TRANSFER AND TRANSPORT IN A GEOLOGIC ENVIRONMENT

P. L. Chambré, T. H. Pigford, W. W.-L. Lee, J. Ahn, S. Kajiwara,
C. L. Kim, H. Kimura, H. Lung, W. J. Williams, S. J. Zavoshy

Earth Sciences Division, Lawrence Berkeley Laboratory

and

Department of Nuclear Engineering, University of California

Berkeley, California 94720

April, 1985

*Prepared for the U. S. Department of Energy under contract no. DE-AC03-76SF00098

The authors invite comments and would appreciate being notified of any errors in the report.

T. H. Pigford
Department of Nuclear Engineering
University of California
Berkeley, CA 94720

CONTENTS

MASS TRANSFER AND TRANSPORT IN A GEOLOGIC ENVIRONMENT

Chapter 1. Introduction and Summary

Chapter 2. Radionuclide Mass Transport from a Spherical Waste Form Surrounded by a Backfill

Chapter 3. The Numerical Analysis of Nuclide Migration through a Backfill

Chapter 4. Mass Transport in Backfill with a Non-Linear Sorption Isotherm

Chapter 5. Steady-State Mass Transport from a Prolate Spheroid with Backfill

Chapter 6. The Time-Dependent Mass Transport of a Radioactive Nuclide from a Waste Form by an Integral Method

Chapter 7. The Numerical Evaluation of the Time-Dependent Mass Transport of a Radionuclide from Finite-Sized Waste Forms of Different Geometries — Integral Method

Chapter 8. Transient Mass Transport of a Radionuclide with Temperature - Dependent Solubility, Diffusivity, and Retardation Coefficient

Chapter 9. The Effect of Heating on Waste Dissolution and Migration

Chapter 10. The Transport of a Radionuclide from a Point Source in a Three-Dimensional Flow Field

Chapter 11. On the Transport of Radioactive Chains in Geologic Media

1. INTRODUCTION AND SUMMARY

This report is in a continuing series of reports that present analytic solutions for the dissolution and hydrogeologic transport of radionuclides from geologic repositories of nuclear waste. Previous reports (P1, H1, C1) have dealt mainly with radionuclide transport in the far-field, away from the effects of the repository. In the present report, the emphasis is on near-field processes, the transfer and transport of radionuclides in the vicinity of the waste packages. The primary tool used in these analyses is mass transfer theory (S1) from chemical engineering. In the chapters that follow, the general format is that the problem statement, governing equations, and derivations of the solutions are presented first, followed by illustrative applications.

The thrust of our work is to develop methods for predicting the performance of geologic repositories. However, many of the results derived in the present report can be generalized to other situations of tracer or contaminant transport in geologic media. We would be interested in discussions with readers on other applications of this work. The subjects treated in the present report are:

(a) Radionuclide transport from a spherical-equivalent waste form through a backfill (Chapter 2, Derivations; Chapter 3, Applications).

(b) Analysis of radionuclide transport through a backfill using a non-linear sorption isotherm (Chapter 4)

(c) Radionuclide transport from a prolate spheroid-equivalent waste form with a backfill (Chapter 5, Steady-State Solutions, Theory and Application; Chapter 6, Transient Solution, Derivations; Chapter 7, Transient Solution, Applications)

(d) Radionuclide transport from a spherical-equivalent waste form through a backfill, where the solubility, diffusivity and retardation coefficients are temperature dependent (Chapter 8)

(e) A coupled near-field, far-field analysis where dissolution and migration rates are temperature dependent (Chapter 9)

(f) Transport of radionuclides from a point source in a three-dimensional flow field (Chapter 10)

(g) A general solution for the transport of radioactive chains in geologic media (Chapter 11)

Radionuclide Transport from a Spherical-Equivalent Waste Form with Backfill

In (C1), Chapter 7, we analyzed the transport of radionuclides from a bare waste form in wet, saturated rock. In the present volume we extend the

solutions to waste forms enclosed by a layer of backfill or packing material. The presence of a backfill will help ensure that in the vicinity of the waste package there is little or no advection, and molecular diffusion will be the main mechanism for mass transfer. The aim is to find the rate of dissolution of radionuclides and their rate of release into the rock, and to predict the spatial and temporal concentration of radionuclides in both the backfill and the rock. The approach used here is to set a saturation boundary condition at at the waste form/backfill interface. The solutions allow the prediction of both concentrations and mass flux as a function of position and time.

These results are potentially useful in showing compliance with the U.S. Nuclear Regulatory Commission's release-rate performance objective (U1). The analytic solutions can be used, for example, to compute the flux of radionuclides from the backfill/packing material into the rock, without the potential problems that discontinuity in porosity and retardation at the backfill/rock interface can introduce into numerical approaches.

There are several important results from the numerical evaluations. First, radioactive decay, higher sorption in the rock and the backfill steepens the gradient for mass transfer, and lead to higher dissolution rates. This is contrary to what was expected by some other workers, but is shown clearly in the analytical solutions. Second, the backfill serves to provide sorption sites so that there is a delay in the arrival of radionuclides in the rock, although this effect is not so important for the steady-state transport of long-lived radionuclides.

Non-linear Sorption

In Chapter 4, we analyzed one-dimensional radionuclide transport through the backfill in the presence of diffusion only, using a two-segment linear approximation of the Langmuir isotherm to simulate the effect of saturation of sorption sites in the backfill. The analytical solutions provide a method of predicting the position of the saturation front as it moves through the backfill.

Radionuclide Transport from a Prolate Spheroid-Equivalent Waste Form with Backfill

In (C1) we obtained the steady state solution as well as the early-time and large-time mass transfer from an infinitely-long and finite cylindrical waste forms. The analysis of cylindrical waste forms has attraction because actual nuclear waste packages are expected to be cylinders. In the limit of zero flow, the time-dependent mass transfer form a prolate-spheroid waste in contact with infinite rock was analyzed. In Chapters 5, 6, and 7 of this report, the analysis of prolate spheroid waste shape is extended in the following directions:

- Inclusion of a finite backfill/packing material layer;

- Inclusion of advective transport in the rock;

- Inclusion of an approximate solution between the

previously derived asymptotical results;

The previous comment about the potential usefulness of these analytic solutions in determining compliance with NRC requirements (U1) also apply here.

Radionuclide Transport with Temperature-Dependent Solutility, Diffusivity and Retardation Coefficients

In and around a geologic repository of nuclear waste, the temperature will vary as a function of time. This variation of temperature will have significant effect on the dissolution and transport of radionuclides by changing the saturation concentration, diffusion coefficient and geochemical retardation processes such as sorption. In Chapter 8 we analyze diffusive mass transport from a spherical-equivalent waste form where the solubility, diffusion coefficient, and retardation coefficients are functions of temperature. Chapter 8 gives radionuclide concentrations and mass fluxes where solubility, diffusivity and retardation coefficients are specified functions of time or temperature.

In Chapter 9, we present an application of this temperature dependent theory, as well as a far-field radionuclide migration model. The coupled model calculates concentration profiles of radionuclides in the far field based upon nonisothermal dissolution of the radionuclides at the waste canister surface.

Transport of Radionuclides from a Point Source in a Three-Dimensional Flow Field

In many repository projects, large-scale numerical codes are used for predicting the far-field distribution of radionuclides. There is a need for methods for testing these codes, especially when three-dimensional dispersion is being considered. In this chapter analytical solutions are derived for the advective-diffusion equation for three-dimensional transport from a point source.

A General Solution for the Transport of Radioactive Chains in Geologic Media

Chapter 11 provides solutions to the problem of migration of radioactive chains of arbitary length in geologic media of infinite or finite extent. These solutions are for very general conditions, and are potentially useful in many situations.

Summary

The following table is a summary index for the waste-package models developed in this report.

Table 1. Waste Package Models in This Report

CHAPTER	WASTE PACKAGE CONSIDERED				SOLUTIONS			FLOW CONDITIONS						
	Waste Form		Shape											
	With Backfill	Without Backfill	Spherical Equivalent	Prolate Spheroid	Quantity Predicted	Derivations	Numerical Examples	Steady State	Time Dependent	Diffusion Only	Advection and Diffusion	Constant T,K,D,C	Variable T,K,D,C	Linear Sorption
2	X		X		N	X			X	X		X		X
3	X		X		N, M		X		X	X		X		X
4	X			X	N, T_b	X	X		X	X		X		
5	X			X	N, M	X	X	X			X	X		X
6		X		X	N	X			X	X		X		X
7		X		X	M, t*		X		X	X		X		X
8		X	X		N, M	X			X	X			X	
9		X	X		N, M		X		X		X		X	X

Key

N = Radionuclide concentration at r at time t

M = Radionuclide flux at r at time t

t*= Time to steady state

T_b= Time to sorption saturation breakthrough

T,K,D,C = Temperature, retardation coefficient, diffusion coefficient and saturation concentration

REFERENCES

C1. Chambre', P.L., T. H. Pigford, Y. Sato, A. Fujita, H. Lung, S. Zavoshy, R. Kobayashi, "Analytical Performance Models", LBL-14842, 1982, 411 pages.

H1. Harada, M., P.L. Chambre', M. Foglia, K. Higashi, F. Iwamoto, D. Leung, T. H. Pigford, and D. Ting, "Migration of Radionuclides Through Sorbing Media: Analytical Solutions - I", LBL-10500, 1980, 233 pages.

P1. Pigford, T. H., P.L. Chambre', M. Albert, M. Foglia, M. Harada, F. Iwamoto, T. Kanki, D. Leung, S. Masuda, S. Muraoka, and D. Ting, "Migration of Radionuclides through Sorbing Media: Analytical Solutions - II", LBL-11616, 1980, 416 pages.

S1. Sherwood, T.K., R. L. Pigford, and C. L. Wilke. 1975. Mass Transfer. New York: McGraw-Hill.

U1. U.S. Nuclear Regulatory Commission. 1983. "Disposal of High Level Radioactive Waste in Geologic Repositories," Title 10, Code of Federal Regulations, Part 60.

2. RADIONUCLIDE MASS TRANSPORT FROM A SPHERICAL WASTE FORM SURROUNDED BY A BACKFILL

P.L. Chambré

In the following we investigate the time dependent mass transport of a radionuclide from a spherical waste form which is surrounded by a spherical shell of backfill material. Both waste and backfill are imbedded in rock extending infinitely in all directions, see Fig. 1. The mass transport through backfill and rock is assumed to occur by diffusion only and the transport by convection is not treated in this paper.

The waste form has a radius R_o and the outer edge of the backfill shell a radius R_1. The backfill porosity is ε_1 and its retardation coefficient is K_1. The rock has the corresponding properties ε_2 and K_2. The radionuclide's diffusion coefficient in the water is D_f and its decay constant is λ. The geometric factors for backfill and rock are σ_1 and σ_2, respectively. The nuclide is released at its solubility limit c_s at the surface of the waste form into the surrounding which is initially at zero concentration. Then if $N_1(r,t)$ and $N_2(r,t)$ denote respectively the nuclide's concentration in the backfill and rock regions the governing equations read, see Fig. 1 with $\nabla^2 = \frac{\partial^2}{\partial r^2} + \frac{2}{r}\frac{\partial}{\partial r}$

$$\frac{\partial N_1}{\partial t} = D_1 \nabla^2 N_1 - \lambda N_1,\ R_o < r < R_1,\ t > 0,\ D_1 = \frac{\sigma_1 D_f}{K_1} \tag{1}$$

$$\frac{\partial N_2}{\partial t} = D_2 \nabla^2 N_2 - \lambda N_2,\ R_1 < r < \infty,\ t > 0,\ D_2 = \frac{\sigma_2 D_f}{K_2} \tag{2}$$

$$N_1(r,0) = 0,\ R_o < r \leqslant R_1;\ N_2(r,0) = 0,\ R_1 \leqslant r < \infty \tag{3}$$

$$N_1(R_o,t) = c_s,\ t \geqslant 0 \tag{4}$$

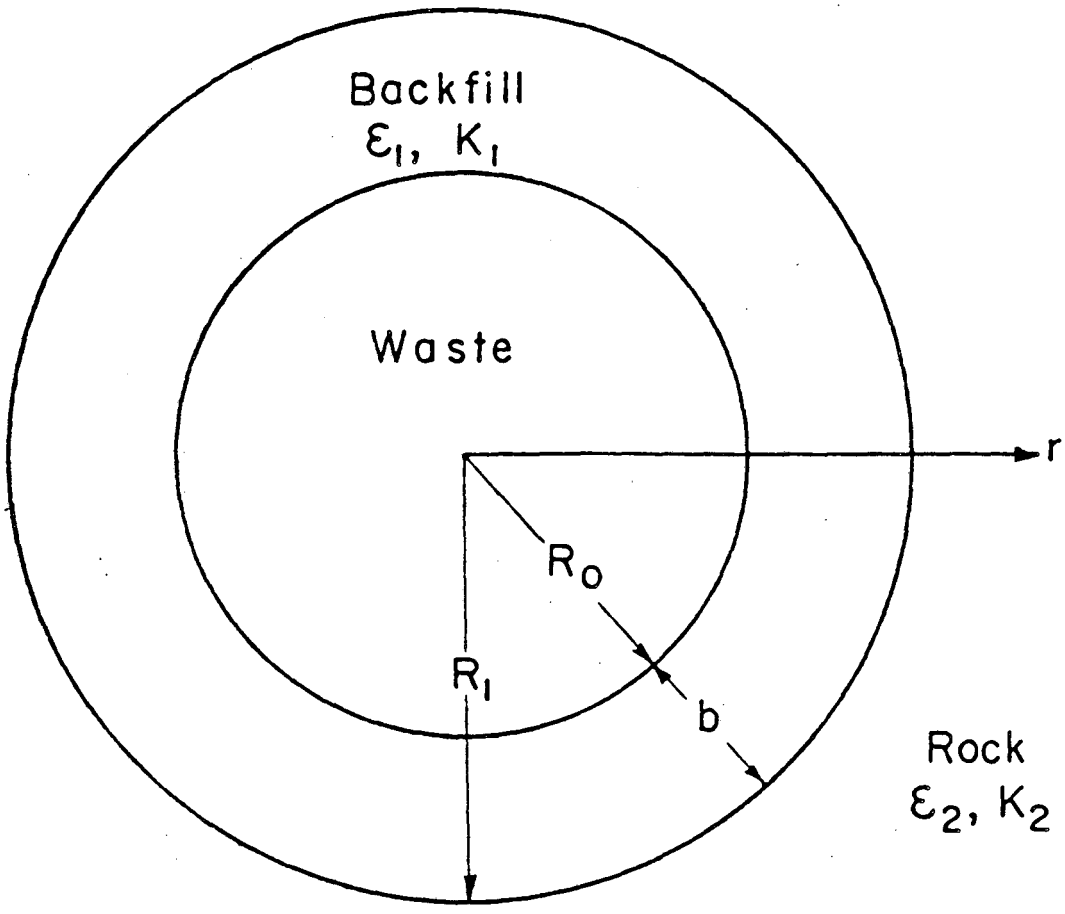

XBL 845-6988

Fig. 1 Geometry of spherical waste form with backfill layer.

$$N_1(R_1,t) = N_2(R_1,t) \ , \quad t \geq 0 \tag{5}$$

$$- \varepsilon_1 \sigma_1 D_f \frac{\partial N_1}{\partial r} = - \varepsilon_2 \sigma_2 D_f \frac{\partial N_2}{\partial r} \quad \text{at } r = R_1, \ t \geq 0 \tag{6}$$

$$N_2 \ (\infty,t) = 0, \ t \geq 0 \tag{7}$$

Equations (1) and (2) describe the conservation of the diffusing specie in the backfill and rock regions respectively. The initial conditions are given by (3). Equation (4) sets the solubility limited release on the waste form surface. Equations (5) and (6) assure the continuity of concentration and flux at the interface between backfill and rock and (7) regulates the concentration in the rock region far from the waste form. The purpose in obtaining the solution to this equation system is to analyze the space and time dependent concentration and transport flux of the nuclide as a function of the eleven parameter system c_s, λ, D_f, R_o, R_1, K_ℓ, ε_ℓ and σ_ℓ (ℓ=1,2). This will be done in Chapter 3.

The analysis of equations (1) - (7) is facilitated through the introduction of new dependent variables which satisfy the equation system in absence of radioactive decay

$$\frac{\partial c_1}{\partial t} = D_1 \nabla^2 c_1, \ R_o < r < R_1, \ t > 0 \tag{1'}$$

$$\frac{\partial c_2}{\partial t} = D_1 \nabla^2 c_2, \ R_1 < r < \infty, \ t > 0 \tag{2'}$$

$$c_1(r,0) = 0, \ R_o < r \leq R_1; \ c_2 \ (r,0) = 0, \ R_1 \leq r < \infty \tag{3'}$$

$$c_1(R_o,t) = c_s, \ t \geq 0 \tag{4'}$$

$$c_1(R_1,t) = c_2(R_1,t), \ t \geq 0 \tag{5'}$$

$$\varepsilon_1 \sigma_1 \frac{\partial c_1}{\partial r} = \varepsilon_2 \sigma_2 \frac{\partial c_2}{\partial r} \quad \text{at } r = R_1, \ t \geq 0 \tag{6'}$$

$$c_2(\infty,t) = 0, \quad t \geq 0 \tag{7'}$$

One can then express $N_1(r,t)$, $N_2(r,t)$ in terms of the solutions of (1')-(7') as follows

$$N_1(r,t) = \lambda \int_o^t e^{-\lambda\tau} c_1(r,\tau)\, d\tau + e^{-\lambda t} c_1(r,t) \qquad R_o \leq r \leq R_1, \; t > 0 \tag{8}$$

$$N_2(r,t) = \lambda \int_o^t e^{-\lambda\tau} c_2(r,\tau) d\tau + e^{-\lambda t} c_2(r,t), \; R_1 \leq r < \infty, \; t > 0 \tag{9}$$

This is readily verified by substitution (8) and (9) into the equation system (1) - (7) utilizing the fact that c_1 and c_2 satisfy eqs. (1') - (7').

In turn the system (1') - (7') is simplified through the dependent variables

$$n_1(r,t) = rc_1(r,t), \quad n_2(r,t) = rc_2(r,t) \; . \tag{10}$$

There results

$$\frac{\partial n_1}{\partial t} = D_1 \frac{\partial^2 n_1}{\partial r^2}, \quad R_o < r < R_1, \; t > 0 \tag{1''}$$

$$\frac{\partial n_2}{\partial t} = D_2 \frac{\partial^2 n_2}{\partial r^2}, \; R_1 < r < \infty, \; t > 0 \tag{2''}$$

$$n_1(r,0) = 0, \; R_o < r \leq R_1; \; n_2(r,o) = 0, \; R_1 \leq r < \infty \tag{3''}$$

$$n_1(R_o,t) = R_o c_s, \; t \geq 0 \tag{4''}$$

$$n_1(R_1,t) = n_2(R_1,t), \; t \geq 0 \tag{5''}$$

$$\varepsilon_1\sigma_1 \left(\frac{\partial n_1}{\partial r} - \frac{n_1}{r}\right) = \varepsilon_2\sigma_2 \left(\frac{\partial n_2}{\partial r} - \frac{n_2}{r}\right) \text{ at } r = R_1, \; t \geq 0 \tag{6''}$$

$$n_2(\infty,t) = 0, \; t \geq 0 \; . \tag{7''}$$

This is the principal equation system to be solved.

We take a Laplace transform of (1'') and (2'') with respect to the t variable and apply the initial conditions (3''). This yields with

$$\bar{n}_\ell(r,p) \equiv \int_o^\infty e^{-pt} n_\ell(r,t)dt, \quad \ell = 1,2 \tag{11}$$

the equation system

$$\frac{d^2\bar{n}_1}{dr^2} - \mu_1^2\bar{n}_1 = 0, \; R_o < r < R_1, \; \mu_1^2 = \frac{p}{D_1}$$

$$\frac{d^2\bar{n}_2}{dr^2} - \mu_2^2\bar{n}_2 = 0, \; R_1 < r < \infty, \; \mu_2^2 = \frac{p}{D_2} \tag{12}$$

The general solutions are

$$\bar{n}_1(r,p) = A \sinh \mu_1(R_1-r) + B \cosh \mu_1(R_1-r), \; R_o \leq r \leq R_1, \tag{13}$$

$$\bar{n}_2(r,p) = De^{-\mu_2(r-R_1)}, \; r \geq R_1 \tag{14}$$

with $\bar{n}_2$ satisfying the Laplace transform of the boundary condition (7''). The three constants A,B and D are found with help of the transforms of equations (4'')-(6''). With

$$b = R_1-R_o, \quad \gamma = \frac{\varepsilon_1'\mu_1}{\varepsilon_2'\mu_2+\alpha}, \quad \alpha = \frac{\varepsilon_2'-\varepsilon_1'}{R_1}, \quad \varepsilon_\ell' = \varepsilon_\ell\sigma_\ell, \; \ell = 1,2 \tag{15}$$

there results

$$A = \frac{R_o c_s}{p} \frac{1}{\gamma\cosh\mu_1 b+\sinh\mu_1 b} \tag{16}$$

$$B = D = \frac{R_o c_s}{p} \frac{\gamma}{\gamma\cosh\mu_1 b+\sinh\mu_1 b} \tag{17}$$

Substitution into (13) and (14) yields after a rearrangement

$$\bar{n}_1(r,p) = \frac{R_o c_s}{p} \left\{ \frac{\varepsilon_1'\mu_1\cosh\mu_1(R_1-r)+(\varepsilon_2'\mu_2+\alpha)\sinh\mu_1(R_1-r)}{\varepsilon_1'\mu_1\cosh\mu_1 b+(\varepsilon_2'\mu_2+\alpha)\sinh\mu_1 b} \right\}, R_o \leq r \leq R_1 \tag{18}$$

$$\bar{n}_2(r,p) = \frac{R_o c_s}{p} \left\{ \frac{\varepsilon_1'\mu_1 e^{-\mu_2(r-R_1)}}{\varepsilon_1'\mu_1\cosh\mu_1 b+(\varepsilon_2'\mu_2+\alpha)\sinh\mu_1 b} \right\}, \; r \geq R_1 \tag{19}$$

We turn next to the inversion of the Laplace transform $\bar{n}_1(r,p)$, which is accomplished through the application of the complex inversion integral

$$n_1(r,t) = \frac{1}{2\pi i} \int_{Br} e^{pt} \bar{n}_1(r,p)dp \ . \tag{20}$$

Since $\bar{n}_1(r,p)$ has a branch point at $p = 0$ due to the term $\mu_1 = \sqrt{\frac{p}{D_1}}$ we adopt the integration contour shown in Fig. 2. One can show that the integrand has no singularities inside this contour and furthermore that the contributions of the integral along the semi-circular arc Γ vanishes as $R_1 \to \infty$. Hence by the extended Cauchy theorem the integral (20) is equal to the contributions along the paths $\overline{BA}$, $\overline{DC}$ and the small circular contour s about the origin. We indicate the necessary steps to express these contributions in the real valued form.

Along the circle set

$$p = \rho e^{i\theta} \ , \ dp = \rho e^{i\theta} i d\theta, \ -\pi < \theta < \pi \tag{21}$$

Then

$$\mu_\ell = \sqrt{\frac{p}{D_\ell}} = \sqrt{\frac{1}{D_\ell}} \ \rho^{1/2} \ e^{i\theta/2} \ , \quad \ell = 1,2 \tag{22}$$

As the circle radius $\rho \to 0$, the hyperbolic function contribution in $\bar{n}_1(r,p)$ of equation (18) are approximated by

$$\cosh\rho = 1 + 0(\rho^2), \quad \sinh\rho = \rho + 0(\rho^3) \tag{23}$$

Hence the bracketed term in (18) becomes, correct to first order terms

$$\frac{\varepsilon_1'\mu_1 + \alpha\mu_1(R_1 - r)}{\varepsilon_1'\mu_1 + \alpha\mu_1 b} = \frac{\varepsilon_1' + \alpha(R_1 - r)}{\varepsilon_1' + \alpha b} \tag{24}$$

Substituting for this into (20) one obtains with (21) the contribution

$$\lim_{\rho \to 0} \frac{1}{2\pi i} \int_s e^{pt} \bar{n}_1(r,p)dp = R_o c_s \frac{\varepsilon_1' + \alpha(R_1 - r)}{\varepsilon_1' + \alpha b} \tag{25}$$

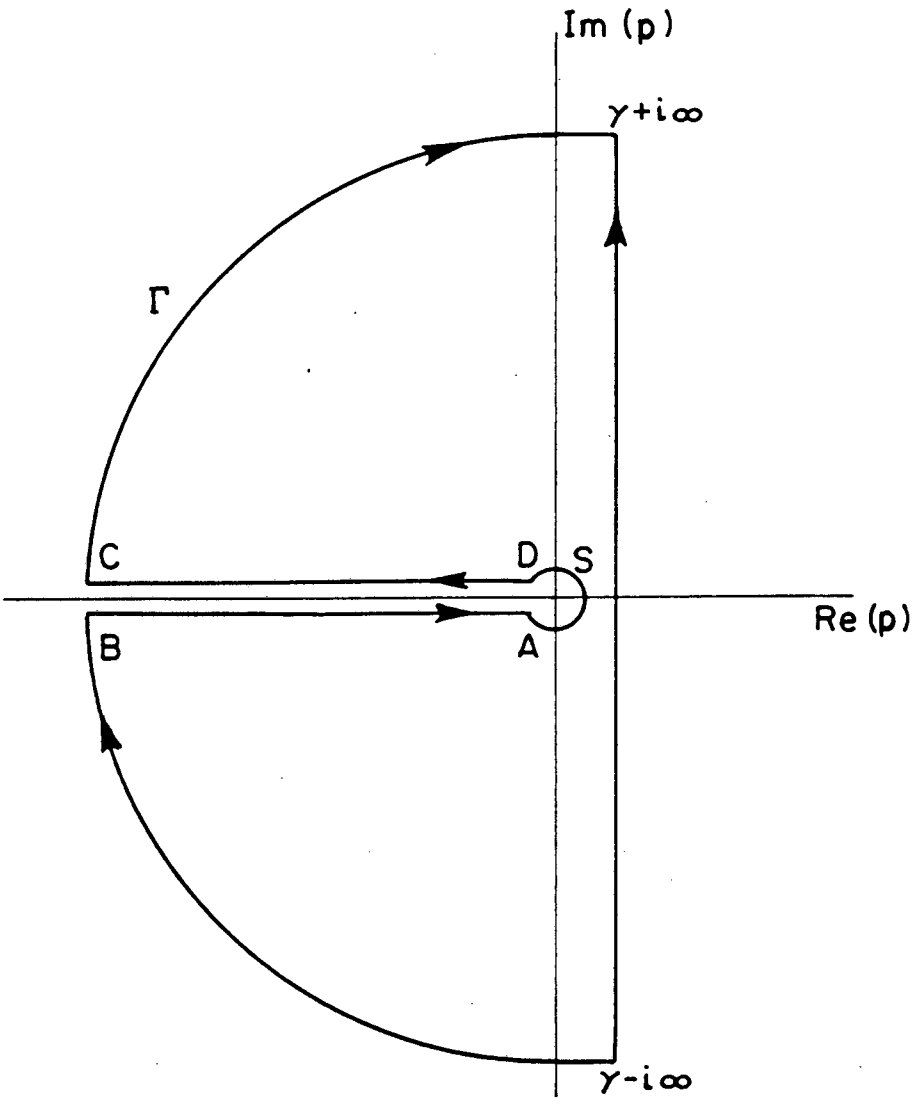

XBL 8412-5878

Fig. 2 Contour integral for inversion of Laplace transform.

For the path $\overline{BA}$ set

$$p = D_1\eta^2 e^{-i\pi} \ , \ \frac{dp}{p} = 2\,\frac{d\eta}{\eta} \tag{26}$$

and make the following replacements in (18)

$$\mu_1 = \sqrt{\frac{p}{D_1}} = \sqrt{\eta^2 e^{-i\pi}} = -i\eta; \quad \mu_2 = \sqrt{\frac{p}{D_2}} = -\,i\sqrt{\frac{K_2'}{K_1'}}\,\eta, \ K_\ell' = \frac{K_\ell}{\sigma_\ell} \ , \ \ell=1,2 \tag{27}$$

$$\cosh\mu_1[\ \ ] = \cosh(-\,i\eta[\ \ ]) = \cos\eta[\ \ ] \tag{28}$$

$$\sinh\mu_1[\ \ ] = \sinh(-\,i\eta[\ \ ] = -\,i\sin(\eta[\ \ ]) \ . \tag{29}$$

These expressions are substituted into (18) and a common factor of i is cancelled from the quotient. On placing the result into (20) and reversing the direction of integration one obtains the integral contribution

$$\frac{1}{2\pi i}\int_{\overline{BA}} e^{pt}\bar{n}_1(r,p)dp = -\,\frac{R_o c_s}{\pi i}\int_o^\infty e^{-D_1 t\eta^2}\ \frac{G_1 - iG_2}{H_1 - iH_2}\ \frac{d\eta}{\eta} \tag{30}$$

where

$$G_1 = \varepsilon_1'\eta\cos(\eta[R_1-r]) + \alpha\sin(\eta[R_1-r]); \ G_2 = \varepsilon_2'\sqrt{\frac{K_2'}{K_1'}}\ \eta\sin(\eta[R_1-r])$$

$$H_1 = \varepsilon_1'\eta\cos(\eta b) + \alpha\sin(\eta b); \ H_2 = \varepsilon_2'\sqrt{\frac{K_2'}{K_1'}}\ \eta\sin(\eta b) \ .$$

For the path $\overline{DC}$ set

$$p = D_1\eta^2 e^{i\pi} \ ; \ \frac{dp}{p} = 2\,\frac{d\eta}{\eta} \tag{31}$$

This changes the terms - i to i in equations (27) and (29) and thus alters the signs in the integrand quotient. In this case the integral contribution to (20) is

$$\frac{1}{2\pi i}\int_{\overline{DC}} e^{pt}\,\bar{n}_i(r,p)dp = \frac{R_o c_s}{\pi i}\int_o^\infty e^{-D_1 t\eta^2}\ \frac{G_1 + iG_2}{H_1 + iH_2}\ \frac{d\eta}{\eta} \tag{32}$$

Finally combining the integral contributions (25), (30) and (32) one obtains the desired inverse

$$n_1(r,t) = R_o c_s \left\{ \frac{\varepsilon_1'+\alpha(R_1-r)}{\varepsilon_1'+\alpha b} + \frac{2}{\pi}\int_o^\infty e^{-D_1 t\eta^2} \frac{G_2H_1-G_1H_2}{H_1^2+H_2^2} \frac{d\eta}{\eta} \right\} \tag{33}$$

But in view of (30) and the definition of α by (15) this transforms with help of (10) into

$$\frac{c_1(r,t)}{c_s} = f(r) + \int_o^\infty e^{-D_1 t\eta^2} I(r,\eta)d\eta, \quad R_o \leq r \leq R_i, \; t \geq 0 \tag{34}$$

where

$$f(r) = \frac{R_o}{r} \frac{1+\delta\left(\frac{r}{R_1}\right)}{1+\delta\left(\frac{R_o}{R_1}\right)}, \quad I(r,\eta) = -\left(\frac{2R_o\varepsilon_1'\varepsilon_2'\beta}{\pi r}\right) \frac{\eta\sin\left(\eta[r-R_o]\right)}{\left\{\varepsilon_1'\eta\cos(\eta b)+\alpha\sin(\eta b)\right\}^2+\left\{\beta\varepsilon_2'\eta\sin(\eta b)\right\}^2}$$

$$b = R_1-R_o, \quad \beta = \sqrt{\frac{K_2'}{K_1'}}, \quad \delta = \frac{\varepsilon_1'-\varepsilon_2'}{\varepsilon_2'} \tag{35}$$

This is the solution for a stable nuclide in the backfill region. By similar arguments one can determine the concentration field in the rock region. Since our principal interest centers on the nuclide concentration in the backfill and at the rock interface we shall not set out the solution in the rock field.

The solution for a radionuclide is obtained by combining (8) and (34)

$$\frac{N_1(r,t)}{c_s} = \lambda\int_o^t \left\{ f(r) + \int_o^\infty e^{-D_1\tau\eta^2} I(r,\eta)d\eta \right\} e^{-\lambda\tau}d\tau + e^{-\lambda t}\left\{ f(r) + \int_o^\infty e^{-D_1 t\eta^2} I(r,\eta)d\eta \right\} \tag{36}$$

Interchanging the order of integration yields

$$\frac{N_1(r,t)}{c_s} = f(r) + \int_o^\infty \frac{I(r,\eta)}{1+\frac{D_1\eta^2}{\lambda}} d\eta + e^{-\lambda t}\int_o^\infty \frac{e^{-D_1 t\eta^2}}{1+(\lambda/D_1\eta^2)} I(r,\eta)d\eta, \quad R_o \leq r \leq R_1, \; t \geq 0 \tag{37}$$

The first two terms represent the steady state solution and the last term the transient part of the concentration field through the backfill. When $\lambda = 0$ this result agrees with that for a stable nuclide.

The early and large time asymptotic behavior for $N_1(r,t)$ is established as follows. It is plausible by physical arguments that the nuclide concentration at very early times has not penetrated very far through the backfill which can thus be assumed to be of infinite extent. In this case the diffusion in the rock can be ignored and the solution to this single region problem is given by

$$\frac{N_1(r,t)}{c_s} = \frac{1}{2}\frac{R_o}{r}\left\{ e^{-(r-R_o)\sqrt{\frac{\lambda}{D_1}}}\ \text{erfc}\left[\frac{(r-R_o)}{2\sqrt{D_1 t}} - \sqrt{\lambda t}\right] + e^{(r-R_o)\sqrt{\frac{\lambda}{D_1}}}\ \text{erfc}\left[\frac{r-R_o}{2\sqrt{D_1 t}} + \sqrt{\lambda t}\right]\right\} \qquad r \gtrsim R,\ t \text{ small} \tag{38}$$

This result can also be obtained from (37) by setting $\varepsilon_1' = \varepsilon_2'$ and $K_1' = K_2'$.

At large times, when $N_1(r,t)$ tends to the steady state solution, equation (37) can be given a form which is more suitable for physical and numerical interpretation. One observes from (8) that as $t \to \infty$, $\frac{N_1(r,\infty)}{\lambda}$ is represented as the Laplace transform with the parameter p formally replaced by λ, i.e.

$$N_1(r,\infty) = \lambda\, L\left\{c_1(r,\tau)\right\}\Big|_{p=\lambda}$$

$$= \lambda \bar{n}_1(r,\lambda)/r \tag{39}$$

Thus using (18)

$$\frac{N_1(r,\infty)}{c_s} = \frac{R_o}{r}\left\{\frac{\varepsilon_1'\mu_1 \cosh\mu_1(R_1-r)+(\varepsilon_2'\mu_2+\alpha)\sinh\mu_1(R_1-r)}{\varepsilon_1'\mu_1\cosh(\mu_1 b)+(\varepsilon_2'\mu_2+\alpha)\sinh(\mu_1 b)}\right\}, \quad R_o \lesssim r \lesssim R_1 \tag{40}$$

where

$$\alpha = \frac{\varepsilon_2' - \varepsilon_1'}{R_1} \ , \ b = R_1 - R_o, \quad \mu_\ell = \sqrt{\frac{\lambda}{D_\ell}} \quad \ell = 1,2 \ .$$

This expression can be used to replace the first two terms on the right hand side of equation (37) so that

$$\frac{N_1(r,t)}{c_s} = \frac{N_1(r,\infty)}{c_s} + e^{-\lambda t}\int_o^\infty \frac{e^{-D_1 t\eta^2}}{1+(\lambda/D_1\eta^2)} \ I(r,\eta)d\eta, \ R_o \leq r \leq R_1, \ t \geq 0 \qquad (41)$$

With the concentration profile $N_1(r,t)$ known it is a straightforward matter to compute the surface mass flux $-\varepsilon_1\sigma_1 D_f \frac{\partial N_1}{\partial r}$ at the waste form surface and at the backfill-rock interface. The result of such calculations are presented in Chapter 3.

3. THE NUMERICAL ANALYSIS OF NUCLIDE MIGRATION THROUGH A BACKFILL

H. Lung and P.L. Chambré

In this chapter we evaluate and discuss the results of the transient nuclide mass transport through a backfill as developed in chapter 2 . For convenience we consider the transports of stable and radioactive nuclides separately.

A. The Mass Transport of a Stable Nuclide

The nuclide concentration $c_1(r,t)$ in the backfill region is given by equation (34) of chapter 2 . From it one can calculate the three quantities of principal interest in evaluating the performance of the backfill. Since the nuclide concentration at the waste surface is prescribed at the solubility limit, the concentration at the backfill-rock interface is of interest. It is computed from, see Eqs. (34), (35) of chapter 2

$$\frac{c_1(r,t)}{c_s} = f(r) + \int_0^\infty e^{-D_1 t\eta^2} I(r,\eta)d\eta, \quad R_o \le r \le R_1, \ t \ge 0 \tag{1}$$

where

$$f(r) = \frac{R_o}{r}\,\frac{1+\delta\left(\frac{r}{R_1}\right)}{1+\delta\left(\frac{R_o}{R_1}\right)}, \quad I(r,\eta) = -\left(\frac{2R_o\varepsilon_1'\varepsilon_2'\beta}{\pi r}\right)\frac{\eta\,\sin(\eta[r-R_o])}{H(\eta)}$$

$$H(\eta) = [\varepsilon_1'\eta\cos\eta b + \alpha\sin\eta b]^2 + [\beta\varepsilon_2'\eta\sin(\eta b)]^2 \tag{2}$$

The other two quantities of concern are the total mass fluxes $\dot{M}$ from the waste form surface and through the interface between backfill and rock. Since

$$\dot{M}(r,t) = 4\pi r^2\left(-\varepsilon_1\sigma_1 D_f\,\frac{\partial c_1(r,t)}{\partial r}\right), \quad R_o \le r \le R_1, \ t \ge 0, \tag{3}$$

one obtains from (1)

$$\frac{\dot{M}(r,t)}{c_s} = 4\pi\varepsilon_1\sigma_1 D_f R_o r\left\{\frac{1}{r\left(1+\delta\,\frac{R_o}{R_1}\right)} + \frac{2\varepsilon_1'\varepsilon_2'\beta}{\pi}\int_0^\infty e^{-D_1 t\eta^2}\,\frac{\eta\left[\eta\cos(\eta[r-R_o]) - \frac{1}{r}\sin(\eta[r-R_o])\right]}{H(\eta)}\,d\eta\right\} \tag{4}$$

$$R_o \le r \le R_1, \ t \ge 0$$

Some special cases of these results were investigated. With identical rock and backfill properties, i.e. $K_1' = K_2'$, $\varepsilon_1' = \varepsilon_2'$, the results reduce to those of a single region problem

$$\frac{c_1(r,t)}{c_s} = \frac{R_o}{r}\ \text{erfc}\left(\frac{r-R_o}{2\sqrt{D_1 t}}\right),\quad r \geq R_o,\ t \geq 0 \tag{5}$$

which agrees with (38) of chapter 2 and

$$\frac{\dot{M}(r,t)}{c_s} = 4\pi\varepsilon_1\sigma_1 D_f R_o \left\{\text{erfc}\left(\frac{r-R_o}{2\sqrt{D_1 t}}\right) + \frac{r}{\sqrt{\pi D_1 t}}\, e^{-\frac{(r-R_o)^2}{4D_1 t}}\right\} \quad r \geq R_o,\ t \geq 0 \tag{6}$$

As the steady state is approached ($t \to \infty$) the integrals in (1), (2) will vanish leaving

$$\frac{c_1(r,\infty)}{c_s} = f(r)$$

$$= \frac{R_o}{r}\left(\frac{1+\delta\frac{r}{R_1}}{1+\delta\frac{R_o}{R_1}}\right),\quad R_o \leq r \leq R_1 \tag{7}$$

and

$$\dot{M}(R_o,\infty) = \dot{M}(R_1,\infty) = 4\pi\varepsilon_1\sigma_1 D_f R_o \frac{1}{1+\delta\left(\frac{R_o}{R_1}\right)} \tag{8}$$

since there can be no accumulation of the diffusing specie in the backfill. Equation (7) is a special case of (40) of chapter 2 . The last two results are applicable for arbitrary K_ℓ' and ε_ℓ' ($\ell = 1,2$) values.

The evaluations of (1), (3) and (4) were carried out on a CDC-7600. An integration subroutine named D01AJF was used to evaluate the integrals. The description of this subroutine can be found in Appendix 3A.

Since the integrands contain the term $e^{-D_1 t\eta^2}$ which decreases rapidly in magnitude as η increases (when $D_1 t > 0$) a cut-off value Δ was introduced for the upper integration limit. Numerical experiments showed that for $D_1 t\Delta^2 \geq 20$ the relative error bound for the value of the integral is 10^{-6}. In the calculations we used $D_1 t\Delta^2 = 100$.

Figures 1 and 2 show the graphs of $\dot{M}(R_o,t)/c_s$ and $\dot{M}(R_1,t)/c_s$ v.s. time with ε_1' and K_1', K_2' as parameters. Figure 3 exhibits $c_1(R_1,t)/c_s$ in a comparable fashion. The remaining parameters were chosen as follows. The sphere radius was taken as 65.9 cm so that the surface area of the spherical waste form is equal to the surface area of the spent fuel canister which has a radius of 17.8 cm and a height of 470 cm. The backfill thickness is 30 cm. The rock porosity $\varepsilon_2 = \frac{0.01}{\sigma_2}$ and the nuclide's diffusion coefficient $D_f = 10^{-5}$ cm^2/sec in both backfill and rock.

A cursory look of Figures (1)-(3) reveals that one can subdivide the time span into three separate intervals which will be called

a) The early time span, ETS, which is controlled mostly by the backfill,

b) The intermediate time span ITS, which is controlled by both backfill and rock, and

c) The late time span LTS, which is controlled mostly by the rock.

The figures show that these spans do not possess distinct separation points but their existence can be argued on physical grounds as follows.

Initially there is no nuclide present outside the waste form. As time increases the specie diffuses from the waste surface into the backfill but in the ETS has as yet not reached the rock interface. Hence in this time span the migration of the nuclide is controlled by the backfill's properties only.

As the concentration of the backfill-rock interface rises both regions begin to affect the migration until the backfill is mostly penetrated. After this ITS the rock primarily controls the nuclide transport and the backfill properties play a subsidiary role. Eventually the rock will also be fully penetrated and a steady state will have been reached.

A semi-quantitative way to delineate the time spans is to compare the mass transfer rate at the backfill-rock interface with the rate at the waste surface.

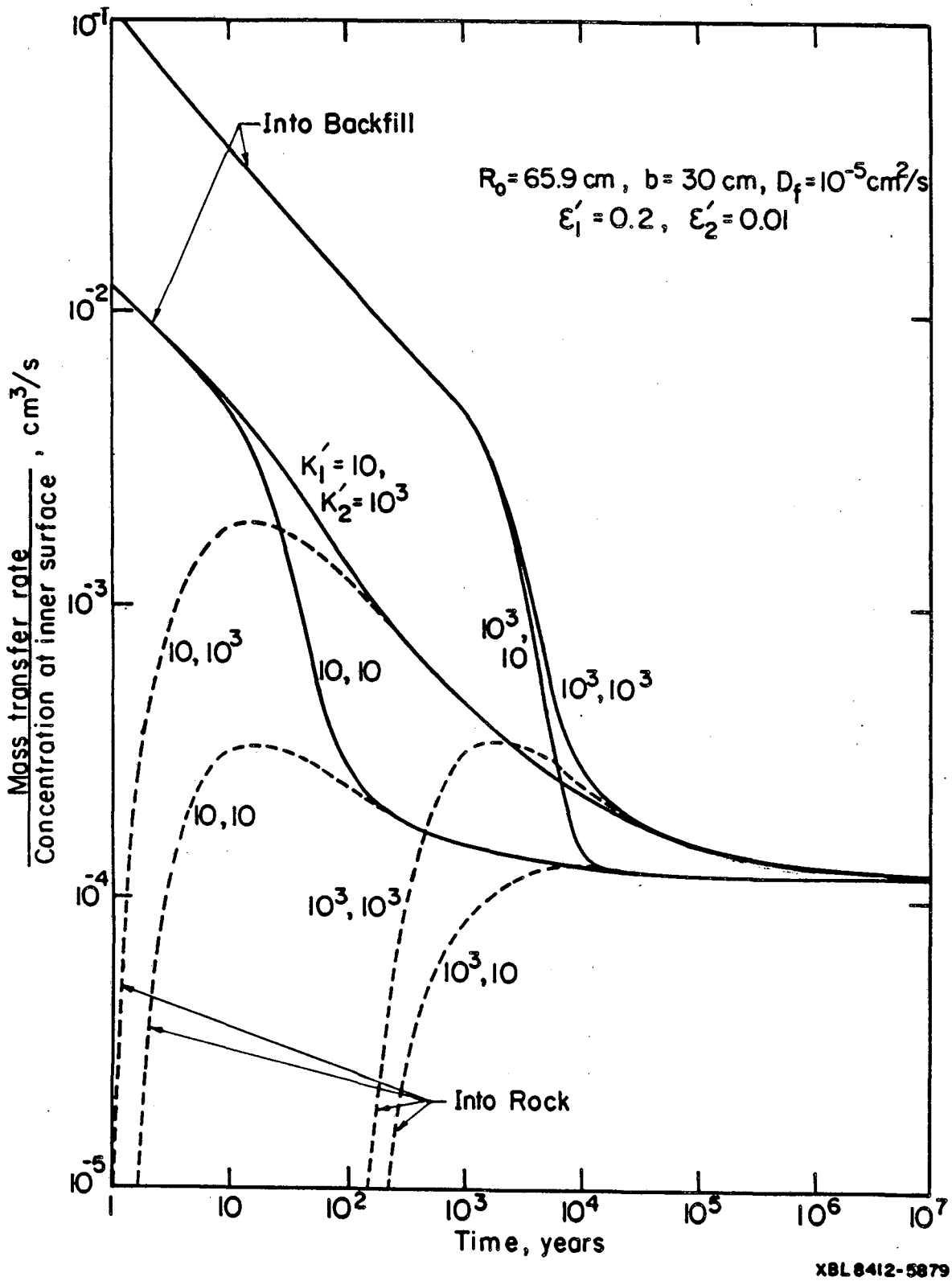

Fig. 1 Normalized mass transfer rate as a function of time and retardation coefficients in backfill and rock; diffusion from a spherical waste form.

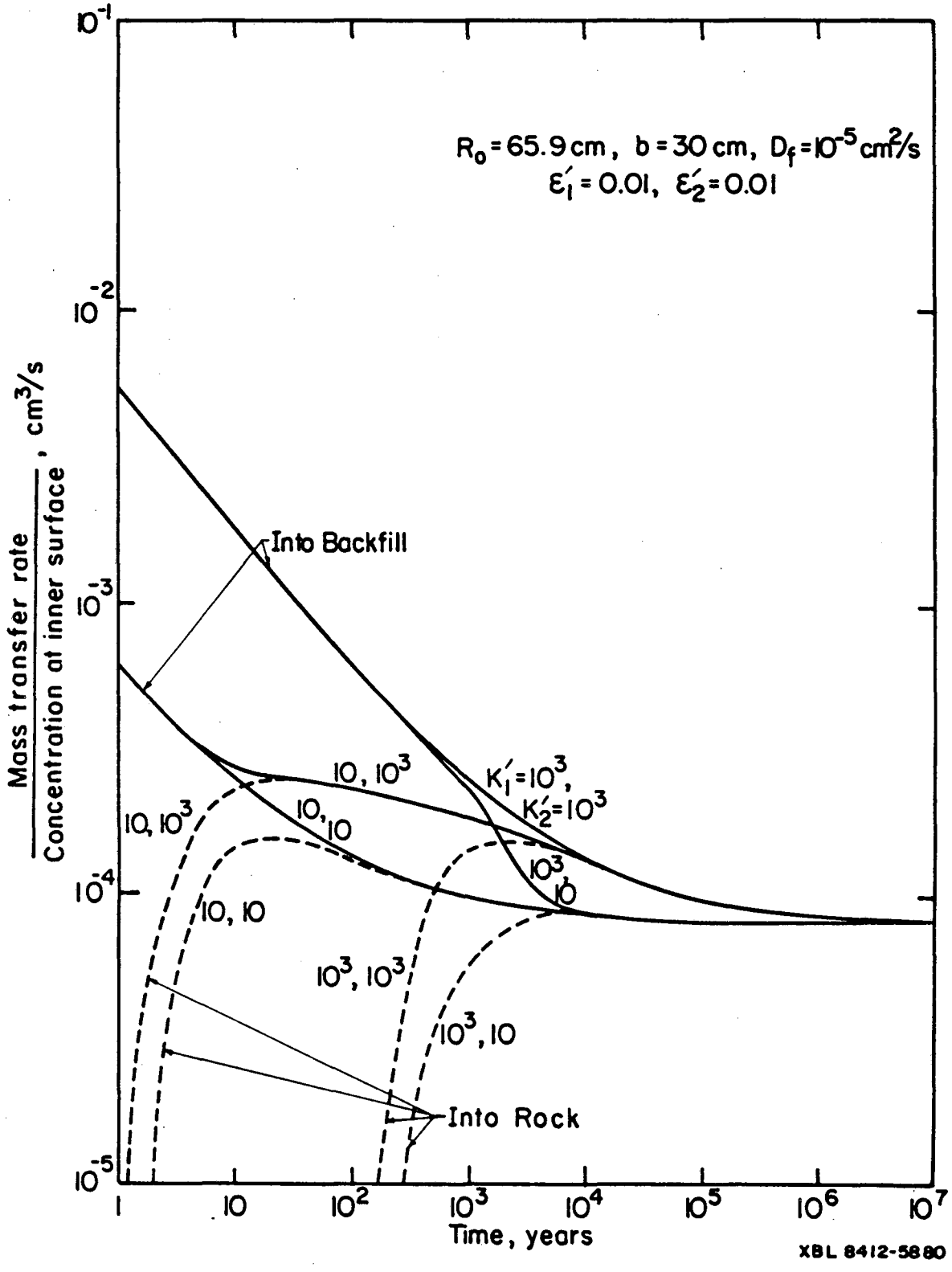

Fig. 2 Normalized mass transfer rate as a function of time and retardation coefficients in backfill and rock; diffusion from a spherical waste form.

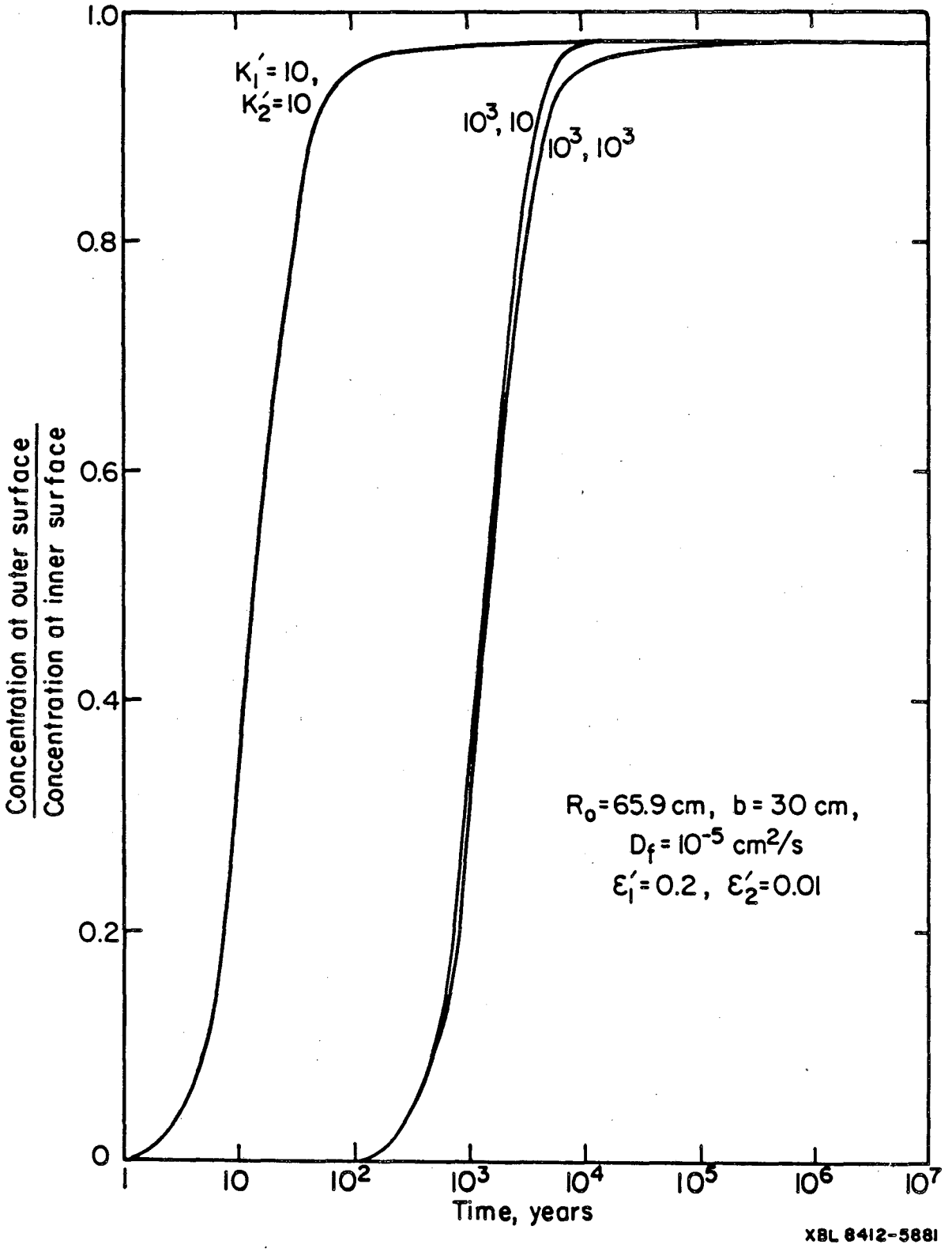

Fig. 3a Normalized backfill-rock interface concentration as a function of time and retardation coefficients in backfill and rock; diffusion from a spherical waste form.

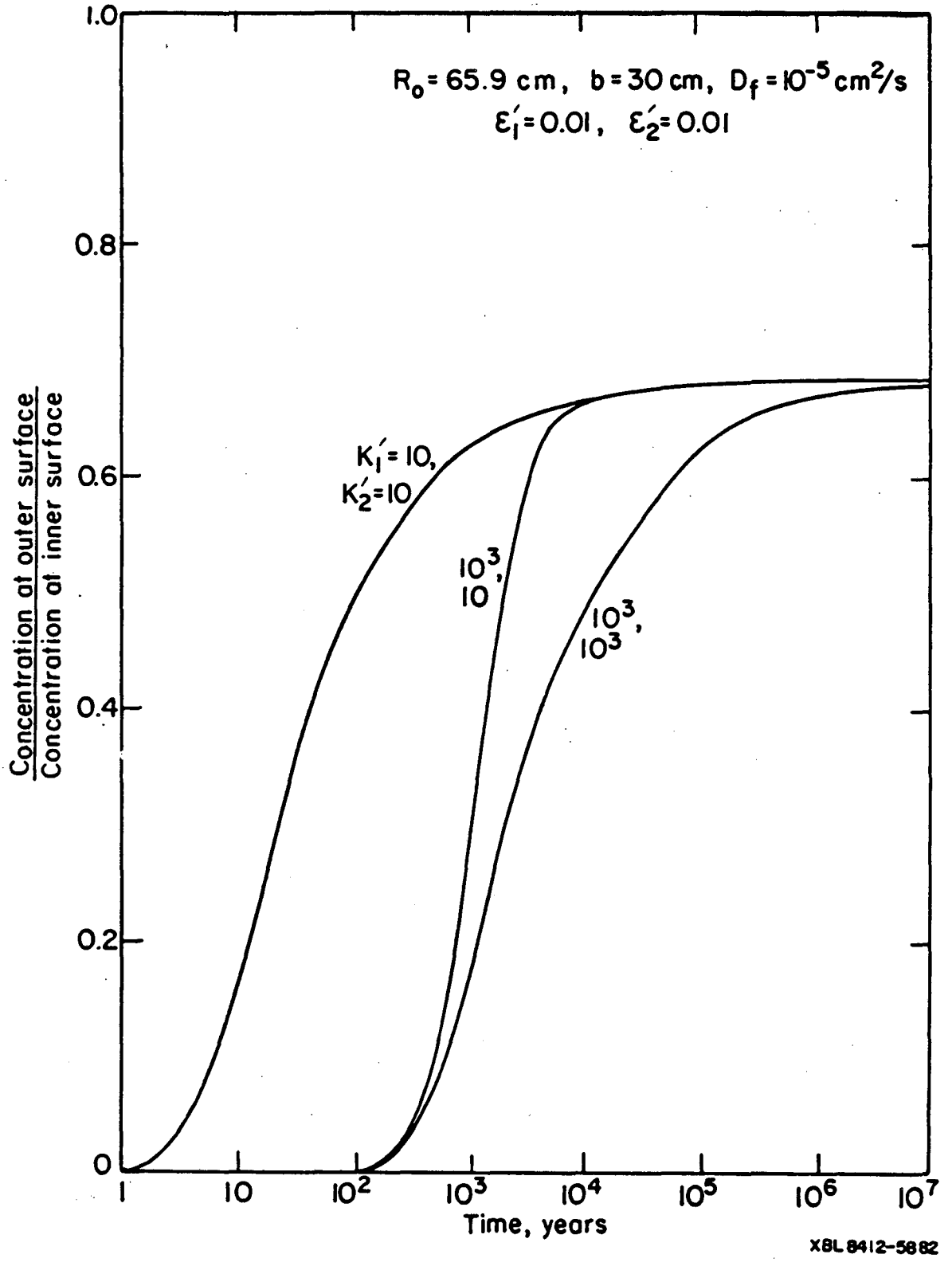

Fig. 3b Normalized backfill-rock interface concentration as a function of time and retardation coefficients in backfill and rock; diffusion from a spherical waste form.

In the ETS, $\dot{M}(R_1,t) \approx 0$, since the nuclide has not yet reached the interface. On the other hand, in the LTS, $\dot{M}(R_1,t) \approx \dot{M}(R_o,t)$, since the backfill is then almost saturated. Thus one can use the ratio $\dot{M}(R_1,t)/\dot{M}(R_o,t)$ as an indicator for the separation points. We adopt the time T_b and T_b^* defined by

$$\frac{M(R_1,T_b)}{M(R_o,T_b)} = 0.05 \quad \text{and} \quad \frac{\dot{M}(R_1,T^*_b)}{\dot{M}(R_o,T^*_b)} = 0.95 \tag{9}$$

as the end points of the ITS. This delineates the three time intervals except for the end point of LTS which borders the steady state. In order to gain insights into the order of magnitude of T_b and T_b^* computations were performed with equations (3), (4) and (9) with the following results

Case Number	ε_1'	ε_2'	K_1'	K_2'	T_b(yr)	T_b^*(yr)	
1	0.01	0.01	10	10	2.2	8.9×10^{1}	without
2	0.01	0.01	10^3	10^3	2.2×10^{2}	8.9×10^{3}	backfill
3	0.2	0.01	10	10	7.6	2.0×10^{2}	
4	0.2	0.01	10^3	10	2.2×10^{3}	1.1×10^{4}	with
5	0.2	0.01	10	10^3	2.0	1.80×10^{2}	backfill
6	0.2	0.01	10^3	10^3	7.6×10^{2}	2.0×10^{4}	

The separation time is an indicator of the backfill retardation function since it shows the breakthrough time of the backfill. Hence a larger T_b represents a better backfill retardation performance.

In the above table, cases 1 and 2 show the results for no-backfill. The rest show the results with backfill. The porosity of the rock is $\frac{0.01}{\sigma_2}$ and the porosity of backfill is $\frac{0.2}{\sigma_1}$ in cases 3-6. From this table one can see that when $K_1' \geq K_2'$, i.e. cases 3, 4, and 6. T_b is longer than that for no-backfill, i.e. case 1 (against cases 3 and 4) and case 2 (against case 6). But when $K_1' < K_2'$ as in case 5, T_b will be shorter as seen in case 2.

Therefore a backfill material with a larger K_1' compared to K_2' is preferred.

The drawback of the concept of T_b is that a larger T_b does not necessarily mean a smaller mass transfer rate at the backfill-rock interface. For example, T_b = 220 years for $K_2' = 10^3$ without backfill as shown in case 2 while it becomes 760 years when a backfill layer with $K_1' = 10^3$ is added. Though the T_b is longer with the backfill present, the mass transfer rate at the backfill-rock interface is always higher than the mass transfer rate with the backfill removed, as seen in Fig. 1 and 2, dashed curves for $K_1' = K_2' = 10^3$.

A better way to evaluate the backfill performance is to use the ratio of the mass transfer rate at the backfill-rock interface for the case with backfill to the rate without backfill. This will be discussed later.

We now consider the detailed behavior of the solution in each of these three time spans.

i) Early Time Span (ETS)

Since backfill controls the mass transport in this time span, one expects that the same mass transfer rate at the waste surface should be obtained for the same backfill properties regardless of the rock region. This is verified in the calculations as can be seen in Fig. 1 and 2, solid curves for $K_1' = K_2' = 10^3$, and $K_1' = 10^3$, $K_2' = 10$. For the mass transfer rate at the backfill-rock interface, one would expect a very low value in this time span. This can be seen from the steep slopes of the dashed curves in Fig. 1 and 2.

Since a large K_1 means a large retardation effect, the appearance of the mass transfer rate at backfill-rock interface will be delayed for larger K_1, as seen in Fig. 1 and 2, dashed curves for $K_1' = 10^3$, $K_2' = 10$ and $K_1' = K_2' = 10$. On the other hand, the mass transfer rate at the waste surface increases with increasing K_1, due to the steepened concentration gradient near the waste surface, as seen in the same Figures, solid curves for $K_1' = 10^3$, $K_2' = 10$ and $K_1' = K_2' = 10$.

ii) Intermediate Time Span

In this time span both backfill and rock exercise control over the mass transport. Nuclides start penetrating into the rock and the interface concentration increases with time as seen in Fig. 3a and 3b. The effect of rock on the mass transfer rate becomes more and more significant and tends to be the controller of the mass transport. This can be seen in Fig. 1 and 2, solid curves for $K_1' = K_2' = 10^3$, and $K_1' = 10^3$, $K_2' = 10$.

iii) Late Time Span

The backfill is now fully penetrated and has only little effect on the mass transport in this time span. The concentration profile and the mass transfer rate only depend on K_2'. This is shown as follows.

The integral term in Eq. (1), $\int_0^\infty e^{-D_1 t^2} \frac{\eta \sin \eta(r-R_o)}{H(\eta)} d\eta$, can be approximated by $\int_0^\Delta e^{-D_1 t\eta^2} \frac{\eta \sin \eta(r-R_o)}{H(\eta)} d\eta$, where Δ is the cut-off point for the integration. As mentioned earlier, the requirement for Δ is that $D_1 t\Delta^2 \geq 20$ to obtain a six-digit precision in the computations. Hence for a very large t, one needs only a very small Δ. For all $\eta b \leq \Delta b << 1$, one gets

$$\sin(\eta b) \approx \eta b, \quad \cos(\eta b) \approx 1, \quad \sin \eta(r-R_o) \approx \eta(r-R_o).$$

If further $\eta\beta\varepsilon_2' b << \varepsilon_1' + \alpha b$, the integral then transforms into

$$\int_0^\Delta e^{-D_1 t\eta^2} \frac{\eta^2(r-R_o)}{(\varepsilon_1'\eta+\alpha\eta b)^2+(\beta\varepsilon_2'\eta^2 b)^2} d\eta$$

$$\approx \int_0^\Delta e^{-D_1 t\eta^2} \frac{(r-R_o)}{(\varepsilon_1'+\alpha b)^2} d\eta$$

$$= \frac{(r-R_o)}{(\varepsilon_1' + \alpha b)^2} \int_o^{\Delta} e^{-D_1 t\eta^2} \, d\eta$$

$$= \frac{(r-R_o)}{(\varepsilon_1' + \alpha b)^2} \frac{\sqrt{\pi}}{2} \sqrt{\frac{1}{D_1 t}} \text{ erf } (\sqrt{D_1 t}\, \Delta)$$

$$\approx \frac{(r-R_o)}{(\varepsilon_1' + \alpha b)^2} \frac{\sqrt{\pi}}{2} \sqrt{\frac{1}{D_1 t}} \text{ , since erf } (\sqrt{D_1 t}\, \Delta) \geq \text{erf } (\sqrt{20}) \approx 1.$$

With this the transient integral contribution in (1) becomes for very large time

$$\frac{2\varepsilon_1'\varepsilon_2'\beta}{\pi} \frac{(r-R_o)}{(\varepsilon_1' + \alpha b)^2} \frac{\sqrt{\pi}}{2} \sqrt{\frac{1}{D_1 t}} = \sqrt{\frac{1}{\pi D_1 t}}\, \beta \frac{(r-R_o)}{(\varepsilon_1' + \alpha b)^2} \varepsilon_1'\varepsilon_2'$$

$$= \sqrt{\frac{1}{\pi D_2 t}}\, \varepsilon_1'\varepsilon_2' \frac{(r-R_o)}{(\varepsilon_1' + \alpha_b)^2} \text{ , since } \beta = \sqrt{\frac{K_2'}{K_1'}} = \sqrt{\frac{D_1}{D_2}} \qquad \text{(A)}$$

A similar form can be obtained for $\dot{M}$ from (3) except that the factor $(r-R_o)$ in (A) is replaced by $\frac{R_o}{r}$. From (A) one finds that at very large t the concentration profile or the mass transfer rate depends on K_2' alone. Eventually the K_2' dependency will also vanish when the steady state is reached.

One observes from Fig. 1 and 2 that both mass transfer rates at waste surface and at backfill-rock interface increase with increasing K_2, as shown in both solid and dashed curves for $K_1' = K_2' = 10^3$, and $K_1' = 10^3$, $K_2' = 10$. This is due to the larger adsorption of the nuclides by the larger K_2 in the rock which causes a steeper concentration gradient in the rock and extracts more nuclides from the waste form. In the LTS the difference between the mass transfer rates at waste surface and backfill-rock interface can hardly be seen. This means that almost all the nuclides released from the waste form are diffusing into the rock. The backfill can no longer retard the nuclides passing through it.

In all these three time spans, the mass transfer rates at waste surface and at backfill-rock interface decrease with decreasing backfill porosity. The

same result also applies to the backfill-rock interface concentration, see the corresponding curves in Fig. 1, 2, and 3. Hence a low porosity material should be used as the backfill when available.

As mentioned earlier in page 3-9, the ratio of the mass transfer rate at the backfill-rock interface with the backfill present to the rate at the same position without backfill can be used to show the effectiveness of the backfill layer. For the case without backfill ($\varepsilon_1' = \varepsilon_2'$, $K_1' = K_2'$), the interface mass transfer rate is calculated at an artificial plane which has the position equal to the actual backfill-rock interface position. Fig. 4 shows this ratio as a function of time with K_1' and K_2' as the parameters. Backfill porosity is taken as $\frac{0.2}{\sigma_1}$ and all other parameters (R_o, b, D_f, and ε_1') are the same as in Fig. 1, 2, and 3. Retardation coefficient K_2' used for rock is 10 and 10^3 and that used for backfill is 10, 10^2 and 10^3 for each value of K_2'. The dotted segments are not reliable due to the limitation of the precision in computations. The solid curves are for $K_2' = 10$ while the dashed ones are for $K_2' = 10^3$. One can see that for $K_1' > K_2'$ such as $K_1' = 10^2$, 10^3 and $K_2' = 10$, this ratio is less than unity up to some time. For $K_1' = 10^2$ it is 100 years and for $K_1' = 10^3$ it is about 1,500 years. This implies that within this time span the interface mass transfer rate in the presence of backfill is always less than that without backfill although the porosity changes from $\frac{0.01}{\sigma_1}$ to $\frac{0.2}{\sigma_1}$. On the other hand, when $K_1' \leq K_2'$ as in all other curves, the ratio is always greater than 1. It means the backfill does not add any benefit to the retardation of the mass transport. Comparing the curves for $K_1' > K_2'$, one finds that the effective time to retard the mass transport increases with increasing K_1'.

As a conclusion, a low-porosity backfill should be used to limit the magnitude of the mass transfer rates and a larger retardation coefficient for backfill compared to that for rock is required to lengthen the effective

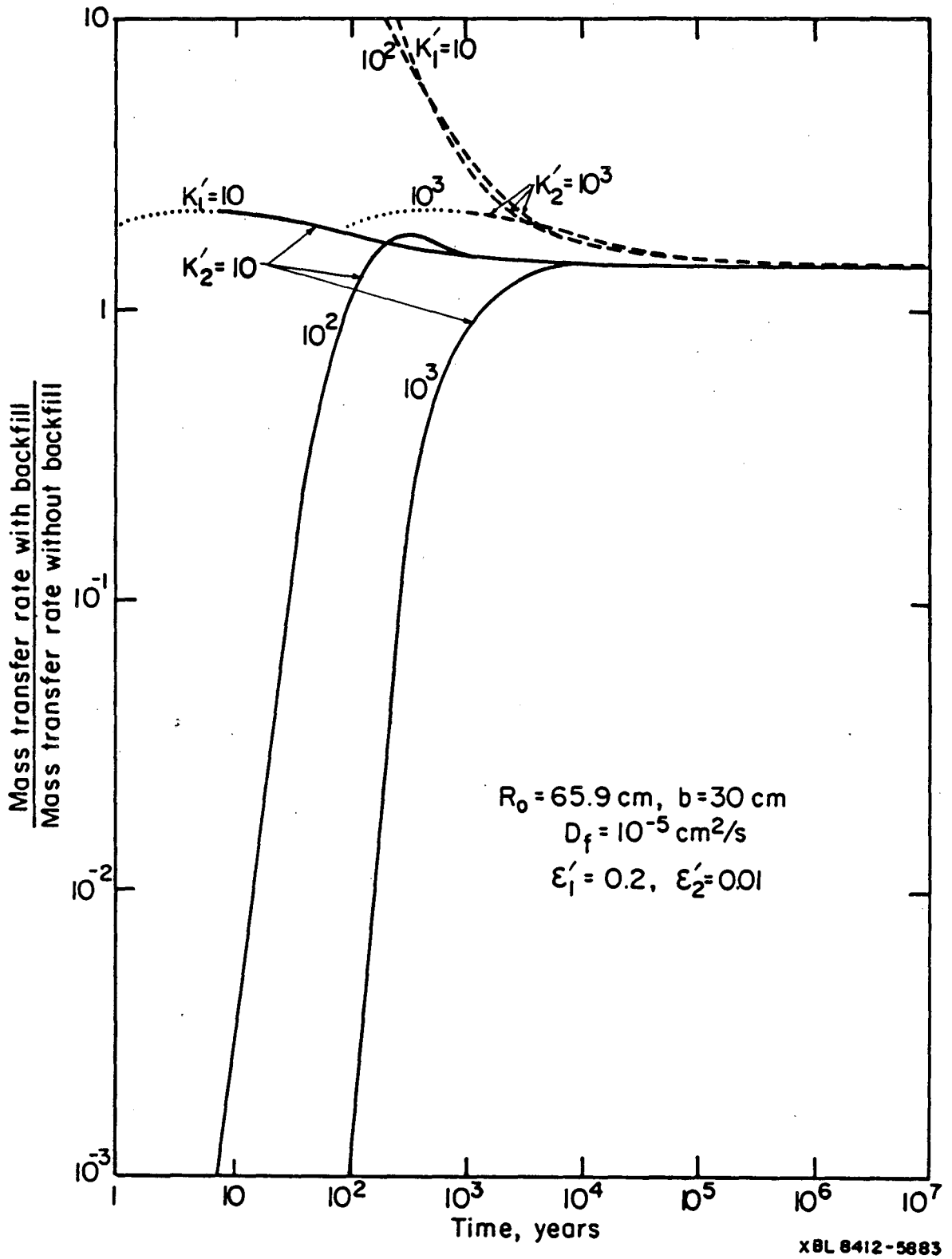

Fig. 4 Ratio of mass transfer rate with backfill to that without backfill as a function of time and retardation coefficients in backfill and rock; diffusion from a spherical waste form.

retarding time in backfill layer.

There is a restriction on the applications of the solutions (1) and (4). One can not use them to calculate the limiting case $\varepsilon_2 = 0$. For $\varepsilon_2 = 0$, the transient integral contribution in both equations vanish leading to the steady state solutions. It means either the problem is time-independent or it reaches the steady state instantaneously. This is certainly not the real situation of this problem. Hence a separate method must be applied. Since $\varepsilon_2 = 0$ implies that the nuclides can not diffuse into the rock, one will have a zero gradient $\left(\frac{\partial c}{\partial r}\right) = 0$ condition at the backfill-rock interface. Therefore the governing equation for rock and the zero concentration B.C. at infinity will not appear, and the interface B.C. should be changed to

$$- \varepsilon_1 \sigma_1 D_f \frac{\partial c_1}{\partial r}\bigg|_{r=R_1} = 0, \quad t \geq 0 \tag{10}$$

By solving the proper governing equation and side conditions, one can get a correct solution for this special case.

B. The Mass Transport of a Radionuclide

The radionuclide concentration $N_1(r,t)$ through the backfill region is given by equations (40) and (41) of chapter 2.

$$\frac{N_1(r,t)}{c_s} = \frac{N_1(r,\infty)}{c_s} + e^{-\lambda t} \int_0^\infty \frac{e^{-D_1 t \eta^2}}{1+\left(\frac{\lambda}{D_1 \eta^2}\right)} I(r,\eta)\, d\eta \tag{11}$$

where $I(r,\eta)$ is defined in (2). The total mass flux at any point in the backfill is then

$$\dot{M}(r,t) = - 4\pi r^2 \varepsilon_1 \sigma_1 D_f \frac{\partial N_1(r,t)}{\partial r}, \quad R_o \leq r \leq R_1, \quad t \geq 0 \tag{12}$$

Again the three principal quantities of interest are the mass transfer rate at the waste form surface and the radionuclide concentration and its mass transfer

rate at backfill-rock interface. The numerical integration was used to calculate $N_1(r,t)$ and $\dot{M}(r,t)$ in Equations (11) and (12). The same subroutine E01AJF used in Part A was adopted again and is described in Appendix 3A. In these computations, three different radionuclides were considered. They are ^{237}Np with half life 2.14×10^6 years, ^{14}C with $T_{1/2}$ = 5730 years, and one artificial nuclide with $T_{1/2}$ = 15.3 years which is close to ^{244}Cm($T_{1/2}$ = 17.6 years). Fig. 5 shows $\dot{M}(R_o t)/C_s$ and $\dot{M}(R_1,t)/C_s$ v.s. time with $T_{1/2}$ as the parameter. Other parameters used are $\varepsilon_1' = 0.2$, $\varepsilon_2' = 0.01$, $K_1' = K_2' = 10^3$. The results for stable specie ($T_{1/2} = \infty$ years) are also plotted for reference. Fig. 6 and Fig. 7 show the same quantities with different parameters. In Fig. 6, ε_1' has been changed to 0.01, i.e. it exhibits the single region results. In Fig. 7 not only ε_1' has been changed to 0.01, but K_2' also changed to 10. Fig. 8 to 10 shows the interface concentration $N_1(R_1,t)/C_s$ as a function of time with the three sets of parameters mentioned above. One observes that for $T_{1/2}$ = 15.3 years the interface concentration is so small that almost all radionuclides released from waste surface have decayed before they reach the interface boundary. This can be seen from Eq. (11) for $N_1(R_1,t)$ at steady state:

$$\frac{N_1(R_1,\infty)}{C_s} = \frac{R_o}{R_1} \frac{\varepsilon_1'\mu_1}{\varepsilon_1'\mu_1\cosh(\mu_1 b)+(\varepsilon_2'\mu_2+\alpha)\sinh(\mu_1 b)} \tag{13}$$

As $T_{1/2}$ decreases (λ increases), $\mu_1 \equiv \sqrt{\frac{\lambda}{D_1}}$ increases, causing $\cosh(\mu_1 b)$ and $\sinh(\mu_1 b)$ increasing very rapidly, resulting a very small $N(R_1,\infty)/C_s$. Eq. (13) can also be used to calculate the range of $T_{1/2}$ for which the radionuclides will have decayed during the diffusion through the backfill layer. From (13) one can solve for λ in terms of $N_1(R_1,\infty)/C_s$ and other parameters. For example, if $N_1(R_1,\infty)/C_s = 0.01$, $\varepsilon_1' = 0.2$, $\varepsilon_2' = 0.01$, $K_1' = K_2' = 10^3$, as used in Fig. 5, one finds that $\lambda = 8.5 \times 10^3$/yr, or $T_{1/2}$ = 81 years. This means if a radionuclide

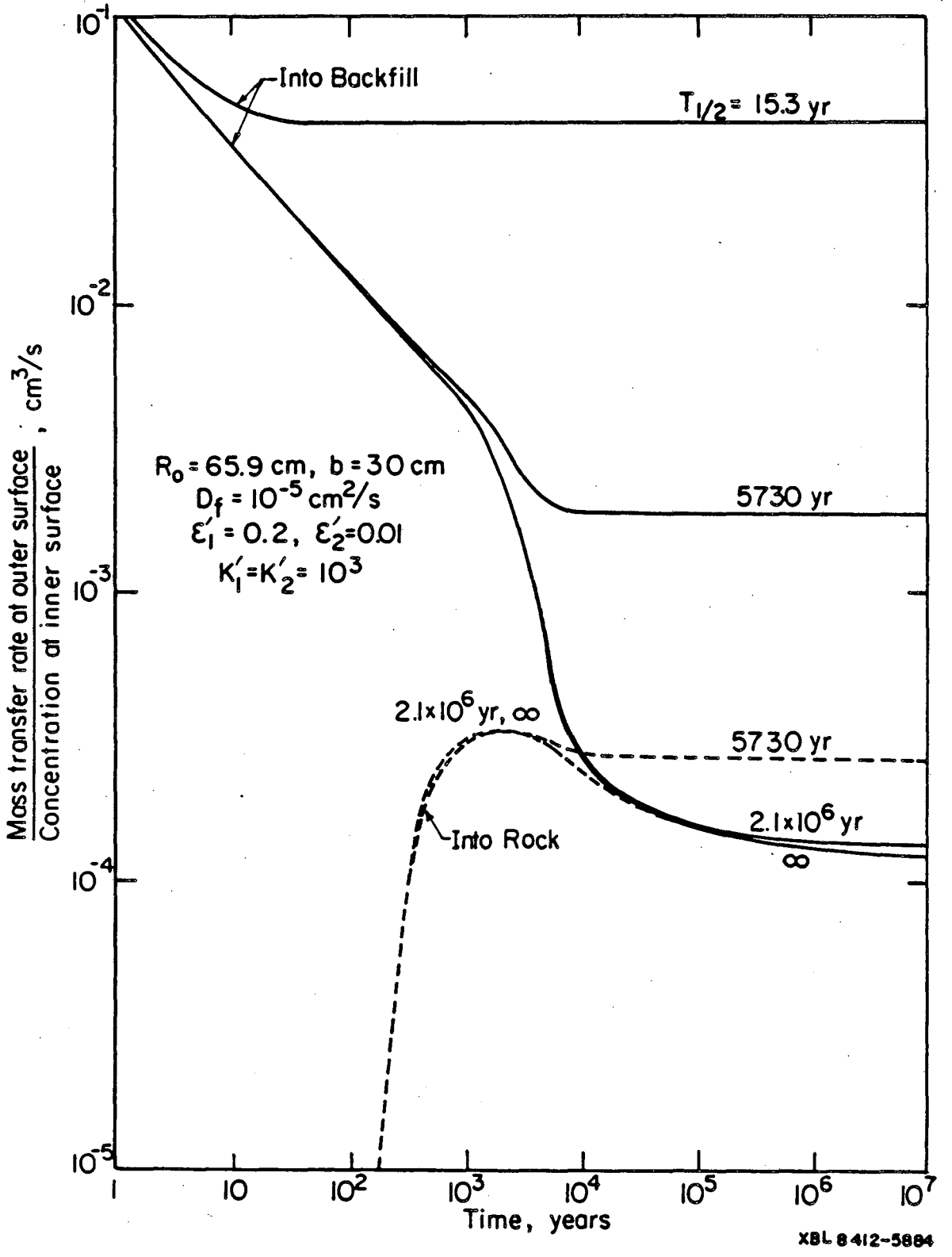

Fig. 5 Normalized mass transfer rate as a function of time and half-life; diffusion from a spherical waste form.

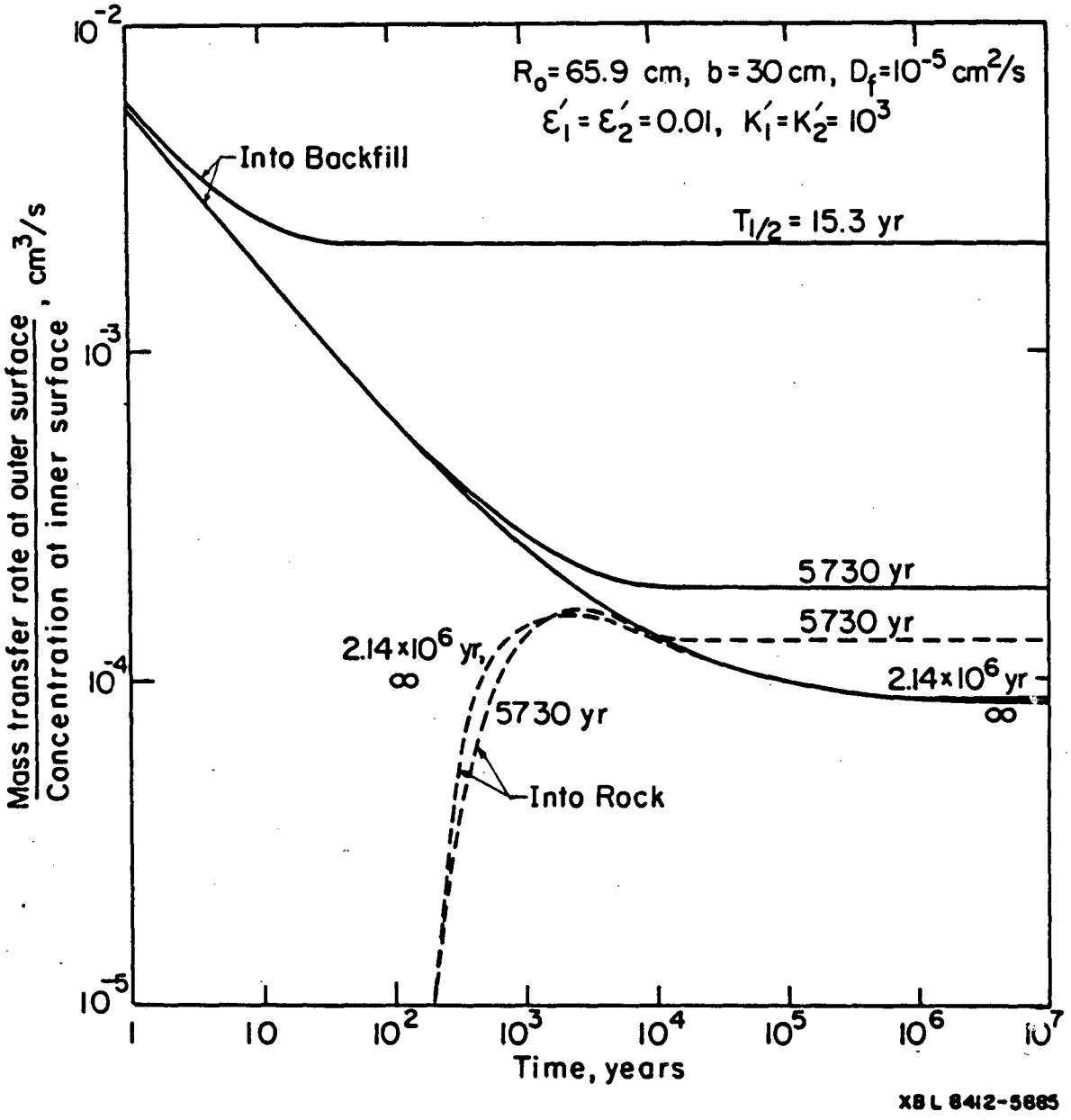

Fig. 6 Normalized mass transfer rate as a function of time and half-life; diffusion from a spherical waste form.

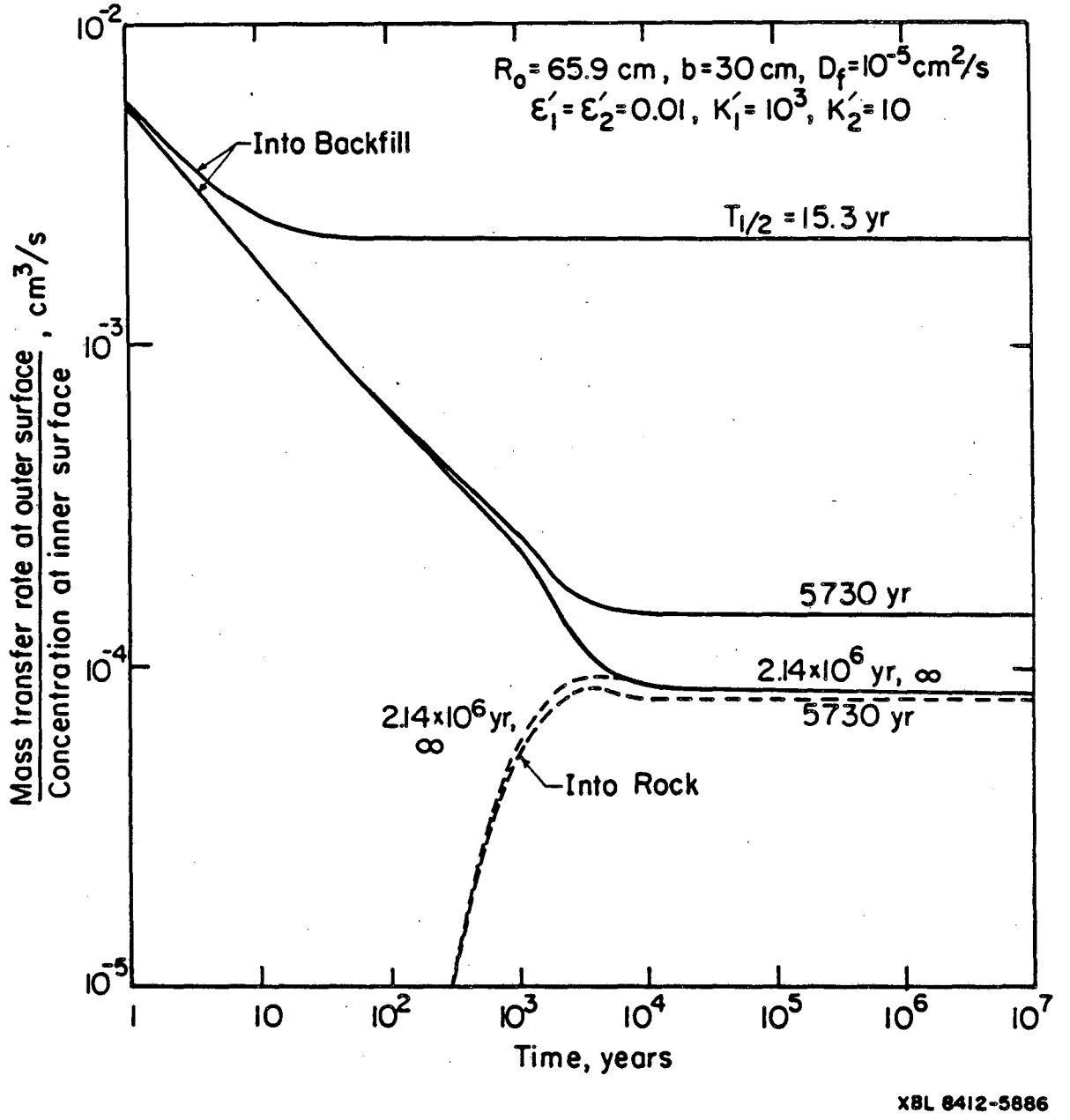

XBL 8412-5886

Fig. 7 Normalized mass transfer rate as a function of time and half-life; diffusion from a spherical waste form.

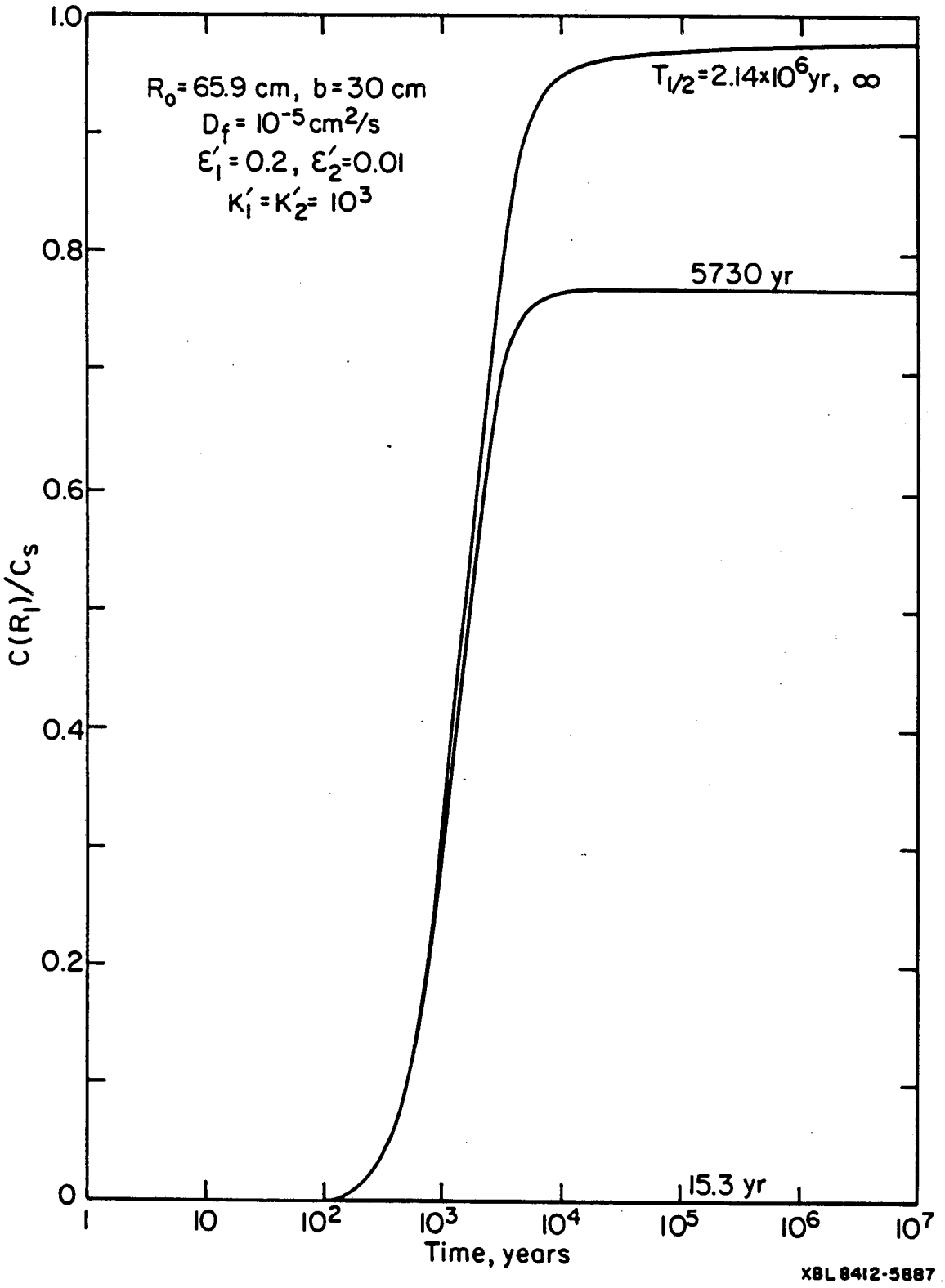

Fig. 8 Normalized backfill-rock interface concentration as a function of time and half-life; diffusion from a spherical waste form.

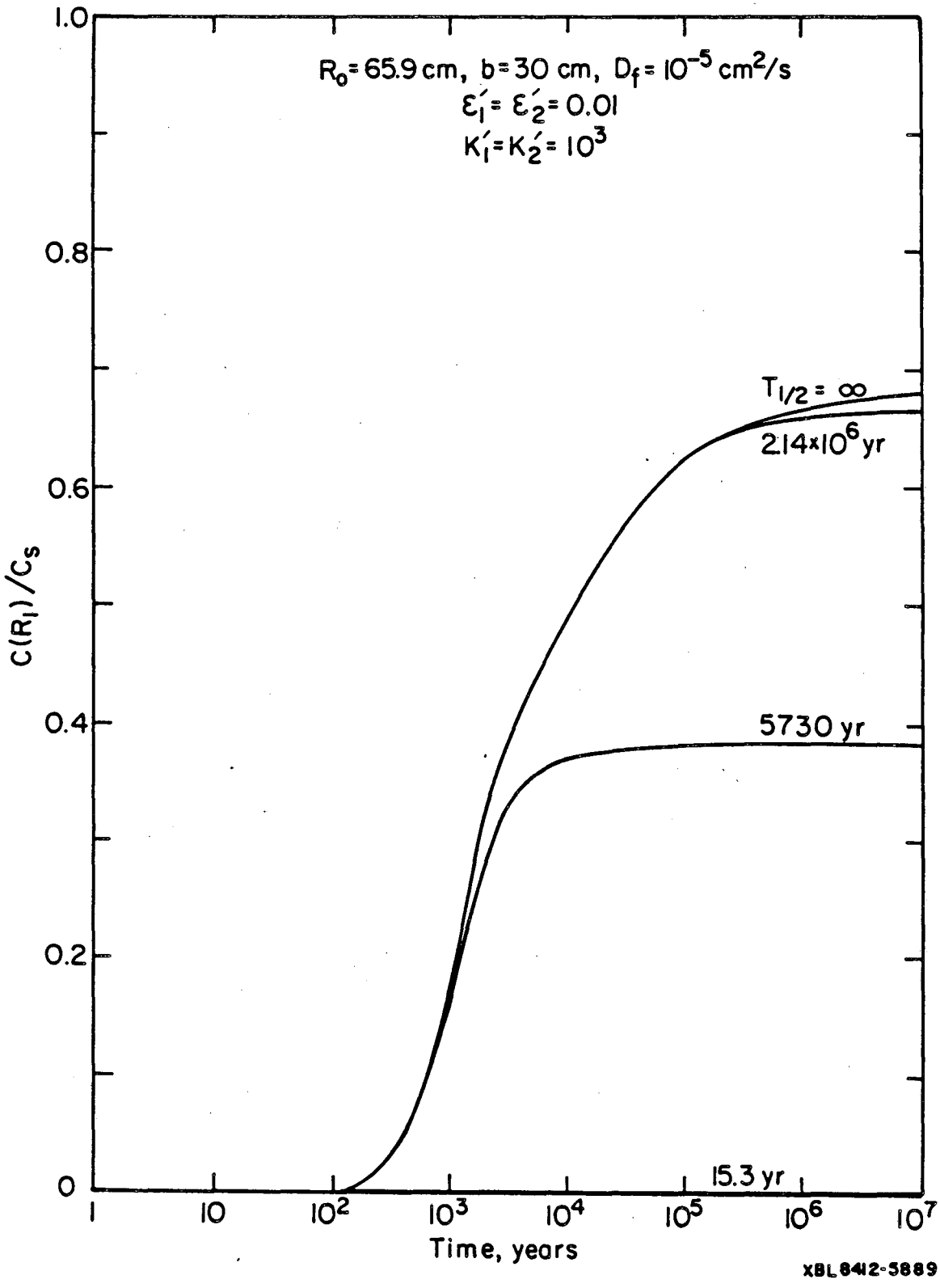

Fig. 9 Normalized backfill-rock interface concentration as a function of time and half-life; diffusion from a spherical waste form.

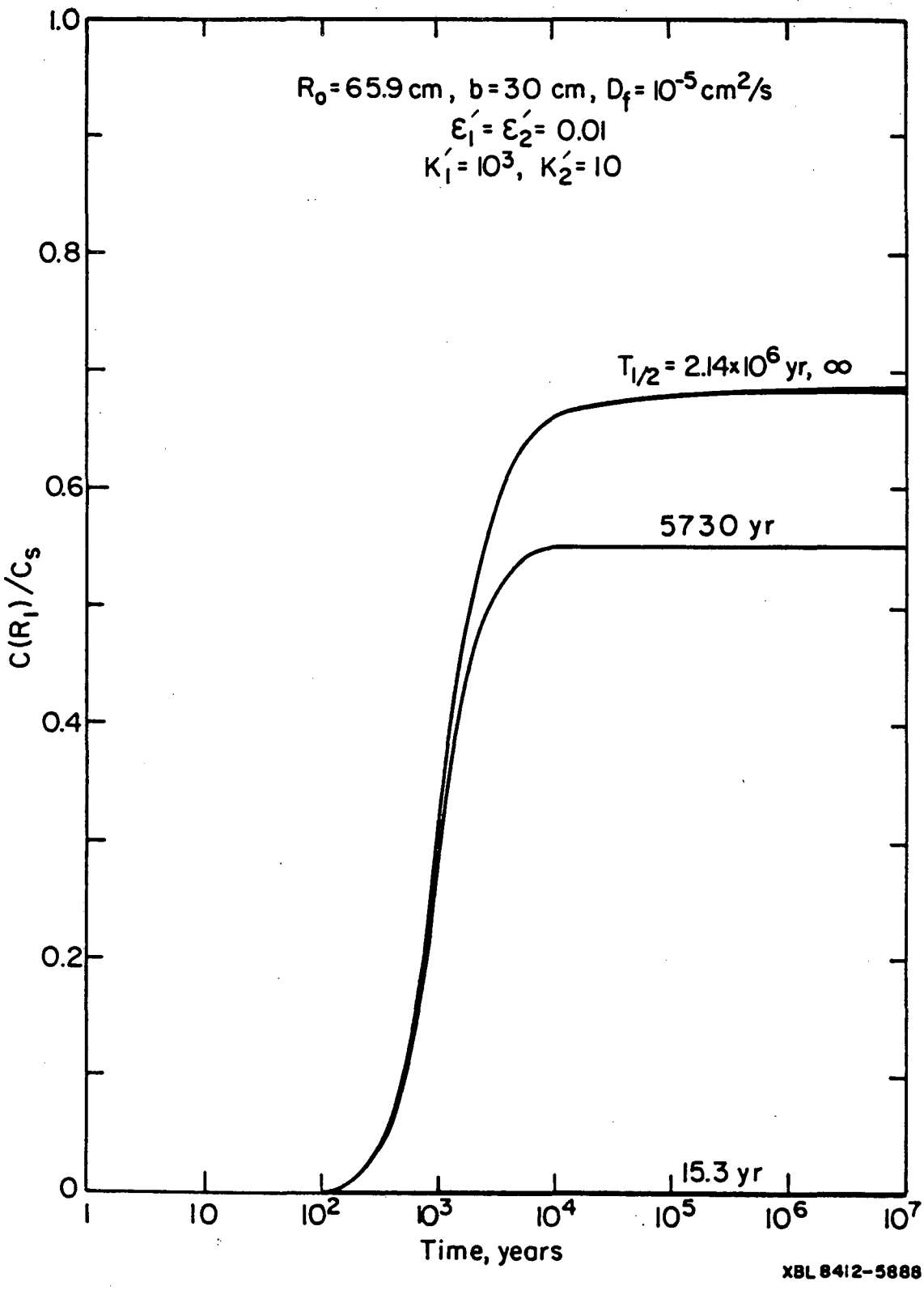

Fig. 10 Normalized backfill-rock interface concentration as a function of time and half-life; diffusion from a spherical waste form.

with half life no longer than 81 years at least 99% of the specie will have decayed in the backfill layer before reaching the interface boundary. One would expect that for larger K_1' or smaller ε_1' this decaying effect will be more significant because of the longer traveling time in the backfill due to the higher retardation. For instance, if $\varepsilon_1' = 0.01$, $T_{1/2}$ may be as long as 110 years if other parameters are fixed. On the other hand, when the half life is so long as 2.14×10^6 years (^{237}Np), the interface concentration is almost equal to that of the stable specie. Hence a radionuclide with half life of a few million years can be treated as a stable nuclide for the backfill calculations. This is also shown in Fig. 5 to 7. In these figures, the mass transfer rates $\dot{M}(R_o,t)/C_s$ and $\dot{M}(R_1,t)/C_s$ for ^{237}Np can hardly be distinguished from the results of stable specie. The results for ^{14}C and ^{244}Cm are somewhat different. Since the radionuclides with relatively short half life will have decayed an appreciable amount in the backfill, a lower concentration profile will be produced in the backfill resulting in a steeper gradient near the waste surface. Hence a higher mass transfer rate at the waste surface will be observed, as shown in curves for $T_{1/2}$ = 15.3 and 5730 years. On the other hand, the mass transfer rate at the backfill-rock interface can not so easily be predicted. For very short-lived radionuclides, such as ^{244}Cm, the concentration drops to such a low level that almost not a single nuclide can reach the interface boundary. Hence the interface mass transfer rate is very close to zero, as shown in Fig. 5 to 7 for the case $T_{1/2}$ = 15.3 years. For ^{14}C, however, the situation is changed. Since not all the nuclides will have decayed in the backfill, the concentration gradient at backfill-rock interface may be either higher or lower than the stable specie. For instance, the curves for ^{14}C in Figs. 5 and 6 have the higher numerical values than the curves for stable specie, while in Fig. 7 they become lower. It is worthwhile noting

that the time to reach the steady state is shorter for radionuclides than for stable specie, as seen in Figs. 5 to 7, since the decay can accelerate the mass balance in addition to the spherical geometry.

As a conclusion, the backfill can effectively stop the mass diffusion for very short-lived radionuclides, but makes no difference between the very long-lived radionuclides and the stable nuclides. For medium-lived radionuclides, though the decay in the backfill will lower the concentration profile, as shown in Figs. 8 to 10, the interface mass transfer rate may not be necessarily lower than the stable species. This is contradictory to what was expected by some other workers. Hence a complete transient analysis like this one should be used to predict the backfill performance.

The following comment was supplied by Dr. W. Lee:

One of the important potential uses of results in Chapters 2 and 3 is to show compliance with the NRC release rates requirement. Within the repository projects the approaches to showing such compliance is not well developed. Part of the reason is that the boundary of the engineered barrier system is not well defined, and may include some host rock in addition to the waste package. The predictive tools developed in Chapters 2 and 3 will apply no matter where the boundary is set. The case of the boundary set in rock is illustrated by the calculations in which the porosity and retardation of the rock and backfill are the same.

Appendix 3A

D01AJF is a general-purpose integrator which calculates an approximation to the integral of a function f(x) over a finite interval (a,b):

$$I = \int_a^b f(x)dx \tag{1}$$

It is an adaptive routine, using the Gauss 10-point and Kronrod 21-point rules, and is suitable as a general-purpose integrator. It can be used when the integrand has singularities, especially when these are of algebraic or logarithmic type.

The user can input the desired accuracy as the absolute and the relative ones. However, it can not guarantee, but in practice usually achieves the following accuracy:

$$\left|I-I_a\right| \leq \max\left(\left|\text{abserr}\right|, \left|\text{relerr} \times I\right|\right) \tag{2}$$

where

I_a = computing result for I

abserr = desired absolute accuracy

relerr = desired relative accuracy

Equation (2) was verified for the limiting case that the backfill and rock have the same properties, that is, Eq. (5) and Eq. (6), and is assumed to be acceptable for other calculations.

4. MASS TRANSPORT IN BACKFILL WITH A NON-LINEAR SORPTION ISOTHERM

H. C. LUNG

P.L. CHAMBRÉ

One of the functions of the backfill is to retard the migration of the radionuclides from the waste form by adsorbing the nuclides on its surface. The sorption effect is usually measured by the so called distribution coefficient defined as

$$K_d(N_f) = \frac{N_s}{N_f} \tag{1}$$

where N_f = concentration of nuclide in liquid phase,

N_s = concentration of nuclide in solid phase.

The relationship between the nuclide concentrations in the liquid phase and that in the solid phase under equilibrium condition is described by the sorption isotherm. The retardation coefficient is then defined by [1]

$$K(N_f) = 1 + \frac{1-\varepsilon}{\varepsilon} K_d(N_f) \tag{2}$$

where ε = porosity of the medium.

Usually one assumes a proportionality between N_f and N_s so that $K_d(N_f)$ and therefore $K(N_f)$ are constants in time and space. However, if the nuclide concentration in liquid phase is sufficiently large so that the solid phase can not adsorb all the nuclides then sorption saturation in the solid phase will occur [2].

Frequently a Langmuir sorption isotherm is assumed to take into account the sorption saturation. Figure 1 shows the Langmuir isotherm with Q the saturation concentration in solid phase. In the present anlaysis we approximate the Langmuir isotherm (the solid curve) by two linear segments (the dashed lines) so that for liquid concentration $N_f < N^*$, we have a linear

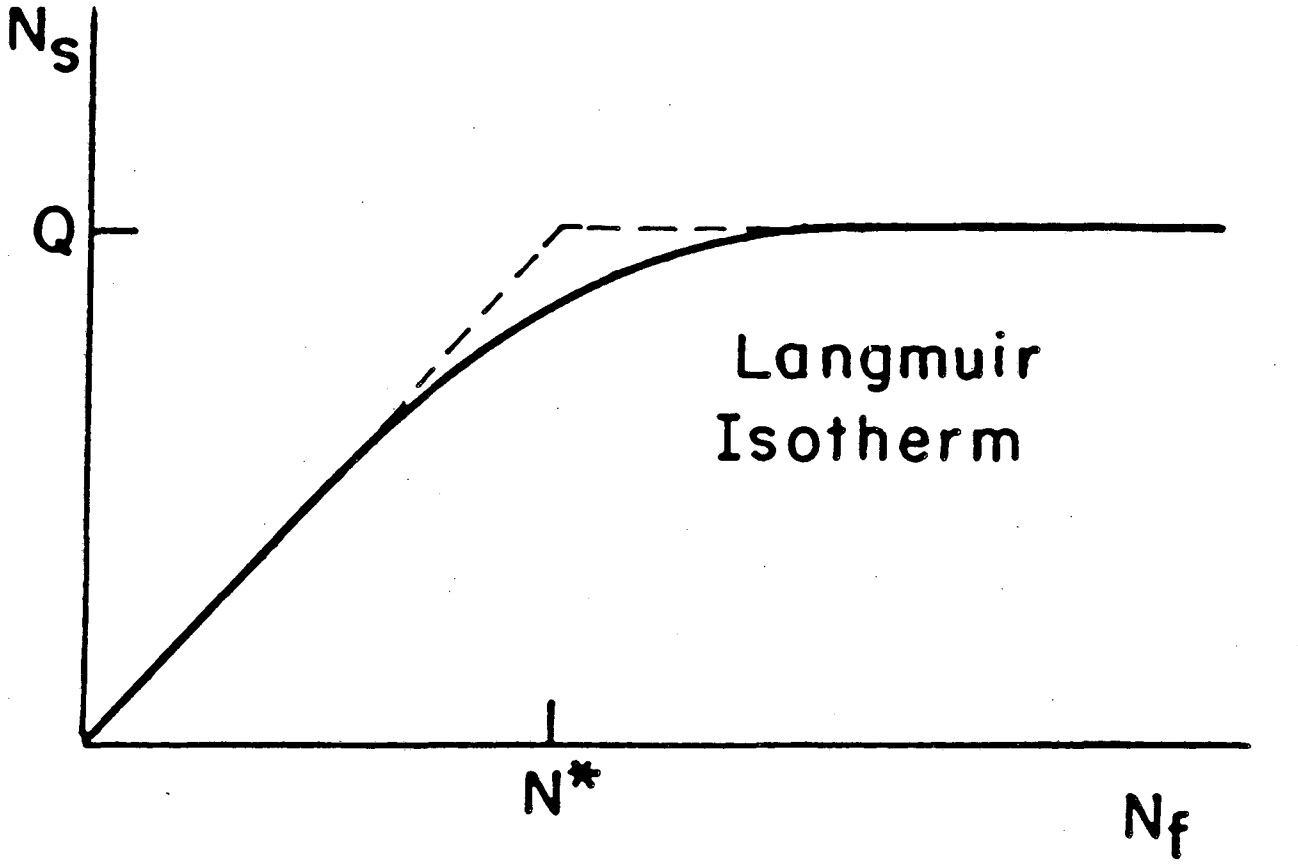

Fig. 1 Approximate Langmuir isotherm.

relationship between N_f and N_s; while for $N_f < N^*$, the solid phase is saturated and $N_s = Q$ for all N_f. N^* is called critical (nuclide) concentration.

We wish to model the radionuclide transport controlled by a sorption isotherm. We assume one-dimensional nuclide transport through the backfill and neglect the effects of convection in the liquid phase and diffusion in its solid phase. The governing equations for the nuclide concentration in the absence of precursors and sources outside the waste form are given by [1]

$$\frac{\partial(\varepsilon N_f)}{\partial t} = D_f \frac{\partial^2(\varepsilon N_f)}{\partial x^2} - \phi(N_f,N_s) - \lambda\varepsilon N_f \tag{3}$$

$$\frac{\partial[(1-\varepsilon)N_s]}{\partial t} = \phi(N_f,N_s) - \lambda(1-\varepsilon)N_s \tag{4}$$

where D_f = diffusion coefficient of nuclide in liquid phase

$\phi(N_f,N_s)$ = interphase reaction rate

λ = decay constant.

On adding Eq. (3) to Eq. (4), one obtains

$$\frac{\partial}{\partial t}\left[\varepsilon N_f + (1-\varepsilon)N_s\right] = D_f \frac{\partial^2(\varepsilon N_f)}{\partial x^2} - \lambda\left[\varepsilon N_f + (1-\varepsilon)N_s\right] \tag{5}$$

Suppose the equilibrium is established for the nuclide concentrations between the phases. If the approximated Langmuir isotherm is applied, then for $N_f > N^*$, $N_s = Q$ = constant, and Eq. (5) reduces to

$$\frac{\partial(\varepsilon N_f)}{\partial t} = D_f \frac{\partial^2(\varepsilon N_f)}{\partial x^2} - \lambda\varepsilon N_f - \lambda(1-\varepsilon)Q, \; N_f > N^* \; . \tag{6}$$

For $N_f < N^*$, we have a linear isotherm so that by equation (1), $\frac{N_s}{N_f} = K_d$. If this is combined with (2) and substituted into (5) one gets

$$\frac{\partial(K\varepsilon N_f)}{\partial t} = D_f \frac{\partial^2(\varepsilon N_f)}{\partial x^2} - \lambda(K\varepsilon N_f), \; N_f < N^* \tag{7}$$

Fig. 2 shows the anticipated concentration profile $N_f(x,t)$ at the fixed time t in the backfill. With the approximation of Langmuir isotherm the backfill can be divided into two parts:

a) an inner saturated region, close to the waste form, within which N_f is greater than N*, and

b) an outer unsaturated region of lower concentration.

If we assume a zero initial condition and a constant boundary concentration at the waste surface (x = 0) which is greater than the critical concentration N*, then at time zero the entire backfill is unsaturated. But as time increases saturation will occur at waste surface and an interface moves outward into the backfill. The interface position s(t), between the saturated and unsaturated regions, is thus a function of time with s(0) = 0.

If one applies the above side conditions to Eqs. (6) and (7) with the assumption of constant properties one obtains for the saturated region, with $N_s \equiv N_f$

$$\frac{\partial N_s(x,t)}{\partial t} = D_f \frac{\partial^2 N_s(x,t)}{\partial x^2} - \lambda N_s(x,t) - \lambda \frac{1-\varepsilon}{\varepsilon} Q, \quad 0 < x \leq s(t), \quad t > 0 \tag{8}$$

unsaturated region, with $N_u \equiv N_f$

$$\frac{\partial N_u(x,t)}{\partial t} = \frac{D_f}{K} \frac{\partial^2 N_u(x,t)}{\partial x^2} - \lambda N_u(x,t), \quad x \geq s(t), \quad t > 0 \tag{9}$$

Initial conditions

$$N_u(x,0) = 0, \quad x > 0; \quad N_s(x,0) \text{ unknown}, \tag{10}$$

Boundary conditions

$$N_s(0,t) = N_o > N^*, \quad t > 0 \tag{11}$$

$$N_s(s(t),t) = N_u(s(t),t) = N^*, \quad t > 0 \tag{12}$$

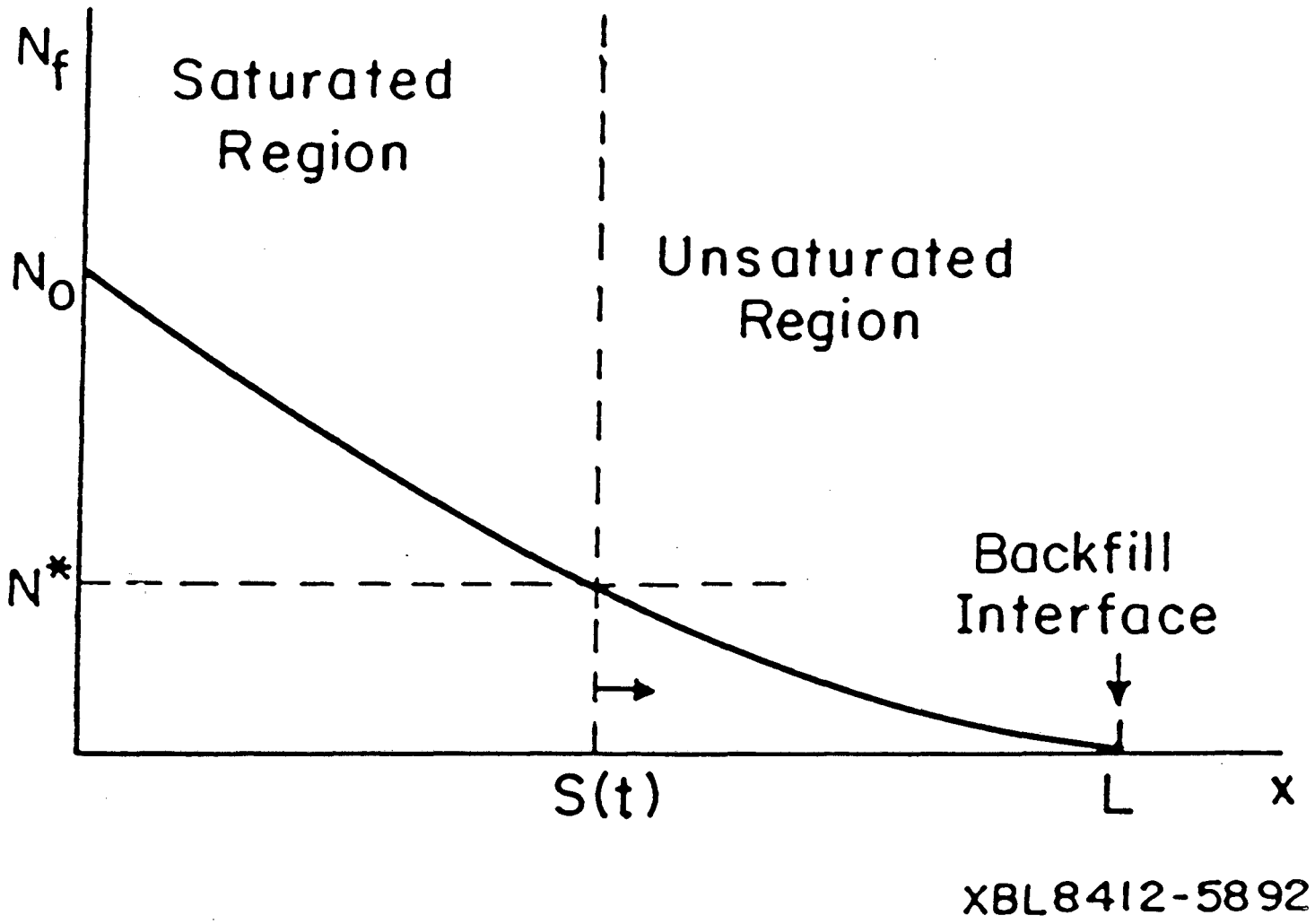

Fig. 2 Conceptual concentration profile in backfill at time t.

$$- \varepsilon D_f \frac{\partial N_s(x,t)}{\partial x} = - \varepsilon D_f \frac{\partial N_u(x,t)}{\partial x}, \quad x = s(t), \; t > 0 \tag{13}$$

$$N_u(\infty,t) = 0, \; t > 0 \tag{14}$$

The initial condition for $N_s(x,t)$ is unspecified because at $t = 0$ there exists no saturated region in the backfill. Equation (11) described the nuclide concentration at the waste form surface to be greater than the critical concentration because otherwise there will be no saturation effects. Equation (12) assures that the critical concentration is reached on both sides of the moving interface and (13) insists on the equality of the flux at this surface. Eqaution (14) is self evident. The last term in (8) can be given an alternate form. It follows from the approximation of (1) that $K_d = Q/N^*$. If this is substituted into (2) and that equation is solved for Q one obtains

$$\frac{1-\varepsilon}{\varepsilon} Q = W$$

where

$$W = (K-1)N^* \tag{15}$$

One can thus replace the term in (8) by λW. Equation (15) shows that for $K = 1$ ($K_d = 0$), $Q = 0$, which verifies that there is no adsorption in the solid phase.

The Early Time Solution

For the time span much shorter than the half life of the radionuclide, the decay terms in both Eq. (8) and (9) can be neglected. The governing equations become

$$\frac{\partial N_s(x,t)}{\partial t} = D_f \frac{\partial^2 N_s(x,t)}{\partial x^2}, \quad 0 < x \leq s(t), \; t > 0 \tag{16}$$

$$\frac{\partial N_u(x,t)}{\partial t} = \frac{D_f}{K} \frac{\partial^2 N_u(x,t)}{\partial x^2}, \quad x \geq s(t), \; t > 0 \tag{17}$$

The side conditions remain unchanged.

The solutions for $N_s(x,t)$ and $N_u(x,t)$ have the following forms

$$\frac{N_s(x,t)}{N_o} = A \operatorname{erf}\left(\frac{x}{2\sqrt{D_f t}}\right) + 1, \quad 0 < x \leq s(t), \quad t > 0 \tag{18}$$

$$\frac{N_u(x,t)}{N_o} = B \operatorname{erfc}\left(\frac{x}{2\sqrt{\frac{D_f}{K}\, t}}\right), \quad x \geq s(t), \quad t > 0 \tag{19}$$

A and B are unknown constants to be determined by the boundary conditions. Equations (18) and (19) already satisfy (10), (11), and (14).

From (12) one obtains

$$\frac{N_s(s(t),t)}{N_o} = \frac{N^*}{N_o}$$

$$= A \operatorname{erf}\left(\frac{s(t)}{2\sqrt{D_f t}}\right) + 1$$

$$= B \operatorname{erfc}\left(\frac{s(t)}{2\sqrt{\frac{D_f t}{K}}}\right)$$

$$= \frac{N_u(s(t),t)}{N_o}, \quad t \geq 0 \quad . \tag{20}$$

Since A, B, D_f, and K are constants, the argument in the error functions must also be constant. Therefore,

$$\frac{s(t)}{\sqrt{t}} = k \text{ or } s(t) = k\sqrt{t}, \quad t \geq 0, \tag{21}$$

where k is constant in time and must be a function of the parameters of the problem, i.e. D_f, K, and $\frac{N^*}{N_o}$. From (20) and (21) one gets

$$A = \frac{\frac{N^*}{N_o} - 1}{\operatorname{erf}\left(\frac{k}{2\sqrt{D_f}}\right)}, \quad B = \frac{\frac{N^*}{N_o}}{\operatorname{erfc}\left(\frac{k}{2\sqrt{\frac{D_f}{K}}}\right)} \tag{22}$$

Substituting into (13) one obtains

$$\frac{\exp\left\{(K-1)\,\frac{k^2}{4D_f}\right\}\,\operatorname{erfc}\left(\frac{k}{2\sqrt{D_f/K}}\right)}{\operatorname{erf}\left(\frac{k}{2\sqrt{D_f}}\right)} - \frac{\frac{N^*}{N_o}\sqrt{K}}{\left(1-\frac{N^*}{N_o}\right)} = 0 \tag{23}$$

One can solve this transcendental equation for k. The results are shown in Fig. 3. There k is plotted as a function of the dimensionless interface concentration N^*/N_o with the retardation coefficient K as the parameter. D_f is fixed in these computations at 10^{-5} cm^2/sec. One sees that as $N^*/N_o \to 1$, $k \to 0$, since the saturated region becomes very narrow, on realizing that $N^* \leq N_s(x,t) < N_o$ and that $N_o \to N^*$. On the other hand, as $N^*/N_o \to 0$, $k \to \infty$. In this case there is almost no unsaturated region in the backfill and hence the interface position will move very rapidly towards infinity. Five different K values were used in the calculations. They are 10^4, 4×10^3, 10^3, 10^2, and 10. It is seen from Fig. 3 that for an increasing K the interface position moves more slowly, since a large K implies a strong retardation effect and hence a slowdown of the saturation in the backfill.

The interface position s(t) is an indicator of the backfill performance because it shows how quickly saturation takes place with a resulting loss of nuclide retardation. If the backfill thickness is L then the retardation by the backfill disappears when the saturation interface penetrates a distance equal to L. The breakthrough time T_b for such penetration is given by

$$T_b = \left(\frac{L}{k}\right)^2 \tag{24}$$

Fig. 3 also shows the breakthrough time as a function of N^*/N_o with the same parameter K. The backfill thickness is taken to be 30 cm. Since T_b is inversely proportional to k^2, as N^*/N_o decreases, T_b decreases, and as K increases, T_b increases also. The importance of saturation in the backfill can be seen by

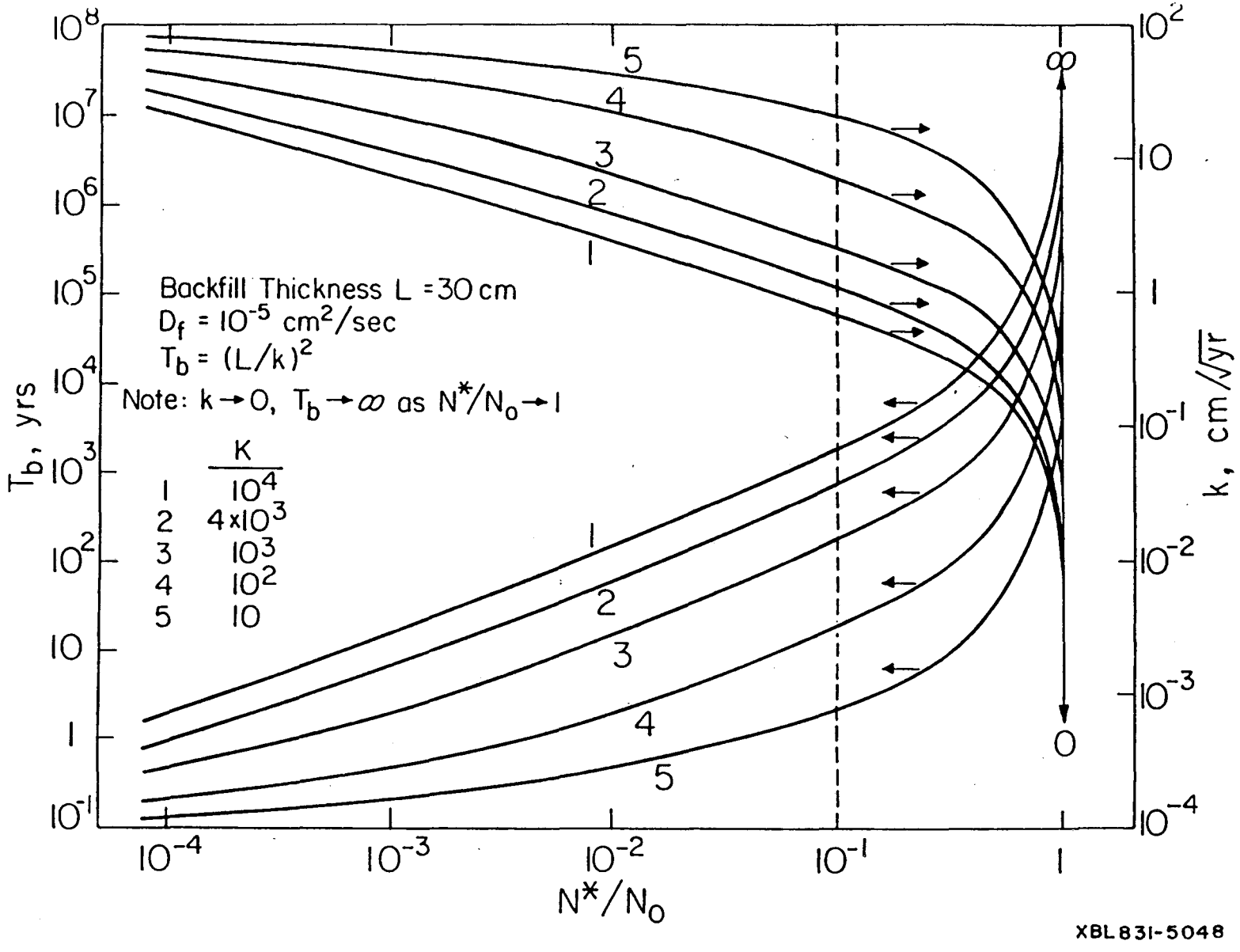

Fig. 3 Breakthrough time T_b as a function of normalized critical concentration and retardation coefficient in backfill.

comparing these results with those in which saturation is assumed absent. Assuming a linear isotherm with slope K = 4000, and for the (same) diffusion coefficient $D_f = 10^{-5}$ cm^2/sec, Nowak [3] showed that it would take 1000 years to raise the concentration at x = 30 cm to 1% of N_o. However, if saturation can occur, with $N^* = 0.01\ N_o$, the breakthrough time is reduced to 60 years as seen in Fig. 3, i.e. only 6% of the breakthrough time in absence of saturation.

In the present analysis, a semi-infinite medium for backfill, as described in B.C. (14) was assumed. Therefore some restriction must be imposed if one wants to apply the results to a finite backfill layer. We assume for this that the concentration at the outer edge of the backfill must not exceed 10% of the concentration at the inner edge of the backfill, N_o. This limits the time span of the solution to a concentration $N^*/N_o \leq 0.1$ at the backfill-rock interface, which is indicated by the vertical dashed line in Fig. 3. Since for $K \leq 10^4$ and $N^*/N_o \leq 0.1$, T_b is always less than 2000 years, nuclides with half lives greater than 5000 years can be treated as nondecaying for the purpose of using the early time solution.

The Steady State Solution

At steady state, time derivations in (8) and (9) vanish so that

$$D_f \frac{\partial^2 N_s(x)}{\partial x^2} - \lambda N_s(x) - \lambda W = 0,\ 0 < x \leq s(\infty). \tag{25}$$

$$\frac{D_f}{K} \frac{\partial^2 N_u(x)}{\partial x^2} - \lambda N_u(x) = 0,\ x \geq s(\infty), \tag{26}$$

where $W = (K-1)N^*$ as defined in (15). The boundary conditions are

$$N_s(0) = N_o > N^*,\ N_u(\infty) = 0 \tag{27}$$

$$N_s(S_\infty) = N_u(S_\infty) = N^*,\ S_\infty = s(t = \infty), \tag{28}$$

$$-\varepsilon D_f \frac{\partial N_s(S_\infty)}{\partial x} = -\varepsilon D_f \frac{\partial N_u(S_\infty)}{\partial x} \tag{29}$$

where S_∞ is the interface position when steady state has been reached. The solutions of (25) and (26) subject to the boundary conditions (27) - (29) take the forms

$$N_s(x) = Ae^{k_s} + Be^{-k_s} - W, \quad 0 < x \leq S_\infty, \tag{30}$$

$$N_u(x) = Ce^{-k_u x}, \quad x \geq S_\infty, \tag{31}$$

$$\text{where } k_s = \sqrt{\frac{\lambda}{D_f}}, \quad k_u = \sqrt{\frac{\lambda K}{D_f}} \tag{32}$$

and A, B, C are constants of integration. After substituting (27) - (29) into (30) and (31), one gets

$$\frac{1}{2}\left[N^*(1+\sqrt{K}) + W\right] = \frac{W(e^{k_s S_\infty}-1) + N_o e^{k_s S_\infty} - N^*}{e^{2k_s S_\infty} - 1} \tag{33}$$

Let

$$\frac{1}{2}[N^*(1+\sqrt{K}) + W] = \beta, \quad e^{k_s S_\infty} = y, \tag{34}$$

then

$$\beta y^2 - (W + N_o)y - (\beta - W - N^*) = 0 \tag{35}$$

Hence

$$y = \frac{(W+N_o) + \sqrt{(W+N_o)^2 + 4\beta(\beta - W - N^*)}}{2\beta}$$

so that

$$S_\infty = \sqrt{\frac{D_f}{\lambda}} \log y \tag{36}$$

In the solution of y the choice of root is determined so that log y is non-negative. The radicand is always greater than $[(W + N_o) - 2\beta]^2$ since N_o is larger than N^* by definition.

Fig. 4 shows the steady state interface position S_∞ as a function of N^*/N_o for a half life $T_{1/2} = 10^4$ yr. Similar to the transient case an increase in the

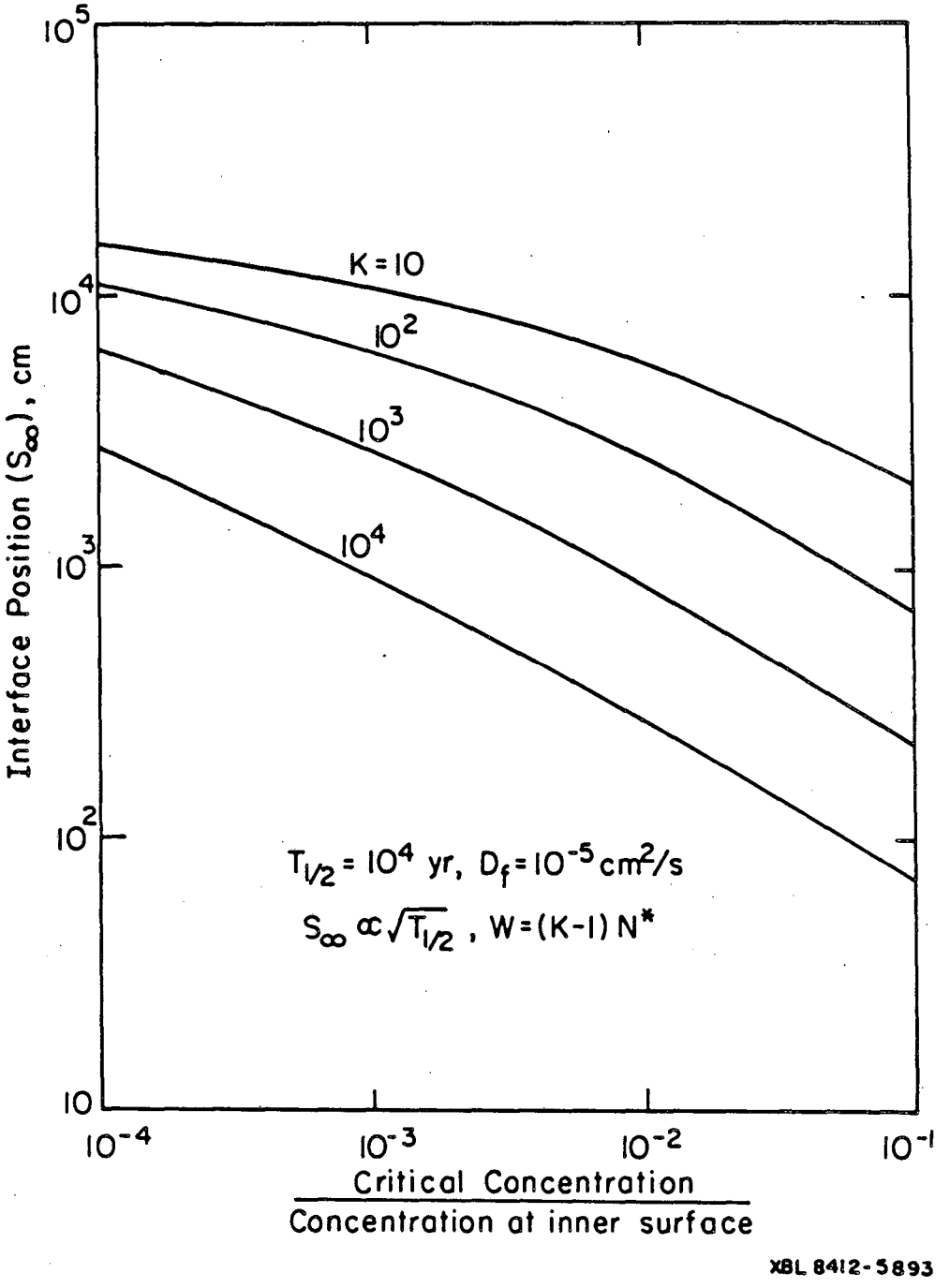

Fig. 4 Steady-state interface position as a function of normalized critical concentration and retardation coefficient in backfill.

retardation coefficient K results in a decrease of S_∞. The effect of decay can be seen from the equation (36). A decrease in $T_{1/2}$ (an increase in λ) decreases S_∞. Although the semi-infinite medium assumption was used in solving this problem, one can still get some insight into the effects of saturation. If, for example, $\frac{N^*}{N_o} = 0.01$ and $K = 10^4$, then S_∞ is about 300 cm for a radionuclide of $T_{1/2} = 10^4$ years or 30 cm for $T_{1/2} = 100$ years. So if for a backfill thickness of 30 cm, and radionuclides with half lives longer than 100 years, the interface position from the waste form will always be greater than the backfill thickness. This implies that the backfill totally saturates before the steady state is reached and is thus rendered useless as a barrier to the migration of the radionuclides. This once more confirms the importance of the saturation of the backfill as already shown in the early time solution. For a boundary condition as $\frac{N^*}{N_o} \to 1$, the saturated region disappears, resulting in a almost zero interface position as shown in Fig. 3. This is also true for S_∞, i.e. $S_\infty \to 0$ as $\frac{N^*}{N_o} \to 1$, though not shown in Fig. 4.

To make the backfill more effective, one can a) increase the backfill thickness to lengthen the breakthrough time T_b as seen in (24); b) use a backfill material with large retardation coefficient K to slow down the interface movement which in turn increases T_b as seen in Fig. 3. A large K also implies a small S_∞ as shown in Fig. 4; c) use a backfill material with high $\frac{N^*}{N_o}$, i.e. $\frac{N^*}{N_o} \to 1$, which will limit the interface position close to the waste form surface even at the steady state, as described in the previous paragraph. With proper combination of the above three suggestions, it is possible to make a backfill not totally saturated and hence effective at all times.

References

1. M. Harada, et al., "Migration of Radionuclides Through Sorbing Media, Analytical Solutions - I," LBL-10500, February 1980.

2. I. Neretnieks, "Retardation of Escaping Nuclides From a Final Repository," KBS Teknisk Rapport nr 30, 1977.

3. E.J. Nowak, "The Backfill Barrier as a Component in a Multiple Barrier Nuclide Waste Isolation System," SAND79-1109, October 1979.

5. STEADY STATE MASS TRANSPORT FROM A PROLATE SPHEROID WITH BACKFILL

P.L. Chambré and H. Lung

In [1], we obtained the steady state solution as well as the early time and large time behaviors of the mass transport from a finite sized waste form by diffusion. The waste shape was approximated by a slender prolate spheroid of the same surface area and volume. Here we extend the steady state analysis to include the effects of a finite backfill layer between the waste and rock and include the transport by advection.

The waste form is approximated by a prolate spheroid with a focal distance f (cf. Fig. 1). The surrounding backfill is idealized by a prolate spheroid layer of the same focal distance. L is the backfill layer thickness at the equator of the waste form, a_I the semi-major axis of the backfill, ε_p the rock porosity, and ε_b the backfill porosity.

Water is flowing perpendicular to the axis of the waste form with a constant pore velocity U far from the waste. The backfill such as bentonite, possesses an extremely low hydraulic permeability. It is assumed that no water can flow inside it once it is saturated with water. Hence the nuclides can only be transported out of the waste by diffusion in the backfill and then carried away by both diffusion and convection into the porous rock.

In the present analysis we consider the steady state solution in the absence of radioactive decay. Under this condition retardation effects in both backfill and rock regions do not arise.

Governing Equation and Side Conditions

The governing equation for the radionuclide concentration $C_b(\alpha)$ in the backfill is given by

$$\frac{d}{d\alpha}\left(\sinh\alpha\ \frac{dC_b}{d\alpha}\right) = 0,\ \alpha_s \leq \alpha \leq \alpha_I\ . \tag{1}$$

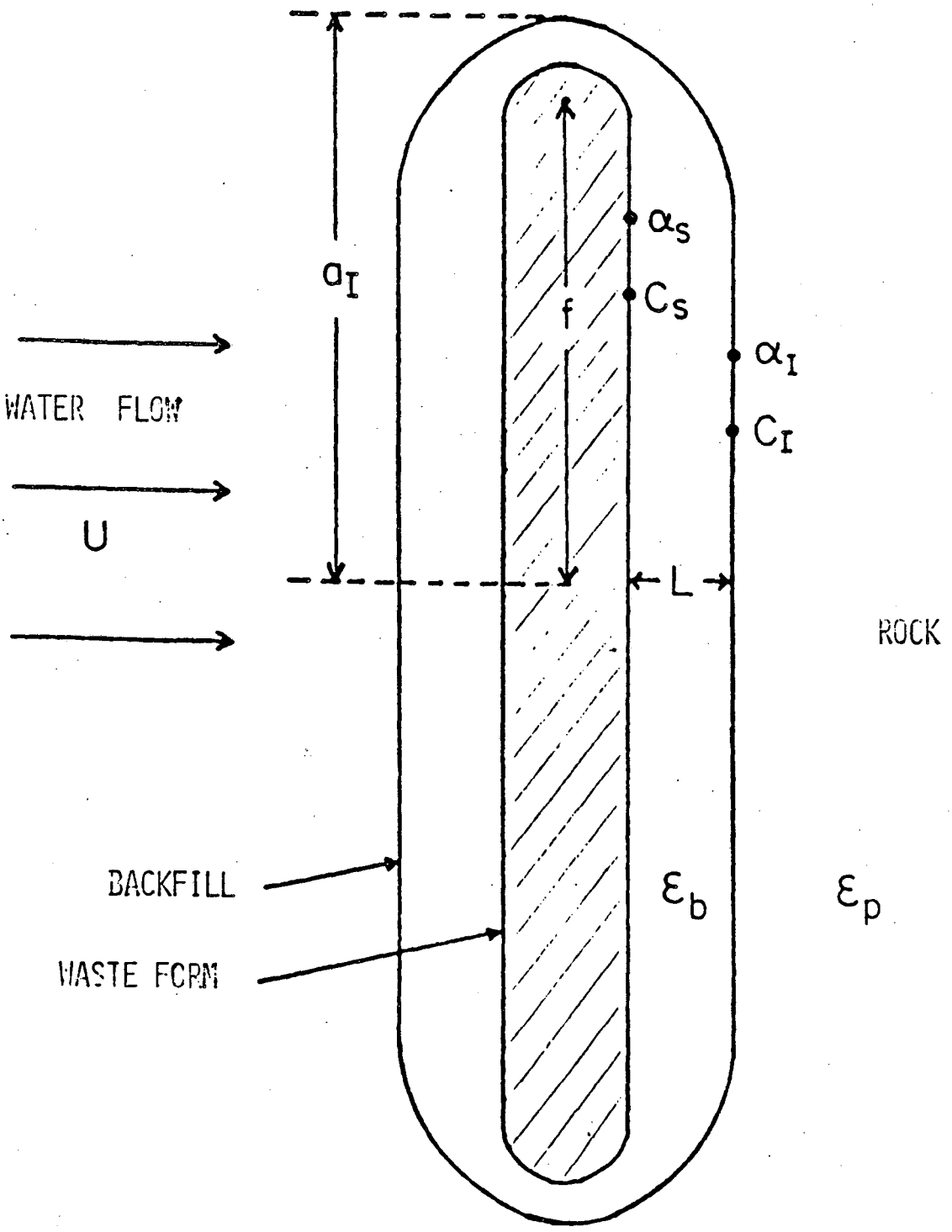

Figure 1. Prolate Spheroid Waste Form

XBL836-5763

Here α is the spatial coordinate in the prolate spheroidal system and α_s and α_I are the coordinates of waste surface and the backfill-rock interface, respectively (cf. Fig. 1). A solubility limited concentration C_s of the nuclide is assumed at the waste surface. The (spatially) average nuclide concentration of backfill-rock interface is C_I which must be determined in the analysis. Thus

$$C_b(\alpha_s) = C_s, \quad C_b(\alpha_I) = C_I. \tag{2}$$

The solution of Eq. (1) subject to side conditions (2) is

$$C_c(\alpha) = C_s - (C_s - C_I)\left[\frac{Q_o(\alpha_s) - Q_o(\alpha)}{Q_o(\alpha_s) - Q_o(\alpha_I)}\right] \quad \alpha_s \leq \alpha \leq \alpha_I , \tag{3}$$

where

$$Q_o(\alpha) = \log\left(\coth\frac{\alpha}{2}\right) \tag{4}$$

From (3) one can compute the local mass flux

$$\vec{j}\,(\alpha_I) = -\,\varepsilon_b \sigma_b D_f \nabla C_b(\alpha)\Big|_{\alpha=\alpha_I} \tag{5}$$

on the backfill-rock interface

$$\vec{j}\,(\alpha_I) = -\,\frac{\varepsilon_b \sigma_b D_f}{h_\alpha}\,\frac{dC_b}{d\alpha}\Bigg|_{\alpha=\alpha_I}$$

$$= \frac{\varepsilon_b \sigma_b D_f}{f(\sinh^2\alpha_I + \sin^2\beta)^{1/2}}\left[\frac{C_s - C_I}{Q_o(\alpha_s) - Q_o(\alpha_I)}\right]\frac{1}{\sinh\alpha_I}, \tag{6}$$

where

$$h_\alpha = f(\sinh^2\alpha + \sin^2\beta)^{1/2}$$

$$\sigma_b = \text{geometric factor for backfill} \tag{7}$$

and D_f is the diffusion coefficient of the nuclide in water. The total mass transfer rate out of the backfill rock interface of surface area S derived from concentration gradient in backfill is then calculated from (6):

$$\dot{M}_b(\alpha_I) = \int_S \vec{j}\,(\alpha_I)\,ds$$

$$= \int_0^{\pi}\int_0^{2\pi} \vec{j}\; h_\beta h_\psi\, d\psi d\beta$$

$$= \int_0^{\pi}\int_0^{2\pi} \left[\frac{C_s - C_I}{Q_o(\alpha_s) - Q_o(\alpha_I)}\right] f \sin\beta\, \varepsilon_b \sigma_b D_f d\psi d\beta$$

$$= 4\pi f \varepsilon_b \sigma_b D_f \left[\frac{C_s - C_I}{Q_o(\alpha_s) - Q_o(\alpha_I)}\right], \tag{8}$$

where

$$h_\beta = h_\alpha = f(\sinh^2\alpha + \sin^2\beta)^{1/2} \tag{9}$$

$$h_\psi = f \sinh\alpha \sin\beta, \tag{10}$$

This mass transfer is carried away by diffusion and convection from the interface boundary into the exterior porous rock where the concentration vanishes far from the waste. The total mass transport rate from the interface into the exterior field calculated from convection and diffusion in rock is represented in the usual form.

$$\dot{M}_p = h_m S_I C_I \tag{11}$$

where h_m is the mass transfer coefficient, and S_I the interface area. If one defines a Sherwood number for mass transport by

$$Sh = \frac{h_m}{2\pi\varepsilon_p \sigma_p D_f}\left(\frac{S_I}{L_o}\right) \tag{12}$$

with L_o some characteristic dimension of the waste form and σ_p the geometric factor for rock one can restate (11) as follows

$$\dot{M}_p = (2\pi\varepsilon_p \sigma_p D_f C_I L_o)\ (Sh) \tag{13}$$

Because L_o can be arbitrarily chosen, we choose it as (cf. Appendix 5A)

$$L_o = 2a_I \tag{14}$$

Since the Sherwood number is primarily a function of the Peclet number $Pe = \frac{Ua_I}{\sigma_p D_f}$ one can express (13) in the form

$$\dot{M}_p = Sh\ (Pe)\ 4\pi C_I \varepsilon_p \sigma_p D_f a_I \tag{15}$$

Under steady state conditions the mass transported out of the backfill

must equal the mass transported into the rock region in a unit of time. Therefore one can equate equations (8) and (15) and solve for the interface concentration C_I as follows

$$C_I = \frac{C_s}{\left(\frac{\varepsilon_p \sigma_p}{\varepsilon_b \sigma_b}\right)\left[Q_o(\alpha_s) - Q_o(\alpha_I)\right]\cosh(\alpha_I)\mathrm{Sh}(\mathrm{Pe}) + 1} \tag{16}$$

On combining this expression with (15) one obtains the total mass transfer rate valid in either backfill or rock region

$$\dot{M} = \frac{4\pi\varepsilon_p\sigma_p D_f C_s a_I}{\left(\frac{\varepsilon_p \sigma_p}{\varepsilon_b \sigma_b}\right)\left[Q_o(\alpha_s) - Q_o(\alpha_I)\right]\cosh(\alpha_I) + \left[\mathrm{Sh}(\mathrm{Pe})\right]^{-1}} \tag{17}$$

The physical content of this result is brought out by introducing the dimensionless mass transfer resistances for backfill and rock

$$R_b = \left(\frac{\varepsilon_p \sigma_p}{\varepsilon_b \sigma_b}\right)\left[Q_o(\alpha_s) - Q_o(\alpha_I)\right]\cosh(\alpha_I);\quad R_p = \left[\mathrm{Sh}(\mathrm{Pe})\right]^{-1} \tag{18}$$

so that

$$\dot{M} = \frac{4\pi\varepsilon_p\sigma_p D_f C_s a_I}{R_b + R_p} \tag{19}$$

The Sherwood number dependence on Pe used in (16) and (17) is given by (cf. Appendix I)

$$\mathrm{Sh}(\mathrm{Pe}) = \begin{cases} \dfrac{1}{Q_o(\alpha_I)\cosh(\alpha_I)}\left[1 + \dfrac{\mathrm{Pe}}{2Q_o(\alpha_I)\cosh(\alpha_I)}\right] \\ \left[\dfrac{\mathrm{Pe}}{\pi}\tanh(\alpha_I)\right]^{1/2}, \quad \mathrm{Pe} \geq 4\coth(\alpha_I) \end{cases} \tag{20}$$

Equation (19) shows that the resistance to the mass transport consists of two parts: the backfill resistance and the exterior medium resistance. The backfill resistance is due to the properties and geometries of both media, as can be seen from (18), and is independent of the flow conditions. On the other hand, the exterior medium resistance is determined by the backfill-rock interface geometric factors α_I and a_I as well as the flow speed U. From (20) one

can see that Sherwood number is a monotone increasing function of Pe. An increase in Sh will thus reduce the exterior medium resistance in accordance with (18). The result is a decrease in the total resistance and hence an increase in the mass transfer rate. The effect of the flow condition on the concentration drop can also be seen from (16). As U increases and thus Sh increases, C_I will decrease causing the concentration drop across the backfill to increase.

Figure 2 shows the dimensionless interface concentration as a function of backfill layer thickness L with the parameters $\frac{\varepsilon_p}{\varepsilon_b}$ and Pe. Figure 3 shows the normalized mass transfer rate as a function of L with the same parameters as in Fig. 2. In all these calculations, a fixed diffusion coefficient $D_f = 10^{-5}$ cm^2/sec and a fixed rock porosity $\varepsilon_p = 0.01$ were used. The waste form is taken to be that of a spent fuel canister with the radius 17.8 cm and height 470 cm. The approximating prolate spheroid of this waste form has a semi-major axis of 272 cm and a semi-minor axis of 20.3 cm and has the same surface area and volume as the spent fuel canister.

The solid lines in Fig. 2 and Fig. 3 represent the case for $\frac{\varepsilon_p}{\varepsilon_b} = \frac{\sigma_b}{20\sigma_p}$, i.e. backfill porosity is 20 times the porosity of the rock times $\frac{\sigma_p}{\sigma_b}$. The dashed lines in Fig. 2 and Fig. 3 are for the case that $\frac{\varepsilon_p}{\varepsilon_b} = \frac{\sigma_b}{\sigma_p}$, i.e. backfill porosity $\varepsilon_b = \varepsilon_p \frac{\sigma_p}{\sigma_b} = 0.01 \frac{\sigma_p}{\sigma_b}$. In both cases the Peclet numbers are taken to be 0, 10^2, and 10^3. For the waste form geometry, consider here Pe = 100 corresponds to a pore velocity $U = 1.1\sigma_p$ m/year.

As L increases, the distance traveled by the nuclide inside the backfill increases. Since the nuclide can only be transported by diffusion, a longer travel distance implies a layer concentration drop across the backfill to maintain an equilibrium concentration gradient at constant exterior conditions. Hence the interface concentration C_I is lowered as L increases for all the cases in Fig. 2.

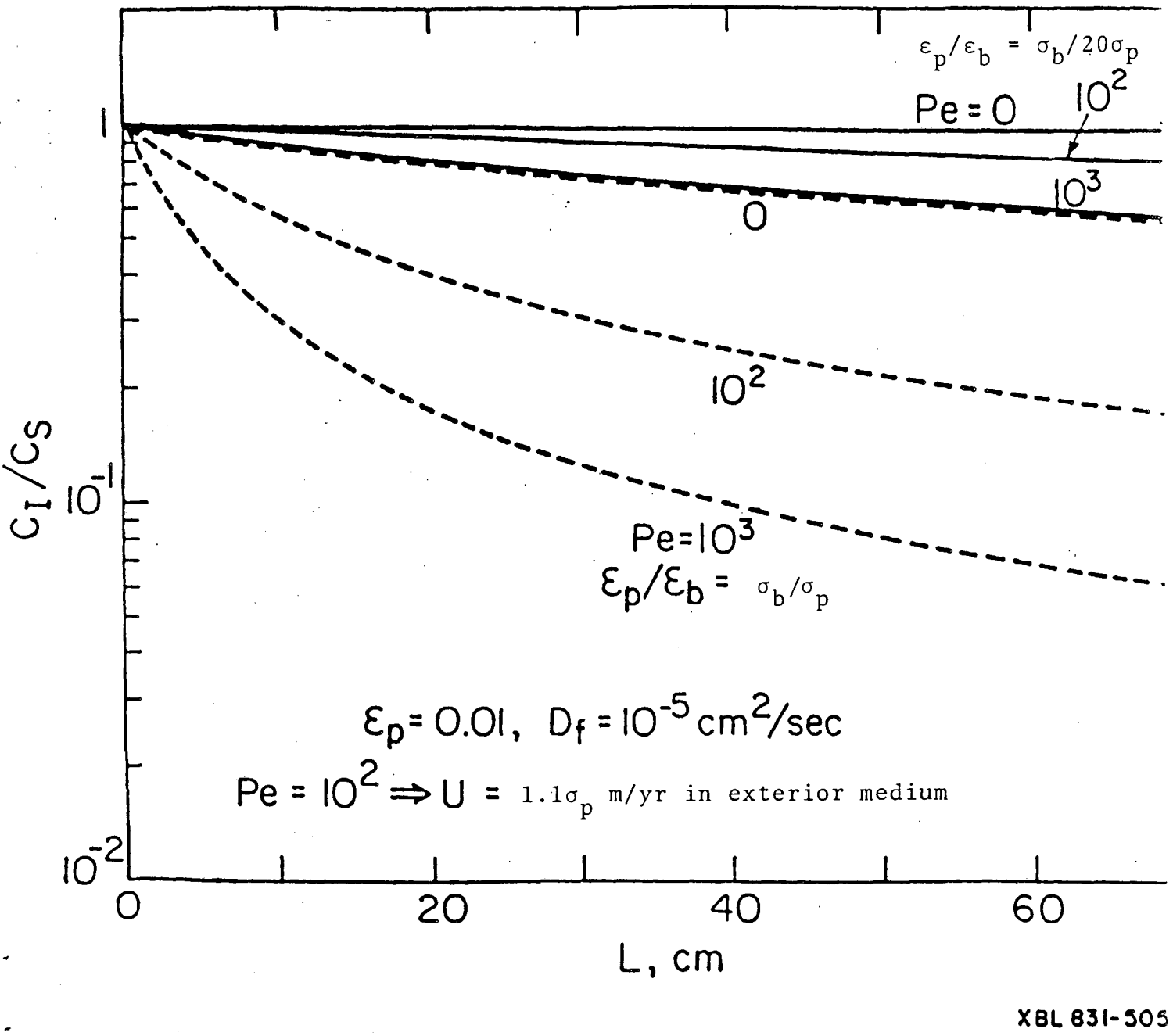

XBL 831-505

Fig. 2 The dimensionless backfill-rock interface concentration as a function of backfill thickness L, porosity ratio $\varepsilon_p/\varepsilon_b$ and Peclet number Pe.

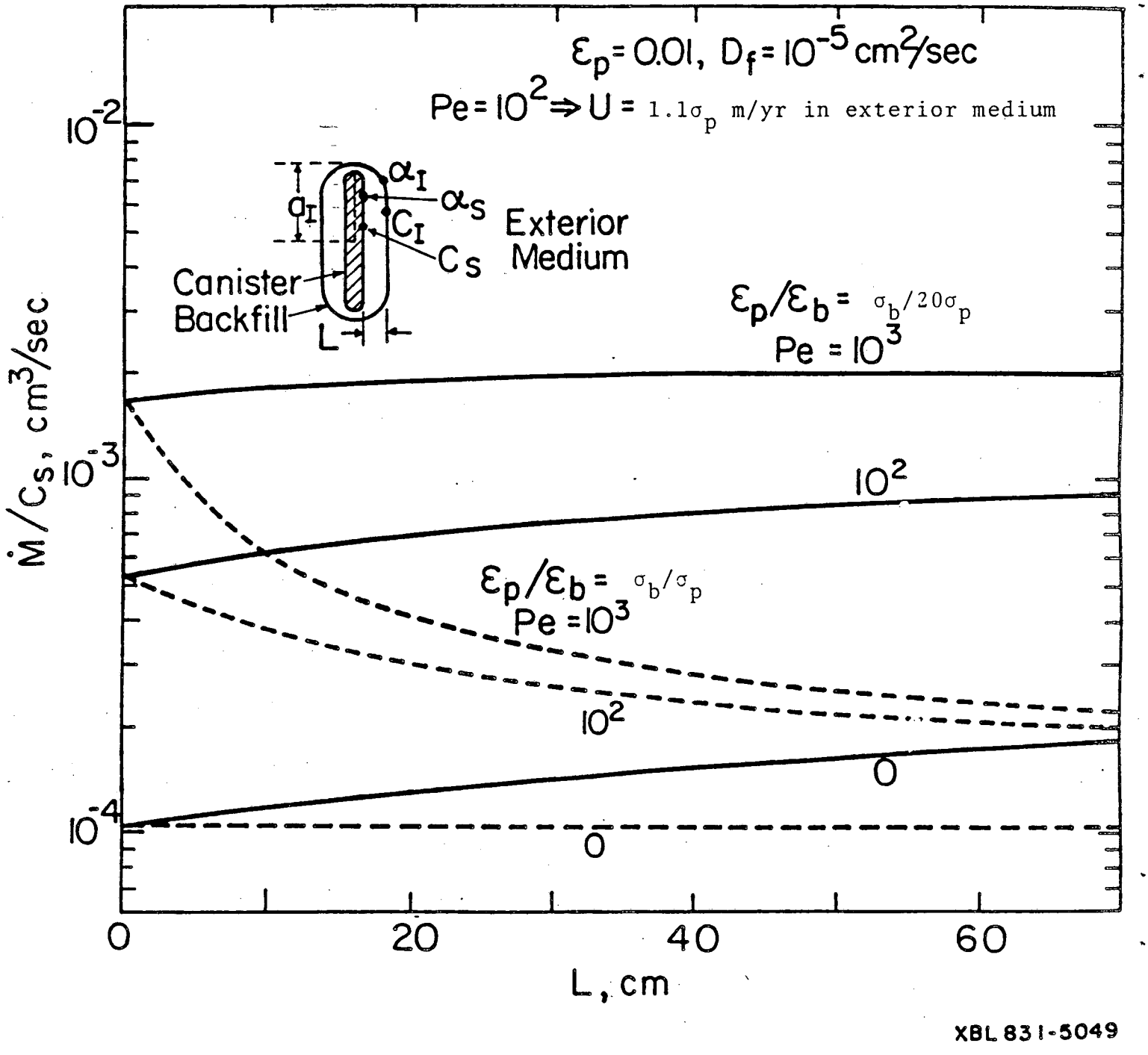

Fig. 3 The mass transfer rate as a function of backfill thickness L, porosity ratio $\varepsilon_p/\varepsilon_b$ and Peclet number Pe.

The effects of $\frac{\varepsilon_p}{\varepsilon_b}$ on Cz is noteworthy. When $\frac{\varepsilon_p}{\varepsilon_b} = \frac{\sigma_b}{20\sigma_p}$, the concentration drop is small even for Pe = 10^3. On the other hand when $\frac{\varepsilon_p}{\varepsilon_b} = \frac{\sigma_b}{\sigma_p}$, C_I decreases in a more pronounced fashion as L increaaes. For Pe = 10^3 and L = 30 cm, C_I drops to about 10% of C_s. This is due to the fact that when the backfill porosity ε_b becomes so small $=\left(0.01\ \frac{\sigma_p}{\sigma_b}\right)$, most of the resistance to the mass transport resides in the backfill especially at highwater flow speeds. From (16) one observes that as the Sh number increases with increasing flow speed, C_I decreases. This can also be seen in Fig. 2.

From (18) one can see that the backfill resistance is proportional to the ratio $\frac{\varepsilon_p}{\varepsilon_b}$ but the rock resistance $Sh(Pe)^{-1}$ is independent of it. Therefore an increase in $\frac{\varepsilon_p}{\varepsilon_b}$ will increase the backfill resistance but will not affect the rock resistance. The final result is an increase in the total resistance and this causes a decrease in the mass transport according to (19). One can see this by comparing the solid curves with the dashed curves in Fig. 3.

Consider next the effects of flow speed. As already mentioned an increase in the water flow or Pe number will increase the magnitude of the Sh number. This decreases the rock resistance but leaves backfill resistance unchanged. The net result is then a decrease in the total resistance and a higher mass transfer rate, as can be seen in Fig. 3 for different Peclet numbers.

The effect of layer thickness on the mass transport, however, is more complicated. Since a change in the layer thickness L will cause both backfill resistance and rock resistance to be changed due to the changes in α_I and a_I, the net effect also depends on these parameters. From Fig. 3 one sees that for $\frac{\varepsilon_p}{\varepsilon_b} = \frac{\sigma_b}{20\sigma_p}$ (the solid lines), $\dot{M}$ increases with increasing L. But for $\varepsilon_p = \varepsilon_b \frac{\sigma_b}{\sigma_p} = 0.01$ (the dashed lines), $\dot{M}$ decreases with increasing L. Since as L increases, both a_I and α_I increase, (cf. Fig. 1), causing $Q_o(\alpha_I)$ to decrease from (4) and Pe to increase from definition. Hence the final results are an increased R_b and a decreased R_p from (18). Thus the competition between

R_b and R_p will determine the total mass transfer rate $\dot{M}$ from (19). If ε_p is fixed as in our calculations, $\left(\frac{a_I}{R_b+R_p}\right)$ and hence $\dot{M}$ increase with the increasing L for $\varepsilon_b = 20\,\varepsilon_p \frac{\sigma_p}{\sigma_b}$, as seen in Fig. 3, due to the fact that part of the rock is replaced by a more porous backfill material which results in an increasing diffusive mass transport. On the other hand, $\left(\frac{a_I}{R_b+R_p}\right)$ and $\dot{M}$ decrease with the increasing L for $\varepsilon_b = \varepsilon_p \frac{\sigma_p}{\sigma_b}$. In this case the diffusive mass transport remains the same but the convective mass transport decreases for there is no water flow in the backfill.

In either case the mass transfer rate tends to a limiting value as L approaches to infinity. As the backfill thickness is increases, the convective transport effects in the rock region become less significant since the radionuclide has more backfill to diffuse through. When L becomes infinite, so that there is no more rock region, one is left with a diffusion problem in the backfill. The limiting value is then given by

$$\dot{M} = \frac{4\pi\varepsilon_b\sigma_b D_f C_s f}{Q_o(\alpha_s)} \tag{21}$$

which was already obtained in [1], eq. (7.1.35). In conclusion, for the ranges of the parameters used in the calculations, a thick backfill is prefered if a low interface concentration C_I is desired, as can be seen from Fig. 2. However, if a low mass transfer rate is to be achieved then for $\frac{\varepsilon_p}{\varepsilon_b} = \frac{\sigma_b}{20\sigma_p}$ one should use as thin a backfill layer as possible. For $\varepsilon_b = \varepsilon_p \frac{\sigma_p}{\sigma_b}$ the situation is reversed, as seen in Fig. 3.

Reference

1. Chambré, P.L., et al., "Analytical Performance Models for Geologic Repositories," LBL-14842, Vol. II, Ch. 7, October 1982.

APPENDIX 5A Derivation of Sherwood Number

From (13)

$$\dot{M}_p = 2\pi\varepsilon_p\sigma_p D_f C_I (L_o Sh) \tag{13a}$$

Since for fixed geometry and properties, $\dot{M}_p$ is also fixed, one finds from (13a) that $(L_o Sh)$ is also fixed. Hence for different choice of L_o, one will have different Sh. We choose

$$L_o = 2a_I \ . \tag{14}$$

From Eq. (17), the mass transfer rate out of the backfill is

$$\dot{M} = \frac{4\pi\varepsilon_p\sigma_p D_f C_s a_I}{\left(\frac{\varepsilon_p\sigma_p}{\varepsilon_b\sigma_b}\right)\left[Q_o(\alpha_s)-Q_o(\alpha_I)\right]\cosh(\alpha_I)+\left[Sh(Pe)\right]^{-1}} \tag{17}$$

As Pe = 0, we want (17) gives the correct answer and the solution for the transport by pure diffusion in both backfill and rock regions

$$\dot{M}(Pe=0) = \frac{4\pi\varepsilon_p\sigma_p D_f C_s f}{\left(\frac{\varepsilon_p\sigma_p}{\varepsilon_b\sigma_b}\right)\left[Q_o(\alpha_s)-Q_o(\alpha_I)\right]+Q_o(\alpha_I)} \tag{a}$$

Comparing (17) and (a) one obtains, with $\cosh(\alpha_I) = \frac{a_I}{f}$,

$$Sh(o) = \frac{1}{Q_o(\alpha_I)\cosh(\alpha_I)} \ .$$

This is the Sh number for mass transport from the backfill-rock interface for vanishing Pe. Now for small Pe number, the Sherwood number is expressed as [1]

$$Sh(Pe) = Sh(o)\left[1 + \frac{1}{8}\,Sh(o)\,\frac{2L_o U}{\sigma_p D_f}\right]. \tag{c}$$

Substituting (14) and (b) into (c) one gets

$$Sh(Pe) = \frac{1}{Q_o(\alpha_I)\cosh(\alpha_I)}\left[1 + \frac{Pe}{2Q_o(\alpha_I)\cosh(\alpha_I)}\right] \ , \ Pe \text{ small} \tag{20)(i}$$

where

$$Pe = \frac{Ua_I}{\sigma_p D_f} \ . \tag{d}$$

For large Pe, we use the results for the infinite long cylinder with radius $r_o = b_I$, the semi-minor axis of the backfill, and a finite section with length ℓ

$\dot{M} = 8\,\varepsilon_p \sigma_p D_f C_I \sqrt{\frac{Ur_o}{\pi\sigma_p D_f}}\,\ell$, $\frac{Ur_o}{\sigma_p D_f} > 4$, (7,2,28) in LBL-14842. Equating this to (13a) one obtains

$$8\varepsilon_p\sigma_p D_f C_I\sqrt{\frac{Ur_o}{\pi\sigma_p D_f}}\,\ell = 2\pi\varepsilon_p\sigma_p D_f C_I (L_o Sh)$$

$$Sh = \frac{2}{\pi a_I}\sqrt{\frac{Ur_o}{\pi\sigma_p D_f}}\,\ell = \frac{2\ell}{\pi a_I}\sqrt{\frac{1}{\pi}}\sqrt{\frac{a_I U}{\sigma_p D_f}}\sqrt{\frac{r_o}{a_I}}$$

$$= \frac{2\ell}{\pi a_I}\sqrt{\frac{Pe}{\pi}}\sqrt{\frac{r_o}{a_I}}\,, \quad \frac{Ur_o}{\sigma_p D_f} > 4 \qquad \text{(e)}$$

Now we let the surface area of the prolate spheroid be equal to the surface area used for mass transfer of the cylinder section, assuming $b_I = r_o << a_I \approx f$, so that $\sin^{-1}\frac{f}{a_I} \approx \frac{\pi}{2}$ and

$$2\pi r_o \ell = 2\pi b_I\left(b_I + \frac{a_I^2}{f}\sin^{-1}\frac{f}{a_I}\right)$$

$$\approx 2\pi b_I\left(a_I\,\frac{\pi}{2}\right)$$

$$= \pi^2 a_I r_o \,.$$

Hence

$$\ell = \frac{\pi}{2}\,a_I \qquad \text{(f)}$$

Also, $\frac{r_o}{a_I} = \frac{b_I}{a_I} = \tanh(\alpha_I)$ (g)

$$\frac{Ur_o}{\sigma_p D_f} = \frac{Ua_I}{\sigma_p D_f}\left(\frac{r_o}{a_I}\right) = Pe\,\tanh(\alpha_I) \qquad \text{(h)}$$

Substituting (f)-(h) into (e) one obtains

$$Sh(Pe) = \sqrt{\frac{Pe}{\pi}\,\tanh\alpha_I}\,, \quad Pe\,\tanh\,(\alpha_I) > 4$$

or

$$Sh(Pe) = \left(\frac{Pe}{\pi} \tanh\alpha_I\right)^{1/2} , \quad Pe > 4 \coth(\alpha_I) . \qquad (20)(ii)$$

If any other choice for L_o is made, the expressions for the Sh number (20)(i)(ii) will be different. This will alter the form of eqs. (16) and (17). However, if the new Sh number forms are substituted into the altered eqs. (16) and (17) the present result is recovered. This shows that the choice of L_o is arbitrary.

Reference

1. P.L. Chambré, to be published.

6. THE TIME DEPENDENT MASS TRANSPORT OF A RADIOACTIVE NUCLIDE FROM A WASTE FORM BY AN INTEGRAL METHOD

Paul L. Chambré

In reference [1] we investigated the diffusive mass transport from a cylindrically shaped waste form imbedded in a porous medium in absence of convection. On emplacement of the waste form the diffusing species is released from its surface at the solubility limit c_s where upon it diffuses into the exterior unbounded space.

Due to the mathematical complexities of the equations, only the early time and the asymptotically large time behaviors of the solution were investigated. We now fill this gap by constructing the complete time dependent solution to this problem by a suitable approximation method. Furthermore, the analysis is extended to include the effect of radioactive decay on the mass transport.

As in [1], the shape of the waste form is approximated by a slender prolate spheroid. With (ζ,μ,ψ) the prolate spheroid coordinates, a solution is sought for the species concentration $\hat{c}(\zeta,u,t;\lambda)$ which is independent of the longitudinal angle ψ on account of the uniformity of the surface concentration c_s. The species concentration satisfies the governing equation, see (7.1.19), reference [1]

$$\frac{\partial \bar{c}}{\partial \tau} = \frac{1}{(\zeta^2-\mu^2)} \left\{\frac{\partial}{\partial \zeta}\left[(\zeta^2-1)\frac{\partial \bar{c}}{\partial \zeta}\right]\right\} + \frac{\partial}{\partial \mu}\left\{(1-\mu^2)\frac{\partial \bar{c}}{\partial \mu}\right\} - \bar{\lambda}\bar{c} \qquad (1)$$

$$\zeta_s < \zeta < \infty, \quad -1 \leq \mu \leq 1, \quad \tau > 0$$

where

$$\bar{c}(\zeta,\mu,t;\lambda) = \frac{\hat{c}(\zeta,\mu,t;\lambda)}{c_s} \qquad (2)$$

$$\tau = \frac{D_f t}{Kf^2}, \quad \bar{\lambda} = \lambda \frac{Kf^2}{D_f}$$

Here D_f is the diffusion coefficient of the radioactive species in water, K its retardation coefficient in the porous medium and f the focal distance of the prolate spheroid (see Fig. 7.1.1, reference [1]). ζ_s defines the surface coordinate of the prolate spheroid.

The initial condition for the concentration is

$$\bar{c}(\zeta,\mu,0;\lambda) = 0, \quad \zeta_s \leqslant \zeta < \infty, \quad -1 \leqslant \mu \leqslant 1 \tag{3}$$

The boundary conditions are

$$\left.\begin{aligned} \bar{c}(\zeta_s,\mu,\tau;\lambda) &= 1, \\ \bar{c}(\infty,\mu,\tau;\lambda) &= 0, \end{aligned}\right\} \quad -1 \leqslant \mu \leqslant 1, \ \tau \geqslant 0 \tag{4}$$

(5)

together with a condition of symmetry about the midplane $\mu=0$,

$$\frac{\partial \bar{c}(\zeta,0,\tau;\lambda)}{\partial \mu} = 0 \qquad \zeta_s \leqslant \zeta < \infty, \qquad \tau \geqslant 0 \tag{6}$$

At this point it is convenient to remove the radioactive decay term from (1) and construct the function $\bar{c}(\zeta,\mu,\tau;0)$. We have shown [2] that with knowledge of $\bar{c}(\zeta,\mu,\tau;0)$ the solution with radioactive decay is given by

$$\bar{c}(\zeta,\mu,\tau;\lambda) = \bar{\lambda} \int_0^{\tau} e^{-\bar{\lambda}\tau'} \bar{c}(\zeta,\mu,\tau';0)d\tau' + e^{-\bar{\lambda}\tau} \bar{c}(\zeta,u,\tau;0) \tag{7}$$

However, for simplicity of writing, all references to λ are now suppressed until needed.

The above problem (1)-(6) is solved for the average surface mass flux of the diffusing species which is the quantity of primary interest to us. For this purpose an approximation method is employed and its effectiveness and accuracy is tested later by comparing it with an exact analytical solution.

As in [1], equation (1) is first subjected to a Legendre transform with respect to μ

$$c(\zeta,2n,\tau) = \int_0^1 \bar{c}(\zeta,\mu,\tau) \, P_{2n}(\mu)d\mu \tag{8a}$$

On account of the symmetry condition (6) only even orders of the Legendre polynomial set $\{P_{2n}(\mu)\}$ are required. It has been shown that only $P_o(\mu)=1$ is needed in order to obtain the leading term of the early and late time solutions. Hence one of the assumptions of the approximation method consists in ignoring the μ dependence of the surface mass flux and treating it as an average defined by

$$c(\zeta,\tau) = \int_0^1 \bar{c}(\zeta,\mu,\tau)P_o(\mu)d\mu = \int_0^1 \bar{c}(\zeta,\mu,\tau)\, d\mu \tag{8b}$$

assumed valid for all time. For simplicity of writing, the dependence on n has been suppressed.

If one applies the integral operator (8b) to every term of (1), with $\bar{\lambda}=0$, there results

$$\frac{\partial}{\partial\tau}\int_0^1 \left(\zeta^2-\mu^2\right)\bar{c}(\zeta,\mu,\tau)d\mu = \frac{\partial}{\partial\zeta}\left[\left(\zeta^2-1\right)\frac{\partial c(\zeta,\tau)}{\partial\zeta}\right] + (1-\mu^2)\frac{\partial\bar{c}(\zeta,\mu,\tau)}{\partial\mu}\Bigg|_{\mu=0}^{\mu=1} \tag{9a}$$

$$\zeta_s<\zeta<\infty, \quad \tau>0$$

The second term on the right hand side vanishes at the lower limit by the symmetry condition (6) and vanishes also at $\mu=1$. The integral is in view of (8b)

$$\int_0^1 \left(\zeta^2-\mu^2\right)\bar{c}(\zeta,\mu,\tau)d\mu = \left(\zeta^2-\frac{1}{3}\right)c(\zeta,\tau) - \frac{2}{3}\int_0^1 \bar{c}(\zeta,\mu,\tau)P_2(\mu)d\mu \tag{9b}$$

The integral on the right hand side gives no contribution to the terms for the early and late time solutions and the approximation method assumes this term to be negligible for all times. Hence there results for $c(\zeta,\tau)$

$$\left(\zeta^2-\frac{1}{3}\right)\frac{\partial c(\zeta,\tau)}{\partial\tau} = \frac{\partial}{\partial\zeta}\left[\left(\zeta^2-1\right)\frac{\partial c(\zeta,\tau)}{\partial\zeta}\right], \quad \zeta_s<\zeta<\infty, \quad \tau>0 \tag{10}$$

with the transformed side conditions

$$c(\zeta,0) = 0, \quad \zeta_s\leqslant\zeta<\infty \tag{11}$$

$$c(\zeta_s,\tau) = 1, \quad \tau\geqslant 0 \tag{12}$$

$$c(\infty,\tau) = 0, \quad \tau\geqslant 0 \tag{13}$$

This parabolic equation problem is solved by a moment method which in continuum mechanics is commonly called an integral method. Its physical motivation is the following.

The diffusing species spreads from time $\tau = 0$ onward into the surrounding porous medium which is at zero concentration causing a concentration boundary layer to form about the prolate spheroid. The thickness of this layer, denoted by $\delta(\tau)$, will increase in a monotone fashion with time. The species concentration varies from $c(\zeta_s,\tau) = 1$ at the inner edge of the boundary layer next to the waste form to an approximately zero value at its outer edge. This outer boundary progresses into the porous medium where c=0. It is customary to assume that the gradient of the concentration also vanishes at this outer boundary. These conditions replace those of equations (11) and (13) and their forms are

$$\delta(0) = 0 \tag{14a}$$

$$c(\zeta_s+\delta(\tau),\ \tau) = \frac{\partial c\left(\zeta_s+\delta(\tau),\tau\right)}{\partial \zeta} = 0 \tag{14b}$$

One now integrates (10) with respect to ζ over the boundary layer thickness, which yields with (14b)

$$\int_{\zeta_s}^{\zeta_s+\delta(\tau)} \left(\zeta^2-1/3\right) \frac{\partial c}{\partial \tau}\, d\zeta = -\left(\zeta_s^2-1\right) \frac{\partial c\left(\zeta_s,\tau\right)}{\partial \zeta}\ ,\ \tau>0 \tag{15}$$

One can interchange the order of differentiation and integration by Leibnitz's rule and using once more (14b) there results the integral form for the concentration boundary layer

$$\frac{d}{d\tau} \int_{\zeta_s}^{\zeta_s+\delta(\tau)} \left(\zeta^2-1/3\right) c(\zeta,\tau) d\tau = -\left(\zeta_s^2-1\right) \frac{\partial c\left(\zeta_s,\tau\right)}{\partial \zeta}\ ,\ \tau>0 \tag{16}$$

The physical content of this equation is the following. The surface flux issuing from the waste surface, which is proportioned to the right hand side of (16), gives rise to the rate of accumulation of the species in the boundary layer of

thickness $\delta(\tau)$.

The principal part of the approximation method consists in a choice of a suitable concentration profile $c(\zeta,\tau)$ for the boundary layer. I assume the form

$$c(\zeta,\tau) = \left[1 - \frac{(\zeta-\zeta_s)}{\delta(\tau)}\right]^2 \frac{Q_0(\zeta)}{Q_0(\zeta_s)} \quad , \quad \zeta_s \leqslant \zeta \leqslant \zeta_s + \delta(\tau) \quad , \quad \tau > 0 \tag{17}$$

where

$$Q_0(\zeta) = \frac{1}{2} \log\left(\frac{\zeta+1}{\zeta-1}\right)$$

is the Legendre function of the second kind of zeroth order. One observes that this form automatically satisfies the required boundary conditions (12) and (14b). On substitution of (17) into the integral form for the concentration boundary layer there results

$$\frac{d}{d\tau} \int_{\zeta_s}^{\zeta_s+\delta(\tau)} \left(\zeta^2 - 1/3\right) \left[1 - \frac{\zeta-\zeta_s}{\delta(\tau)}\right]^2 \frac{Q_0(\zeta)}{Q_0(\zeta_s)} \, d\zeta = \left(\zeta_s^2 - 1\right) \left[\frac{2}{\delta(\tau)} - \frac{Q_0'(\zeta_s)}{Q_0(\zeta_s)}\right], \tau > 0 \tag{18}$$

This can be transformed into an ordinary differential equation for the unknown boundary layer thickness $\delta(\tau)$. With

$$I(\delta(\tau)) \equiv \int_{\zeta_s}^{\zeta_s+\delta(\tau)} \left(\zeta^2 - 1/3\right) \left[1 - \frac{(\zeta-\zeta_s)}{\delta(\tau)}\right]^2 \frac{Q_0(\zeta)}{Q_0(\zeta_s)} \, d\zeta \tag{19}$$

(18) becomes

$$\frac{dI(\delta(\tau))}{d\tau} = \left(\zeta_s^2 - 1\right) \left[\frac{2}{\delta(\tau)} - \frac{Q_0'(\zeta_s)}{Q_0(\zeta_s)}\right] \tag{20}$$

One can now separate variables and express, since the boundary layer thickness is initially equal to zero by (14a), τ explicitly as a function of δ in the following form

$$\tau(\delta) = \int_0^{\delta} \frac{\eta I'(\eta)}{\left(\zeta_s^2-1\right)\left[2-\frac{Q_0'(\zeta_s)}{Q_0(\zeta_s)}\eta\right]}\, d\eta \tag{21}$$

To simplify this one has from (17)

$$Q_0'(\zeta_s) = -\frac{1}{\zeta_s^2-1} \tag{22}$$

and from (19)

$$I'(\eta) = 2\int_{\zeta_s}^{\zeta_s+\eta} \left(\zeta^2-1/3\right)\left(1-\frac{\zeta-\zeta_s}{\eta}\right)\frac{(\zeta-\zeta_s)}{\eta^2}\,\frac{Q_0(\zeta)}{Q_0(\zeta_s)}\, ds \tag{23}$$

With these, there results the solution for the growth of the boundary layer in the form

$$\tau(\delta) = \int_0^{\delta} \frac{2}{\eta^2(A+B\eta)}\left\{\int_{\zeta_s}^{\zeta_s+\eta} \left(\zeta^2-1/3\right)(\zeta_s+\eta-\zeta)(\zeta-\zeta_s)\,\frac{Q_0(\zeta)}{Q_0(\zeta_s)}\, d\zeta\right\} d\eta \tag{24a}$$

where

$$A = 2\left(\zeta_s^2-1\right)\ ,\ B = \left[Q_0(\zeta_s)\right]^{-1}$$

The inner integral can be readily evaluated which leads to

$$\tau(\delta) = \frac{1}{Q_0(\zeta_s)}\int_0^{\delta} \frac{\left[I_2(\eta)-I_1(\eta)\right]d\eta}{\eta^2(A+B\eta)} \tag{24b}$$

The functions $I_1(\eta)$, $I_2(\eta)$ are listed in Appendix 6A. The remaining integration in (24b) was performed numerically and yields the inverse function $\delta=\delta(\tau)$ describing the boundary layer thickness as a function of time.

With knowledge of $\delta=\delta(\tau)$ one can at once calculate the transform of the concentration profile $c(\zeta,\tau)$. By applying the Legendre inversion formula with n = 0 to this, one recovers $\bar{c}(\zeta,\mu,\tau) = c(\zeta,\tau)$ to the present approximation.

The quantity of primary interest to us is the surface mass flux of the species from the prolate spheroid surface which is given by [1], eq. (7.1.60) and (17)

$$\vec{j}(\tau;0) = -\frac{D_f \varepsilon c_s}{h_\zeta(\zeta)} \left.\frac{\partial c}{\partial \zeta}\right|_{\zeta=\zeta_s}$$

$$= \frac{D_f \varepsilon c_s}{h_\zeta(\zeta_s)} \left[\frac{2}{\delta(\tau)} - \frac{Q_o'(\zeta_s)}{Q_o(\zeta_s)}\right] \quad , \tau>0 \tag{25}$$

where

$$h_\zeta(\zeta_s) = f\left(\frac{\zeta_s^2-\mu^2}{\zeta_s^2-1}\right)^{1/2} \tag{26}$$

From the above discussion $\delta(\tau)$ can be considered to be a known function in (25). This result is valid in absence of radioactive decay. The application of (7) to the surface flux yields then in presence of decay

$$\vec{j}(\tau;\bar{\lambda}) = \bar{\lambda}\int_0^\tau e^{-\bar{\lambda}\tau'} \vec{j}(\tau';0)d\tau' + e^{-\bar{\lambda}\tau}\, \vec{j}(\tau;0) \tag{27}$$

which will be used in next section for calculational purposes.

The surface mass transport as derived in (25) consists of two parts. The first term in the bracket describes the transient behavior of the flux. Since $\delta(0) = 0$ by (14a), the flux is initially infinite in magnitude. From the monotone trend of $\tau(\delta)$ given by (24) one obtains a boundary layer thickness $\delta(\tau)$ which tends to infinity as $\tau\to\infty$. Hence the first term in the bracket of (25) tends to zero leaving the second term which exactly represents the steady state mass transport from the prolate spheroid, see [1] eq.(7.1.28) and sequel.

Of considerable interest is the time needed for the surface flux to attain the steady state to some degree of approximation. This time t^* is a function of the prolate spheroid geometry. Consider a set of prolate spheroids with identical surface areas but differing ratios of minor to major axis (b/a). The limiting cases for this class are the sphere with b/a = 1 and the needle with b/a = 0. We will show in next section that t* decreases with decreasing (b/a) which could be of importance to waste form designs which operate within the framework of the present theory.

To test the effectiveness and accuracy of the integral method we apply it

to the determination of the mass transport from a sphere. The sphere is a member of the family of prolate spheroids. In this case the major and minor axis of the spheroid are identical and the focal distance f = 0. We consider a limit procedure in which ζ becomes large but in such a way that the (new) radial coordinate r is given by

$$r = f\zeta \tag{28}$$

The radius R of the sphere is then defined by

$$R = f\zeta_s \tag{29}$$

In the same way one scales the position in the boundary layer by the new coordinate

$$\alpha = f\eta \tag{30}$$

and the boundary layer thickness by

$$\Delta = f\delta \ . \tag{31}$$

We proceed in making these scaling transformations in (24a). With (2)

$$\frac{D_f t}{Kf^2} = \frac{1}{f^2} \int_0^{\Delta} \frac{1}{\alpha^2 \left[R^2 - f^2 + \frac{f\alpha}{2} Q_o^{-1}\left(\frac{R}{f}\right)\right]} \left\{ \int_R^{R+\alpha} \left[r^2 - \frac{f^2}{3}\right]\left[R+\alpha-r\right]\left[r-R\right] \cdot \cdot \frac{Q_o(r/f)}{Q_o(R/f)} dr \right\} d\alpha \tag{32}$$

From (17), as f→0

$$Q_o\left(\frac{r}{f}\right) = \frac{1}{2} \log\left(\frac{1+f/r}{1-f/r}\right) \to \frac{f}{r} \tag{33}$$

Hence

$$\frac{f\alpha}{2} Q_o^{-1}\left(\frac{R}{f}\right) \to \frac{1}{2} \alpha R; \ \frac{Q_o(r/f)}{Q_o(R/f)} \to \frac{R}{r} \tag{34}$$

so that, on cancelling $\frac{1}{f^2}$ from both sides of (32), one obtains on letting f→0

$$\frac{D_f t}{KR^2} = \frac{2}{R^2} \int_0^{\Delta} \frac{1}{\alpha^2 [2R+\alpha]} \left\{ \int_R^{R+\alpha} r(R+\alpha-r)(r-R) dr \right\} d\alpha \tag{35}$$

This is readily integrated and yields

$$\frac{D_f t}{KR^2} = \frac{1}{12}\left(\frac{\Delta}{R}\right)^2 \tag{36}$$

Next one applies the same limit considerations to (25).

With

$$h_\zeta(\zeta_s) \to f; \left|\frac{Q_0'(\zeta_s)}{Q_0(\zeta_s)}\right| \to \frac{f}{R} \tag{37}$$

one obtains for the surface mass flux from the sphere

$$\begin{aligned} \vec{j}(\tau;0) &= \frac{D_f \varepsilon c_s}{R}\left[\frac{2}{(\Delta/R)} + 1\right] \\ &= \frac{D_f \varepsilon c_s}{R}\left[\frac{1}{\sqrt{3}\left(\frac{D_f t}{KR^2}\right)^{1/2}} + 1\right], \quad \tau>0 \end{aligned} \tag{38}$$

using (36).

The exact analytical solution yields precisely the same form but with $\sqrt{3}$ replaced by $\sqrt{\pi}$. The numerical error of the approximation is less than 3% throughout the entire time span. Although this "spot check" for a single geometry does not uniformly validate the integral method for prolate spheroids of arbitrary slenderness ratios, it is hoped that the principle of this method will be substantiated by future refinements and extensions.

References:

1. Chambré, P.L., et al, "Analytical Performance Models for Geological Repositories," LBL-14842, V.II, October, 1982.

2. Chambré, P.L., "Nuclear Waste Management Seminar, NE 298)", Spring Quarter, 1982.

APPENDIX 6A Evaluation of the Integral

$$\tau = \int_0^{\delta} \frac{2}{\delta'^2(A+B\delta')} \int_{\zeta_s}^{\zeta_s+\delta'} (\zeta^2-\bar{\mu}^2)(\zeta_s+\delta'-\zeta)(\zeta-\zeta_s)\frac{Q_o(\zeta)}{Q_o(\zeta_s)}\, d\zeta d\delta'$$

$$= \frac{1}{Q_o(\zeta_s)} \int_0^{\delta} \frac{-1}{\delta'^2(A+B\delta')} \int_{\zeta_s}^{\zeta_s+\delta'} (\zeta^2-\bar{\mu}^2)(\zeta-\zeta_s-\delta')(\zeta-\zeta_s)\ln\left(\frac{\zeta+1}{\zeta-1}\right) d\zeta d\delta'$$

$$= \frac{-1}{Q_o(\zeta_s)} \int_0^{\delta} \frac{1}{\delta'^2(A+B\delta')} \int_{\zeta_s}^{\zeta_s+\delta'} (\delta^2-\bar{\mu}^2)(\zeta-\zeta_s-\delta')(\zeta-\zeta_s)[\ln(\zeta+1)-\ln(\zeta-1)]d\zeta d\delta'$$

Let $I_1 = \int_{\zeta_s}^{\zeta_s+\delta'} (\zeta^2-\bar{\mu}^2)(\zeta-\zeta_s-\delta')(\zeta-\zeta_s)\ln(\zeta+1)d\zeta$

$$I_2 = \int_{\zeta_s}^{\zeta_s+\delta'} (\zeta^2-\bar{\mu}^2)(\zeta-\zeta_s-\delta')(\zeta-\zeta_s)\ln(\zeta-1)d\zeta$$

then

$$\tau = \frac{-1}{Q_o(\zeta_s)} \int_0^{\delta} \frac{1}{\zeta'^2(A+B\delta')} (I_1-I_2)d\delta' .$$

Now let $U = \zeta+1$, $C_1 = \zeta_s+1$, $D_1 = \zeta_s + \delta' +1$,

$$I_1 = \int_{C_1}^{D_1} [(U-1)^2-\bar{\mu}^2](U-D_1)(U-C_1)\ln U\, dU$$

$$= \int_{C_1}^{D_1} (U^2-2U+1-\bar{\mu}^2)[U^2-(C_1+D_1)U + C_1D_1]\ln U\, dU$$

$$= \int_{C_1}^{D_1} \left\{U^4-(C_1+D_1+2)U^3 + [(1-\bar{\mu}^2) + 2(C_1+D_1) + C_1D_1]U^2 - [(1-\bar{\mu}^2)(C_1+D_1) + \right.$$

$$\left. + 2C_1D_1]U+(1-\bar{\mu}^2)C_1D_1\right\} \ln U dU$$

$$= \left\{\frac{1}{5}\left(U^5\ln U - \frac{U^5}{5}\right) - \frac{1}{4}(C_1+D_1+2)\left(U^4\ln U - \frac{U^4}{4}\right) + \frac{1}{3}[(1-\bar{\mu}^2) + 2(C_1+D_1)+C_1D_1]\cdot\right.$$

$$\left.\left(U^3\ln U - \frac{U^3}{3}\right) - \frac{1}{2}[(1-\bar{\mu}^2)(C_1+D_1) + 2C_1D_1]\left(U^2\ln U - \frac{U^2}{2}\right) + (1-\bar{\mu}^2)C_1D_1(U\ln U-U)\right\}\Bigg|_{C_1}^{D_1}$$

Let $v = \zeta-1$, $C_2 = \zeta_s-1$, $D_2 = \zeta_s + \delta'-1$,

$$I_2 = \int_{C_2}^{D_2} [(v+1)^2 - \bar{\mu}^2](v-D_2)(U-C_2)\ln v\, dv$$

$$= \int_{C_2}^{D_2} \left\{v^4-(C_2+D_2-2)v^3+[(1-\bar{\mu}^2)-2(C_2+D_2)+C_2D_2]v^2-[(1-\bar{\mu}^2)(C_2+D_2)-2C_2D_2]v\right.$$

$$\left. + (1-\bar{\mu}^2)C_2D_2\right\} \ln v\, dv$$

$$= \left\{ \frac{1}{5}\left(v^5 \ell nv - \frac{v^2}{5}\right) - \frac{1}{4}(C_2+D_2-2)\left(v^4 \ell nv - \frac{v^4}{4}\right) + \frac{1}{3}\left[(1-\bar{\mu}^2)-2(C_2+D_2)+C_2D_2\right]\left(v^3 \ell nv - \frac{v^3}{3}\right)\right.$$

$$\left. - \frac{1}{2}\left[(1-\bar{\mu}^2)(C_2+D_2) - 2C_2D_2\right]\left(v^2 \ell nv - \frac{v^2}{2}\right) + (1-\bar{\mu}^2)C_2D_2(v \ell nv - v)\right\} \Bigg|_{C_2}^{D_2}$$

Then

$$\tau(\delta) = -\frac{1}{Q_o(\zeta_s)} \int_o^{\delta} \frac{(I_1-I_2)}{\zeta'^2(A+B\delta')}\, d\delta' .$$

I am indebted to H. Lung for this calculation.

7. THE NUMERICAL EVALUATION OF THE TIME DEPENDENT MASS TRANSPORT OF A RADIONUCLIDE FROM FINITE SIZED WASTE FORMS OF DIFFERENT GEOMETRIES - INTEGRAL METHOD

H. Lung

P. L. Chambré

In last section equation (25) an expression for the surface mass flux $\vec{j}(\tau;0)$ from a prolate spheroid was given. We turn now to the numerical evaluation of this result which is reformulated in terms of the total mass loss $\dot{M}(\tau;0)$ from the waste form

$$\dot{M}(\tau;0) = \int_{-1}^{+1}\int_{0}^{2\pi} \vec{j}(\tau;0)\, h_\mu h_\psi d\psi d\mu \tag{1a}$$

Here the metric coefficients are evaluated at $\zeta=\zeta_s$ and are given by

$$h_\mu = f\left(\frac{\zeta_s^2-\mu^2}{1-\mu^2}\right)^{1/2} \quad ; \quad h_\psi = f\left\{\left(\zeta_s^2-1\right)\left(1-\mu^2\right)\right\}^{1/2} \tag{1b}$$

The result of the integration is obtained with (25) in the last section

$$\dot{M}(\tau;0) = 4\pi\varepsilon D_f C_s \frac{b^2}{f}\left[\frac{2}{\delta(\tau)} - \frac{Q_0'(\zeta_s)}{Q_0(\zeta_s)}\right], \quad \tau>0 \tag{2}$$

where b is the minor semi-axis of the prolate spheroid

$$b = f\left(\zeta_s^2-1\right)^{1/2} . \tag{3}$$

The numerical evaluation of $\dot{M}(\tau;0)$ is based on the following porous medium parameter values

$$D_f = 10^{-5}\ \text{cm}^2/\text{sec}; \quad \varepsilon = 0.01; \quad K = 10^3 \tag{4}$$

The cyclindrical spent fuel canister, which is to be modelled, has a radius r and a height h

$$r = 17.8\ \text{cm}; \quad h = 4.70\ \text{cm} \tag{5}$$

The prolate spheroid dimensions are chosen so that its surface area and volume

are equal to those of the spent fuel canister. This determines the prolate spheroid semi-major axis a and semi-minor axis b, the surface coordinate ζ_s and the focal distance f

$$a = 272 \text{ cm}; \; b = 20.3 \text{ cm}; \; \zeta_s = 1.003; \; f = 271 \text{ cm} . \tag{6}$$

In addition we shall refer to a spherical body of radius R which has the same surface area as the cylindrical spent fuel canister

$$R = 65.9 \text{ cm} \tag{7}$$

With the values given by (4) and (6) $\frac{\dot{M}(t;0)}{c_s}$ has been computed and is shown as curve 1 in Fig. 1 as a function of the physical time in the range 1 yr<t<10^7 yr. Starting at t = 0 from an infinite value (not shown), $\frac{\dot{M}(t;0)}{c_s}$ decreases in time to a steady state value which is reached at about $2\text{x}10^5$yr. Shown also in Fig. 1 are the early time and the large time solutions which were derived in [1] Section 7.1. It is seen that the present solution, which covers the entire time range, tends to these asymptotic forms. Finally, curve 4 gives the mass transport from the equal surface area sphere defined by (7) and computed from the exact solution. The trend of that curve is close to that of the prolate spheroid up to time t = 10^5 yrs and for larger times it falls about 20% below the steady state solution of the prolate spheroid. The equal surface area sphere solution will be used as an approximation in part of the following discussion.

The time t* necessary to reach the steady state plateau in Fig. 1 is a quantity of interest since it gives an indication when the minimum mass transport rate is achieved. It will be shown that t*, aside from the parameters K and D_f, is a function of the prolate spheroid geometry. We define t* as the time at which the transient part of the solution (2) is a fraction χ of its steady state part, i.e.

$$\frac{2}{\delta(\tau^*)} = \chi \left| \frac{Q_0'(\zeta_s)}{Q_0(\zeta_s)} \right| \tag{8}$$

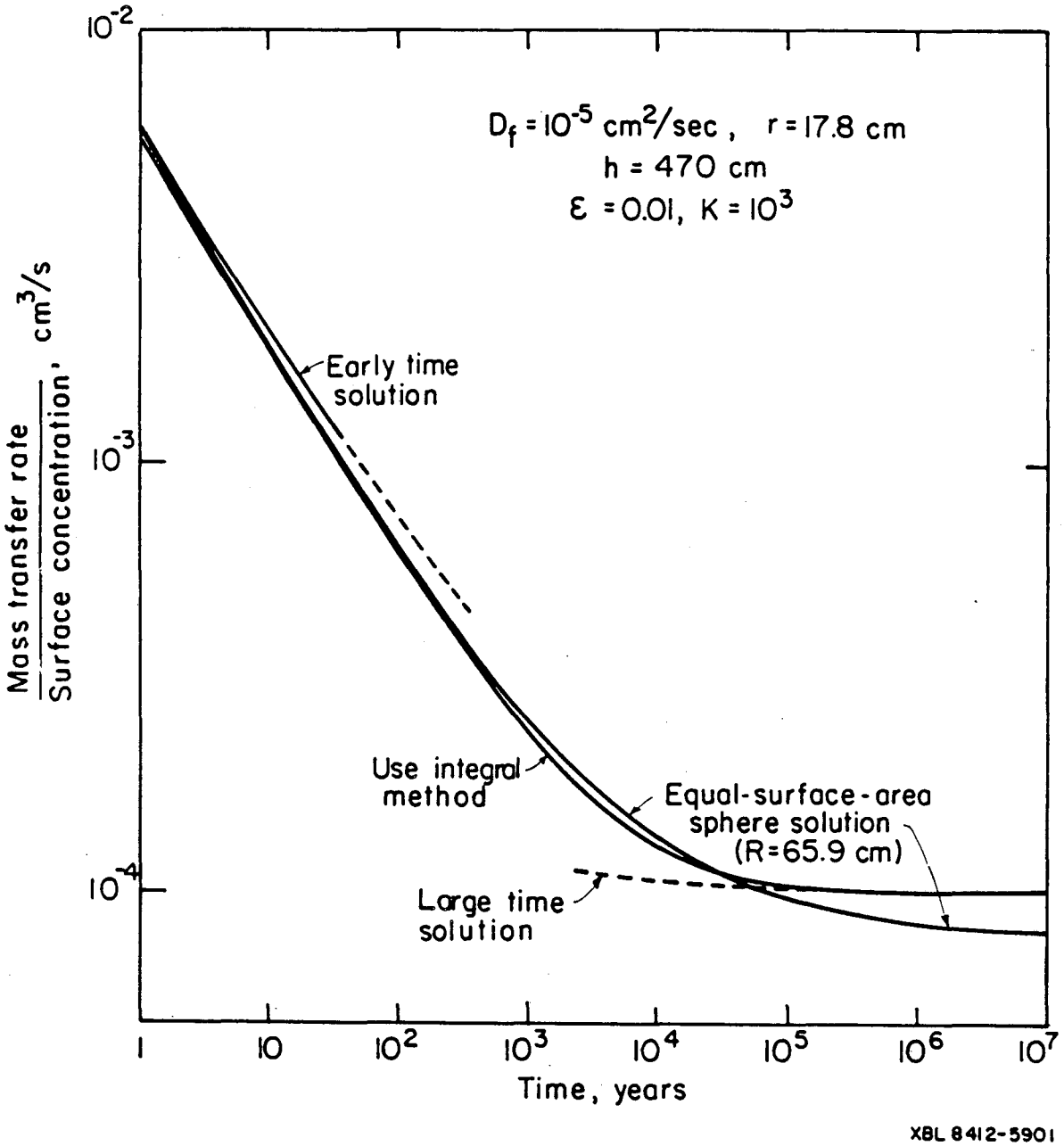

Fig. 1 Normalized mass transfer rate as a function of time; diffusion from a prolate spheroidal waste form and from a spherical waste form.

This can be solved for τ^* which yields with (2) of last section,

$$t^* = \frac{Kf^2}{D_f} \cdot \tau^* \ , \tag{9}$$

τ^* is the inverse function of δ as given in equation (8). We wish to compare the mass transport from a set of prolate spheroids of identical surface area S, but of different eccentricities $e \equiv b/a$. For this it is convenient to express f in terms of S and e and ζ_s in terms of e. The relationships are the following (S = surface area of the prolate spheroid)

$$\zeta_s = \frac{a}{f}$$

$$= \frac{a}{\sqrt{a^2-b^2}}$$

$$= \frac{1}{\sqrt{1-e^2}} \tag{10}$$

$$S = 2\pi b^2\left(1+ \frac{a^2}{bf} \sin^{-1} \frac{f}{a}\right)$$

$$= 2\pi f^2 \frac{e^2}{1-e^2} \left(1+ \frac{1}{e\sqrt{1-e^2}} \sin^{-1}\sqrt{1-e^2}\right) \tag{11}$$

If one solves (11) for f^2 in terms of S and e and substitutes this together with ζ_s from (10) into (9) one obtains

$$t^* = \frac{SK}{D_f} F(\chi,e) \tag{12}$$

where $F(\chi,e)$ is a known numerical function of the steady state criterion χ and prolate spheroid eccentricity e.

The time to reach steady state is thus directly proportional to the surface area of the waste form as well as to the retardation coefficient and inversely proportional to the diffusion coefficient. The dependence of t^* on waste form geometry is less obvious. It is shown in Fig. 2 as a function of e with χ as a parameter. The other parameter values are those of (4) and (5) with a value of

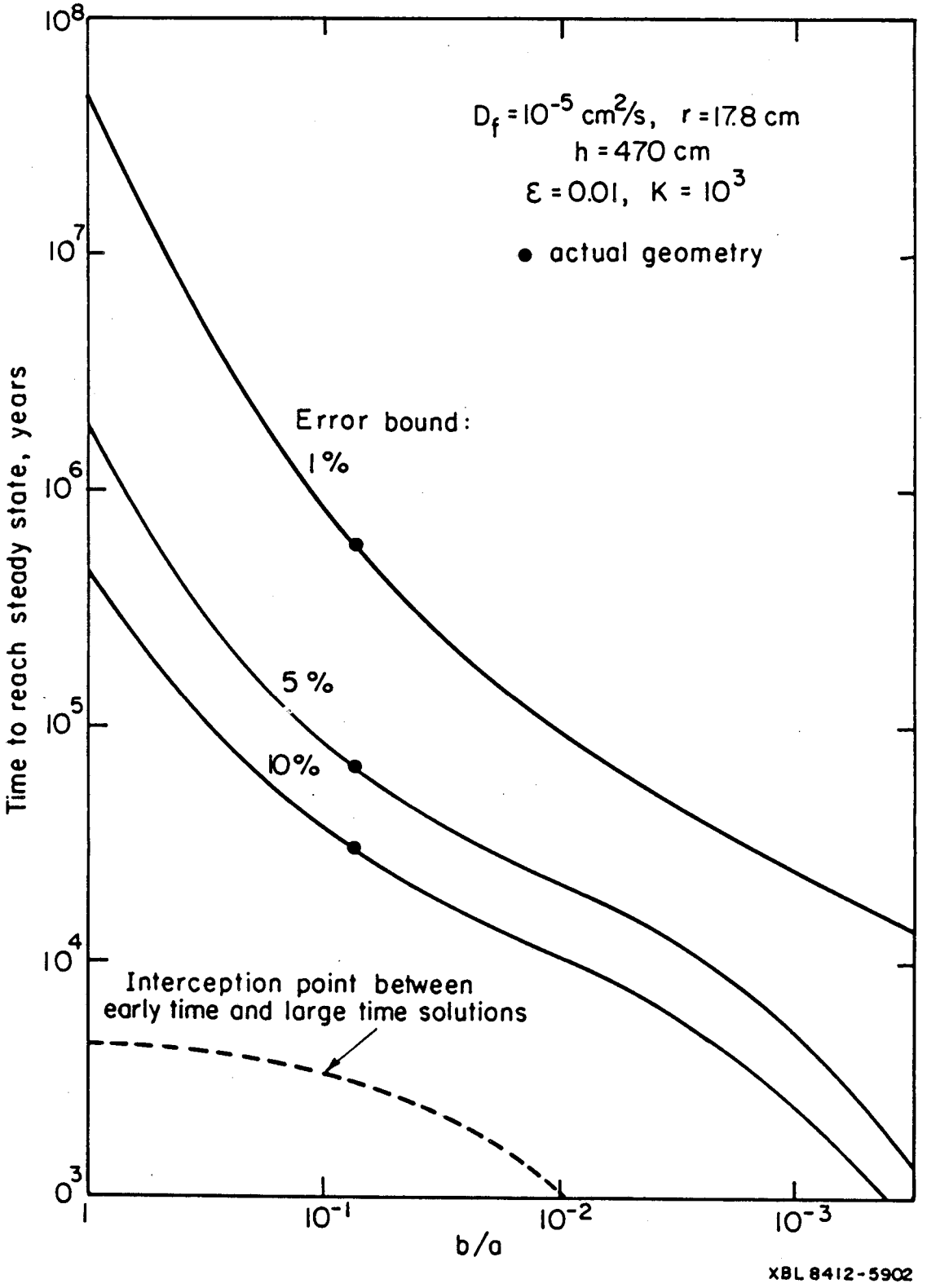

Fig. 2 Time to reach steady state as a function of body slenderness and error bound.

$S = 5.46\ m^2$. One observes the principal feature that the time necessary to reach steady state decreases with decreasing values of $e = b/a$. Hence the sphere with $\frac{b}{a} = 1$ requires the longest time and the needle, for which $\frac{b}{a} \to 0$, the shortest time to reach steady state. The χ criterion which characterizes the closeness to the steady state affects the value of t^* in an understandable way. Holding $e = b/a$ constant, t^* increases as χ decreases. The marked point on the χ parameter curves represents the operating point for the prolate spheroid form specified by (6).

As an illustration of the effect of the eccentricity e of the waste form on the time t^*, consider $\chi = 0.1$, i.e. curve 3. If a spherical waste form is used t^* will be approximately 4.5×10^5 yr which is about one order of magnitude greater than t^* at the operating point specified by (6). Hence a slender waste form geometry shortens the time to reach steady state at which the mass transport attains its lowest value.

We turn next to the discussion of the effects of radioactive decay on the mass transport. As stated in last section, equation (7), the transport in presence of decay $\dot{M}(\tau;\lambda)$ can be compactly expressed in terms of $\dot{M}(\tau;0)$ by

$$\dot{M}(\tau;\lambda) = \bar{\lambda}\int_0^{\tau} e^{-\bar{\lambda}s}\, \dot{M}(s;0)\, ds + e^{-\bar{\lambda}\tau}\, \dot{M}(\tau;0) \qquad (13)$$

With $\dot{M}(\tau;0)$ given by (2) one can readily carry out the integration numerically, since $\delta(\tau)$ is a known numerical function. However, an analytical formula for $\dot{M}(\tau;\lambda)$ offers the advantage of exhibiting its parameter dependence on λ as well as on some of the geometric characteristics of the waste form. One can accomplish this by approximating curve 1 of Figure 1 by two curve segments.

The first segment covers the transient time interval $0<\tau<T^*$. As shown in Fig. 1, the equal surface area sphere of radius R, given by (7), closely approximates the mass transport from a prolate spheroid defined by (5). Thus in this time span we apply the surface integral of (38) of last section with its correct numerical factor

$$\dot{M}(t;0) = 4\pi\varepsilon D_f C_s R \left[1+\sqrt{\frac{KR^2}{\pi D_f t}}\right] \quad 0<t\leqslant T^* \tag{14}$$

When used in (13) this expression can be readily integrated analytically.

The intersection of (14) with the exact steady state mass transport from the prolate spheroid determines the beginning of the second segment which is given by (7.1.13), (7.1.29) and (7.1.35) of [1]

$$\dot{M}(t;0) = 4\pi\varepsilon D_f C_s f Q_0^{-1}(\zeta_s) \quad , \quad t>T^* \tag{15}$$

The transition time T^* is obtained by equating (14) and (15)

$$T^* = \frac{\left(\frac{KR^2}{\pi D_f}\right)}{\left[\frac{f}{R} Q_0^{-1}(\zeta_s)-1\right]^2} \tag{16}$$

With the last three equations one can evaluate (13). With the total flux expressed in terms of the physical time variable t,

$$\dot{M}(t;\lambda) = 4\pi\varepsilon D_f C_s R \begin{cases} \left[1+\left(\operatorname{erf}\sqrt{\lambda t} + \frac{e^{-\lambda t}}{\sqrt{\pi\lambda t}}\right) Da^{1/2}\right] & 0<t\leqslant T^* \\ \left[1+\left(\operatorname{erf}\sqrt{\lambda T^*} + \frac{e^{-\lambda T^*}}{\sqrt{\pi\lambda T^*}}\right) Da^{1/2}\right] & , \ t>T^* \end{cases} \tag{17}$$

where

$$Da = \frac{K\lambda R^2}{D_f} \quad .$$

For K=1, Da represents the dimensionless Damkohler modulus used by chemical engineers in analysis of problems involving a chemical reaction of the first order and subject to diffusive transport of the reactants. Retardation of the diffusing specie modifies ϕ in our application.

Equation (17) is the approximation for the total mass transfer rate from a prolate spheroid for a specie undergoing radioactive decay. It is evaluated with the data given in (4) and (7) for the radio nuclides Np^{237}, C^{14}, and Cm^{244}

with half lives

$$T_{1/2}\left(Np^{237}\right) = 2.14 \times 10^{6} \text{ yr};\ T_{1/2}\left(C^{14}\right) = 6.14 \times 10^{3} \text{ yr};\ T_{1/2}\left(Cm^{244}\right) = 17.6 \text{ yr} \tag{18a}$$

The corresponding λ values are

$$\lambda\left(Np^{237}\right) = 3.24\times10^{-7} \text{ yr}^{-1};\ \lambda\left(C^{14}\right) = 1.13\times10^{-4} \text{ yr}^{-1};\ \lambda\left(Cm^{244}\right) = 3.94\times10^{-2} \text{ yr}^{-1} \tag{18b}$$

The results of the calculations are shown in Fig. 3. Curve 1 represents the total mass transfer rate without decay and curves 2 to 4 show those of the three radionuclides. The effects of decreasing the half life are quite pronounced. The transition time T* decreases from 10^5 years to about 80 years. The steady state (plateau) value of the mass transfer rate increases by more than one order of magnitude. The physical explanation for this increase resides in the fact that the radioactive decay removes the specie close to the waste form surface thereby causing the concentration profile to become steeper. In turn, this increased gradient increases the mass flux.

For a radionuclide of very long half life such as Np^{237}, which exceeds the time T* to reach steady state, i.e. 2.14×10^6 yr >> 6.89×10^4 yr, the effect of the decay on the mass transfer is negligible as curves 1 and 2 in Fig. 3 show. This can also be seen from (17). If $T_{1/2} >> T^*$, then λt is very small for $t<T^*$. Therefore $\text{erf}\sqrt{\lambda t} \simeq 0$, $e^{-\lambda t} \simeq 1$ and the first line ot (17) shows that $\dot{M}(t;\lambda) \simeq \dot{M}(t;0)$. This approximation even holds for some time span beyond T* as seen in Fig. 3.

If on the other hand $T_{1/2} << T^*$, as is the case for Cm^{244}, then even for small and moderate values of t, λt is large, so that $\text{erf}\sqrt{\lambda t} \simeq 1$ and $e^{-\lambda t} \simeq 0$. Equation (17) shows that then a steady state is reached relatively quickly, within several times of $T_{1/2}$, with a value

$$\dot{M}(\infty;\lambda) = 4\pi\varepsilon D_f C_s R \left[1+Da^{1/2}\right] \tag{19}$$

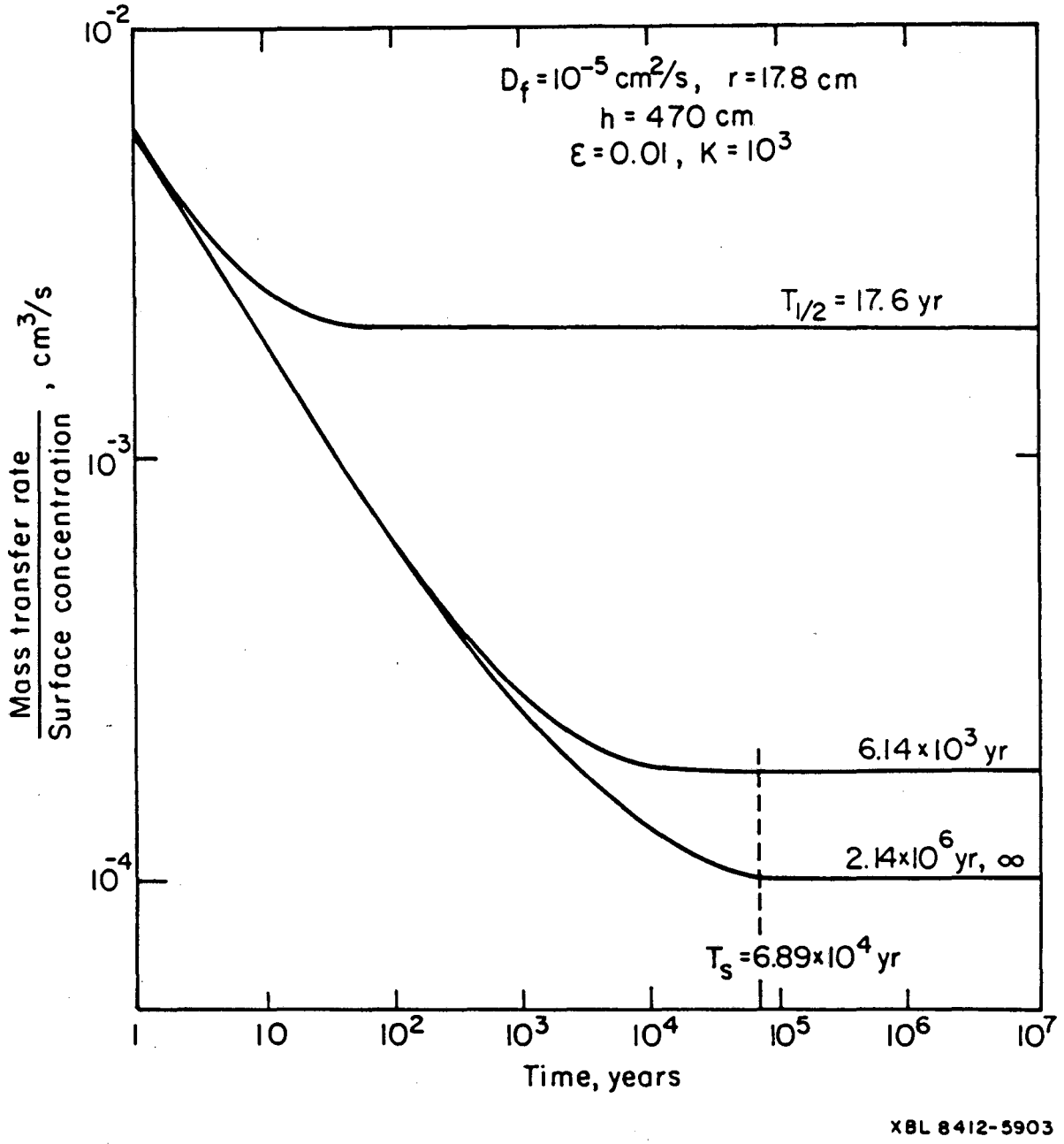

XBL 8412-5903

Fig. 3 Normalized mass transfer rate as a function of time and half-life; diffusion from a prolate spheroidal waste form.

This can be compared with the total mass transport at steady state ($t>T^*$) in absence of decay. From (14),

$$\dot{M}(\infty,0) = 4\pi\epsilon D_f C_s R \left[1+\sqrt{\frac{KR^2}{\pi D_f T^*}}\right] \tag{20}$$

With the definition of the Damköhler modulus

$$\frac{\dot{M}(\infty;\lambda)}{\dot{M}(\infty;0)} = \frac{1+\left(\frac{K\lambda R^2}{D_f}\right)^{1/2}}{1+\left(\frac{KR^2}{\pi D_f T^*}\right)^{1/2}}$$

$$= \frac{1+\left(\frac{KR^2 \ln 2}{D_f T_{1/2}}\right)^{1/2}}{1+\left(\frac{KR^2}{\pi D_f T^*}\right)^{1/2}} \tag{21}$$

From this it is seen that if $T_{1/2} \ll T^*$ then $\dot{M}(\infty;\lambda)$ will have a much larger steady state value than $\dot{M}(\infty;0)$ as shown in Fig. 3.

It should be noted that the effects of radioactive decay on the mass transfer have been made specifically for a waste form described by (6) in terms of its replacement defined by (7). For other waste form geometries the qualitative trends shown in Fig. 3 should remain unchanged. To obtain quantitative results for other waste form geometries the numerical integration of (13) is readily carried out.

Reference

1. Chambré, P.L., et al, "Analytical Performance Models for Geological Repositories," LBL-14842, V.II, October, 1982.

8. TRANSIENT MASS TRANSPORT OF A RADIONUCLIDE WITH TEMPERATURE-DEPENDENT SOLUBILITY, DIFFUSIVITY, AND RETARDATION COEFFICIENT

P.L. Chambré

This analysis focuses on the time dependent, diffusive mass transport of a radioactive specie from a spherically shaped waste form, imbedded in a porous medium, in absence of water convection. It was shown in chapter 7 that one can approximate, subject to stated restrictions, the mass transport from a cylindrically shaped waste by that from an equivalent surface area sphere. The analysis given below incorporates a number of physical features of practical importance and leads to a convenient analytical formula from which their effects on the mass transport is readily judged. The analysis includes aside from the effects of decay, the influence of a time variable temperature environment. Thus it applies to the non-isothermal time span which arises shortly after the emplacement of the waste form.

The surface temperature of the waste package is time dependent, on account of the time variable heat release of the waste. Since we are primarily interested in the surface mass flux, it is the effect of the variable surface temperature on the mass transport which we wish to take into account. Since the solubility concentration and the diffusion coefficient of the diffusing specie are assumed known functions of temperature, they in turn depend on time. They are respectively $c_s(t)$ and $D_f(t)$. The analysis applies of course also to isothermal conditions where these parameters are constant in time.

The concentration $N(r,t)$ of the diffusing specie, in absence of precursors, is governed by for constant porosity

$$\frac{\partial K(t)N}{\partial t} = D_f(t)\,\frac{1}{r^2}\,\frac{\partial}{\partial r}\left(r^2\,\frac{\partial N}{\partial r}\right) - K(t)\lambda N,\quad R_o<r<\infty\ ,\ t>0 \tag{1}$$

The initial conditions are

$$N(r,0) = 0;\ r>R_o \tag{2}$$

and the boundary conditions,

$$N(R_o,t) = c_s(t),\ t\geq 0 \tag{3}$$

$$N(\infty,t) = 0,\ t\geq 0 \tag{4}$$

Let

$$c(r,t) = rK(t)N(r,t)e^{\lambda t};\ \frac{D_f(t)}{K(t)} = \frac{D_0}{K_0}\,g(t) \tag{5}$$

then (1) - (4) transform to

$$\frac{\partial c}{\partial t} = \frac{D_0}{K_0}\,g(t)\,\frac{\partial^2 c}{\partial r^2}\ ;\ r>R_0,\ t>0 \tag{6}$$

$$c(r,0) = 0,\ r>R_0 \tag{7}$$

$$c(R_0,t) = R_0K(t)c_s(t)e^{\lambda t},\ t>0 \tag{8}$$

$$c(\infty,t) = 0\ ,\ t>0 \tag{9}$$

The solubility concentration is given by

$$K(t)c_s(t) = c_{s0}f(t)\ ,\ t\geq 0 \tag{10}$$

The dimensionless functions $f(t)$, $g(t)$ represent the known time dependence of $K(t)c_s(t)$ and $\frac{D(t)}{K(t)}$ respectively. In order to reduce (6) to a constant coefficient equation let

$$x(r) = \frac{r-R_0}{R_0}\ ,\ r\geq R_0 \tag{11}$$

$$\tau(t) = \frac{D_0}{K_0R_0^2}\int_0^t g(t')dt'\ ,\ t\geq 0 \tag{12}$$

$$C(x,\tau) = c(r,t) \tag{13}$$

then (6) - (9) transform into

$$\frac{\partial C}{\partial \tau} = \frac{\partial^2 C}{\partial x^2}\ ,\ 0<x<\infty\ ,\ \tau>0 \tag{14}$$

$$C(x,0) = 0 \tag{15}$$

$$C(0,\tau) = \beta\bar{f}(\tau) \tag{16}$$

$$C(\infty,\tau) = 0 \tag{17}$$

where

$$\beta = R_0 c_{s0} \ , \ \bar{f}(\tau) = f(t(\tau))e^{\lambda t(\tau)} \tag{18}$$

To solve this problem apply a Laplace transform, with respect to the variable τ, to (14) and impose the side conditions (15) - (17) with the result

$$C(x,s) = \beta\bar{f}(s)e^{-x\sqrt{s}} \ , \ x \geq 0 \tag{19}$$

The primary interest is in the surface concentration gradient which will be denoted by $\phi(\tau)$

$$\phi(\tau) = -\frac{\partial C(0,\tau)}{\partial x} \tag{20}$$

Its Laplace transform is obtained, with help of (19),

$$\phi(s) = -\frac{\partial C(0,s)}{\partial x}$$

$$= \beta s\bar{f}(s)\frac{1}{\sqrt{s}} \tag{21}$$

Since

$$L\left\{(\pi t)^{-1/2}\right\} = s^{-1/2} \text{ and } L\left\{\bar{f}'(\tau)\right\} + \bar{f}(0+) = s\bar{f}(s) \tag{22}$$

(21) takes on the alternate form

$$\phi(s) = \beta\left[\frac{\bar{f}(0+)}{\sqrt{s}} + L\left\{\bar{f}'(\tau)\right\} \cdot \frac{1}{\sqrt{s}}\right] \ , \tag{23}$$

provided $\bar{f}(\tau)$ is a continuously differentiable function for $\tau>0$. $\phi(s)$ can be inverted with help of the convolution theorem

$$\phi(\tau) = \frac{\beta}{\sqrt{\pi}}\left[\frac{\bar{f}(0+)}{\sqrt{\tau}} + \int_0^\tau \frac{\bar{f}'(\tau-\eta)}{\sqrt{\eta}}\,d\eta\right] , \tag{24}$$

where the ' denotes differentiation with respect to the first variable.

One can now compute the surface mass flux per unit surface area from

the spherical waste form into the exterior field. It is given by

$$\dot{m}(t;\lambda) = -D_f(t)\varepsilon \frac{\partial N(R_0,t)}{\partial r} \tag{25}$$

where ε is the porosity of the exterior medium, assumed independent of temperature. From (5), (11) and (13)

$$\frac{\partial N(r,t)}{\partial r} = \frac{e^{-\lambda t}}{K(t)} \frac{\partial}{\partial r} \left[\frac{c(r,t)}{r}\right]$$

$$= \frac{e^{-\lambda t}}{K(t)} \left[-\frac{c(r,t)}{r^2} + \frac{1}{r} \frac{\partial c(r,t)}{\partial r}\right]$$

$$= \frac{e^{-\lambda t}}{K(t)} \left[-\frac{C(x,\tau(t))}{\left[R_0(1+x)\right]^2} + \frac{1}{R_0(1+x)} \frac{1}{R_0} \frac{\partial C(x,\tau(t))}{\partial x}\right] \tag{26}$$

Hence

$$\frac{\partial N(R_0,t)}{\partial r} = \frac{e^{-\lambda t}}{K(t)} \left[-\frac{C(0,\tau(t))}{R_0^2} + \frac{1}{R_0^2} \frac{\partial C(0,\tau(t))}{\partial x}\right]$$

$$= -\frac{e^{-\lambda t}}{R_0^2 K(t)} \left[\beta \overline{f}(\tau(t)) + \phi(\tau(t))\right] \tag{27}$$

on using (16) and (20). If one combines this with (24) there results the desired solution for the mass flux per unit sphere surface

$$\dot{m}(t;\lambda) = \frac{D_f(t) c_{s0} \varepsilon e^{-\lambda t}}{R_0 K(t)} \left[\overline{f}(\tau(t)) + \frac{1}{\sqrt{\pi}} \left\{\frac{\overline{f}(0+)}{\sqrt{\tau(t)}} + \int_0^{\tau(t)} \overline{f}'(\tau(t)-\eta) \frac{d\eta}{\sqrt{\eta}}\right\}\right] \tag{28}$$

Equation (28) shows that if initially $\overline{f}(0+) \neq 0$, the mass flux is infinite at $\tau = t = 0$. To evaluate the right hand side of (28) one uses $\overline{f}(\tau)$ as defined by (18) with $\tau(t)$ defined by (12). An application of the determination of $\dot{m}(t)$ in a time varying temperature environment for a stable nuclide is given in Section 9.

We illustrate (28) for a radioactive nuclide diffusing into a uniform and time invariant temperature field.

For this case

$$g(t) = 1,\ f(t) = K(t) = K_0,\ t \geq 0 \tag{29}$$

From (12) and (18)

$$\tau(t) = \frac{D_0}{K_0 R_0^2}\, t \tag{30}$$

$$\bar{f}(\tau) = e^{\lambda t(\tau)} K_0$$

$$= \exp\left(\frac{\lambda K_0 R_0^2}{D_0}\,\tau\right) K_0 \tag{31}$$

With this there results from (28),

$$\dot{m}(t;\lambda) = \frac{D_0 c_{s0} \varepsilon e^{-\lambda t}}{R_0}\left[\exp\left(\frac{\lambda K_0 R_0^2 \tau(t)}{D_0}\right) + \frac{1}{\sqrt{\pi}}\left\{\frac{1}{\sqrt{\tau(t)}} + \frac{\lambda K_0 R_0^2}{D_0}\cdot\right.\right.$$

$$\left.\left.\cdot\int_0^{\tau(t)} e^{\frac{\lambda K_0 R_0^2}{D_0}(\tau(t)-\eta)}\,\frac{d\eta}{\sqrt{\eta}}\right\}\right] \tag{32}$$

which with (30) reduces to the convenient formula

$$\dot{m}(t;\lambda) = \frac{D_0 c_{s0} \varepsilon}{R_0}\left[1 + \sqrt{\frac{K_0 R_0^2}{\pi D_0 t}}\, e^{-\lambda t} + \sqrt{\frac{\lambda K_0 R_0^2}{D_0}}\ \mathrm{erf}\left(\sqrt{\lambda t}\right)\right] \tag{33}$$

In absence of radioactive decay this reduces to

$$\dot{m}(t;0) = \frac{D_0 c_{s0} \varepsilon}{R_0}\left[1 + \sqrt{\frac{K_0 R_0^2}{\pi D_0 t}}\right] \tag{34}$$

a well known result. A comparison with (33) shows that the mass transport is enhanced by the decay. As already discussed in chapter 7 this is due to the removal of the diffusing specie due to decay which increases the concentration gradient close to the waste surface. Quantitatively (33) and (34) give the

following expression for small and large times, with $\lambda \neq 0$

$$\frac{\dot{m}(t;\lambda)}{\dot{m}(t;0)} = \begin{cases} 1, \text{ for } t \ll 1 \\ 1 + \dfrac{\lambda K_0 R_0^2}{D_0}, \text{ for } t \to \infty \end{cases} \tag{35}$$

In Figure 1, the total mass transport $\dot{m}(t;\lambda)$ from a sphere is shown as a function of time with λ as a parameter. Three nuclides of widely different half lives have been chosen to compare the effect of λ on $\dot{m}(t;\lambda)$. For convenience $\dot{m}$ has been normalized with the solubility concentration c_{s0}. Starting at $t = 0$ from an infinite value where according to (35) there is no effect with λ, $\frac{\dot{m}(t;\lambda)}{c_{s0}}$ decreases in time to a steady value which is reached approximately at t^*. It is seen that t^* decreases with the nuclide half life. On the other hand, the steady state plateau increases in magnitude with the decrease in half life in accordance with (35). These results are similar to those discussed in chapter 7 which the reader might consult.

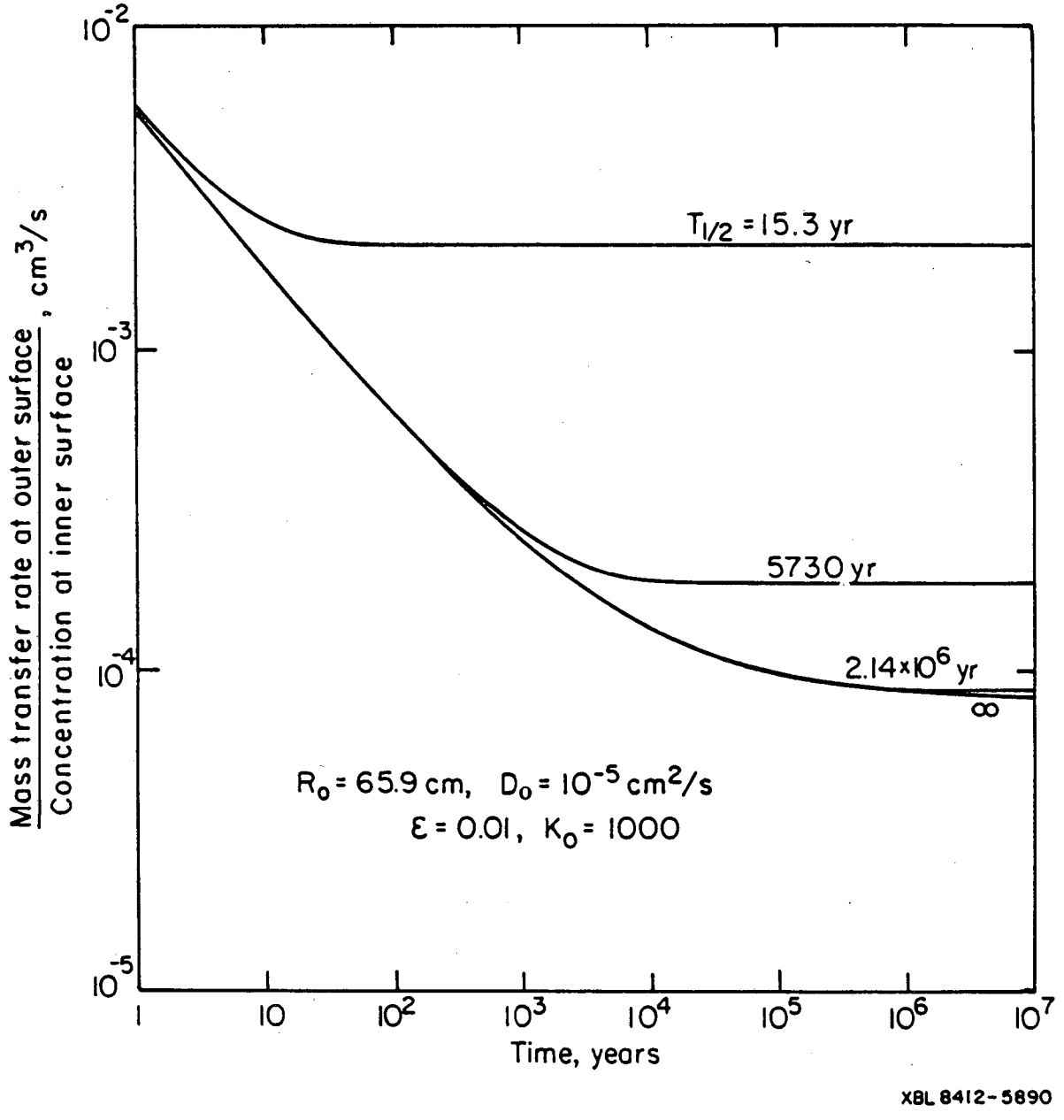

Fig. 1 Normalized mass transfer rate as a function of time and half-life; diffusion from a spherical waste form.

9. THE EFFECT OF HEATING ON WASTE DISSOLUTION AND MIGRATION

W.J. Williams, III, C.L. Kim, T.H. Pigford, P.L. Chambré

9.1. THEORETICAL DEVELOPMENT

The time dependent theory for the near-field mass transport from a spherical waste canister embedded in a purely diffusive field with time dependent temperatures, solubilities, and diffusion coefficients has already been developed in chapter 8 . An existing far-field one dimensional nondispersive migration model is coupled to this near-field model. The coupled model can be used to calculate waste concentration profiles in the far field based upon the nonisothermal dissolution of material at the waste canister surface. This method is applied to a conceptual commercial high level waste repository in basalt.

In the present study several assumptions were made in developing the waste canister mass transport and migration models:

- The cylindrical waste canister can be modeled as a sphere of the same lateral surface area.
- The waste is embedded in a purely diffusive isotropic field.
- The near-field mass transfer of material from the waste surface is controlled by diffusion, and near-field convective effects on mass transfer are negligible.
- The surface temperature of the spherical waste package is spatially uniform. This temperature is the spatially averaged surface temperature of the actual cylinder and is a known function of time.
- The solubility and liquid diffusion coefficients of each chemical species of interest are known functions of temperature.
- The retardation coefficeint is constant and not a function of temperature for each chemical species of interest.

- The initial concentration of each chemical species of interest is zero outside the waste canister.
- The maximum surface temperature of the waste canister occurs at the time of emplacement in the repository.
- The steel waste canister fails instantaneously at the time of emplacement in the repository.
- The waste is infinitely massive, i.e., the concentration of material in the ground water next to the waste surface is never less than the solubility limit.
- The radius of the waste form is constant even though mass is being lost to the surrounding ground water.
- The waste package surface temperature is determined by considering the heat generation of all the canisters in the emplacement array. These canisters are identical and were deposited in the repository at the same time.
- The concentration plumes resulting from the dissolution of other waste packages in the repository are neglected.
- The ground water concentration of each chemical species dissolved from the waste falls rapidly toward zero in the region within a few canister diameters of the waste (see Figure 9.1).
- A transition zone (see Figure 9.1) exists near the waste where diffusive and flow effects are both significant.

The last two assumptions are needed to couple the waste surface mass flux to the far-field ground water concentration. In the transition zone dissolved waste tends to be swept away by the flowing ground water. Since the concentration in this region is generally much less than the solubility limit at the waste surface, the transition zone concentration is assumed equal to zero in the near-field mass transport model. This assumption, however, does not apply to the far-field

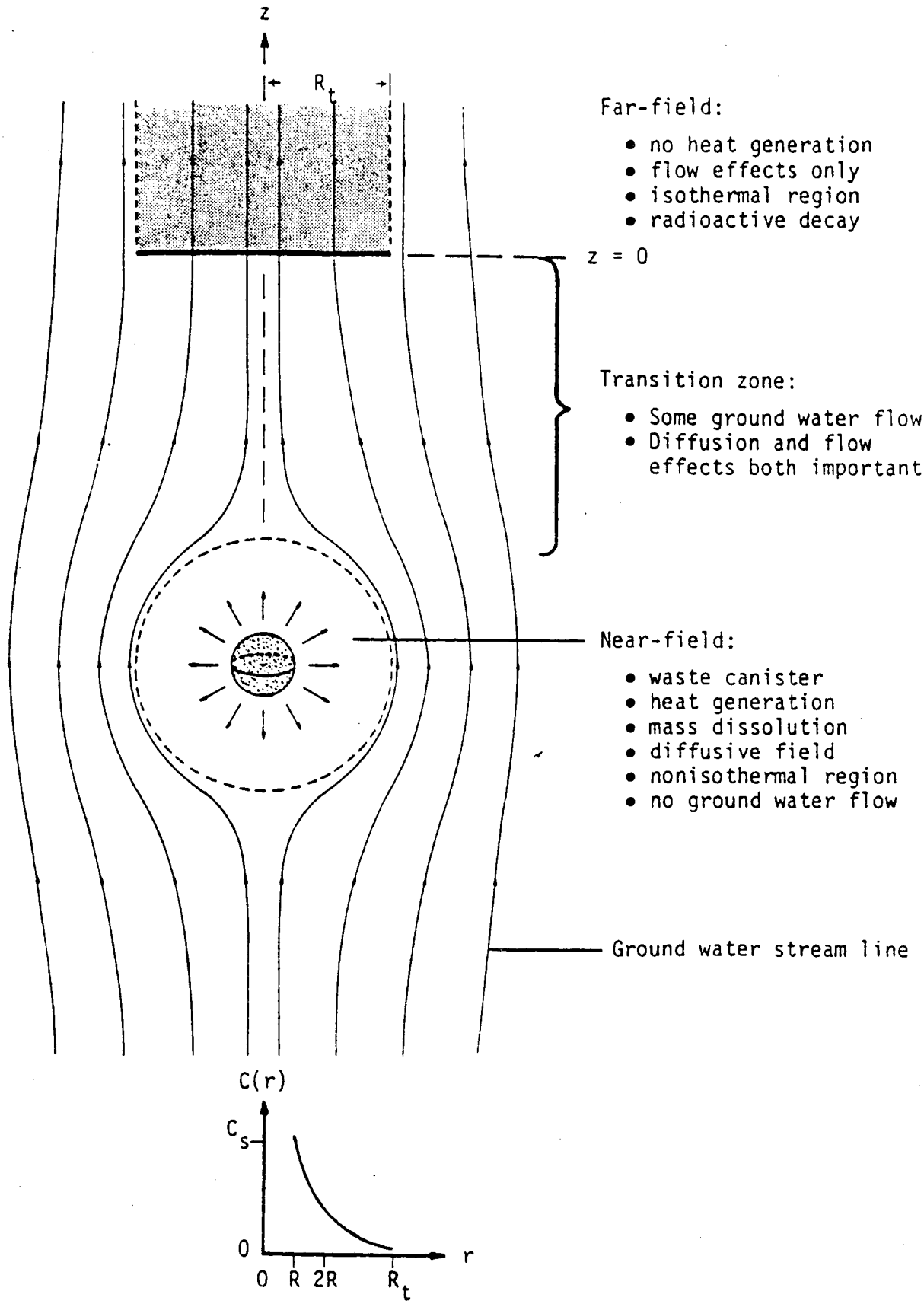

Figure 9.1 -- Coupling between the near and far fields.

migration calculations, since the far-field concentrations are of the same order.

Given the above assumptions, the solutions obtained in chapter 8 can be applied for near-field diffusive mass transport and the theory which governs the subsequent migration of radionuclides from a repository is developed in the next section 9.2.

Section 9.3 describes the method used to find the best polynomial fitting curves for solubility C_s and diffusion coefficient D as the functions of temperature. These two quantities are then tabulated as the functions of time according to the temperature history. Section 9.4 uses the cubic spline functions to fit the above two quantities as smooth functions of time. Section 9.5 then applies the cubic spline technique to obtain the mass transport from the waste surface developed in chapter 8. This mass transport is used as the boundary condition for far-field migration model developed in section 9.2. Section 9.6 presents the results of these calculations and finally section 9.7 gives conclusions about this analysis.

9.2. Radionuclide Migration through Nondispersive Porous Media[1]

The one dimensional migration of a radionuclide through a water saturated nondispersive porous medium is described by the following differential equation:

$$K \frac{\partial N}{\partial t} + v \frac{\partial N}{\partial z} + \lambda K N = 0 \tag{2.1}$$

where $N(z,t)$ is the ground water concentration of the radionuclide, v is the ground water pore velocity, K is the retardation coefficient, and λ is the nuclide's radioactive decay constant.

For $N(z,t)$ the following side conditions apply:

$$N(z,0) = 0 \quad , \quad z > 0 \tag{2.2}$$

$$N(0,t) = N_0 \, \omega(t) \quad , \quad t > 0 \tag{2.3}$$

$$N(\infty,t) = 0 \quad , \quad t > 0 \tag{2.4}$$

Taking the Laplace transform of equation (2.1) yields the ordinary differential equation

$$\frac{d\bar{N}}{dz} + \frac{K}{v} (\lambda + s) \bar{N} = 0 \tag{2.5}$$

where $\bar{N}(z,s) = \mathcal{L}\{N(z,t)\}$. Equation (2.5) may be solved to produce

$$\bar{N}(z,s) = A(s) \exp \left\{ - \frac{K}{v} (\lambda + s) z \right\} = e^{-\lambda \frac{K}{v} z} \left\{ A(s) \, e^{-\frac{K}{v} z s} \right\} \tag{2.6}$$

Assuming that its Laplace transform exists, boundary condition (2.3) may be transformed to the s domain to obtain

$$\bar{N}(0,s) = N_0 \Omega(s) \tag{2.7}$$

where $\Omega(s) = \mathcal{L}\{\omega(t)\}$. The function $A(s)$ may be determined by applying this transformed boundary condition to equation (2.6):

$$A(s) = N_0 \Omega(s) \tag{2.8}$$

Thus,

$$\bar{N}(z,s) = e^{-\lambda \frac{K}{v} z} \left\{ N_0 \Omega(s)\, e^{-\frac{K}{v} z s} \right\} \tag{2.9}$$

The inverse Laplace transform of equation (2.9) may be determined by applying the Laplace transform translation theorem[2]:

$$e^{-bs} F(s) = \mathcal{L}\{f(t-b)\, u(t-b)\} \quad , \quad b > 0 \tag{2.10}$$

where $F(s) = \mathcal{L}\{f(t)\}$ and

$$u(t-b) \equiv \begin{cases} 0 & (t < b) \\ 1 & (t > b) \end{cases} \tag{2.11}$$

Hence N(z,t) is given by

$$N(z,t) = N_0\, e^{-\lambda \frac{K}{v} z}\, \omega(t - \tfrac{K}{v} z)\, u(t - \tfrac{K}{v} z) \tag{2.12}$$

A dimensionless relative concentration may be defined as

$$N^*(z,t) = \frac{N(z,t)}{N(0,\infty)} \tag{2.13}$$

Substituting equation (2.12) yields

$$N^*(z,t) = \frac{\omega(t - \frac{K}{v} z)\, u(t - \frac{K}{v} z)}{\omega(\infty)}\, e^{-\lambda \frac{K}{v} z} \tag{2.14}$$

Boundary condition (2.3) must be coupled to the surface mass flux at the waste canister. As shown in Figure 9.1, a plane z=0 is assumed where the ground water stream lines become parallel. Since the migration is nondispersive, all of the dissolved radionuclides are contained within a cylinder of radius R_t whose axis coincides with the z-axis. The intersection of the plane z=0 and this cylinder is a disc of radius R_t. This disc is the migration source plane. Because all of the waste must pass through this disc, the coupling between the surface mass flux and the far-field migration may be achieved by assuming the following

proportionality:

$$\omega(t - \frac{K}{v}z) \propto \dot{M}(t - \frac{K}{v}z) \tag{2.15}$$

Thus,

$$N^*(z,t) = \frac{\dot{M}(t - \frac{K}{v}z)\, u(t - \frac{K}{v}z)}{\dot{M}(\infty)} e^{-\lambda \frac{K}{v}z} \tag{2.16}$$

Note that since $\dot{M}(0^+)$ is infinite, the maximum concentration passing a given point, $N^*_{max}(z)$, cannot be defined for nondispersive migration.

The mass transport and migration models just developed require functional representations of diffusion coefficients, solubilities, and surface temperatures. Generally the values of these functions are known only at a few discrete points. In the next two sections, two curve fitting techniques, polynomial least squares analysis and the method of cubic splines, are developed.

9.3. Method of the Least Squares for Polynomial Fitting

The mass transport equations (5) and (10) in chapter 8 presume that the solubility (C_s) and the diffusion coefficient (D) of each chemical species of interest are known at the waste canister surface as functions of time. Generally, however, these functions are tabulated with respect to temperature as discrete experimental data points. Thus, one must construct approximations to $C_s(t)$ and D(t) based upon the tabulated data and the surface temperature history, T(t), of the waste canister.

The first step of the construction procedure is the fitting of the tabulated $C_s(T)$ and D(T) to continuous functions. Since the ranges of C_s, D, and T are only a few orders of magnitude, the method of polynomial least squares is an appropriate fitting technique.

Consider a set of data points (x_i,y_i). The polynomial to be fitted to these points can be represented as

$$y(x) = \sum_{j=0}^{n} a_j x^j \tag{3.1}$$

where the a_j are to be determined. Define the error, ϵ_i, as follows:

$$\epsilon_i \equiv y(x_i) - y_i = \sum_{j=0}^{n} a_j x_i^j - y_i \tag{3.2}$$

where n is the order of the polynomial to be fitted.

In a least squares analysis the best fit of the data to the function y(x) is obtained when σ^2, the sum of the squared errors, is minimum:

$$\sigma^2 = \sum_{i=1}^{m} \epsilon_i^2 \tag{3.3}$$

where m is the number of data points. Since σ^2 is generally greater than zero, curve smoothing is an integral characteristic of the least

squares technique. The set of coefficients a_j for which σ^2 is minimum is given by the following system of equations (normal equations):[3]

$$\begin{aligned}
a_0 \sum_{i=1}^{m} x_i^0 x_i^0 + a_1 \sum_{i=1}^{m} x_i^0 x_i^1 + a_2 \sum_{i=1}^{m} x_i^0 x_i^2 + \ldots + a_n \sum_{i=1}^{m} x_i^0 x_i^n &= \sum_{i=1}^{m} x_i^0 y_i \\
a_0 \sum_{i=1}^{m} x_i^1 x_i^0 + a_1 \sum_{i=1}^{m} x_i^1 x_i^1 + a_2 \sum_{i=1}^{m} x_i^1 x_i^2 + \ldots + a_n \sum_{i=1}^{m} x_i^1 x_i^n &= \sum_{i=1}^{m} x_i^1 y_i \\
a_0 \sum_{i=1}^{m} x_i^2 x_i^0 + a_1 \sum_{i=1}^{m} x_i^2 x_i^1 + a_2 \sum_{i=1}^{m} x_i^2 x_i^2 + \ldots + a_n \sum_{i=1}^{m} x_i^2 x_i^n &= \sum_{i=1}^{m} x_i^2 y_i \\
&\vdots \qquad\qquad \vdots \qquad\qquad \vdots \qquad\quad \ldots \quad \vdots \qquad\qquad \vdots \\
a_0 \sum_{i=1}^{m} x_i^n x_i^0 + a_1 \sum_{i=1}^{m} x_i^n x_i^1 + a_2 \sum_{i=1}^{m} x_i^n x_i^2 + \ldots + a_n \sum_{i=1}^{m} x_i^n x_i^n &= \sum_{i=1}^{m} x_i^n y_i
\end{aligned} \tag{3.4}$$

In matrix form the normal equations reduce to

$$\underline{Q}\,\vec{a} = \underline{X}'\vec{y} \tag{3.5}$$

where $\underline{X}'$ is the transpose of $\underline{X}$ and

$$\vec{a} \equiv \begin{bmatrix} a_0 \\ a_1 \\ a_2 \\ \vdots \\ a_n \end{bmatrix} \tag{3.6}$$

$$\vec{y} \equiv \begin{bmatrix} y_1 \\ y_2 \\ y_3 \\ \vdots \\ y_m \end{bmatrix} \tag{3.7}$$

$$\underline{X} \equiv \begin{bmatrix} 1 & x_1 & x_1^2 & x_1^3 & x_1^4 & \ldots & x_1^n \\ 1 & x_2 & x_2^2 & x_2^3 & x_2^4 & \ldots & x_2^n \\ 1 & x_3 & x_3^2 & x_3^3 & x_3^4 & \ldots & x_3^n \\ \vdots & \vdots & \vdots & \vdots & \vdots & & \vdots \\ 1 & x_m & x_m^2 & x_m^3 & x_m^4 & \ldots & x_m^n \end{bmatrix} \tag{3.8}$$

$$\underline{Q} \equiv \begin{bmatrix} \sum_{i=1}^{m} x_i^0 x_i^0 & \sum_{i=1}^{m} x_i^0 x_i^1 & \sum_{i=1}^{m} x_i^0 x_i^2 & \cdots & \sum_{i=1}^{m} x_i^0 x_i^n \\ \sum_{i=1}^{m} x_i^1 x_i^0 & \sum_{i=1}^{m} x_i^1 x_i^1 & \sum_{i=1}^{m} x_i^1 x_i^2 & \cdots & \sum_{i=1}^{m} x_i^1 x_i^n \\ \sum_{i=1}^{m} x_i^2 x_i^0 & \sum_{i=1}^{m} x_i^2 x_i^1 & \sum_{i=1}^{m} x_i^2 x_i^2 & \cdots & \sum_{i=1}^{m} x_i^2 x_i^n \\ \vdots & \vdots & \vdots & \cdots & \vdots \\ \sum_{i=1}^{m} x_i^n x_i^0 & \sum_{i=1}^{m} x_i^n x_i^1 & \sum_{i=1}^{m} x_i^n x_i^2 & \cdots & \sum_{i=1}^{m} x_i^n x_i^n \end{bmatrix} \quad (3.9)$$

The quadratic matrix, $\underline{Q}$, can be represented in terms of $\underline{X}$:

$$\underline{Q} = \underline{X}'\underline{X} \quad (3.10)$$

Thus, equation (3.5) can be expressed in terms of equations (3.6) through (3.10) as follows:

$$(\underline{X}'\underline{X})\vec{a} = \underline{X}'\vec{y} \quad (3.11)$$

Solving for $\vec{a}$ yields the desired result:

$$\vec{a} = (\underline{X}'\underline{X})^{-1}\,\underline{X}'\vec{y} \quad (3.12)$$

provided that $(\underline{X}'\underline{X})$ is invertible. The best fitting polynomial of order n is now given by substituting the elements of $\vec{a}$ into equation (3.1).

In general n should be chosen such that there are more equations than unknown coefficients, i.e., $m \geq n$. If $n \geq 4$, y(x) may oscillate wildly.[3] Hence polynomial fitting is not always an appropriate curve fitting technique. In the case of the functions $C_s(T)$ and D(T), the selected values of n were all less than 4.

Consider a data point (t_i, T_i) on the T(t) curve. Since T(t) is monotonically decreasing, values of $C_s(t_i)$ and $D(t_i)$ can be determined by evaluating the polynomial expressions for $C_s(T)$ and D(T) at several T_i. Thus, the transformation from the temperature (T) domain to the

time (t) domain has been accomplished.

Unfortunately, C_s and D are once again in tabular form, now as functions of time. At first glance it may be tempting to apply the least squares fitting technique a second time. However, because the range of t is at least seven orders of magnitude, the resulting fit is very poor and σ^2 is very large.

A better approximation might be calculated by analyzing C_s and D as funtions of ℓn t instead of t. Substitution of logarithmic polynomials into equations (12) and (28) in chapter 8 for g(t) and f'(t) results in intractable integrals. While numerical integration theoretically could be performed, such calculations require large amounts of computational effort to achieve a result which has reasonable accuracy.

Because of these shortcomings of least squares curve fitting over large orders of magnitude, another technique, the method of cubic spline functions, was used instead. The theory of cubic splines is developed in the next section.

9.4. Cubic Spline Functions

Consider an interval [a,b] containing the nodes x_i such that

$$a = x_0 < x_1 < x_2 \ . \ . \ . \ < x_n = b \quad , \quad 0 \leq i \leq n \tag{4.1}$$

and

$$y_i = \psi(x_i) \tag{4.2}$$

Suppose that $\Psi_i(x)$ is the set of cubic functions (spline functions) which best approximates the actual function $\psi(x)$ on each interval $[x_{i-1}, x_i]$, where

$$\Psi_i(x) = \alpha_3 x^3 + \alpha_2 x^2 + \alpha_1 x + \alpha_0 \quad , \quad 1 \leq i \leq n \tag{4.3}$$

and α_0, α_1, α_2, and α_3 are coefficients. Since the method of cubic splines is not a smoothing technique,

$$y_0 = \psi(x_0) = \Psi_1(x_0) \tag{4.4}$$

$$y_i = \psi(x_i) = \Psi_i(x_i) = \Psi_{i+1}(x_i) \quad , \quad 1 \leq i \leq n-1 \tag{4.5}$$

$$y_n = \psi(x_n) = \Psi_n(x_n) \tag{4.6}$$

The Ψ_i are constrained by continuity considerations at the nodes:

$$\Psi_i(x_i) = \Psi_{i+1}(x_i) \quad , \quad 1 \leq i \leq n-1 \tag{4.7}$$

$$\Psi_i'(x_i) = \Psi_{i+1}'(x_i) \quad , \quad 1 \leq i \leq n-1 \tag{4.8}$$

$$\Psi_i''(x_i) = \Psi_{i+1}''(x_i) \quad , \quad 1 \leq i \leq n-1 \tag{4.9}$$

Note that only the third derivative of Ψ_i may be discontinuous at a nodal point. Two additional boundary conditions are required to perform the analysis. Since $\psi(x)$ is of no interest for $x < a$ or $x > b$, one sets

$$\Psi_1''(a) = 0 \tag{4.10}$$

$$\Psi_n''(b) = 0 \tag{4.11}$$

Define the following parameters:

$$h_i \equiv x_i - x_{i-1} \quad , \quad 1 \leq i \leq n \tag{4.12}$$

$$d_i \equiv \frac{y_i - y_{i-1}}{x_i - x_{i-1}} = \frac{y_i - y_{i-1}}{h_i} \quad , \quad 1 \leq i \leq n \tag{4.13}$$

$$t \equiv \frac{x-x_{i-1}}{x_i-x_{i-1}} = \frac{x-x_{i-1}}{h_i} , \quad 1 \leq i \leq n, \quad x_{i-1} \leq x \leq x_i . \tag{4.14}$$

Given the data (x_i,y_i), constraints (4.4) through (4.9), and definitions (4.12) through (4.14), the solution may be expressed as[4]

$$\psi_i[t(x)] = ty_i + (1-t)y_{i-1} + h_i t(1-t)[(k_{i-1}-d_i)(1-t) - (k_i-d_i)t] , \quad 1 \leq i \leq n \tag{4.15}$$

where

$$2k_0 + k_1 = 3d_1 \tag{4.16}$$

$$h_{i+1}k_{i-1} + 2(h_i+h_{i+1})k_i + h_i k_{i+1} = 3(h_i d_{i+1} + h_{i+1} d_i) , \quad 1 \leq i \leq n-1 \tag{4.17}$$

$$k_{n-1} + 2k_n = 3d_n \tag{4.18}$$

represent a non-recursive system of equations. Equations (4.16) through (4.18) however, can be represented in matrix form:

$$\underline{A}\,\vec{k} = \vec{b} \tag{4.19}$$

where

$$\underline{A} = \begin{bmatrix} 2 & 1 & 0 & 0 & \cdots & 0 & 0 & 0 & 0 \\ h & 2(h_1+h_2) & h_1 & 0 & \cdots & 0 & 0 & 0 & 0 \\ 0 & h_3 & 2(h_2+h_3) & h_2 & \cdots & 0 & 0 & 0 & 0 \\ \vdots & \vdots & \vdots & \vdots & & \vdots & \vdots & \vdots & \vdots \\ 0 & 0 & 0 & 0 & \cdots & h_{n-1} & 2(h_{n-2}+h_{n-1}) & h_{n-2} & 0 \\ 0 & 0 & 0 & 0 & \cdots & 0 & h_n & 2(h_{n-1}+h_n) & h_{n-1} \\ 0 & 0 & 0 & 0 & \cdots & 0 & 0 & 1 & 2 \end{bmatrix} \tag{4.20}$$

and $\vec{k}$ and $\vec{b}$ are given by

$$\vec{k} = \begin{bmatrix} k_0 \\ k_1 \\ k_2 \\ \vdots \\ k_{n-2} \\ k_{n-1} \\ k_n \end{bmatrix} \quad (4.21) \qquad \vec{b} = 3 \begin{bmatrix} d_1 \\ h_1 d_2 + h_2 d_1 \\ h_2 d_3 + h_3 d_2 \\ \vdots \\ h_{n-2} d_{n-1} + h_{n-1} d_{n-2} \\ h_{n-1} d_n + h_n d_{n-1} \\ d_n \end{bmatrix} \quad (4.22)$$

Equation (4.15) requires $\vec{k}$. Solving equation (4.19) for $\vec{k}$ yields

$$\vec{k} = \underline{A}^{-1} \vec{b} \tag{4.23}$$

provided that $\underline{A}^{-1}$ exists. Equation (4.15) can be expanded in terms of the definitions (4.12) through (4.14) to obtain for each i:

$$\alpha_3 = c_1 \tag{4.24}$$

$$\alpha_2 = -(c_1 c_3 + c_4 + c_5) \tag{4.25}$$

$$\alpha_1 = d_i + c_1 c_2 + c_3(c_4 + c_5) \tag{4.26}$$

$$\alpha_0 = \frac{x_i y_{i-1} - x_{i-1} y_i}{h_i} - c_2(c_4 + c_5) \tag{4.27}$$

where

$$c_1 = \frac{k_i + k_{i-1} - 2d_i}{h_i} \tag{4.28}$$

$$c_2 = x_i x_{i-1} \tag{4.29}$$

$$c_3 = x_i + x_{i-1} \tag{4.30}$$

$$c_4 = \frac{k_{i-1} - d_i}{h_i} \tag{4.31}$$

$$c_5 = c_1 x_{i-1} \tag{4.32}$$

Boundary conditions (4.10) and (4.11) were chosen primarily in the interest of computational simplicity. The actual curve to be fitted,

however, may not have vanishing second derivatives at the end points a and b of equation (4.1). It has been found, fortuitously, that only the spline functions near the coordinates a and b are sensitive to the above boundary conditions. By extrapolating the actual function in the regions just outside the end points, dummy data points may be computed. These dummy points "insulate" the actual data from the effects of the assumed boundary conditions.

One must also exercise caution in the selection of the points on the interval [a,b]. In low slope regions the time interval between adjacent points must be small in order for the spline approximation to accurately represent the actual function. It should also be noted that adjacent points may not have the same ordinate value.

The fitting of solubilities and diffusion coefficients is now complete. The next section describes the application of the cubic spline technique to the mass transport equations developed in chapter 8.

9.5. Cubic Spline Functions Applied to the Mass Transport Equations

The functions f(t) and g(t) of equations (5) and (10) in chapter 8 respectively, can be approximated up to the time $t=t_n$ by cubic splines:

$$f_i(t) = a_{i,3}t^3 + a_{i,2}t^2 + a_{i,1}t + a_{i,0} \quad , \quad 1 \leq i \leq n \tag{5.1}$$

$$g_i(t) = b_{i,3}t^3 + b_{i,2}t^2 + b_{i,1}t + b_{i,0} \quad , \quad 1 \leq i \leq n \tag{5.2}$$

Define

$$G_i(t) \equiv \int_0^t g_i(t')\,dt' \quad , \quad t_{i-1} \leq t \leq t_i \quad , \; 1 \leq i \leq n \tag{5.3}$$

$$= \frac{b_{i,3}}{4}t^4 + \frac{b_{i,2}}{3}t^3 + \frac{b_{i,1}}{2}t^2 + b_{i,0}t \tag{5.4}$$

The defining equation for $\tau(t)$ must be adapted in order to account for the piecemeal nature of $g_i(t)$. From the transport analysis in chapter 8 one recalls that

$$\tau(t) \equiv \frac{D_0}{KR_0^2}\int_0^t g(t')\,dt' \quad , \quad t \geq 0 \quad \text{(chapter 8, eq. 12)}$$

For $t_{i-1} \leq t \leq t_i$, $1 \leq i \leq n$, $t_0 = 0$, and $\tau_0 = 0$

$$\tau(t) = \frac{D_0}{KR_0^2}\sum_{j=1}^{i-1}\int_{t_{j-1}}^{t_j} g_j(t')\,dt' + \frac{D_0}{KR_0^2}\int_{t_{i-1}}^{t} g_i(t')\,dt'$$

$$= \frac{D_0}{KR_0^2}\sum_{j=1}^{i-1}[G_j(t_j) - G_j(t_{j-1})] + \frac{D_0}{KR_0^2}[G_i(t) - G_i(t_{i-1})]$$

$$= \tau_{i-1} + \frac{D_0}{KR_0^2}[G_i(t) - G_i(t_{i-1})] \tag{5.5}$$

where

$$\tau_{i-1} = \frac{D_0}{KR_0^2}\sum_{j=1}^{i-1}[G_j(t_j) - G_j(t_{j-1})] = \frac{D_0}{KR_0^2}\int_0^{t_{i-1}} g(t')\,dt' \tag{5.6}$$

Consider the convolution integral used in equation 28 of chapter 8:

$$I(t) = \int_0^{\tau(t)} \frac{f'\{\tau(t)-\tau'\}}{\sqrt{\tau}}\, d\tau' \qquad (5.7)$$

The approximation of f'(t) by quadratic (derivative of cubic) spline functions is shown in Figure 9.2. Note that in equation (5.7) τ is fixed and τ' is the variable of integration. Define

$$\tau'' \equiv \tau(t) - \tau' \qquad (5.8)$$

The transformation of f' from the time (t) domain to the τ'' domain is obtained by applying eq 12 of chap. 8.) Figure 9.3 shows the transformation when $D(t)/KR_o^2$ is taken to be constant. In general, however, D(t) is not constant and the proportionality between each t_i and τ_i is lost. The upper bound of integration, $\tau(t)$, is selected to lie in the i^{th} interval. A simple change of coordinates is made so that $f'(\tau'')$ is plotted against τ''. Now equation (5.7) can be rewritten as below:

$$I(t) = \int_0^{\tau(t)} \frac{f'(\tau'')}{\sqrt{\tau(t)-\tau''}}\, d\tau'' \qquad (5.9)$$

$$= \sum_{j=1}^{i-1} \int_{\tau_{j-1}}^{\tau_j} \frac{f'_j(\tau'')}{\sqrt{\tau(t)-\tau''}}\, d\tau'' + \int_{\tau_{i-1}}^{\tau(t)} \frac{f'_i(\tau'')}{\sqrt{\tau(t)-\tau''}}\, d\tau'' \qquad (5.10.a)$$

(where $\tau_o \equiv 0$, $\tau_{i-1} < \tau(t) \leq \tau_i$, and $2 \leq i \leq n$)

or

$$\int_0^{\tau(t)} \frac{f'_1(\tau'')}{\sqrt{\tau(t)-\tau''}}\, d\tau'' \quad (o < \tau(t) \leq \tau_1,\ i = 1) \qquad (5.10.b)$$

Notice that one must take care to perform the convolution integral using the appropriate spline function f', between the limits τ_j and τ_{j-1} in each interval j, $i \leq j \leq i$. Thus, the convolution integral can be treated as the summation of the i separate integrations. And to remove the singularity which appears in the second term of the right hand side in equation (5.10.a) define

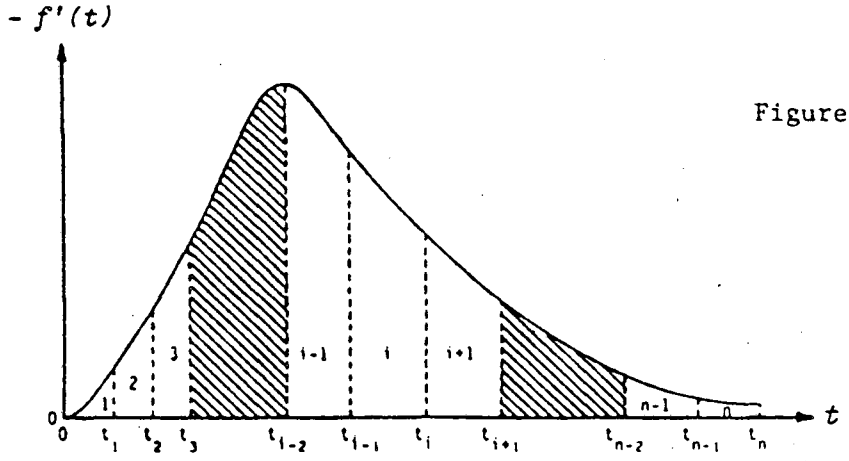

Figure 9.2 -- Plot of f' in the t domain.

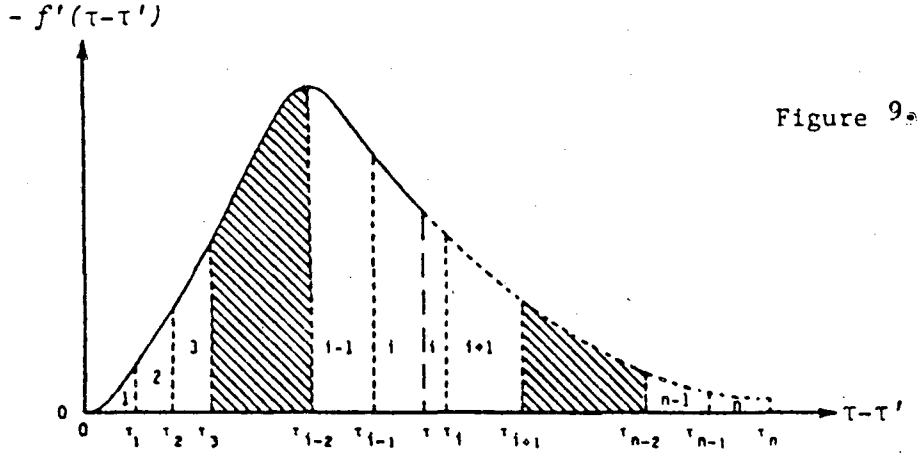

Figure 9.3 -- Plot of f' in the τ-τ' domain.

$$u^2 \equiv \tau(t) - \tau'' \tag{5.11}$$

Then,

$$\int_{\tau_{i-1}}^{\tau(t)} \frac{f_i'(\tau'')}{\sqrt{\tau(t)-\tau''}}\, d\tau'' = 2\int_0^{\sqrt{\tau(t)-\tau_{i-1}}} f_i' \left\{\tau(t)-u^2\right\} du \tag{5.12}$$

Similarly, equation (5.10.b) can be reformed as

$$\int_0^{\tau(t)} \frac{f_1(\tau'')}{\sqrt{\tau(t)-\tau''}}\, d\tau'' = 2\int_0^{\sqrt{\tau(t)}} f_1' \left\{\tau(t)-u^2\right\} du \tag{5.13}$$

Now combine the equations (5.12) and (5.13) into the equation (5.10).

$$I(t) = \sum_{j=1}^{i-1} \int_{\tau_{j-1}}^{\tau_j} \frac{f_j'(\tau'')}{\sqrt{\tau(t)-\tau''}}\, d\tau'' + 2\int_0^{\sqrt{\tau(t)-\tau_{i-1}}} f'_i \left\{\tau(t)-u^2\right\} du$$

$$\tau_{i-1} < \tau(t) \leq \tau_i, \quad 2 \leq i \leq n \tag{5.14a}$$

or $$2\int_0^{\sqrt{\tau(t)}} f_1' \left\{\tau(t)-u^2\right\} du$$

$$0 < \tau(t) \leq \tau_1, \; i = 1 \tag{5.14b}$$

At this point apply the trapezoidal rule to the equations (5.14.a) and (5.14.b) and obtain the following results:

$$I(t) = \sum_{j=1}^{i-1} \frac{1}{2}\left[\frac{f_j'(\tau_j)}{\sqrt{\tau(t)-\tau_j}} + \frac{f_j'(\tau_{j-1})}{\sqrt{\tau(t)-\tau_{j-1}}}\right]\left(\tau_j-\tau_{j-1}\right) +$$

$$\left[f_i' \left\{\tau(t)\right\} + f_i'(\tau_{i-1})\right] \sqrt{\tau(t)-\tau_{i-1}} \tag{5.15.a}$$

where

$$\tau_{i-1} < \tau(t) \leq \tau_i, \quad 2 \leq i \leq n.$$

$$I(t) = \left[f_1' \left\{\tau(t)\right\} + f_1'(o)\right] \sqrt{\tau(t)} \tag{5.15.b}$$

where

$$0 < \tau(t) \leq \tau_1, \; i = 1$$

9.6. RESULTS

The results of the waste dissolution and migration from a canister embedded in a conceptual basalt repository are presented in this section. Two species, SiO_2 (silica) and ^{237}Np, were considered in the analysis. The dissolution of silica is indicative of the performance of the borosilicate glass matrix in the repository environment. ^{237}Np is representative of many long lived ($t_{\frac{1}{2}} = 2.14 \cdot 10^6$ y) radionuclides. Their activity can be appreciable even after thousands of years.

The time dependent rock temperature at the emplacement hole surface was supplied by Altenhofen[5] for commercial high level waste that has been cooled ten years prior to emplacement. In the present study it was assumed that the emplacement hole surface temperature was the same as the waste package surface temperature, T(t). Furthermore, the time axis was shifted such that the maximum surface temperature occurred at time t = 0, an adjustment of six years. The assumed waste package surface temperature history is shown in Figure 9.4.

The temperature dependence of silica solubility[6] and liquid diffusion coefficient[7] is shown in Figures 9.5 and 9.6 and also is tabulated in Appendix 9A. Using the construction technique described earlier in this study, Figures 9.4, 9.5 and 9.6 were combined to yield discrete time dependent values of the silica solubility and diffusion coefficient. The resulting 47 data points of each variable were then splined to produce the continuous functions plotted in Figures 9.7 and 9.8. These results are also tabulated in Appendix 9B. The interval of each cubic spline function is delimited by a vertical string of dots in these figures.

The neptunium solubility and diffusion coefficients were not known

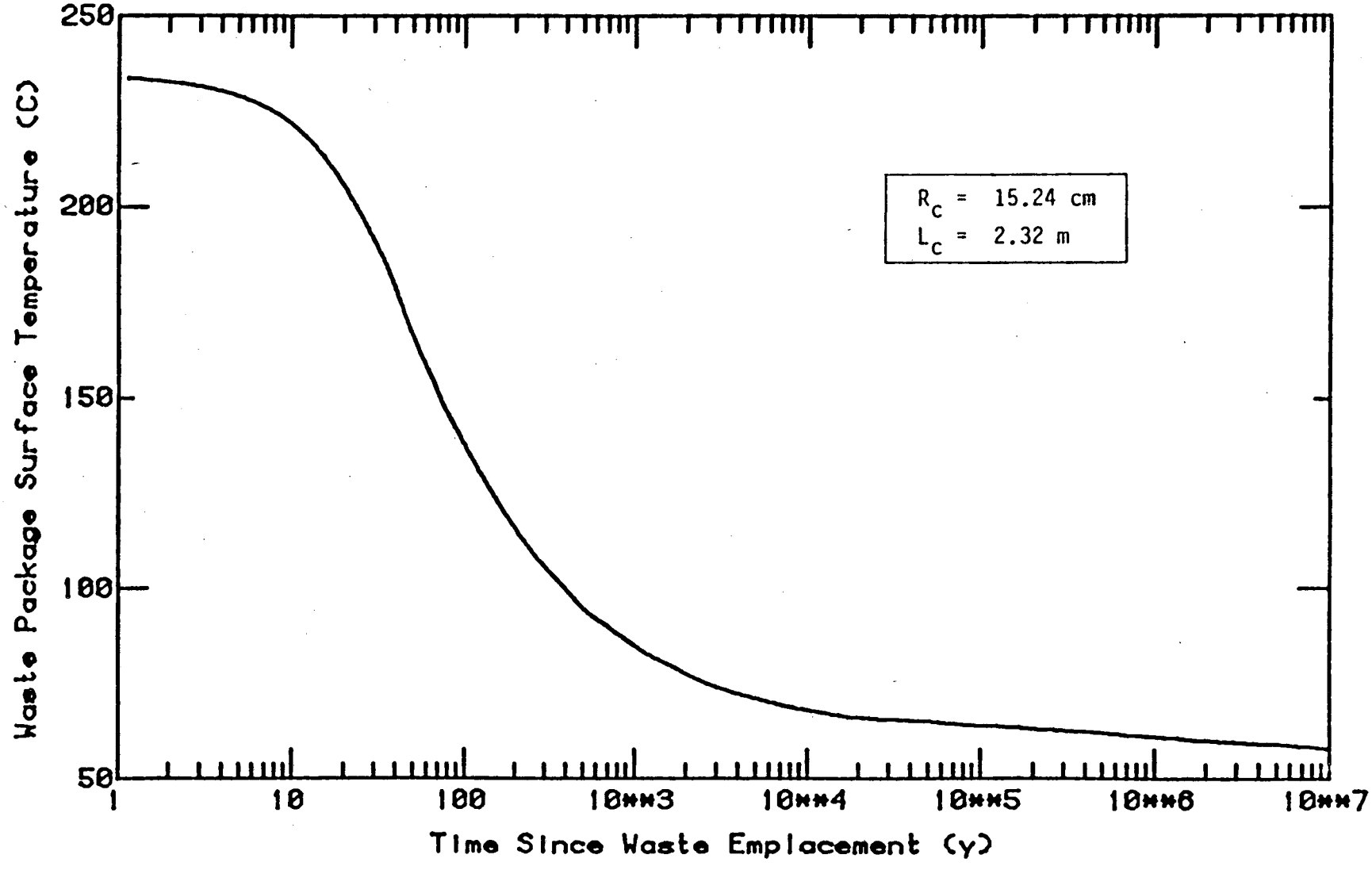

Figure 9.4 -- Waste package surface temperature history for a conceptual commercial high level waste repository in basalt. (Adapted from reference 5)

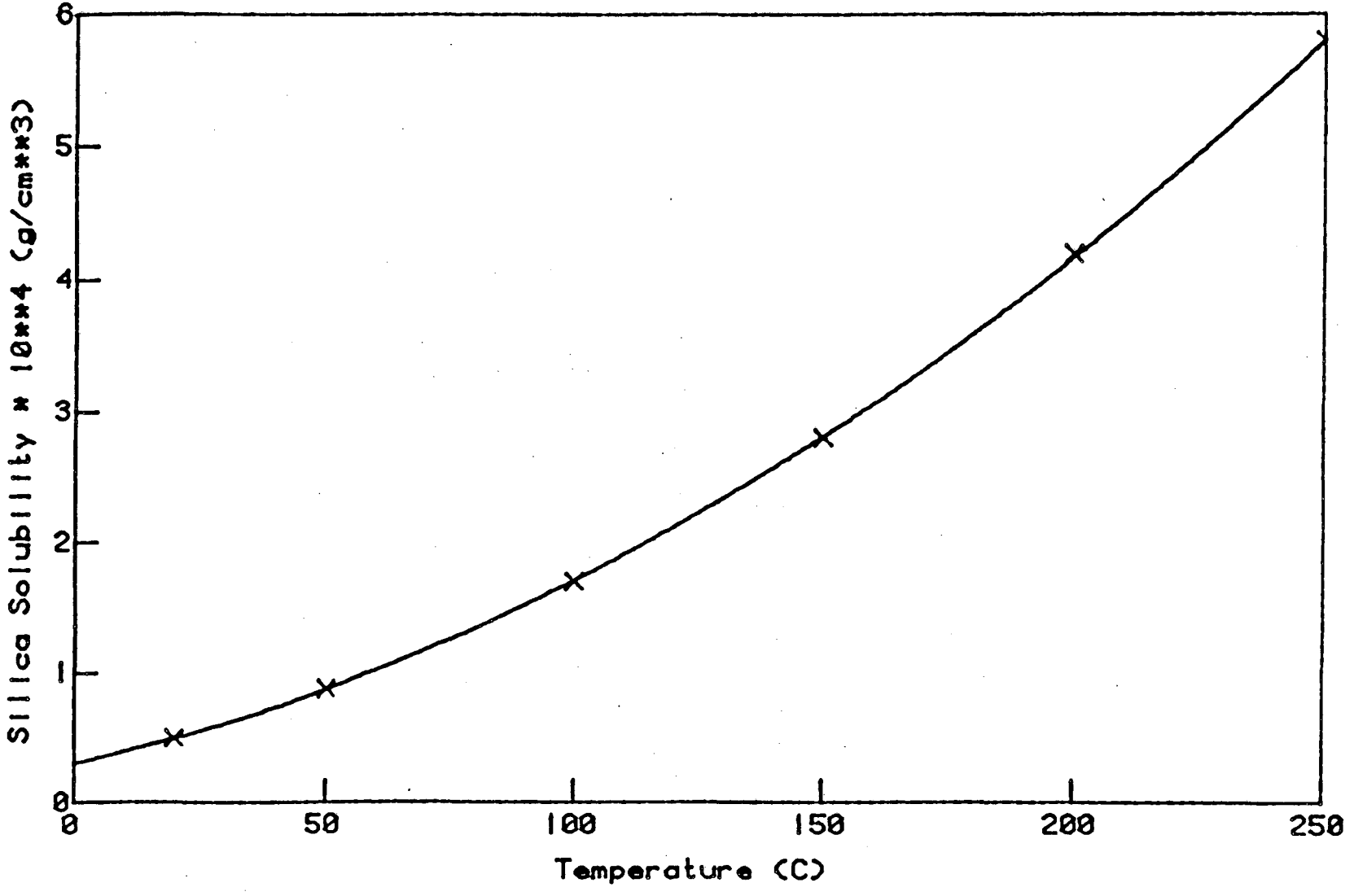

Figure 9.5 -- The effect of temperature on silica solubility.
(Data from reference 6)

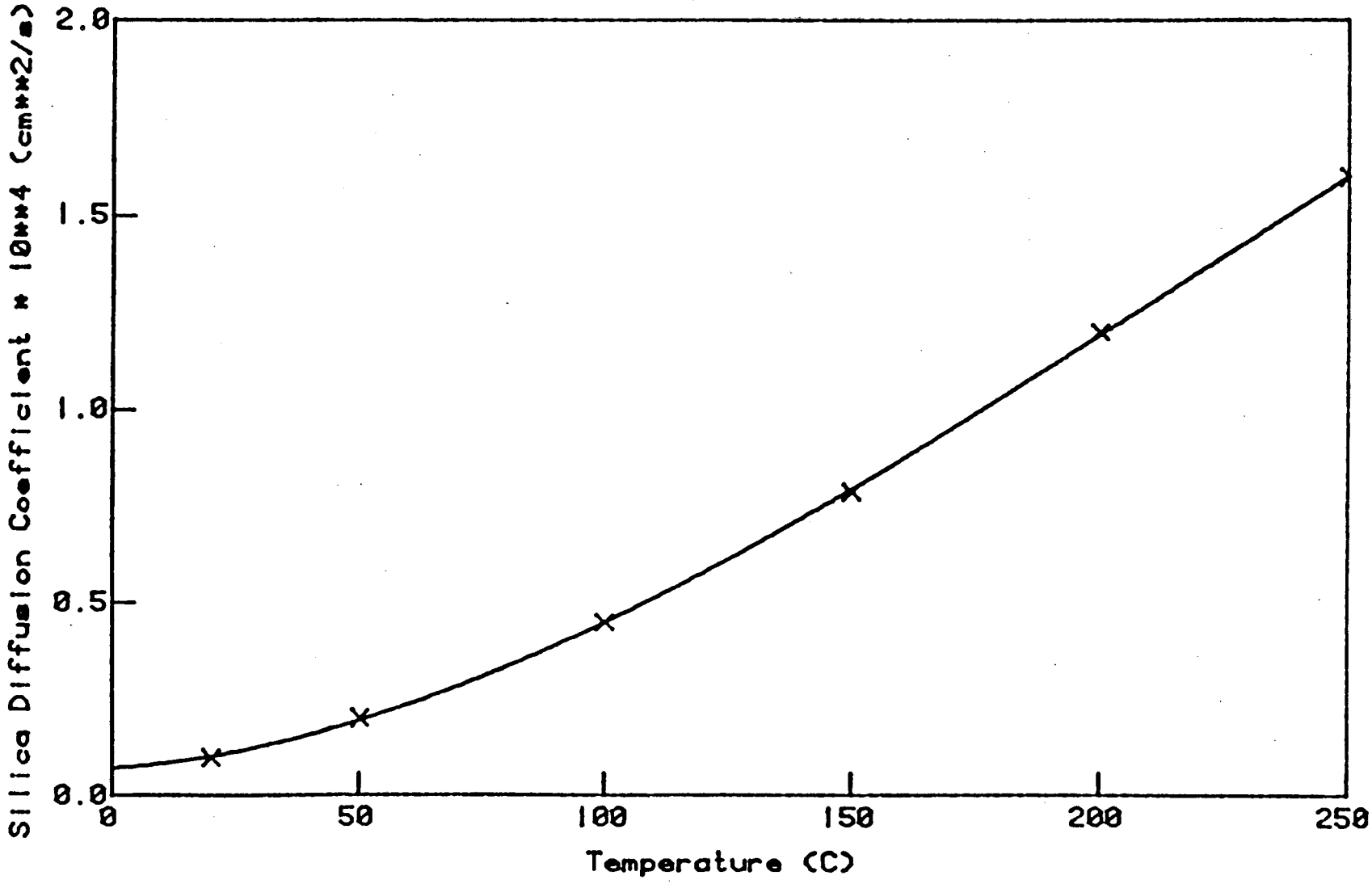

Figure 9.6 -- The effect of temperature on the liquid diffusion coefficient of silica. (Data from reference 6)

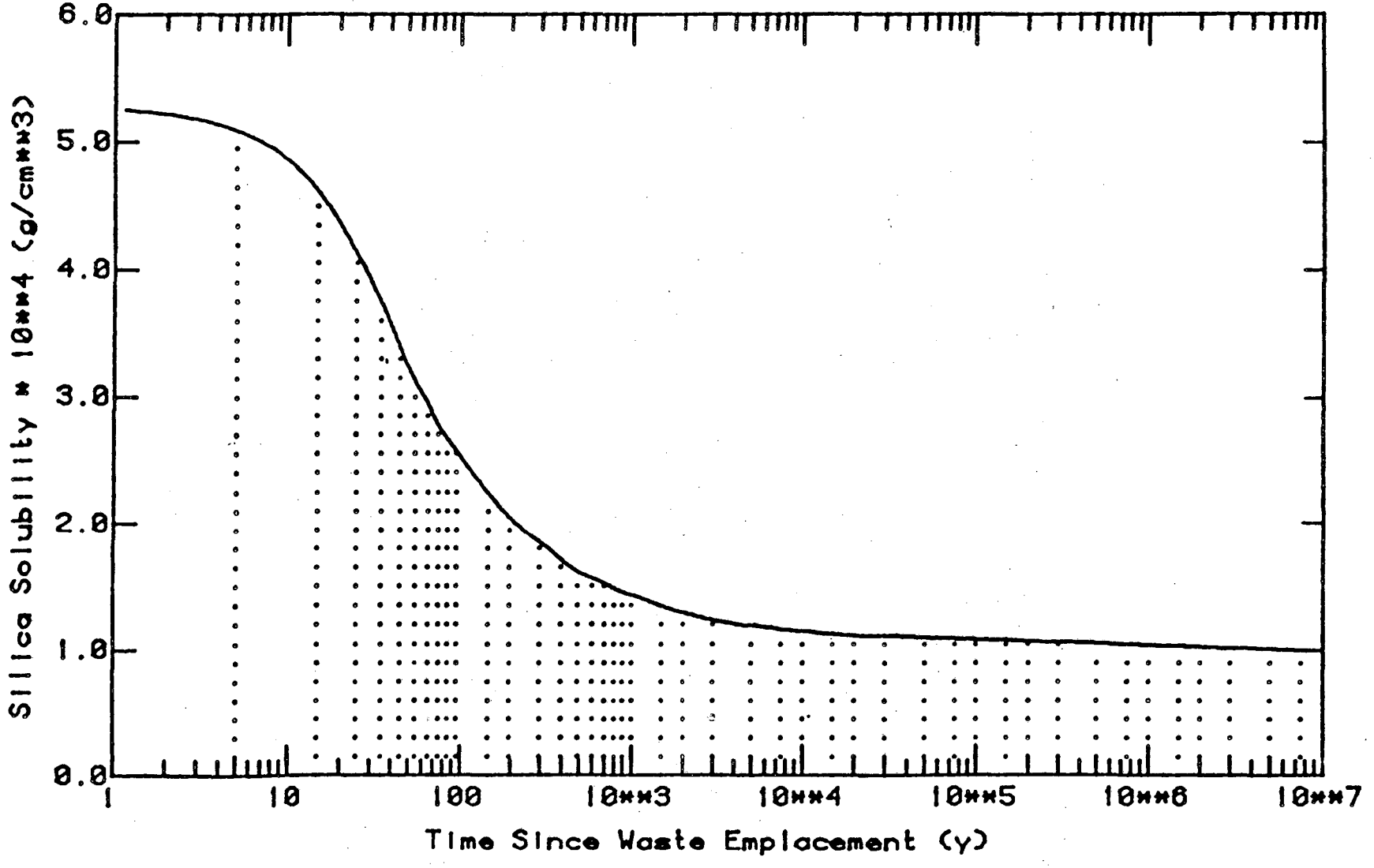

Figure 9.7 -- Silica solubility history at the waste canister surface. The vertical dotted lines delimit the intervals used in approximating this curve by spline functions. (See §4)

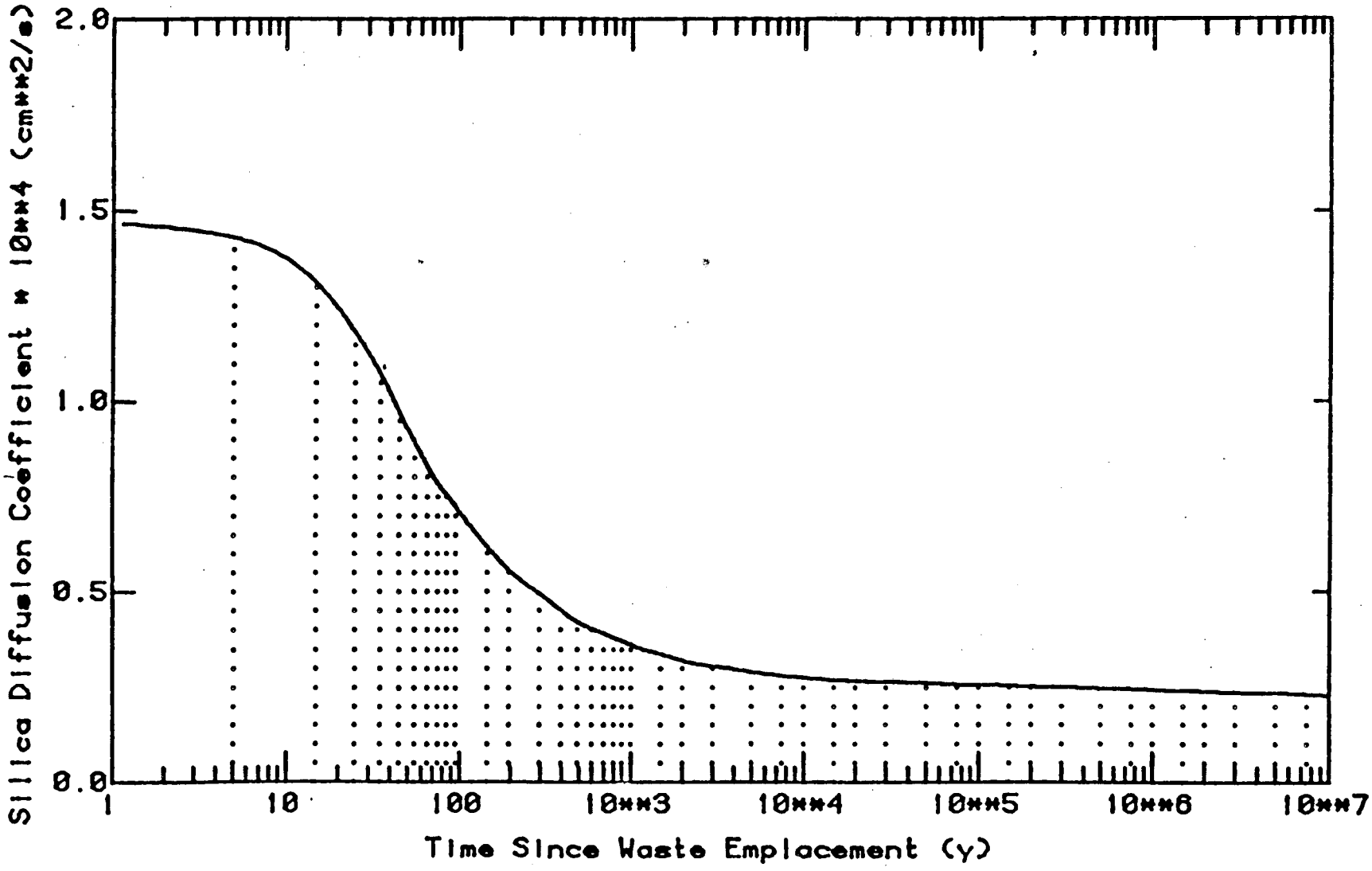

Figure 9.8 -- Silica liquid diffusion coefficient history at the waste canister surface. The vertical dotted lines delimit the intervals used in approximating this curve by splines. (See §4)

functions of temperature. It was assumed that silica and neptunium have the same specific heats of solution. Consequently, the following relationship is valid (see Appendix 9D for derivation):

$$\frac{C_{Np}(T)}{C_{SiO_2}(T)} = \frac{C_{Np}(T_0)}{C_{SiO_2}(T_0)} \qquad (6.1)$$

where T_0 is a reference temperature at which the solubilities of both species are known. This ratio was determined to be $2.0 \cdot 10^{-7}$.[8] The diffusion coefficient of both species was assumed to be the same. The retardation coefficient of silica was assumed to be $K = 1$, the worst case value, and that of neptunium was taken as $K = 100$, the generally accepted value for basalt.

Using the time varying solubility and diffusion coefficient functions, the total surface mass flux from the waste canister was computed using equation (28) in chapter 8. The results are shown in Figures 9.9 and 9.10 and are also tabulated in Appendix 9C. A steady state waste dissolution rate is reached after about 10,000 years for silica and 100,000 years for neptunium. Less than two percent of the total silica inventory was dissolved from the waste after 10,000 years of emplacement (see Appendix 9E).

Applying the one dimensional nondispersive migration model of Section 9.2. the concentration profiles of the waste were computed. The ratio of the waste concentration at a particular time and displacement to that under ambient temperature conditions is denoted by $N^*(z,t)$ [see equation 2.13)], where $N(0,\infty)$ is constant. Since $N^*(z,t)$ is hard to visualize, it is plotted with one coordinate fixed. Thus, the function $N^*(t)$ is the concentration ratio at a fixed position and $N^*(z)$ is the concentration ratio at a fixed time. The $N^*(t)$ and $N^*(z)$ for silica and ^{237}Np are plotted in Figures 9.11 through 9.14 for various values of z and t.

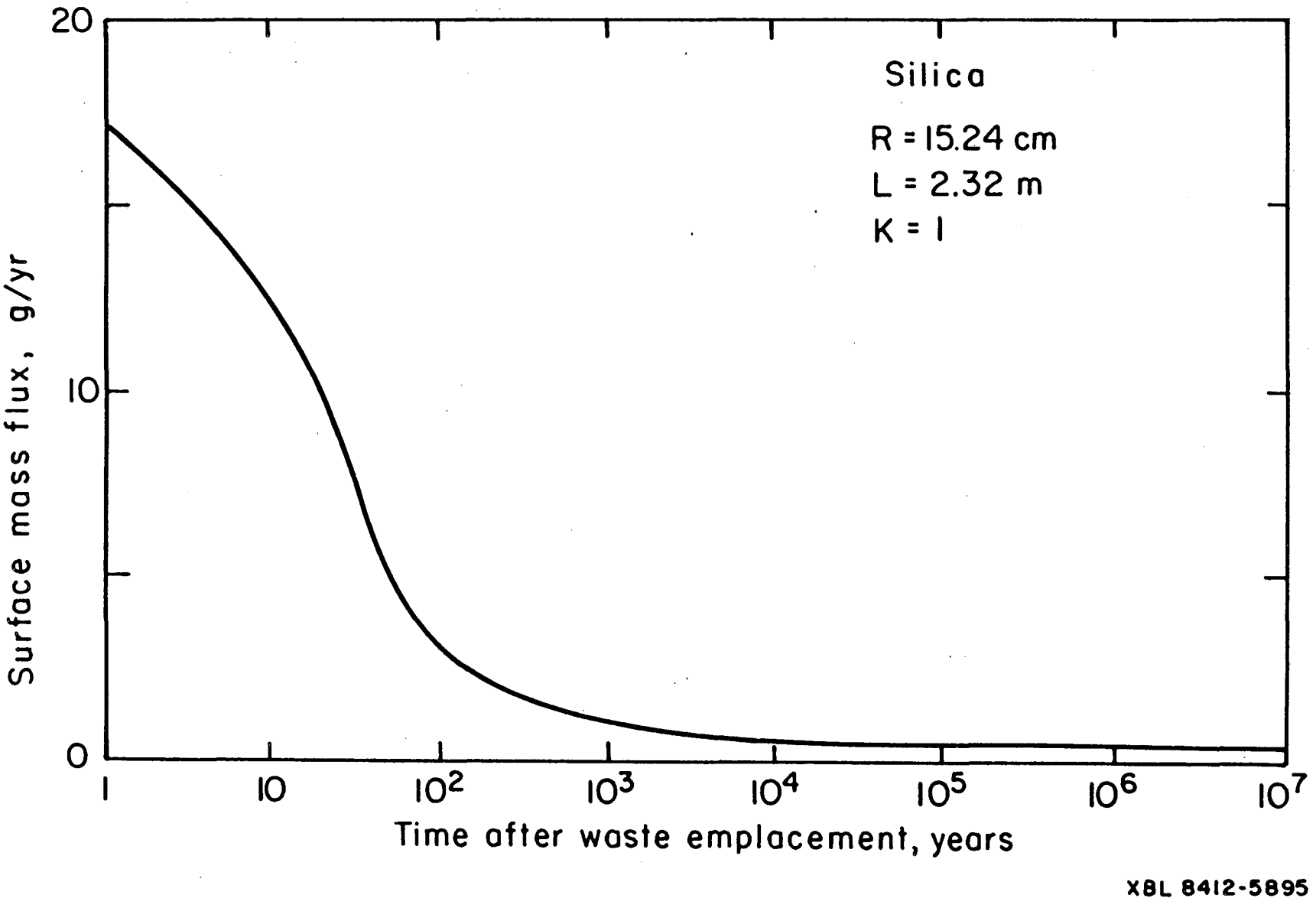

Fig. 9.9 Total surface mass flux of Silica from a spherical waste form as a function of time.

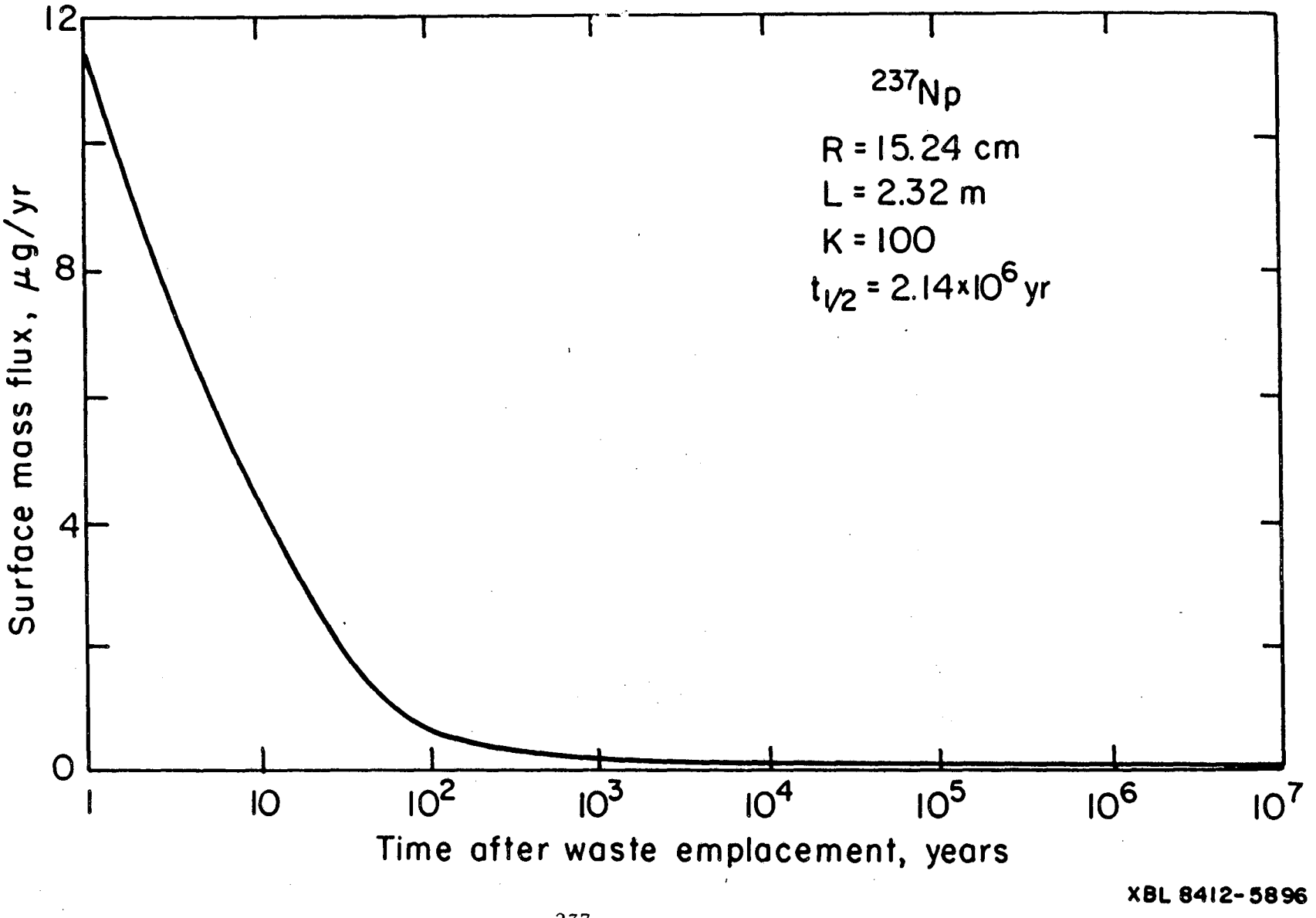

Fig. 9.10 Total surface mass flux of ^{237}Np from a spherical waste form as a function of time.

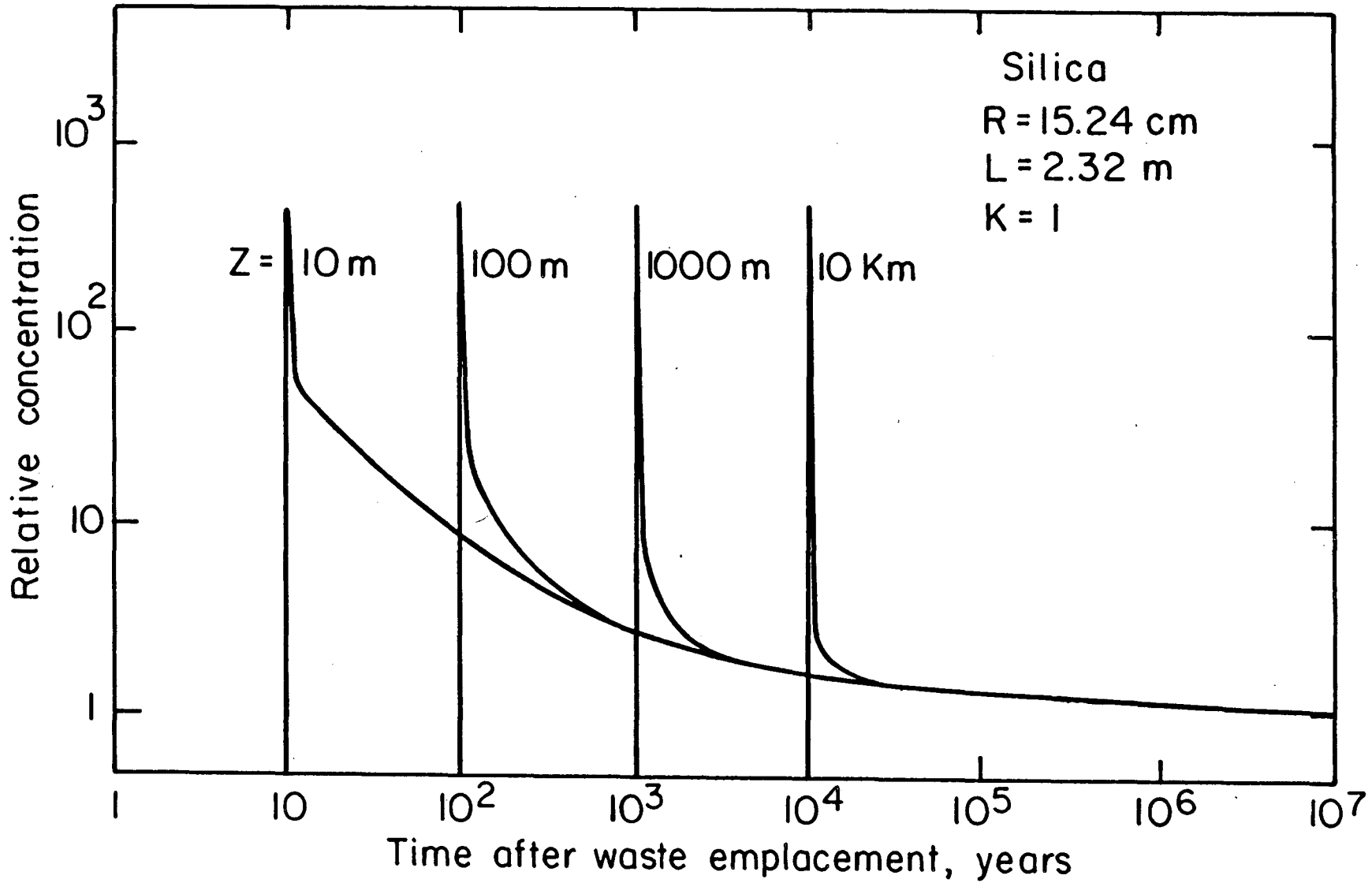

Fig.9.11 Far-field relative concentration of Silica from a spherical waste form as a function of time and distance.

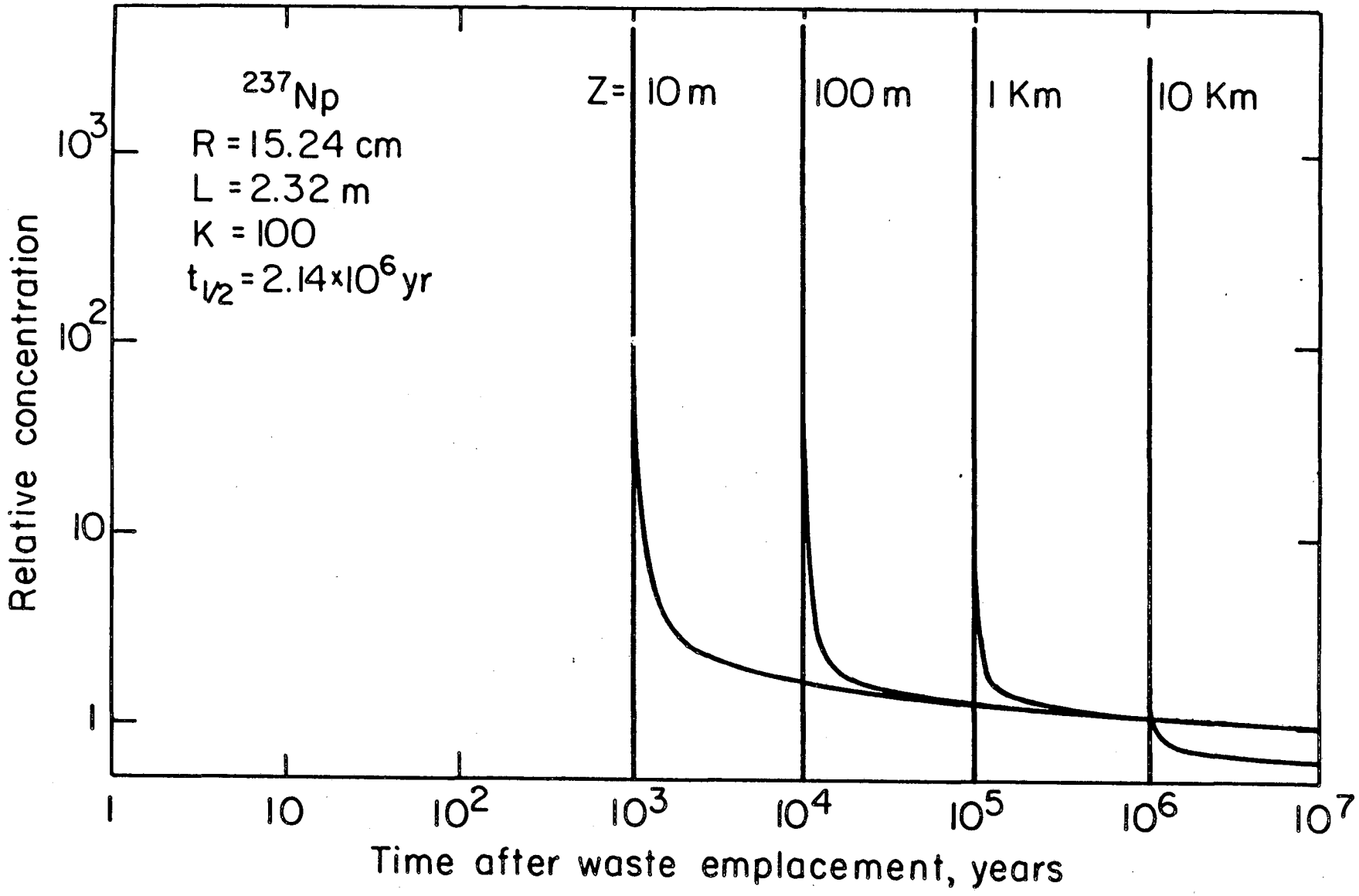

XBL 8412-5898

Fig.9.12 Far-field relative concentration of ^{237}Np from a spherical waste form as a function of time and distance.

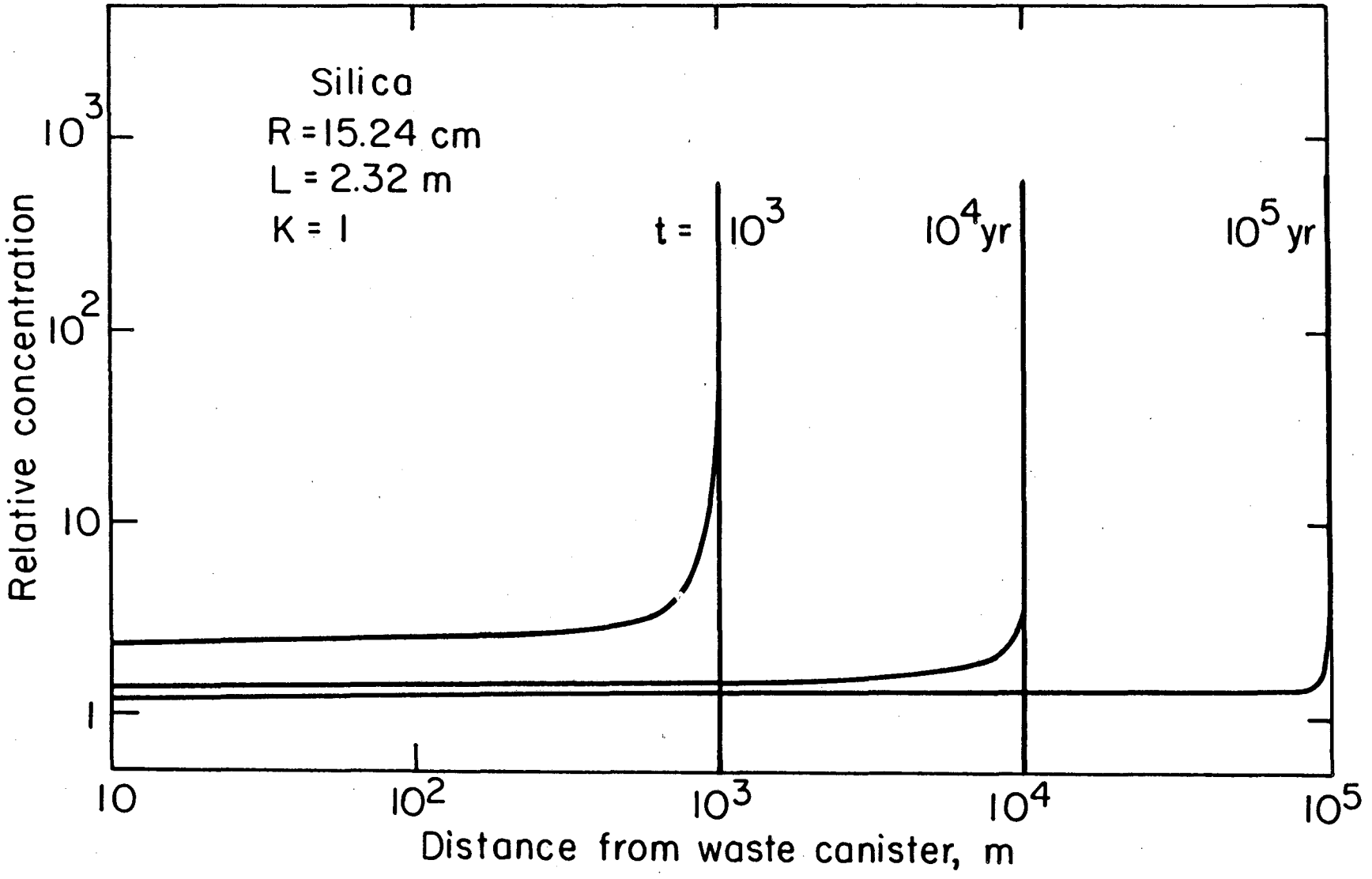

Fig. 9.13 Far-field relative concentration of Silica from a spherical waste form as a function of time and distance.

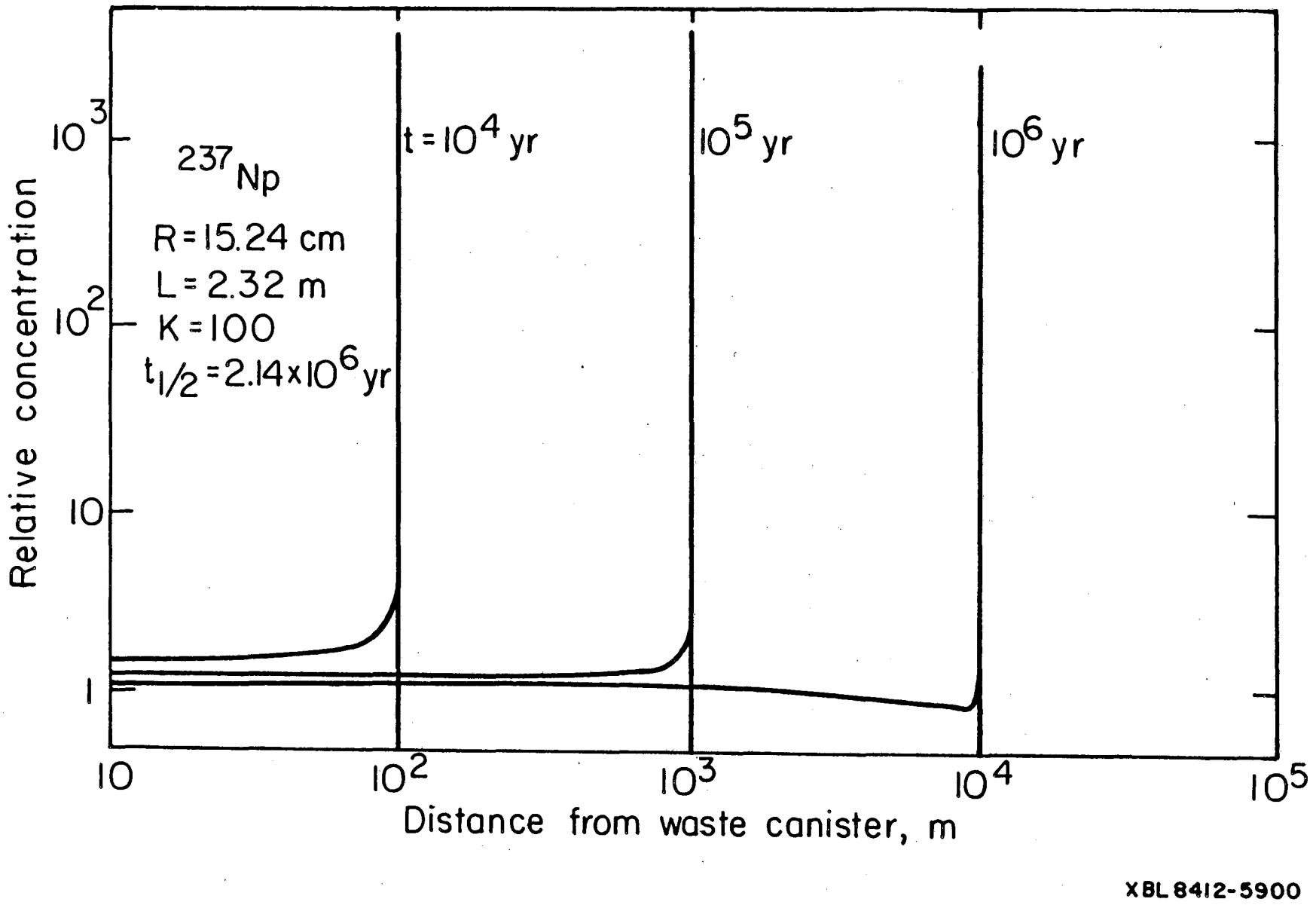

Fig. 9.14 Far-field relative concentration of ^{237}Np from a spherical waste form as a function of time and distance.

Since silica is stable, $N^*(z,t)$ appraoches unity at large times. ^{237}Np, however, decays, though very slowly. The limit as t tends to infinity for $N^*(z,t)$ of radioactive species tends to zero instead of unity. This effect can be seen for ^{237}Np in Figure 9.12.

The retardation coefficient, K, appears in both the mass transport and migration equations. By comparing the shapes of Figures 9.9 and 9.10, however, its effect in the near-field region is negligible on the shape of the surface mass flux curve. In the far-field region, the effect of K is very dramatic. Comparing Figures 9.13 and 9.14 shows a K-fold increase in the time necessary for the waste dissolution front to reach a given point over the water travel time. One should also note that the initial impulse magnitude increases with K, but decays rapidly to the same order of magnitude as the K=1 case.

9.7. CONCLUSIONS

The results of the total surface mass flux calculations demonstrate that the dissolution rate of the borosilicate waste glass matrix in a basalt repository is indeed very small. The quantity of ^{237}Np leached from the waste would hardly be detectable, less than one gram over 10 million years.

At first glance these results appear to verify the adequacy of the conceptual basalt repository. One should note, however, that many of the assumptions made in this analysis are not strictly valid in the actual repository environment. The effect of fissures in the host rock, for example, was not studied. Other practical considerations such as finite waste mass, convective ground water flow, sequential waste canister emplacement, varying canister corrosion properties, and the interactions of adjacent canisters in a repository may play an important role in future theoretical developments.

References

1. Harada, M., P. L. Chambre', M. Foglia, K. Higashi, F. Iwamoto, D. Leung, T. H. Pigford, and D. Ting, "Migration of Radionuclides Through Sorbing Media: Analytical Solutions - I", LBL-10500, 1980.

2. Abramowitz, M. and I. A. Stegun, (eds.). 1964. **Handbook of Mathematical Functions**, U. S. National Bureau of Standards Applied Mathematics Series 55.

3. Merriman, M. 1877. **Elements of the Methods of Least Squares**, London: MacMillan.

4. Dahlquist G. and A. Bjorck. 1974. **Numerical Methods**, Englewood Cliffs, NJ: Prentice-Hall.

5. Altenhofen, M. K., written communication to T. H. Pigford, April 1983.

6. Williams, G. H. 1978. **Computational Linear Algebra with Models**, Second Edition, Boston: Allyn & Bacon.

7. Fournier, R. O. and J. J. Power, **Amer. Minerologist, 61**, 1977.

8. Pigford, T. H., P. L. Chambre' and S. J. Zavoshy, "Effect of Repository Heating on Dissolution of Glass Waste," **Trans. Am. Nuc. Soc., 44**, 115, 1983.

APPENDIX 9A

Computer Program LSQR

LSQR performs a polynomial least squares analysis on a set of data points (see Section 3 for theoretical development). Sample program outputs for $C_s(T)$ and D(T) follow the FORTRAN listing.

```
      PROGRAM LSQR
C     ************************************************************
C     : FIT THE NTH ORDER LEAST SQUARES POLYNOMIAL TO A SET OF DATA :
C     ************************************************************
      PARAMETER M0=30,N0=15,N2=30
      DIMENSION XTRANS(N0,M0),X(M0,N0),XQUAD(N0,N0),XVECT(M0),Y(M0),
     1          XY(N0),A(N0),XQINV(N0,N0),GJ(N0,N2)
      DOUBLE PRECISION GJ
      EQUIVALENCE (XQUAD(1,1),XQINV(1,1))
      OPEN(UNIT=1,NAME='LSQR.GDA',TYPE='NEW')
C
      WRITE(5,5)
    5 FORMAT(//53H ENTER NUMBER OF DATA POINTS AND ORDER OF POLYNOMIAL:)
      READ(5,*) M,N
      N=N+1
C     CHECK ARRAY BOUNDS
      IF (M .GT. M0 .OR. N .GT. N0) GOTO 6000
      WRITE(5,15)
   15 FORMAT(//36H ENTER X VECTOR, ONE VALUE PER LINE:)
C     LOAD THE X AND X TRANSPOSE MATRICES
      DO 2000 I=1,M
          READ(5,*) XVECT(I)
          X(I,1)=1.
          XTRANS(1,I)=1.
          DO 1000 J=2,N
              X(I,J)=XVECT(I)**(J-1)
              XTRANS(J,I)=X(I,J)
 1000     CONTINUE
 2000 CONTINUE
C
      WRITE(5,45)
   45 FORMAT(//36H ENTER Y VECTOR, ONE VALUE PER LINE:)
      DO 3000 I=1,M
          READ(5,*) Y(I)
 3000 CONTINUE
C     XQUAD=XTRANS*X
      CALL MULT(XTRANS,X,XQUAD,N,M,N,N0,M0,N0)
C     XY=XTRANS*Y
      CALL MULT(XTRANS,Y,XY,N,M,1,N0,M0,1)
C     XQINV=XQUAD**(-1)
      CALL INV(GJ,XQUAD,XQINV,N,2*N,N0)
C     A=XQINV*XY
      CALL MULT(XQINV,XY,A,N,N,1,N0,N0,1)
      WRITE(5,90)
   90 FORMAT(//18H A VECTOR:)
      CALL PRT(A,N,1,N0,1)
C
      WRITE(5,101)
  101 FORMAT(//9X,1HX,10X,12HCALCULATED Y,6X,8HACTUAL Y,7X,8HREL DIFF/
     1         9X,1H-,10X,12H------------,6X,8H--------,7X,8H---------/)
      EPSLON=0.
C     CHECK LEAST SQUARES FIT AGAINST INPUT DATA
      DO 4000 I=1,M
          CALC=POLY(A,N,XVECT(I))
          EPSLON=EPSLON+(CALC-Y(I))**2
          IF (Y(I) .EQ. 0.) GOTO 3500
              RDIFF=(CALC-Y(I))/Y(I)
              WRITE(5,100) XVECT(I),CALC,Y(I),RDIFF
  100         FORMAT(3E16.6,F13.5)
              GOTO 4000
 3500     WRITE(5,100) XVECT(I),CALC,Y(I)
 4000 CONTINUE
C
      WRITE(5,105) EPSLON
  105 FORMAT(//29H SUM OF THE SQUARED ERRORS = ,E13.6)
C     COMPUTE ADDITIONAL DATA POINTS
      WRITE(5,110)
  110 FORMAT(//51H INITIAL, FINAL, AND STEP -- POLYNOMIAL EVALUATION:/)
      READ(5,*) START,FINAL,STEP
C
      IF (START .GE. 0.) GOTO 5000
          CLOSE(UNIT=1,DISPOSE='DELETE')
          GOTO 8000
C
 5000 IF (START .GT. FINAL) GOTO 7000
          WRITE(1,120) START,POLY(A,N,START)
  120     FORMAT(2E16.6)
          START=START+STEP
          GOTO 5000
 6000 WRITE(5,130)
  130 FORMAT(//37H DIMENSION PARAMETER(S) ARE TOO LARGE/)
 7000 CONTINUE
      CLOSE(UNIT=1,DISPOSE='SAVE')
```

```
 8000 CONTINUE
      END
C     ***************************************************************************
C     ***************************************************************************
      SUBROUTINE PRT(A,K,L,K0,L0)
C     ***************************
C     : PRINT THE CONTENTS OF ARRAY A :
C     ***************************
      DIMENSION A(K0,L0)
C
      DO 1 I=1,K
          WRITE(5,10) (A(I,J),J=1,L)
   10     FORMAT(10E13.5)
    1 CONTINUE
      RETURN
      END
C     ***************************************************************************
C     ***************************************************************************
      SUBROUTINE MULT(A,B,C,I,J,K,I0,J0,K0)
C     *****************************
C     : MULTIPLY MATRICES:  C=A*B :
C     *****************************
      DIMENSION A(I0,J0),B(J0,K0),C(I0,K0)
C
      DO 3 II=1,I
          DO 2 KK=1,K
              C(II,KK)=0.
              DO 1 JJ=1,J
                  C(II,KK)=C(II,KK)+A(II,JJ)*B(JJ,KK)
    1         CONTINUE
    2     CONTINUE
    3 CONTINUE
      RETURN
      END
C     ***************************************************************************
C     ***************************************************************************
      SUBROUTINE INV(A,B,C,N,M,N0)
C     ****************
C     : INVERT MATRIX A :
C     ****************
C
C     ..... .....
C     :                                                                 :
C     : SUBROUTINE INV WAS ADAPTED FROM A BASIC PROGRAM IN APPENDIX J   :
C     : (INVERSE OF A MATRIX USING GAUSS-JORDAN ELIMINATION) OF THE     :
C     : TEXTBOOK 'COMPUTATIONAL LINEAR ALGEBRA WITH MODELS' BY GARETH   :
C     : WILLIAMS, SECOND EDITION, ALLYN & BACON, INC., BOSTON, 1978.    :
C     :.....:
C
      DIMENSION A(N,M),B(N0,N0),C(N0,N0)
      DOUBLE PRECISION A,T,Y,Z
C
      DO 17 I=1,N
          DO 16 J=1,M
              IF (J .GT. N) GOTO 12
                  A(I,J)=DBLE(B(I,J))
                  GOTO 16
   12         IF (J .EQ. N+I) GOTO 15
                  A(I,J)=0.
                  GOTO 16
   15         A(I,J)=1.
   16     CONTINUE
   17 CONTINUE
C
      DO 125 K=1,N
          IF (A(K,K) .NE. 0.) GOTO 76
              DO 70 I=K+1,N
                  IF (A(I,K) .EQ. 0.) GOTO 70
                      DO 60 J=K,M
                          T=A(K,J)
                          A(K,J)=A(I,J)
                          A(I,J)=T
   60                     CONTINUE
                          GOTO 76
   70             CONTINUE
                  GOTO 170
   76     IF (A(K,K) .EQ. 1.) GOTO 95
              Y=A(K,K)
              DO 90 L=K,M
                  A(K,L)=A(K,L)/Y
   90         CONTINUE
   95         DO 120 I=1,N
                  IF (I .EQ. K .OR. A(I,K) .EQ. 0.) GOTO 120
```

```
                    Z=A(I,K)
                    DO 115 J=K,M
                        A(I,J)=A(I,J)-Z*A(K,J)
  115               CONTINUE
  120         CONTINUE
  125 CONTINUE
C
      DO 150 I=1,N
          DO 145 J=N+1,M
              C(I,J-N)=SNGL(A(I,J))
  145     CONTINUE
  150 CONTINUE
      GOTO 200
C
  170 WRITE(5,999)
  999 FORMAT(//27H THE INVERSE DOES NOT EXIST/)
C
  200 CONTINUE
      RETURN
      END
C     ***************************************************************************
C     ***************************************************************************
      FUNCTION POLY(A,N,X)
C     ********************************************************
C     ! COMPUTE THE (N-1)TH ORDER POLYNOMIAL F(X) !
C     ********************************************************
C
C     A(1) IS THE CONSTANT TERM
C     A(N) IS THE COEFFICIENT OF THE (N-1)TH TERM
C
      DIMENSION A(N)
C
      SUM=A(N)*X
      DO 1 I=1,N-2
          SUM=(SUM+A(N-I))*X
    1 CONTINUE
      POLY=SUM+A(1)
      RETURN
      END
```

```
>RUN LSQR      (C8)

ENTER NUMBER OF DATA POINTS AND ORDER OF POLYNOMIAL:
6 2


ENTER X VECTOR, ONE VALUE PER LINE:
20
50
100
150
200
250


ENTER Y VECTOR, ONE VALUE PER LINE:
5E-5
8.8E-5
1.7E-4
2.8E-4
4.2E-4
5.8E-4


A VECTOR:
 0.30399E-04
 0.87371E-06
 0.53143E-08
```

X	CALCULATED Y	ACTUAL Y	REL DIFF
0.200000E+02	0.499992E-04	0.500000E-04	-0.00001
0.500000E+02	0.873706E-04	0.880000E-04	-0.00715
0.100000E+03	0.170913E-03	0.170000E-03	0.00537
0.150000E+03	0.281028E-03	0.280000E-03	0.00367
0.200000E+03	0.417713E-03	0.420000E-03	-0.00544
0.250000E+03	0.580970E-03	0.580000E-03	0.00167

```
SUM OF THE SQUARED ERRORS =  0.845712E-11


INITIAL, FINAL, AND STEP -- POLYNOMIAL EVALUATION:

0 -1 0
```

```
>RUN LSQR       (D)

ENTER NUMBER OF DATA POINTS AND ORDER OF POLYNOMIAL:
6 3


ENTER X VECTOR, ONE VALUE PER LINE:
20
50
100
150
200
250


ENTER Y VECTOR, ONE VALUE PER LINE:
1E-5
2E-5
4.5E-5
7.9E-5
1.2E-4
1.6E-4


A VECTOR:
 0.71642E-05
 0.88650E-07
 0.34343E-08
-0.53642E-11

        X            CALCULATED Y        ACTUAL Y         REL DIFF
        -            ------------        --------         --------

   0.200000E+02     0.102680E-04     0.100000E-04       0.02680
   0.500000E+02     0.195118E-04     0.200000E-04      -0.02441
   0.100000E+03     0.450076E-04     0.450000E-04       0.00017
   0.150000E+03     0.796284E-04     0.790000E-04       0.00795
   0.200000E+03     0.119351E-03     0.120000E-03      -0.00541
   0.250000E+03     0.160153E-03     0.160000E-03       0.00095


SUM OF THE SQUARED ERRORS =  0.114943E-11


INITIAL, FINAL, AND STEP -- POLYNOMIAL EVALUATION:

0 -1 0
```

APPENDIX 9B

Computer Program SPLINE

SPLINE performs a cubic spline fitting on a set of data points (see Section 4 for theoretical development). Sample program outputs for $C_s(t)$ and $D(t)$ follow the FORTRAN listing.

```
      PROGRAM SPLINE
C     ********************************************************
C     : COMPUTE THE CUBIC SPLINE FUNCTIONS WHICH BEST FIT THE DATA :
C     ********************************************************
      PARAMETER N0=47,N2=94
      DIMENSION A(N0,N2),AINV(N0,N0),ALPHA(4),H(N0),D(N0),F(6),
     1          H(N0),K(N0),X(N0),Y(N0)
      DOUBLE PRECISION A
      REAL K
      EQUIVALENCE (A,AINV)
      OPEN(UNIT=1,NAME='SPLINE.DDA',TYPE='NEW')
      OPEN(UNIT=2,NAME='SPLINE.OUT',TYPE='NEW')
C
      WRITE(5,10) N0
   10 FORMAT(//39H ENTER NUMBER OF DATA POINTS (MAXIMUM =,I3,2H):)
      READ(5,*) N
      IF (N .GT. N0) GOTO 9999
C
      WRITE(5,20)
   20 FORMAT(//47H ENTER X AND Y VECTORS, ONE DATA POINT PER LINE:)
      DO 1000 I=1,N
          READ(5,*) X(I),Y(I)
 1000 CONTINUE
C
C
      H(1)=0.
      D(1)=0.
C
      DO 1200 I=1,N
C         ZERO THE 'A' MATRIX
          DO 1100 J=1,2*N
              A(I,J)=0.
 1100     CONTINUE
C         LOAD THE IDENTITY MATRIX IN THE RIGHT HALF OF 'A'
          A(I,N+I)=1.
C
          IF (I .EQ. 1) GOTO 1200
              H(I)=X(I)-X(I-1)
              D(I)=(Y(I)-Y(I-1))/H(I)
 1200 CONTINUE
C     LOAD THE 'A' MATRIX AND THE 'B' VECTOR
      A(1,1)=2.
      A(1,2)=1.
      B(1)=3.*D(1)
      DO 1400 I=2,N-1
          A(I,I-1)=DBLE(H(I+1))
          A(I,I)=DBLE(2.*(H(I)+H(I+1)))
          A(I,I+1)=DBLE(H(I))
          B(I)=3.*(H(I+1)*D(I)+H(I)*D(I+1))
 1400 CONTINUE
      A(N,N-1)=1.
      A(N,N)=2.
      B(N)=3.*D(N)
C     INVERT THE LEFT HALF OF THE 'A' MATRIX
      CALL INV(A,AINV,N,2*N,N0,N2)
C
      WRITE(5,60)
   60 FORMAT(//49H ENTER NUMBER OF POINTS TO COMPUTE BETWEEN NODES:)
      READ(5,*) NSPLIN
C     COMPUTE THE K(I)'S
      CALL MULT(AINV,B,K,N,N,1,N0,N0,1)
C
      WRITE(5,70)
   70 FORMAT(//2X,1HI,4X,6HX(I-1),5X,9HF(X(I-1)),3X,10HF'(X(I-1)),2X,
     1        10HF"(X(I-1)),3X,7HF(X(I)),5X,8HF'(X(I)),4X,
     2        8HF"(X(I)),6X,4HA(3),7X,4HA(2),7X,4HA(1),7X,4HA(0)/
     3          2X,1H-,4X,6H-------,5X,9H---------,3X,10H----------,2X,
     4        10H----------,3X,7H-------,5X,8H--------,4X,
     5        8H---------,6X,4H----,3(7X,4H----)/)
C
      DO 1600 I=2,N
C         EVALUATE EXPRESSIONS TO COMPUTE THE CUBIC COEFFICIENTS
          C1=(K(I)+K(I-1)-2.*D(I))/(H(I)*H(I))
          C2=X(I)*X(I-1)
          C3=X(I)+X(I-1)
          C4=(K(I-1)-D(I))/H(I)
          C5=C1*X(I-1)
C         CALCULATE THE COEFFICIENTS OF THE CUBIC SPLINE
C         NOTE THAT A3 = ALPHA(1), A2 = ALPHA(2), A1 = ALPHA(3), ETC.
          ALPHA(1)=C1
          ALPHA(2)=-(C4+C1*(C3+X(I-1)))
          ALPHA(3)=D(I)+C3*(C4+C5)+C1*C2
          ALPHA(4)=(X(I)*Y(I-1)-X(I-1)*Y(I))/H(I)-C2*(C4+C5)
```

```
C          CALCULATE F(X) AT THE TWO SPLINE NODES
           F(1)=POLY(ALPHA,4,X(I-1))
           F(4)=POLY(ALPHA,4,X(I))
C          CALCULATE THE CUBIC SPLINE'S FIRST DERIVATIVE COEFFICIENTS
           ALPHA(1)=3.*ALPHA(1)
           ALPHA(2)=2.*ALPHA(2)
C          CALCULATE F'(X) AT THE TWO SPLINE NODES
           F(2)=POLY(ALPHA,3,X(I-1))
           F(5)=POLY(ALPHA,3,X(I))
C          CALCULATE THE CUBIC SPLINE'S SECOND DERIVATIVE COEFFICIENTS
           ALPHA(1)=2.*ALPHA(1)
C          CALCULATE F"(X) AT THE TWO SPLINE NODES
           F(3)=POLY(ALPHA,2,X(I-1))
           F(6)=POLY(ALPHA,2,X(I))
C          RESTORE THE COEFFICIENTS OF THE CUBIC SPLINE
           ALPHA(1)=ALPHA(1)/6.
           ALPHA(2)=ALPHA(2)/2.
C          TO TERMINAL
           WRITE(5,80) I-1,X(I-1),(F(J),J=1,6),(ALPHA(L),L=1,4)
    80     FORMAT(I4,E11.3,X,6E12.4,X,4E11.3)
C          TO GRAPHICS FILE
           WRITE(1,90) X(I-1),F(1)
    90     FORMAT(2E16.5)
C          TO COEFFICIENTS FILE
           WRITE(2,100) X(I-1),X(I),(ALPHA(5-L), L=1,4)
   100     FORMAT(6E16.8)
           DELTAX=(X(I)-X(I-1))/FLOAT(NSPLIN+1)
           DO 1500 J=1,NSPLIN
               X(I-1)=X(I-1)+DELTAX
               WRITE(1,90) X(I-1),POLY(ALPHA,4,X(I-1))
  1500     CONTINUE
  1600 CONTINUE
C
       WRITE(1,90) X(N),F(4)
  9999 CONTINUE
       CLOSE(UNIT=1,DISPOSE='SAVE')
       CLOSE(UNIT=2,DISPOSE='SAVE')
       END
C      ***************************************************************************
C      ***************************************************************************
       SUBROUTINE MULT(A,B,C,I,J,K,I0,J0,K0)
C      ************************
C      : MULTIPLY MATRICES:  C=A*B :
C      ************************
       DIMENSION A(I0,J0),B(J0,K0),C(I0,K0)
C
       DO 3 II=1,I
           DO 2 KK=1,K
               C(II,KK)=0.
               DO 1 JJ=1,J
                   C(II,KK)=C(II,KK)+A(II,JJ)*B(JJ,KK)
     1         CONTINUE
     2     CONTINUE
     3 CONTINUE
       RETURN
       END
C      ***************************************************************************
C      ***************************************************************************
       SUBROUTINE INV(A,AINV,N,M,N0,M0)
C      ********************
C      : INVERT MATRIX A :
C      ********************
C
C      ..........................................................
C      :                                                        :
C      : SUBROUTINE INV WAS ADAPTED FROM A BASIC PROGRAM IN APPENDIX J  :
C      : (INVERSE OF A MATRIX USING GAUSS-JORDAN ELIMINATION) OF THE    :
C      : TEXTBOOK 'COMPUTATIONAL LINEAR ALGEBRA WITH MODELS' BY GARETH  :
C      : WILLIAMS, SECOND EDITION, ALLYN & BACON, INC., BOSTON, 1978.   :
C      :........................................................:
C
       DIMENSION A(N0,M0),AINV(N0,N0)
       DOUBLE PRECISION A,T,Y,Z
C
       DO 125 K=1,N
           IF (A(K,K) .NE. 0.) GOTO 76
               DO 70 I=K+1,N
                   IF (A(I,K) .EQ. 0.) GOTO 70
                       DO 60 J=K,M
                           T=A(K,J)
                           A(K,J)=A(I,J)
                           A(I,J)=T
   60                  CONTINUE
```

```
                    GOTO 76
   70          CONTINUE
               GOTO 170
   76     IF (A(K,K) .EQ. 1.) GOTO 95
               Y=A(K,K)
               DO 90 L=K,M
                  A(K,L)=A(K,L)/Y
   90          CONTINUE
   95          DO 120 I=1,N
                  IF (I .EQ. K .OR. A(I,K) .EQ. 0.) GOTO 120
                     Z=A(I,K)
                     DO 115 J=K,M
                        A(I,J)=A(I,J)-Z*A(K,J)
  115                 CONTINUE
  120          CONTINUE
  125 CONTINUE
C
      DO 150 I=1,N
         DO 145 J=N+1,M
            AINV(I,J-N)=SNGL(A(I,J))
  145    CONTINUE
  150 CONTINUE
      GOTO 200
C
  170 WRITE(5,999)
  999 FORMAT(//27H THE INVERSE DOES NOT EXIST/)
C
  200 CONTINUE
      RETURN
      END
C     ***************************************************************
C     ***************************************************************
      FUNCTION POLY(A,N,X)
C     ********************************************
C     : COMPUTE THE (N-1)TH ORDER POLYNOMIAL F(X) :
C     ********************************************
C
C     A(1) IS THE COEFFICIENT OF THE (N-1)TH ORDER TERM
C     A(N) IS THE CONSTANT TERM
C
      DIMENSION A(N)
C
      SUM=A(1)*X
      IF (N .LE. 2) GOTO 2
         DO 1 I=2,N-1
            SUM=(SUM+A(I))*X
    1    CONTINUE
    2 POLY=SUM+A(N)
      RETURN
      END
```

```
>RUN SPLINE        (C)

ENTER NUMBER OF DATA POINTS (MAXIMUM = 47):
47


ENTER X AND Y VECTORS, ONE DATA POINT PER LINE
-0.400E+01  0.5460E-03
-0.220E+01  0.5390E-03
 0.000E+00  0.5290E-03
 0.500E+01  0.5090E-03
 0.150E+02  0.4610E-03
 0.250E+02  0.4120E-03
 0.350E+02  0.3740E-03
 0.450E+02  0.3380E-03
 0.550E+02  0.3110E-03
 0.650E+02  0.2940E-03
 0.750E+02  0.2770E-03
 0.850E+02  0.2660E-03
 0.950E+02  0.2570E-03
 0.145E+03  0.2240E-03
 0.195E+03  0.2040E-03
 0.295E+03  0.1850E-03
 0.395E+03  0.1710E-03
 0.495E+03  0.1610E-03
 0.600E+03  0.1560E-03
 0.700E+03  0.1520E-03
 0.800E+03  0.1480E-03
 0.900E+03  0.1450E-03
 0.100E+04  0.1430E-03
 0.150E+04  0.1340E-03
 0.200E+04  0.1290E-03
 0.300E+04  0.1230E-03
 0.500E+04  0.1190E-03
 0.750E+04  0.1160E-03
 0.100E+05  0.1144E-03
 0.150E+05  0.1122E-03
 0.200E+05  0.1112E-03
 0.300E+05  0.1106E-03
 0.500E+05  0.1096E-03
 0.750E+05  0.1086E-03
 0.100E+06  0.1081E-03
 0.150E+06  0.1073E-03
 0.200E+06  0.1067E-03
 0.300E+06  0.1059E-03
 0.500E+06  0.1050E-03
 0.750E+06  0.1041E-03
 0.100E+07  0.1035E-03
 0.150E+07  0.1026E-03
 0.200E+07  0.1020E-03
 0.300E+07  0.1012E-03
 0.500E+07  0.1004E-03
 0.750E+07  0.9955E-04
 0.100E+08  0.9895E-04


ENTER NUMBER OF POINTS TO COMPUTE BETWEEN NODES:
25
```

Table of Cubic Spline Functions for $C_s(t)$

I	X(I-1)	F(X(I-1))	F'(X(I-1))	F''(X(I-1))	F(X(I))	F'(X(I))	F''(X(I))	A(3)	A(2)	A(1)	A(0)
1	-0.400E+01	0.5460E-03	0.3153E-05	-0.1296E-04	0.5390E-03	-0.6307E-05	0.2452E-05	0.143E-05	0.106E-04	0.198E-04	0.546E-03
2	-0.220E+01	0.5390E-03	-0.6307E-05	0.2452E-05	0.5290E-03	-0.3720E-05	-0.1008E-06	-0.193E-06	-0.504E-07	-0.372E-05	0.529E-03
3	0.000E+00	0.5290E-03	-0.3720E-05	-0.1008E-06	0.5090E-03	-0.4308E-05	-0.1342E-06	-0.111E-08	-0.504E-07	-0.372E-05	0.529E-03
4	0.500E+01	0.5090E-03	-0.4308E-05	-0.1342E-06	0.4610E-03	-0.5114E-05	-0.2713E-07	0.178E-08	-0.938E-07	-0.350E-05	0.529E-03
5	0.150E+02	0.4610E-03	-0.5114E-05	-0.2713E-07	0.4120E-03	-0.4336E-05	0.1827E-06	0.350E-08	-0.171E-06	-0.235E-05	0.523E-03
6	0.250E+02	0.4120E-03	-0.4336E-05	0.1827E-06	0.3740E-03	-0.3641E-05	-0.4356E-07	-0.377E-08	0.374E-06	-0.160E-04	0.636E-03
7	0.350E+02	0.3740E-03	-0.3641E-05	-0.4356E-07	0.3380E-03	-0.3301E-05	0.1116E-06	0.259E-08	-0.293E-06	0.739E-05	0.364E-03
8	0.450E+02	0.3380E-03	-0.3301E-05	0.1116E-06	0.3110E-03	-0.2057E-05	0.1372E-06	0.427E-09	-0.192E-08	-0.573E-05	0.561E-03
9	0.550E+02	0.3110E-03	-0.2057E-05	0.1372E-06	0.2940E-03	-0.1673E-05	-0.6051E-07	-0.330E-08	0.612E-06	-0.395E-04	0.118E-02
10	0.650E+02	0.2940E-03	-0.1673E-05	-0.6051E-07	0.2770E-03	-0.1451E-05	0.1048E-06	0.276E-08	-0.568E-06	0.372E-04	-0.482E-03
11	0.750E+02	0.2770E-03	-0.1451E-05	0.1048E-06	0.2660E-03	-0.9211E-06	0.1284E-08	-0.173E-08	0.441E-06	-0.384E-04	0.141E-02
12	0.850E+02	0.2660E-03	-0.9210E-06	0.1284E-08	0.2570E-03	-0.8643E-06	0.1006E-07	0.146E-09	-0.367E-07	0.214E-05	0.259E-03
13	0.950E+02	0.2570E-03	-0.8643E-06	0.1006E-07	0.2240E-03	-0.5029E-06	0.4396E-08	-0.189E-10	0.104E-07	-0.233E-05	0.401E-03
14	0.145E+03	0.2240E-03	-0.5029E-06	0.4396E-08	0.2040E-03	-0.3041E-06	0.3555E-08	-0.280E-11	0.342E-08	-0.132E-05	0.352E-03
15	0.195E+03	0.2040E-03	-0.3041E-06	0.3555E-08	0.1850E-03	-0.1396E-06	-0.2643E-09	-0.637E-11	0.550E-08	-0.172E-05	0.378E-03
16	0.295E+03	0.1850E-03	-0.1396E-06	-0.2643E-09	0.1710E-03	-0.1277E-06	0.5017E-09	0.128E-11	-0.126E-08	0.272E-06	0.182E-03
17	0.395E+03	0.1710E-03	-0.1277E-06	0.5017E-09	0.1610E-03	-0.6972E-07	0.6577E-09	0.260E-12	-0.573E-10	-0.204E-06	0.245E-03
18	0.495E+03	0.1610E-03	-0.6972E-07	0.6577E-09	0.1560E-03	-0.3795E-07	-0.5257E-10	-0.113E-11	0.200E-08	-0.122E-05	0.413E-03
19	0.600E+03	0.1560E-03	-0.3795E-07	-0.5257E-10	0.1520E-03	-0.4147E-07	-0.1786E-10	0.578E-13	-0.130E-09	0.561E-07	0.157E-03
20	0.700E+03	0.1520E-03	-0.4147E-07	-0.1786E-10	0.1480E-03	-0.3616E-07	0.1240E-09	0.236E-12	-0.506E-09	0.319E-06	0.955E-04
21	0.800E+03	0.1480E-03	-0.3616E-07	0.1240E-09	0.1450E-03	-0.2387E-07	0.1218E-09	-0.378E-14	0.711E-10	-0.143E-06	0.219E-03
22	0.900E+03	0.1450E-03	-0.2387E-07	0.1218E-09	0.1430E-03	-0.1834E-07	-0.1105E-10	-0.221E-12	0.659E-09	-0.671E-06	0.377E-03
23	0.100E+04	0.1430E-03	-0.1834E-07	-0.1105E-10	0.1340E-03	-0.1456E-07	0.2616E-10	0.124E-13	-0.427E-10	0.299E-07	0.143E-03
24	0.150E+04	0.1340E-03	-0.1456E-07	0.2616E-10	0.1290E-03	-0.7421E-08	0.2392E-11	-0.792E-14	0.487E-10	-0.107E-06	0.212E-03
25	0.200E+04	0.1290E-03	-0.7421E-08	0.2392E-11	0.1230E-03	-0.4354E-08	0.3742E-11	0.225E-15	-0.154E-12	-0.951E-08	0.147E-03
26	0.300E+04	0.1230E-03	-0.4354E-08	0.3742E-11	0.1190E-03	-0.1034E-08	-0.4222E-12	-0.347E-15	0.499E-11	-0.249E-07	0.162E-03
27	0.500E+04	0.1190E-03	-0.1034E-08	-0.4222E-12	0.1160E-03	-0.1004E-08	0.4462E-12	0.579E-16	-0.108E-11	0.542E-08	0.112E-03
28	0.750E+04	0.1160E-03	-0.1004E-08	0.4462E-12	0.1144E-03	-0.4695E-09	-0.1852E-13	-0.310E-16	0.920E-12	-0.958E-08	0.149E-03
29	0.100E+05	0.1144E-03	-0.4695E-09	-0.1852E-13	0.1122E-03	-0.3346E-09	0.7248E-13	0.303E-17	-0.100E-12	0.626E-09	0.115E-03
30	0.150E+05	0.1122E-03	-0.3346E-09	0.7248E-13	0.1112E-03	-0.1119E-09	0.1660E-13	-0.186E-17	0.120E-12	-0.268E-08	0.132E-03
31	0.200E+05	0.1112E-03	-0.1119E-09	0.1660E-13	0.1106E-03	-0.3916E-10	-0.2048E-14	-0.311E-18	0.270E-13	-0.817E-09	0.119E-03
32	0.300E+05	0.1106E-03	-0.3916E-10	-0.2048E-14	0.1096E-03	-0.5120E-10	0.8439E-15	0.241E-19	-0.319E-14	0.874E-10	0.110E-03
33	0.500E+05	0.1096E-03	-0.5120E-10	0.8439E-15	0.1086E-03	-0.2815E-10	0.1001E-14	0.104E-20	0.265E-15	-0.856E-10	0.113E-03
34	0.750E+05	0.1086E-03	-0.2815E-10	0.1001E-14	0.1081E-03	-0.1622E-10	-0.4638E-16	-0.698E-20	0.207E-14	-0.221E-09	0.116E-03
35	0.100E+06	0.1081E-03	-0.1622E-10	-0.4638E-16	0.1073E-03	-0.1441E-10	0.1188E-15	0.551E-21	-0.188E-15	0.494E-11	0.109E-03
36	0.150E+06	0.1073E-03	-0.1441E-10	0.1188E-15	0.1067E-03	-0.1016E-10	0.5114E-16	-0.226E-21	0.161E-15	-0.475E-10	0.112E-03
37	0.200E+06	0.1067E-03	-0.1016E-10	0.5114E-16	0.1059E-03	-0.6241E-11	0.2719E-16	-0.399E-22	0.495E-16	-0.252E-10	0.110E-03
38	0.300E+06	0.1059E-03	-0.6241E-11	0.2719E-16	0.1050E-03	-0.3737E-11	-0.2149E-17	-0.245E-22	0.356E-16	-0.210E-10	0.110E-03
39	0.500E+06	0.1050E-03	-0.3737E-11	-0.2149E-17	0.1041E-03	-0.3058E-11	0.7581E-17	0.649E-23	-0.108E-16	0.220E-11	0.106E-03
40	0.750E+06	0.1041E-03	-0.3058E-11	0.7581E-17	0.1035E-03	-0.2032E-11	0.6241E-18	-0.464E-23	0.142E-16	-0.166E-10	0.110E-03
41	0.100E+07	0.1035E-03	-0.2032E-11	0.6241E-18	0.1026E-03	-0.1492E-11	0.1537E-17	0.304E-24	-0.601E-18	-0.174E-11	0.106E-03
42	0.150E+07	0.1026E-03	-0.1492E-11	0.1537E-17	0.1020E-03	-0.1001E-11	0.4278E-18	-0.370E-24	0.243E-17	-0.629E-11	0.108E-03
43	0.200E+07	0.1020E-03	-0.1001E-11	0.4278E-18	0.1012E-03	-0.6127E-12	0.3480E-18	-0.133E-25	0.294E-18	-0.202E-11	0.105E-03
44	0.300E+07	0.1012E-03	-0.6127E-12	0.3480E-18	0.1004E-03	-0.3227E-12	-0.5804E-19	-0.338E-25	0.479E-18	-0.257E-11	0.106E-03
45	0.500E+07	0.1004E-03	-0.3227E-12	-0.5804E-19	0.9955E-04	-0.3021E-12	0.7451E-19	0.884E-26	-0.162E-18	0.630E-12	0.100E-03
46	0.750E+07	0.9955E-04	-0.3021E-12	0.7451E-19	0.9895E-04	-0.2090E-12	-0.2585E-25	-0.497E-26	0.149E-18	-0.170E-11	0.106E-03

```
>RUN SPLINE      (D)

ENTER NUMBER OF DATA POINTS (MAXIMUM = 47):
47


ENTER X AND Y VECTORS, ONE DATA POINT PER LINE
-0.400E+01  0.1520E-03
-0.220E+01  0.1510E-03
 0.000E+00  0.1480E-03
 0.500E+01  0.1430E-03
 0.150E+02  0.1310E-03
 0.250E+02  0.1180E-03
 0.350E+02  0.1070E-03
 0.450E+02  0.9670E-04
 0.550E+02  0.8890E-04
 0.650E+02  0.8270E-04
 0.750E+02  0.7810E-04
 0.850E+02  0.7510E-04
 0.950E+02  0.7220E-04
 0.145E+03  0.6180E-04
 0.195E+03  0.5560E-04
 0.295E+03  0.4940E-04
 0.395E+03  0.4500E-04
 0.495E+03  0.4200E-04
 0.600E+03  0.4020E-04
 0.700E+03  0.3910E-04
 0.800E+03  0.3790E-04
 0.900E+03  0.3710E-04
 0.100E+04  0.3620E-04
 0.150E+04  0.3360E-04
 0.200E+04  0.3190E-04
 0.300E+04  0.3040E-04
 0.500E+04  0.2890E-04
 0.750E+04  0.2790E-04
 0.100E+05  0.2739E-04
 0.150E+05  0.2672E-04
 0.200E+05  0.2644E-04
 0.300E+05  0.2633E-04
 0.500E+05  0.2597E-04
 0.750E+05  0.2564E-04
 0.100E+06  0.2550E-04
 0.150E+06  0.2527E-04
 0.200E+06  0.2509E-04
 0.300E+06  0.2486E-04
 0.500E+06  0.2459E-04
 0.750E+06  0.2432E-04
 0.100E+07  0.2414E-04
 0.150E+07  0.2387E-04
 0.200E+07  0.2369E-04
 0.300E+07  0.2347E-04
 0.500E+07  0.2325E-04
 0.750E+07  0.2299E-04
 0.100E+08  0.2282E-04


ENTER NUMBER OF POINTS TO COMPUTE BETWEEN NODES:
25
```

Table of Cubic Spline Functions for D(t)

I	X(I-1)	F[X(I-1)]	F'[X(I-1)]	F''[X(I-1)]	F[X(I)]	F'[X(I)]	F''[X(I)]	A(3)	A(2)	A(1)	A(0)
1	-0.400E+01	0.1520E-03	0.6301E-06	-0.1852E-05	0.1510E-03	-0.1260E-05	-0.2486E-06	0.148E-06	0.855E-06	0.348E-06	0.149E-03
2	-0.220E+01	0.1510E-03	-0.1260E-05	-0.2486E-06	0.1480E-03	-0.1297E-05	0.2153E-06	0.351E-07	0.108E-06	-0.130E-05	0.148E-03
3	0.000E+00	0.1480E-03	-0.1297E-05	0.2153E-06	0.1430E-03	-0.9445E-06	-0.7434E-07	-0.965E-08	0.108E-06	-0.130E-05	0.148E-03
4	0.500E+01	0.1430E-03	-0.9445E-06	-0.7434E-07	0.1310E-03	-0.1339E-05	-0.4632E-08	0.116E-08	-0.546E-07	-0.486E-06	0.147E-03
5	0.150E+02	0.1310E-03	-0.1339E-05	-0.4631E-08	0.1180E-03	-0.1198E-05	0.3287E-07	0.625E-09	-0.304E-07	-0.848E-06	0.148E-03
6	0.250E+02	0.1180E-03	-0.1198E-05	0.3287E-07	0.1070E-03	-0.1068E-05	-0.6839E-08	-0.662E-09	0.661E-07	-0.326E-05	0.169E-03
7	0.350E+02	0.1070E-03	-0.1068E-05	-0.6839E-08	0.9670E-04	-0.9198E-06	0.3649E-07	0.722E-09	-0.792E-07	0.183E-05	0.109E-03
8	0.450E+02	0.9670E-04	-0.9198E-06	0.3649E-07	0.8890E-04	-0.6829E-06	0.1088E-07	-0.427E-09	0.759E-07	-0.515E-05	0.214E-03
9	0.550E+02	0.8890E-04	-0.6829E-06	0.1088E-07	0.8270E-04	-0.5486E-06	0.1598E-07	0.849E-10	-0.857E-08	-0.511E-06	0.129E-03
10	0.650E+02	0.8270E-04	-0.5486E-06	0.1598E-07	0.7810E-04	-0.3627E-06	0.2120E-07	0.871E-10	-0.899E-08	-0.483E-06	0.128E-03
11	0.750E+02	0.7810E-04	-0.3627E-06	0.2120E-07	0.7510E-04	-0.2806E-06	-0.4794E-08	-0.433E-09	0.108E-06	-0.926E-05	0.348E-03
12	0.850E+02	0.7510E-04	-0.2806E-06	-0.4794E-08	0.7220E-04	-0.2848E-06	0.3972E-08	0.146E-09	-0.397E-07	0.329E-05	-0.808E-05
13	0.950E+02	0.7220E-04	-0.2848E-06	0.3972E-08	0.6180E-04	-0.1538E-06	0.1267E-08	-0.902E-11	0.456E-08	-0.906E-06	0.125E-03
14	0.145E+03	0.6180E-04	-0.1538E-06	0.1267E-08	0.5560E-04	-0.9609E-07	0.1041E-08	-0.751E-12	0.960E-09	-0.385E-06	0.997E-04
15	0.195E+03	0.5560E-04	-0.9609E-07	0.1041E-08	0.4940E-04	-0.4589E-07	-0.3743E-10	-0.180E-11	0.157E-08	-0.504E-06	0.107E-03
16	0.295E+03	0.4940E-04	-0.4589E-07	-0.3743E-10	0.4500E-04	-0.3834E-07	0.1884E-09	0.376E-12	-0.352E-09	0.634E-07	0.516E-04
17	0.395E+03	0.4500E-04	-0.3834E-07	0.1884E-09	0.4200E-04	-0.2273E-07	0.1240E-09	-0.107E-12	0.221E-09	-0.163E-06	0.815E-04
18	0.495E+03	0.4200E-04	-0.2273E-07	0.1240E-09	0.4020E-04	-0.1248E-07	0.7127E-10	-0.836E-13	0.186E-09	-0.146E-06	0.786E-04
19	0.600E+03	0.4020E-04	-0.1248E-07	0.7127E-10	0.3910E-04	-0.1161E-07	-0.5379E-10	-0.208E-12	0.411E-09	-0.280E-06	0.106E-03
20	0.700E+03	0.3910E-04	-0.1161E-07	-0.5379E-10	0.3790E-04	-0.1010E-07	0.8388E-10	0.229E-12	-0.509E-09	0.363E-06	-0.447E-04
21	0.800E+03	0.3790E-04	-0.1010E-07	0.8388E-10	0.3710E-04	-0.7993E-08	-0.4173E-10	-0.209E-12	0.544E-09	-0.479E-06	0.180E-03
22	0.900E+03	0.3710E-04	-0.7993E-08	-0.4173E-10	0.3620E-04	-0.8927E-08	0.2305E-10	0.108E-12	-0.312E-09	0.292E-06	-0.513E-04
23	0.100E+04	0.3620E-04	-0.8927E-08	0.2305E-10	0.3360E-04	-0.3507E-08	-0.1368E-11	-0.814E-14	0.359E-10	-0.564E-07	0.648E-04
24	0.150E+04	0.3360E-04	-0.3507E-08	-0.1368E-11	0.3190E-04	-0.2843E-08	0.4026E-11	0.180E-14	-0.878E-11	0.107E-07	0.313E-04
25	0.200E+04	0.3190E-04	-0.2843E-08	0.4026E-11	0.3040E-04	-0.8266E-09	0.7499E-14	-0.670E-15	0.603E-11	-0.189E-07	0.510E-04
26	0.300E+04	0.3040E-04	-0.8266E-09	0.7499E-14	0.2890E-04	-0.6044E-09	0.2147E-12	0.173E-16	-0.152E-12	-0.383E-09	0.324E-04
27	0.500E+04	0.2890E-04	-0.6044E-09	0.2147E-12	0.2790E-04	-0.2597E-09	0.6104E-13	-0.102E-16	0.261E-12	-0.245E-08	0.359E-04
28	0.750E+04	0.2790E-04	-0.2597E-09	0.6104E-13	0.2739E-04	-0.1690E-09	0.1153E-13	-0.330E-17	0.105E-12	-0.127E-08	0.330E-04
29	0.100E+05	0.2739E-04	-0.1690E-09	0.1153E-13	0.2672E-04	-0.9291E-10	0.1889E-13	0.245E-18	-0.159E-14	-0.211E-09	0.294E-04
30	0.150E+05	0.2672E-04	-0.9291E-10	0.1889E-13	0.2644E-04	-0.2939E-10	0.6525E-14	-0.412E-18	0.280E-13	-0.654E-09	0.316E-04
31	0.200E+05	0.2644E-04	-0.2939E-10	0.6525E-14	0.2633E-04	-0.6848E-11	-0.2017E-14	-0.142E-18	0.118E-13	-0.331E-09	0.295E-04
32	0.300E+05	0.2633E-04	-0.6848E-11	-0.2017E-14	0.2597E-04	-0.2014E-10	0.6880E-15	0.225E-19	-0.304E-14	0.115E-09	0.250E-04
33	0.500E+05	0.2597E-04	-0.2014E-10	0.6880E-15	0.2564E-04	-0.7929E-11	0.2885E-15	-0.266E-20	0.744E-15	-0.745E-10	0.282E-04
34	0.750E+05	0.2564E-04	-0.7929E-11	0.2885E-15	0.2550E-04	-0.4548E-11	-0.1801E-16	-0.204E-20	0.604E-15	-0.640E-10	0.279E-04
35	0.100E+06	0.2550E-04	-0.4548E-11	-0.1801E-16	0.2527E-04	-0.4254E-11	0.2978E-16	0.159E-21	-0.568E-16	0.203E-11	0.257E-04
36	0.150E+06	0.2527E-04	-0.4254E-11	0.2978E-16	0.2509E-04	-0.3037E-11	0.1889E-16	-0.363E-22	0.312E-16	-0.112E-10	0.264E-04
37	0.200E+06	0.2509E-04	-0.3037E-11	0.1889E-16	0.2486E-04	-0.1771E-11	0.6427E-17	-0.208E-22	0.219E-16	-0.931E-11	0.262E-04
38	0.300E+06	0.2486E-04	-0.1771E-11	0.6427E-17	0.2459E-04	-0.1151E-11	-0.2294E-18	-0.555E-23	0.821E-17	-0.520E-11	0.258E-04
39	0.500E+06	0.2459E-04	-0.1151E-11	-0.2294E-18	0.2432E-04	-0.9092E-12	0.2164E-17	0.160E-23	-0.251E-17	0.161E-12	0.249E-04
40	0.750E+06	0.2432E-04	-0.9092E-12	0.2164E-17	0.2414E-04	-0.6122E-12	0.2116E-18	-0.130E-23	0.401E-17	-0.473E-11	0.262E-04
41	0.100E+07	0.2414E-04	-0.6122E-12	0.2116E-18	0.2387E-04	-0.4485E-12	0.4429E-18	0.771E-25	-0.125E-18	-0.593E-12	0.248E-04
42	0.150E+07	0.2387E-04	-0.4485E-12	0.4429E-18	0.2369E-04	-0.2936E-12	0.1768E-18	-0.887E-25	0.621E-18	-0.171E-11	0.253E-04
43	0.200E+07	0.2369E-04	-0.2936E-12	0.1768E-18	0.2347E-04	-0.1611E-12	0.8828E-19	-0.147E-25	0.177E-18	-0.824E-12	0.247E-04
44	0.300E+07	0.2347E-04	-0.1611E-12	0.8828E-19	0.2325E-04	-0.9606E-13	-0.2323E-19	-0.929E-26	0.128E-18	-0.677E-12	0.246E-04
45	0.500E+07	0.2325E-04	-0.9606E-13	-0.2323E-19	0.2299E-04	-0.9084E-13	0.2741E-19	0.338E-26	-0.623E-19	0.273E-12	0.230E-04
46	0.750E+07	0.2299E-04	-0.9084E-13	0.2741E-19	0.2282E-04	-0.5658E-13	-0.1292E-25	-0.183E-26	0.548E-19	-0.605E-12	0.252E-04

APPENDIX 9C

Computer Program SURMF

SURMF calculates the total surface mass flux from the spherical waste canister (see chapter 8 for theoretical development). The data created by SPLINE (see Appendix 9B are used as input to SURMF. In SURMF the input data are again interpolated to increase the number of data points being used in the calculation of the total surface mass flux by routines called SPLIFT, SPLINT and SPLIQ. These three routines are obtainable from the SANDIA Mathematics Library which is one of the Background Mathematics Libraries at LBL. SPLIFT computes the parameters of an exact spline fit to data. Then SPLINT interpolates values on a spline using parameters from SPLIFT. And SPLIQ integrates a cubic spline defined by SPLIFT or SPLINT. Besides the routines from SANDIA one more subroutine CONVOL is included in this program. CONVOL calculates the convolution integral (see equation (5.7)) by method explained in Section 5. List of $\dot{M}_{NP-237}(t)$ obtained from this program follow the FORTRAN listing. In the next page the symbols used in SURMF are explained.

Symbols Used in SURMF

T	Array of abscissas (actually time in increasing order) that define the spline.
F	Array of ordinates that define the spline. See eq. 10 in chapter 8 and eq. (5.1) for definitions.
FP	Array of first derivatives of F at abscissas T.
FPP	Array of second derivatives of F at T.
G	Array of ordinates that define the spline. See eq. 5, ch. 8 and (5.2) for definition and details.
GP	Array of first derivatives of G at abscissas T.
GPP	Array of second derivatives of G at T.
N	The number of data points. The arrays F, G, FP, GP, FPP, GPP must be dimensioned at least N. ($N \geq 4$).
W	Array of working storage dimensioned at least 3N used in routine SPLIFT.
ISX	Must be zero on the initial call to SPLIFT. If a spline is to be fitted to a second set of data that has the same set of abscissas as a previous set, ISX may be set to 1 for faster execution.
A1, B1, AN, BN	Specify the end conditions for the spline determined by the routine SPLIFT. The end condition constraints are FPP(i) = A1 * FPP(2) + B1 FPP(n) = AN*FPP(N-1) + BN where $\|A1\| < 1$ and $\|AN\| < 1$.
TLO	Left end point of integration intervals in the routine SPLIQ.

TUP	Array of abscissas (in arbitrary order) at which the spline is to be evaluated by the routine SPLINT. At the same time it is the array of right end points of integration intervals used in the routine SPLIQ.
NUP	The number of right end points in the routine SPLIQ. Same as the number of abscissas at which the spline is to be evaluated by the routine SLINT.
ANS	Array of integral values, that is, ANS(I) = integral of G from TLO to TUP(I).
TAU	Array of dimensionless times defined by eq. 12 of ch. 8.
FI	Array of values of the spline F at TUP.
FPI	Array of values of the first derivative of spline F at TUP.
FPPI	Array of values of the second derivative of spline F at TUP.
GI	Array of values of the spline G at TUP.
GPI	Array of values of the first derivative of spline G at TUP.
GPPI	Array of values of the second derivative of spline G at TUP.
FPT	Array of values of the first derivative of spline F at TAU which is to be used by subroutine CONVOL.
Fϕ	Value of the spline F at time t = 0.
FPϕ	Value of the first derivative of spline F at dimensionless time $\tau = 0$ (see eq. 12 of ch. 8 for definition of τ).
Dϕ	D_o defined by equation (x.5).
CSϕ	C_{so} defined by equation (x.12).

EPS	The porosity of the surrounding medium.
R	The radius of the spherical waste canister.
COEFK	Retardation factor.
FLUX	The total mass flux from the entire sphere surface expressed by eq. 28 in chapter 8.
CONVIN	The convolution integral used in eq. 28, chap. 8.
CUMFL	The accumulated mass flux since the beginning of dissolution.

```
**PROGRAM SURMFO1(INPUT,OUTPUT,TAPE5=INPUT,TAPE6=OUTPUT)**

PROGRAM SURMFC1(INPUT,OUTPUT,TAPE5=INPUT,TAPE6=OUTPUT)

      DIMENSION OF ARRAYS FOR SPLIQ AND SPLIFT

      PARAMETER N=47,NUP=64
      DIMENSION T(N),G(N),GP(N),GPP(N),TUP(NUP),ANS(NUP)
      DIMENSION F(N),FP(N),FPP(N),FI(NUP),FPI(NUP),FPPI(NUP)
      DIMENSION GI(NUP),GPI(NUP),GPPI(NUP)
      DIMENSION W(N,3),TAU(NUP),FPT(NUP)
      COMMON/CAL/FPO
      DATA PAI/3.1415926535/

      SET VARIABLES NEEDED FOR SPLIQ

      TLO=C.
      READ(5,500) DO,CSO,EPS,R,COEFK
  500 FORMAT(5F10.0)
      WRITE(6,610) DO,CSO,EPS,R,COEFK,NUP
  610 FORMAT(1H1,4HDO =F8.0,7HCM**2/S,/,5H CSO=,  E8.1,7HG/CM**3,/,
     1       5H EPS=,F8.3,/,5H R. =,F8.3,2HCM,/,5H K  =,F8.0,/,
     2       2CH NO OF CALCULATIONS: ,I3)
      READ(5,501) (T(I),G(I),F(I),I=1,N)
  501 FORMAT(3F10.0)
      NO=0
      DO 10 L=1,8
      DO 10 LL=1,9
      FL=LL
      TM=1.*10.**(L-1)*FL
      NC=NC+1
      TUP(NO)=TM
      IF(NC.EQ.NUP) GO TO 11
   10 CONTINUE

         SET VARIABLES FOR SPLIFT AND THEN CALL SPLIFT TO
                  OBTAIN THE OTHER NEEDED INPUT FOR SPLIQ

   11 ISX=0
      A1=0.
      B1=C.
      AN=0.
      BN=C.
      CALL SPLIFT(T,G,GP,GPP,N,W,IERR1,ISX,A1,B1,AN,BN)
      IF(IERR1.EQ.1) GO TO 20
      PRINT 600
  600 FORMAT(/1X,30HMISTAKE MADE IN SPLIFT ABOUT G)
   20 CONTINUE
      CALL SPLIQ(T,G,GP,GPP,N,TLO,TUP,NUP,ANS,IERR2)
      IF(IERR2.EQ.1) GO TO 30
      PRINT 601
  601 FORMAT(/1X,21HMISTAKE MADE IN SPLIQ)
   30 CONTINUE
      CALL SPLINT(T,G,GPP,N,TUP,GI,GPI,GPPI,NUP,IERR3)
      IF(IERR3.EQ.1) GO TO 40
      PRINT 602, IERR3
  602 FORMAT(/1X,6HIERR3=,I3)
   40 CONTINUE

         A SPLINE IS TO BE FITTED TO A SECOND SET OF DATA
```

```
**FFCCFAM SURMFO1(INPUT,OUTPUT,TAPE5=INPUT,TAPE6=OUTPUT)**

                    THAT HAS THE SAME SET CF ABSCISSAS
      ISX=1
      CALL SPLIFT(T,F,FP,FPP,N,W,IERR1,ISX,A1,B1,AN,BN)
      IF(IERR1.EQ.1) GC TO 5C
      PRINT 603
  603 FCRMAT(/1X,30HMISTAKE MADE IN SPLIFT ABOUT F)
   5C CONTINUE
      CALL SPLINT(T,F,FPP,N,TUP,FI,FPI,FPPI,NUP,IERR4)
      IF(IERR4.EQ.1) GC TO 60
      PRINT 6C4, IERR4
  604 FCRMAT(/1X,6HIERR4=,I3)
   6C CONTINUE
C          FO=F(TIME T = 0+ YEAR)
C          FPO=F'(TIME T = 0+ YEAR)
      FO=F(3)
      FPO=FP(3)
      PRINT 62C
  620 FORMAT(4(/),4X,1HT,15X,3HTAU,10X,4HF(T), 9X,5HF'(T),8X,6HF''(T),
     1                                 10X,4HG(T), 9X,5HG'(T),8X,6HG''(T),
     2                                 2X,12HSURFACE FLUX,11H CUMMU.FLUX,
     3            /4X,1H-,15X,3(1H-),1CX,4(1H-), 9X,5(1H-),8X,6(1H-),
     4                                  10X,4(1H-), 9X,5(1H-),8X,6(1H-),
     5                                  2X,12(1H-),1X,10(1H-))
      FLUXC=4.*PAI*R*DO*CSO*EPS*365.25*24.*36CC.
      CCNST=CO/CCEFK/(R**2)*365.25*3600.*24.
C
C          CALCULATE THE FIRST DELIVATIVE OF F IN TAU.
      DC 90 LN=1,NUP
      FPT(LN)=FPI(LN)/CONST/GI(LN)
   90 CCNTINUE
      FPC=FPC/CCNST/G(3)
C
C          CALCULATE STEADY-STATE SURFACE MASS FLUX AND
C                    TIME-DEPENDENT SURFACE MASS FLUX.
C
      DC 100 J=1,NUP
      TAU(J)=CCNST*ANS(J)
      CALL CONVOL(FPT,TAU,J,NUP,CONVIN)
      FLUX=FLUXO*GI(J)*(FI(J)+(FO/SQRT(TAU(J))+CONVIN)/SQRT(PAI))
      IF(J.EQ.1) GC TC 1C1
      CUMFL=CUMFL+(FLUX+FMEMO)/2.*(TUP(J)-TUP(J-1))
      GC TC 1C2
  1C1 CUMFL=FLUX*TUP(1)
  1C2 FMEMC=FLUX
      WRITE(6,630) TUP(J),TAU(J),FI(J),FPI(J),FPPI(J),GI(J),GPI(J),
     *             GPPI(J),FLUX,CUMFL
  630 FCRMAT(1X,1PE8.2,8E14.5,E11.3)
  1CC CONTINUE
      STOP
      END
```

```
**SUBROUTINE CONVOL(FPT,TAU,KK,NUP,CONVIN)**

      SUBROUTINE CONVOL(FPT,TAU,KK,NUP,CONVIN)
      DIMENSION FPT(NUP),TAU(NUP)
      COMMON/CAL/FPO
      SUM=0.
      DO 200 II=1,KK
      IF(II.NE.1) GO TO 201
      IF(II.EQ.KK) GO TO 203
      SUM=SUM+(FPT(1)/SQRT(TAU(KK)-TAU(1))+FPO/SQRT(TAU(KK)))*.5*TAU(1)
      GO TO 200
  203 SUM=SUM+(FPT(1)+FPO)*SQRT(TAU(1))
      GO TO 200
  201 IF(II.EQ.KK) GO TO 202
      SUM=SUM+(FPT(II)/SQRT(TAU(KK)-TAU(II))+FPT(II-1)/SQRT(TAU(KK)-TAU(
     * II-1)))*.5*(TAU(II)-TAU(II-1))
      GO TO 200

              REMOVAL OF SINGULARITY

  202 SUM=SUM+(FPT(KK)+FPT(KK-1))*SQRT(TAU(KK)-TAU(KK-1))
  200 CONTINUE
      CONVIN=SUM
      RETURN
      END
```

```
DO =        1.   CM**2/S
CSO=    .1E+C1   G/CM**3
EPS=      .010
R  =    42.C4C   CM
K  =        1.
NO OF CALCULATIONS: 64
```

(For SIO_2)

STEADY STATE SURFACE MASS FLUX = 0.376 g/y

TIME ELAPSED [y]	SURFACE MASS FLUX [g/y]	TOTAL MASS DISSOLUTION [g]
1.00E+00	1.72628E+01	1.726E+01
2.00E+00	1.57110E+01	3.375E+01
3.00E+00	1.49258E+01	4.9C7E+C1
4.00E+00	1.43884E+01	6.373E+01
5.00E+00	1.395S9E+C1	7.7SCE+01
6.00E+00	1.35828E+01	9.167E+01
7.CCE+00	1.32344E+01	1.051E+02
8.00E+00	1.29042E+01	1.181E+02
9.00E+00	1.25863E+01	1.309E+02
1.00E+01	1.22776E+01	1.433E+02
2.00E+01	9.58371E+00	2.526E+02
3.00E+01	7.65706E+00	3.388E+02
4.00E+01	6.20799E+00	4.082E+C2
5.00E+01	5.08211E+00	4.646E+02
6.00E+01	4.39CC7E+CC	5.12CE+02
7.00E+01	3.87296E+00	5.533E+02
8.00E+01	3.50121E+00	5.902E+02
9.00E+01	3.25750E+00	6.240E+02
1.00E+02	3.02671E+00	6.554E+02
2.00E+02	1.87268E+0C	9.0C3E+02
3.00E+02	1.52357E+00	1.070E+03
4.00E+02	1.28343E+00	1.211E+03
5.00E+02	1.13079E+CC	1.331E+03
6.00E+02	1.05531E+00	1.441E+03
7.00E+02	1.C0049E+CC	1.543E+03
8.00E+02	9.43787E-01	1.641E+03
9.CCE+02	9.05229E-01	1.733E+03
1.00E+03	8.71429E-01	1.822E+03
2.00E+03	6.92CC5E-01	2.604E+03
3.00E+03	6.28613E-01	3.264E+03
4.00E+03	5.97719E-01	3.877E+03
5.00E+03	5.77932E-01	4.465E+03
6.00E+03	5.61856E-01	5.035E+C3
7.00E+03	5.48694E-01	5.590E+03
8.COE+03	5.38747E-01	6.134E+C3
9.00E+03	5.31533E-01	6.669E+03

TIME ELAPSED [y]	SURFACE MASS FLUX [g/y]	TOTAL MASS DISSOLUTION [g]
1.00E+04	5.25741E-01	7.198E+03
2.00E+04	4.92589E-01	1.229E+04
3.00E+04	4.87574E-01	1.719E+04
4.00E+04	4.82561E-01	2.204E+04
5.00E+04	4.76147E-01	2.683E+04
6.00E+04	4.70882E-01	3.157E+04
7.00E+04	4.67027E-01	3.626E+04
8.00E+04	4.64287E-01	4.092E+04
9.00E+04	4.62316E-01	4.555E+04
1.00E+05	4.60705E-01	5.016E+04
2.00E+05	4.47113E-01	9.555E+04
3.00E+05	4.39554E-01	1.399E+05
4.00E+05	4.34697E-01	1.836E+05
5.00E+05	4.30948E-01	2.269E+05
6.00E+05	4.27352E-01	2.698E+05
7.00E+05	4.23978E-01	3.124E+05
8.00E+05	4.21133E-01	3.546E+05
9.00E+05	4.18847E-01	3.966E+05
1.00E+06	4.16879E-01	4.384E+05
2.00E+06	4.03083E-01	8.484E+05
3.00E+06	3.96167E-01	1.248E+06
4.00E+06	3.92172E-01	1.642E+06
5.00E+06	3.89311E-01	2.033E+06
6.00E+06	3.86228E-01	2.421E+06
7.00E+06	3.83092E-01	2.805E+06
8.00E+06	3.80422E-01	3.187E+06
9.00E+06	3.78336E-01	3.566E+06
1.00E+07	3.76551E-01	3.944E+06

DO = 1. CM**2/S
CSO= .2E-06 G/CM**3
EPS= .C10
R = 42.C40 CM (For $^{237}N_p$)
K = 100.
NO OF CALCULATIONS: 64

STEADY STATE SURFACE MASS FLUX = 0.752E-07 g/y

TIME ELAPSED [y]	SURFACE MASS FLUX [g/y]	TOTAL MASS DISSOLUTION [g]
1.00E+00	1.14225E-05	1.142E-05
2.00E+00	8.66198E-06	2.146E-05
3.00E+00	7.40453E-06	2.950E-05
4.00E+00	6.62994E-06	3.652E-05
5.00E+00	6.C7728E-06	4.287E-05
6.00E+00	5.64512E-06	4.873E-05
7.C0E+00	5.28833E-06	5.420E-05
8.00E+00	4.98334E-06	5.933E-05
9.00E+00	4.71577E-06	6.418E-05
1.00E+01	4.47653E-06	6.878E-05
2.00E+01	2.92498E-06	1.058E-04
3.00E+01	2.09345E-06	1.309E-04
4.00E+01	1.56834E-06	1.492E-04
5.00E+01	1.19939E-06	1.630E-04
6.00E+01	1.C19C8E-06	1.741E-04
7.00E+01	8.842C6E-07	1.836E-04
8.00E+01	7.85098E-07	1.920E-04
9.00E+01	7.36615E-07	1.996E-04
1.00E+02	6.80445E-07	2.067E-04
2.00E+02	3.947C6E-07	2.604E-04
3.00E+02	3.27734E-07	2.966E-04
4.00E+02	2.75894E-07	3.267E-04
5.00E+02	2.42082E-07	3.526E-04
6.00E+02	2.28701E-07	3.762E-04
7.00E+02	2.17489E-07	3.985E-04
8.00E+02	2.04318E-07	4.196E-04
9.00E+02	1.96132E-07	4.396E-04
1.00E+03	1.89422E-07	4.589E-04
2.00E+03	1.49117E-07	6.281E-04
3.00E+03	1.35136E-07	7.703E-04
4.00E+03	1.28215E-07	9.019E-04
5.00E+03	1.23830E-07	1.028E-03
6.00E+03	1.19989E-07	1.150E-03
7.00E+03	1.16720E-07	1.268E-03
8.00E+03	1.143C9E-07	1.384E-03
9.00E+03	1.12588E-07	1.497E-03

TIME ELAPSED [y]	SURFACE MASS FLUX [g/y]	TOTAL MASS DISSOLUTION [g]
1.00E+04	1.11181E-07	1.669E-03
2.00E+04	1.02880E-07	2.679E-03
3.00E+04	1.01262E-07	3.700E-03
4.00E+04	9.97986E-08	4.705E-03
5.00E+04	9.81489E-08	5.695E-03
6.00E+04	9.68278E-08	6.670E-03
7.00E+04	9.58559E-08	7.633E-03
8.00E+04	9.51523E-08	8.588E-03
9.00E+04	9.46320E-08	9.537E-03
1.00E+05	9.42017E-08	1.048E-02
2.00E+05	9.08579E-08	1.973E-02
3.00E+05	8.90730E-08	2.873E-02
4.00E+05	8.79421E-08	3.758E-02
5.00E+05	8.70826E-08	4.633E-02
6.00E+05	8.62797E-08	5.500E-02
7.00E+05	8.55391E-08	6.359E-02
8.00E+05	8.49185E-08	7.212E-02
9.00E+05	8.44200E-08	8.058E-02
1.00E+06	8.39914E-08	8.900E-02
2.00E+06	8.10392E-08	1.715E-01
3.00E+06	7.95759E-08	2.518E-01
4.00E+06	7.87301E-08	3.310E-01
5.00E+06	7.81259E-08	4.094E-01
6.00E+06	7.74846E-08	4.872E-01
7.00E+06	7.68375E-08	5.644E-01
8.00E+06	7.62882E-08	6.409E-01
9.00E+06	7.58587E-08	7.170E-01
1.00E+07	7.54912E-08	7.927E-01

APPENDIX 9D

Derivation of Solubility Proportionality Law

The dissolution of a chemical species into a liquid such as water is governed by the following equation:

$$C(T) = A \exp\left\{ - \frac{\Delta H_s}{RT} \right\} \qquad (D.1)$$

where $C(T)$ [g/cm^3] is the temperature dependent solubility concentration, A is a constant with the same units as $C(T)$, ΔH_s [J/mol] is the specific heat of solution, R [J/mol·K] is the gas constant, and T [K] is the temperature of the liquid.

Suppose $C(T)$ is known for a chemical species at two temperatures T_1 and T_2. Then,

$$\frac{C(T_1)}{C(T_2)} = \exp\left\{ - \frac{\Delta H_s}{R} \left[\frac{1}{T_1} - \frac{1}{T_2} \right] \right\} \qquad (D.2)$$

If one assumes that ΔH_s is constant for all species of interest and that it does not vary with temperature, it is obvious that the right hand side of equation (D.2) will be a constant once T_1 and T_2 are selected. Thus,

$$\frac{C_i(T_1)}{C_j(T_1)} = \frac{C_i(T_2)}{C_j(T_2)} \qquad (D.3)$$

where i and j are the two species of interest. This formula is useful for determining the fourth member of a set of related solubilities when only three members are known.

APPENDIX 9E

Mass Loss From a Waste Canister

In section 1 of this report the assumption was made that the radius of the spherical waste canister, R, does not change with time. It may be of some interest to use the mass transport results to strengthen the basis for making such an assumption.

Consider the actual cylindrical waste canister of radius R_c and length L_c. This cylinder is modeled in the present study by a sphere of equal lateral surface area. The relationship between the sphere radius, R, and the cylinder radius, R_c, can be expressed as follows:

$$R = \sqrt{\frac{R_c L_c}{2}} \qquad (E.1)$$

The total amount of silica mass initially contained within the cylinder is given by

$$m = \frac{4}{3} \pi \gamma \rho R^3 = \frac{\sqrt{2}}{3} \pi \gamma \rho (R_c L_c)^{3/2} \qquad (E.2)$$

where γ is the mass fraction of the waste that is silica and ρ is the density of the waste. Taking $\gamma = .50$, $\rho = 3$ g/cm^3, $R_c = 15.24$ cm, and $L_c = 2.32$ m, one obtains

$$m_{SiO_2} = 470 \text{ kg} \qquad (E.3)$$

At time t=10,000 y the total SiO_2 mass loss from the waste is 7.2 kg (see Appendix 9C). The loss in silica inventory from the canister is thus about 1.5%, a rather small amount. Since

$$m \propto R^3 \qquad (E.4)$$

the effect on R would be much smaller and can be determined from the fol-

lowing expression:

$$\frac{m - \Delta m}{m} = \left[\frac{R - \Delta R}{R}\right]^3$$

$$R\left[\frac{m - \Delta m}{m}\right]^{1/3} = R - \Delta R$$

$$\frac{\Delta R}{R} = 1 - \left[\frac{m - \Delta m}{m}\right]^{1/3} \qquad \text{(E.5)}$$

Substituting the parameters from the previous page into equation (E.5) results in

$$\frac{\Delta R}{R} = .005 \qquad \text{(E.6)}$$

Thus, the waste canister dimensions do not change appreciably during the first 10,000 years of emplacement and the constant R assumption is well founded.

10. THE TRANSPORT OF A RADIONUCLIDE IN A THREE DIMENSIONAL FLOW FIELD FROM A POINT SOURCE

P.L. Chambré

The following analysis describes the concentration pattern in three dimensional space and in time of a radio-nuclide which is emitted from a point source. The source is located in a porous medium permeated by water flow. The magnitude of the advective and dispersive transports in the three principal coordinate directions can be prescribed with some latitude. The solution to the mathematical problem has been obtained in terms of elementary functions, specifically an integral, which can be evaluated in a straightforward manner. The result of the analysis is useful as a benchmark for comparison with numerical solutions of the governing equation. It can also serve as a model for the far field migration of a radionuclide emitted from a single waste form.

The model is based on the governing equation for the nuclide concentration $N(x_1,x_2,x_3,t)$ with a retardation coefficient K

$$K\frac{\partial N}{\partial t} + \left(\hat{u}_1+\hat{\alpha}_1 x_1\right)\frac{\partial N}{\partial x_1} + \left(\hat{u}_2+\hat{\alpha}_2 x_2\right)\frac{\partial N}{\partial x_2} + \left(\hat{u}_3+\hat{\alpha}_3 x_3\right)\frac{\partial N}{\partial x_3} =$$

$$\frac{\partial}{\partial x_1}\left(\hat{D}_1\frac{\partial N}{\partial x_1}\right) + \frac{\partial}{\partial x_2}\left(\hat{D}_2\frac{\partial N}{\partial x_2}\right) + \frac{\partial}{\partial x_3}\left(\hat{D}_3\frac{\partial N}{\partial x_3}\right) - \lambda KN,\ x_i\epsilon\mathcal{D}_\infty,\ i=1,2,3;t>0 \qquad (1)$$

For mathematical convenience the cartesian space coordinates are labelled x_1,x_2,x_3 and the dispersion coefficients $\hat{D}_1,\hat{D}_2,\hat{D}_3$. The unbounded space is $\mathcal{D}_\infty$. The strength of the nuclide source, located at x_i°, i=1,2,3, in D_∞ is $\dot{M}(\tau)d\tau$ and measures the mass of material released at time τ during the time span $d\tau$. The release gives rise to the concentration $N(x_1,x_2,x_3,t)$ at position x_1,x_2,x_3 at time $t>\tau$. This concentration is initially zero throughout $\mathcal{D}_\infty$ and satisfies suitable boundedness conditions at an infinite distance from the source position.

Furthermore N obeys a vanishing flux conditions at interior surfaces of $\mathcal{V}_\infty$ which are not penetrated by the advection nor by the dispersion.

In (1) the pore water velocity components:

$$\left(\hat{u}_1+\hat{\alpha}_1 x_1\right)\ ,\ \left(\hat{u}_2+\hat{\alpha}_2 x_2\right),\ \left(\hat{u}_3+\hat{\alpha}_3 x_3\right);\ \hat{u}_1,\hat{u}_2,\hat{u}_3,\hat{\alpha}_1,\hat{\alpha}_2,\hat{\alpha}_3 \text{ constants}, \tag{2}$$

which are chosen for a linear velocity field, are spatially dependent and are subject to the constraint imposed by the conservation of mass equation for an incompressible liquid moving with velocity $\vec{v}$ through the porous medium

$$\text{div } \vec{v} = 0 \tag{3}$$

This yields with (2)

$$\hat{\alpha}_1+\hat{\alpha}_2+\hat{\alpha}_3 = 0 \tag{4}$$

The coefficients $\hat{\alpha}_1,\hat{\alpha}_2,\hat{\alpha}_3$ can be selected to satisfy a few physically meaningful potential flow patterns.

Illustration A. The choice: $\hat{u}_1 = \hat{u}_2 = \hat{u}_3 = 0$; $\hat{\alpha}_1 = \hat{\alpha}_2$, $\hat{\alpha}_3 = -2\hat{\alpha}_1$, leads to the velocity components

$$\bar{u}_1 = \hat{\alpha}_1 x_1;\ \bar{u}_2 = \hat{\alpha}_1 x_2\ ;\ \bar{u}_3 = -2\hat{\alpha}_1 x_3 \tag{5}$$

for which the three-dimensional flow stream tubes appear as shown in Fig. 1. The flow pattern simulates the streaming past the source point $(x_1^\circ,x_2^\circ,x_3^\circ)$ by a wide jet, which is symmetrical about the x_3 axis and which impinges against an impenetrable (x_1,x_2) plane from both positive and negative x_3 directions. By suitably adjusting the dispersion coefficients D_1,D_2,D_3, additional skewing of the concentration field, over that caused by the velocity field, can be achieved to test the applicability of a numerical code calculation.

Illustration B. If one choses $\hat{\alpha}_1 = \hat{\alpha}_2 = \hat{\alpha}_3 = 0$, the flow pattern is constant in space and without loss of generality one can take the flow direction along one of the coordinate axes such as x_1 by setting $\hat{u}_2 = \hat{u}_3 = 0$ and $\hat{u}_1 \neq 0$. This rectilinear flow pattern in the completely unbounded $\mathcal{V}_\infty$ can be used to

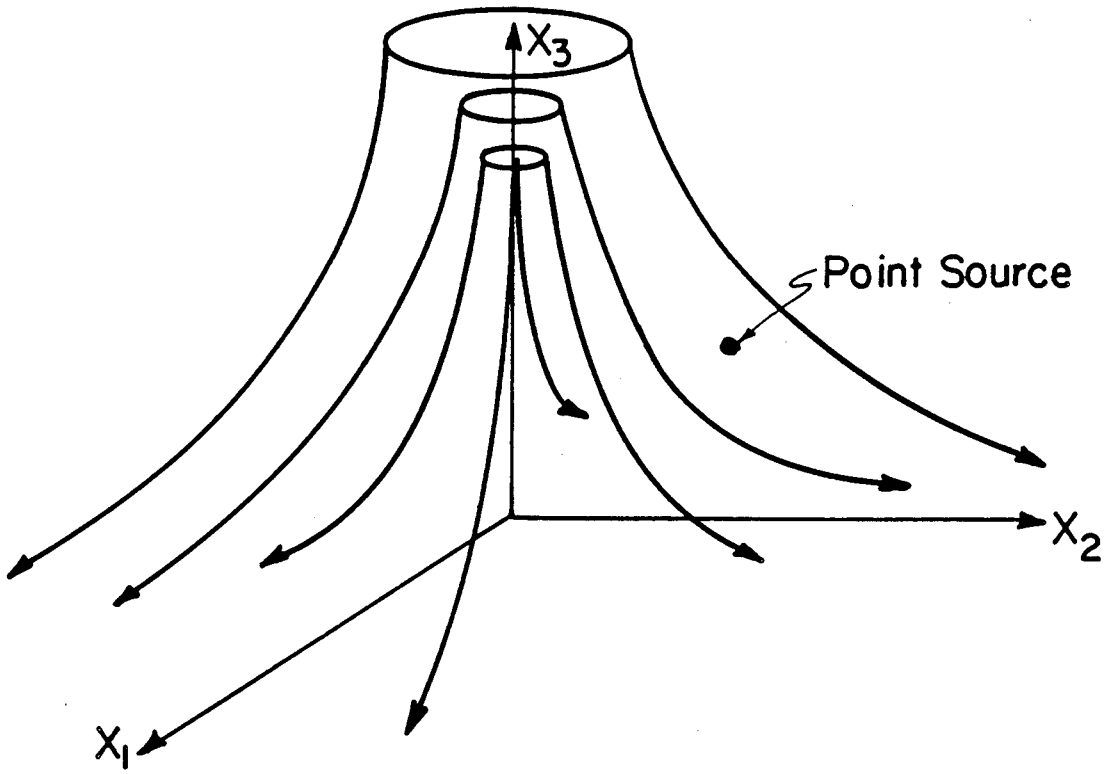

(a) Stagnant Potential Flow Field Bounded by $X_1 - X_2$ Plane

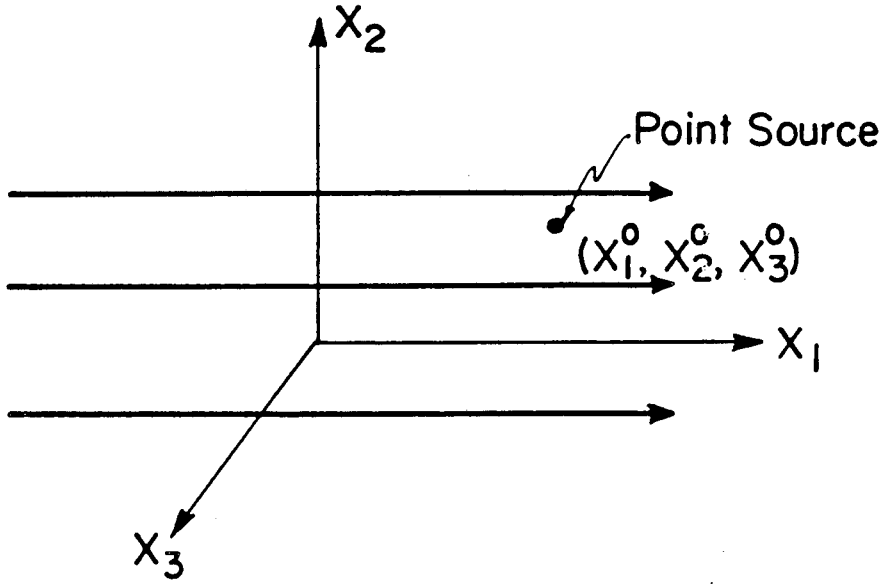

(b) Rectilinear Potential Flow Field Along X_1 Axis

XBL 8412-5894

Fig. 1 Illustrative flow fields for sample problems A and B.

model the far field migration from a single waste form. Other choices for the parameters $\hat{u}_i, \hat{\alpha}_i$ (i=1,2,3) can be made which lead to other useful physical simulations.

To solve equation (1) we first eliminate the decay term with help of

$$c(x_1,x_2,x_3,t) = e^{\lambda t} N(x_1,x_2,x_3,t) \tag{6}$$

If one divides the resulting equation by K and sets

$$D_i = \frac{\hat{D}_i}{K}\ ,\ u_i = \frac{\hat{u}_i}{K}\ ,\ \alpha_i = \frac{\hat{\alpha}_i}{K}\ ,\ i = 1,2,3 \tag{7}$$

there results, if the D_i's are considered constant,

$$\frac{\partial c}{\partial t} + (u_1+\alpha_1 x_1)\frac{\partial c}{\partial x_1} + (u_2+\alpha_2 x_2)\ \frac{\partial c}{\partial x_2} + (u_3+\alpha_3 x_3)\ \frac{\partial c}{\partial x_3} =$$

$$D_1 \frac{\partial^2 c}{\partial x_1^2} + D_2 \frac{\partial^2 c}{\partial x_2^2} + D_3 \frac{\partial^2 c}{\partial x_3^2}\ ,\ x_i \varepsilon \mathcal{D}_\infty,\ t>0;\ i = 1,2,3 \tag{8}$$

To solve this represent $c(x_1,x_2,x_3,t)$ in the product form

$$c(x_1,x_2,x_3,t) = c_1(x_1,t)c_2(x_2,t)c_3(x_3,t) \tag{9}$$

where the $c_i(x_i,t)$ satisfy the "one-dimensional" equations defined by the differential operator L

$$Lc_i(x_i,t) \equiv \frac{\partial c_i}{\partial t} + (u_i+\alpha_i x_i)\frac{\partial c_i}{\partial x_i} - \nu_i \frac{\partial^2 c_i}{\partial x_i^2} = 0,\ i=1,2,3;\ -\infty<x_i<\infty,\ t>0 \tag{10}$$

To show that the product form (9) is a solution of the governing equation (8) is straightforward and leads on substitution of (9) into (8) and some re-arrangements to

$$c_2c_3\left\{Lc_1\right\} + c_1c_3\left\{Lc_2\right\} + c_1c_2\left\{Lc_3\right\} = 0 \tag{11}$$

Since the bracketed terms vanish by (10) the result is established.

Hence the solution of the problem (8) is thus reduced to the much simpler equations (10) which have the common form

$$\frac{\partial c}{\partial t} + (u+\alpha x)\frac{\partial c}{\partial x} = D\frac{\partial^2 c}{\partial x^2} \tag{12}$$

on dropping the subscript labels. As explained in the paragraph below equation (1), $c(x,t)$ must satisfy the initial condition

$$c(x,o) = 0, \quad x\varepsilon\mathcal{D}_\infty \tag{13}$$

and the source condition at $x^\circ\varepsilon\mathcal{D}_\infty$.

We reduce the variable coefficient partial differential equation (12) to one with constant coefficients. Let

$$\zeta(x,t) = \frac{u}{\alpha}\left\{e^{-\alpha t}\left[1+\frac{\alpha x}{u}\right] - 1\right\} \tag{14}$$

$$\tau(t) = \frac{1}{2\alpha}\left(1-e^{-2\alpha t}\right) \tag{15}$$

and

$$c(x,t) = C(\zeta,\tau). \tag{16}$$

From (14)

$$\frac{\partial \zeta}{\partial t} = -ue^{-\alpha t}\left[1+\frac{\alpha x}{u}\right], \quad \frac{\partial \zeta}{\partial x} = e^{-\alpha t} \tag{17}$$

and from (15)

$$\frac{d\tau}{dt} = e^{-2\alpha t}. \tag{18}$$

With these expressions the derivatives of $C(\zeta,\tau)$ are computed from

$$\frac{\partial c}{\partial t} = \frac{\partial C}{\partial \tau}\frac{d\tau}{dt} + \frac{\partial C}{\partial \zeta}\frac{\partial \zeta}{\partial t}$$

$$= e^{-2\alpha t}\frac{\partial C}{\partial \tau} - e^{-\alpha t}(u+\alpha x)\frac{\partial C}{\partial \zeta} \tag{19}$$

$$\frac{\partial c}{\partial x} = \frac{\partial C}{\partial \zeta}\,\frac{\partial \zeta}{\partial x}$$

$$= e^{-\alpha t}\,\frac{\partial C}{\partial \zeta} \tag{20}$$

$$\frac{\partial^2 c}{\partial x^2} = e^{-2\alpha t}\,\frac{\partial^2 C}{\partial \zeta^2} \tag{21}$$

Substitution of (19) - (21) into (12) yields the desired constant coefficient equation

$$\frac{\partial C}{\partial \tau} = D\,\frac{\partial^2 C}{\partial \zeta^2} \tag{22}$$

A solution of (22) with a point source singularity of unit strength at $\zeta=0$, $\tau=0$ is given by the well known Kelvin function

$$C(\zeta,\tau) = \frac{1}{2\sqrt{\pi D\tau}}\quad \exp\left\{-\frac{\zeta^2}{4D\tau}\right\} \tag{23}$$

In terms of the original x,t variables one has in view of (14) - (16) for a point source singularity now located at x°,

$$c(x,t) = \frac{1}{\left(\pi\,\frac{2D}{\alpha}\left[1-e^{-2\alpha t}\right]\right)^{1/2}}\quad \exp\left\{-\frac{\left(e^{-\alpha t}\left[\frac{u}{\alpha}+(x-x^\circ)\right]-\frac{u}{\alpha}\right)^2}{\frac{2D}{\alpha}\left[1-e^{-2\alpha t}\right]}\right\} \tag{24}$$

This is the solution of the system (12) and (13). In turn this allows one now to construct, with help of (9) and (24), the solution for the nuclide concentration c from a point source singularity of unit strength located at x_i° $(i = 1,2,3)$

$$c(x_1,x_2,x_3,t) = \prod_{i=1}^{3} c_i(x_i,t)\ . \tag{25}$$

The source condition produced by integrating Eq.(25) with respect to x_i from $-\infty$ to $+\infty$, $i = 1,2,3$, is $e^{(\alpha_1+\alpha_2+\alpha_3)t} = 1$, since $\alpha_1 + \alpha_2 + \alpha_3 = 0$ from Eq.(4). Hence c indeed is the solution of the unit strength point source condition. By construction $N(x_1,x_2,x_3,t)$ from Eq.(6) is seen to satisfy equation (1). x,x°,u,α and D are replaced by $x_i,x_i^\circ,u_i,\alpha_i$, and D_i respectively in (24) to give the function $c(x_i,t)$ in (25).

In turn the solution due to a point source located at x_i°, releasing the mass $\dot{M}(\tau)d\tau$ at time τ during the time span $d\tau$, creates the concentration dN at the time $t(>\tau)$ at x_i

$$dN = (\dot{m}(\tau)d\tau)e^{-\lambda(t-\tau)} \prod_{i=1}^{3} c_i(x_i,t-\tau) \quad , \quad \dot{m}(\tau) = \frac{\dot{M}(\tau)}{\varepsilon K} \tag{26}$$

where ε is the porosity of the porous medium. The reason for using this form is presented in Appendix 10A. Hence the concentration at time t, at x_i, due to the mass liberated during the time span $0<\tau<t$ is given by the superposition integral

$$N(x_1,x_2,x_3,t) = \int_0^t \dot{m}(\tau)e^{-\lambda(t-\tau)} \prod_{i=1}^{3} c_i(x_i,t-\tau)d\tau \tag{27}$$

where

$$c_i(x_i,t-\tau) = \frac{1}{\left[\pi \frac{2D_i}{\alpha_i} \phi(\alpha_i,t-\tau)\right]^{1/2}} \exp\left\{ - \frac{\left(e^{-\alpha_i(t-\tau)} \left[\frac{u_i}{\alpha_i} + (x_i - x_i^\circ) \right] - \frac{u_i}{\alpha_i} \right)^2}{2 \frac{D_i}{\alpha_i} \phi(\alpha_i,t-\tau)} \right\}$$

and (28)

$$\phi(\alpha_i,t-\tau) \equiv \left[1-\exp(-2\alpha_i[t-\tau])\right]$$

Equation (27) represents the solution to our problem in an unbounded D_∞ space. It should be noted that one can utilize this point source solution to model the emission of a radionuclide from a surface source of arbitrary shape. For this one integrates the source position x_i° (i = 1,2,3) over the surface to obtain the desired answer. This can be carried out analytically for the simulation of line, plane, cylindrical and spherical surface sources but the results are not reported here. As an example of the theory we consider the Illustration B with $u_2 = u_3 = \alpha_1 = \alpha_2 = \alpha_3 = 0$ and $u_1 \neq 0$ representing a rectilinear flow field which is independent of position. Furthermore we assume the source to be located at the origin so that $x_1^\circ = x_2^\circ = x_3^\circ = 0$. The following limits are required in (28)

$$\lim_{\alpha_i \to 0} \frac{\phi(\alpha_i, t-\tau)}{2\alpha_i} = t-\tau, \quad i = 1,2,3$$

$$\lim_{\alpha_i \to 0} \left\{ e^{-\alpha_i (t-\tau)} \left[\frac{u_i}{\alpha_i} + (x_i - x_i^\circ) \right] - \frac{u_i}{\alpha_i} \right\} = (x_i - x_i^\circ) - u_i(t-\tau), \quad i = 1,2,3. \tag{29}$$

With these results (27) reduces to

$$N(x_1,x_2,x_3,t) = \int_0^t \frac{\dot{m}(\tau) e^{-\lambda(t-\tau)}}{(4\pi D(t-\tau))^{3/2}} \exp\left\{ \frac{-1}{4(t-\tau)} \left\{ \frac{[x_1 - u_1(t-\tau)]^2}{D_1} + \frac{x_2^2}{D_2} + \frac{x_3^2}{D_3} \right\} \right\} d\tau \tag{30}$$

where

$$D \equiv (D_1 D_2 D_3)^{1/3} .$$

The integral can be simplified for an easy numerical evaluation with the assumption $D_1 = D_2 = D_3 = D$. Let

$$r^2 = x_1^2 + x_2^2 + x_3^2 \tag{31}$$

and

$$\alpha = \frac{r}{\left(4D[t-\tau]\right)^{1/2}} \tag{32}$$

Then (30) reduces to

$$N(x_1,x_2,x_3,t) = \frac{\exp\left\{\frac{x_1 u_1}{2D}\right\}}{?(\pi)^{3/2} Dr} \int_{r/2\sqrt{Dt}}^{\infty} \exp\left\{ -\alpha^2 - \left(\frac{\lambda r^2}{4D} + \left[\frac{u_1 r}{4D}\right]^2 \right) \frac{1}{\alpha^2} \right\} \cdot \dot{m}\left(t - \frac{r^2}{4D\alpha^2}\right) d\alpha \tag{33}$$

For the special case of a constant mass release for $\tau > 0$

$$\dot{m}(\tau) = \dot{m}_o , \quad \tau > 0$$

one obtains on carrying out the integration

$$N(x_1,x_2,x_3,t) = \frac{\dot{m}_o e^{\frac{x_1 u_1}{2D}}}{8\pi Dr} \left\{ e^{r\phi} \operatorname{erfc} \left(\sqrt{\left(\lambda + \frac{u_1^2}{4D}\right)} t + \frac{r}{2\sqrt{Dt}} \right) \right.$$
$$\left. + e^{-r\phi} \left[2 - \operatorname{erfc} \left(\sqrt{\left(\lambda + \frac{u_1^2}{4D}\right)} t - \frac{r}{2\sqrt{Dt}} \right) \right] \right\} \tag{34}$$

where

$$\phi = 2\sqrt{\frac{\lambda}{4D} + \left(\frac{u_1}{4D}\right)^2} \quad .$$

As with $t \to \infty$ a steady state concentration field is established which has the form

$$N(x_1,x_2,x_3,\infty) = \frac{\dot{m}_o}{4\pi Dr} \exp \left\{ \frac{x_1 u_1}{2D} - 2 \left(\frac{\lambda r^2}{4D} + \left(\frac{u_1 r}{4D}\right)^2 \right)^{1/2} \right\} \tag{35}$$

Equation (33) can be used to describe the far field migration from an isolated waste form. The solution for the case of unequal dispersion coefficients can be obtained in a similar manner but is too lengthy to be reported here.

Eq. (27) is a solution for the governing equation (1) subject to the prescribed initial and boundary conditions. If there is no mass transport through the (x_1,x_2) plane, either by advection or by dispersion, the solution can be obtained by superposing a point source at $(x_1^o, x_2^o, -x_3^o)$ to cancel out the mass flux at x_3^o. The final result for $u_1 = u_2 = u_3 = o$ and $\alpha_1 = \alpha_2 = -\frac{\alpha_3}{2}$, as described in Illustration A is

$$N(x_1,x_2,x_3,t) = \int_o^t \dot{m}(\tau)e^{-\lambda(t-\tau)}\Big[f(x_1-x_1^o,x_2-x_2^o,\ x_3-x_3^o,t-\tau)$$

$$+f(x_1-x_1^o,x_2-x_2^o,x_3+x_3^o,t-\tau)\Big]\,d\tau,\ -\infty<x_1,x_2<\infty,\ o<x_3<\infty,\ t>o, \qquad (36)$$

where

$$f(x_1-x_1^o,x_2-x_2^o,x_3 \pm x_3^o,t)$$

$$=\left(\prod_{i=1}^{2} \frac{\exp\left\{-\frac{\left(x_i-x_i^o\right)^2 e^{-2\alpha_i t}}{2D_i\left(1-e^{-2\alpha_i t}\right)/\alpha_i}\right\}}{\left[\pi\frac{2D_i}{\alpha_i}\left(1-e^{-2\alpha_i t}\right)\right]^{1/2}}\right)\left(\frac{\exp\left\{-\frac{\left(x_3 \pm x_3^o\right)^2 e^{-2\alpha_3 t}}{2D_3\left(1-e^{-2\alpha_3 t}\right)/\alpha_3}\right\}}{\left[\pi\frac{2D_3}{\alpha_3}\left(1-e^{-2\alpha_3 t}\right)\right]^{1/2}}\right) \qquad (37)$$

APPENDIX 10A

In Eq. (26) the source term $\dot{m}(t)$ used in the solution is related to $\dot{M}(t)$ by $\dot{m}(t) = \frac{\dot{M}(t)}{\varepsilon k}$, where $\dot{M}(t)$ is the total mass release rate (g/sec) at the source point, ε is the porosity of the porous medium, and K is the nuclide retardation coefficient. This relation can be derived as follows.

Let $N(x_1,x_2,x_3,t)$ be the nuclide concentration in the liquid and N_s (x_1,x_2,x_3,t) the nuclide concentration in the solid, then conservation of the nuclide specie in the porous medium requires that

$$\int_{-\infty}^{\infty}\int_{-\infty}^{\infty}\int_{-\infty}^{\infty}\left[\varepsilon N + (1-\varepsilon)N_s\right] dx_1dx_2dx_3 = \int_o^t \dot{M}(\tau)e^{-\lambda(t-\tau)}\, d\tau \ . \qquad (I1)$$

Since $\varepsilon N + (1-\varepsilon)N_s = \varepsilon N\left[1 + \left(\frac{1-\varepsilon}{\varepsilon}\right)\left(\frac{N_s}{N}\right)\right]$
$= \varepsilon KN$

Eq. (I1) becomes $\int_{-\infty}^{+\infty}\int_{-\infty}^{+\infty}\int_{-\infty}^{+\infty} \varepsilon kN dx_1dx_2dx_3 = \int_o^t \dot{M}(\tau)e^{-\lambda(t-\tau)}d\tau \qquad (I2)$

But from (27) we have, with help of (25), for the left hand side

$$\int_{-\infty}^{+\infty}\int_{-\infty}^{+\infty}\int_{-\infty}^{+\infty} \varepsilon KN dx_1dx_2dx_3 = \int_o^t \varepsilon k\dot{m}(\tau)e^{-\lambda(t-\tau)}d\tau \qquad (I3)$$

Comparing (12) and (13), one finds $\dot{m}(t) = \frac{\dot{M}(t)}{\varepsilon k}$.

11. ON THE TRANSPORT OF RADIOACTIVE CHAINS IN GEOLOGIC MEDIA

Paul L. Chambré

The following analysis deals with the migration of radioactive chains in geologic media of finite and infinite spatial extent. The governing equations are sufficiently general to model the specie transport by dispersion and advection in a water saturated porous medium. They can also be applied to diffusion of radioactive chains in denser media such as rocks permeated by micro-pores where advection is negligible.

The formulation of the equation system and its solution form is given in Section I. Two classes of problems, dealing with dispersion-advection and diffusion respectively, are formulated together with very general boundary conditions in Section II. Sections III and IV give the exact closed form (non-recursive) analytical solutions for the radioactive specie concentrations of chains of arbitrary length in media of finite and (semi) infinite spatial extents. Section V illustrates the theory by applying it to the problem of radionuclide transport by dispersion and advection from a repository surface to the biosphere, positioned at a finite distance. At the latter position the specie fluxes are shown to be given by explicit analytical formulas.

The results of the analysis generalize the recursive chain calculations on which the Computer Code UCB NE 10.2 and 10.3 are based, to chains of arbitrary length in both finite and infinite spatial geometries.

I. The Governing Equation System and its Solution Form

Consider the canonical system for $z\varepsilon\mathcal{D}$, $t>0$

$$K_1 \frac{\partial N_1}{\partial t} + v \frac{\partial N_1}{\partial z} + \lambda_1 K_1 N_1 = D_1 \frac{\partial^2 N_1}{\partial z^2}$$

$$K_2 \frac{\partial N_2}{\partial \tau} + v \frac{\partial N_2}{\partial z} + \lambda_2 K_2 N_2 = D_2 \frac{\partial^2 N_2}{\partial z^2} + \lambda_1 K_1 N_1 \tag{1}$$

- -

$$K_i \frac{\partial N_i}{\partial t} + v \frac{\partial N_i}{\partial z} + \lambda_i K_i N_i = D_i \frac{\partial^2 N_i}{\partial z^2} + \lambda_{i-1} K_{i-1} N_{i-1}$$

which is to be solved for $N_i = N_i(z,t)$, in a one-dimensional domain $\mathcal{D}$ which is either finite or infinite, for times $t>0$. The D_i are the diffusion coefficients of the individual species to be specified later. All other symbols have their usual meaning. The functions $N_i(z,t)$, $i=1,2,\ldots$ are subject to the initial conditions

$$N_i(z,0) = 0, \quad z\varepsilon\mathcal{D} \tag{2}$$

and the boundary conditions

$$-D_i\varepsilon \frac{\partial N_i}{\partial z} + v N_i = v \overset{\circ}{N_i}\phi_i(t) \qquad \text{for } z=0,\ t>0 \tag{3}$$

$$\phi_i(t) \equiv 0 \text{ for } t<0$$

The left hand side represents the total flux of specie i through the boundary surface $z=0$ of $\mathcal{D}$ while the right hand side describes the rate of supply of specie i in terms of the abitrarily prescribed integrable functions $\overset{\circ}{N_i}\,\phi_i(t)$. These functions describe the time release of the chain members from a repository surface or waste form located at $z=0$. ε is the porosity of the medium. In case of no advection the terms involving v are dropped from (1) and replaced by other parameters in (3) as will be discussed later. The second boundary condition for the $N_i(z,t)$ at the other boundary of $\mathcal{D}$ will be stated in Section II.

The general form of the equation system (1) is

$$\frac{K_i}{D_i}\frac{\partial N_i}{\partial t} + \frac{v}{D_i}\frac{\partial N_i}{\partial z} + \nu_i N_i = \frac{\partial^2 N_i}{\partial z^2} + \nu_{i-1} N_{i-1}, \text{ with } \nu_o = 0,\ i = 1,2,\ldots \tag{4}$$

where

$$\nu_i = \frac{K_i \lambda_i}{D_i}\ ,\ \nu_{i-1} = \frac{K_{i-1}\lambda_{i-1}}{D_i}\ . \tag{5}$$

The aim is to obtain the general (non-recursive) analytical solution for the $N_i(z,t)$.

On account of the linearity of (4), the solution for the individual chain member N_i can be represented as a sum of functions, which satisfy (4), and selected boundary conditions. We specify

$$\begin{aligned} N_1(z,t) &= N_1^{(1)}(z,t) \\ N_2(z,t) &= N_2^{(1)}(z,t) + N_2^{(2)}(z,t) \\ N_3(z,t) &= N_3^{(1)}(z,t) + N_3^{(2)}(z,t) + N_3^{(3)}(z,t) \end{aligned} \tag{6a}$$

and for an arbitrary i^{th} chain member

$$N_i(z,t) = N_i^{(i)}(z,t) + \sum_{j=1}^{i-1} N_i^{(j)}(z,t)\ . \tag{6b}$$

Thus, in order to obtain the concentration of the i^{th} chain member, every function $N_1^{(j)}(z,t)$ must be known. We begin with the construction of $N_1^{(1)}(z,t)$. It is chosen to be a solution of (4) (with $\nu_o = 0$) which satisfies both the initial condition (2) and the boundary condition (3). This determines $N_1(z,t)$. To determine $N_2(z,t)$ we require two solutions of (4). $N_2^{(1)}(z,t)$ is chosen so that it obeys the initial condition (2) and the homogeneous boundary condition (3) with $N_2^{\circ} = 0$. This function yields the contribution to $N_2(z,t)$ which is due to the radioactive decay of its precursor $N_1(z,t)$. $N_2^{(2)}(z,t)$ on the other hand

is chosen to satisfy the inhomogeneous boundary condition (3), as well as of course (2). But since the precursor contribution to $N_2(z,t)$ is already accounted for, the inhomogeneous term $\nu_1 N_1$ is not included in eq.(4) when one solves for $N_2^{(2)}(z,t)$. One proceeds comparably in the construction of $N_3(z,t)$. $N_3^{(1)}(z,t)$ and $N_3^{(2)}(z,t)$ are precursor contributions stemming from chain members $N_1(z,t)$ and $N_2(z,t)$ respectively. Their solutions of eq.(4) satisfy homogeneous boundary concentrations, with $N_3^{\circ} = 0$, while $N_3^{(3)}(z,t)$ yields the contribution to $N_3(z,t)$ due to the inhomogeneous boundary condition (3), with $N_3^{\circ} \neq 0$. However, for the determination of $N_3^{(3)}(z,t)$ the inhomogeneous term $\nu_2 N_2$ is dropped from (4).

According to this decomposition of the problem, the functions $N_\ell^{(j)}(z,t)$ must satisfy the following equation system for $z\varepsilon\mathcal{D}$, $t>0$

$$\frac{K_\ell}{D_\ell}\frac{\partial N_\ell^{(j)}}{\partial t} + \frac{v}{D_\ell}\frac{\partial N_\ell^{(j)}}{\partial z} + \nu_\ell N_\ell^{(j)} = \frac{\partial^2 N_\ell^{(j)}}{\partial z^2} + \nu_{\ell-1} N_{\ell-1}^{(j)}, \quad \nu_0=0, \quad \ell=1,2,..i, \quad j \leqslant \ell. \tag{7}$$

The functions are subject to,

$$N_\ell^{(j)}(z,0) = 0 \tag{8}$$

$$-D_\ell \varepsilon \frac{\partial N_\ell^{(j)}(0,t)}{\partial z} + vN_\ell^{(j)}(o,t) = \delta_{\ell j} N_\ell^{\circ} v\phi_j(t), \quad j\leqslant\ell \tag{9}$$

where $\delta_{\ell j}$ is the Kronecker delta which vanishes for $\ell\neq j$ and is unity for $\ell=j$. Furthermore

$$N_{\ell-1}^{(j)}(z,t) \equiv 0, \text{ for } \ell\leqslant j \tag{10}$$

which assures that for $\ell\leqslant j$ the inhomogeneous (source) term $\nu_{\ell-1}N_{\ell-1}$ vanishes. The second boundary condition which $N_\ell^{(j)}(z,t)$ must satisfy in $\mathcal{D}$ will be discussed in the next section. At this point however one can verify that the solution to equations (7) through (9) when substituted into (6) will satisfy the original equations system (1), (2), and (3) due to the linearity of the

latter equations.

II. Specification of Problems

We now wish to specify a number of problems of practical interest which will be seen to have a common mathematical basis. For this purpose we take the Laplace transform of (7) with respect to the time variable and define

$$\bar{N}_\ell^{(j)}(z,s) = \int_0^\infty e^{-st} N_\ell^{(j)}(z,t)dt; \quad \bar{\phi}_j(s) = \int_0^\infty e^{-st}\phi_j(t)dt \tag{11}$$

The transform of equation (7), on utilizing the initial condition (8), yields

$$\frac{d^2\bar{N}_\ell^{(j)}}{dz^2} - \frac{v}{D_\ell}\frac{d\bar{N}_\ell^{(j)}}{dz} - \left(\frac{K_\ell}{D_\ell}s + \nu_\ell\right)\bar{N}_\ell^{(j)} = -\nu_{\ell-1}\bar{N}_{\ell-1}^{(j)}, \tag{12}$$

for $\bar{N}_\ell^{(j)}(z,s)$. It is convenient to remove the first order derivative term by setting

$$\bar{N}_\ell^{(j)}(z,s) = e^{\frac{v}{2D_\ell}z} n_\ell^{(j)}(z,s) \tag{13}$$

Then

$$\frac{d^2 n_\ell^{(j)}}{dz^2} - \left[\frac{K_\ell}{D_\ell}s + \nu_\ell + \left(\frac{v}{2D_\ell}\right)^2\right] n_\ell^{(j)} = -\nu_{\ell-1} n_{\ell-1}^{(j)} e^{-\frac{vz}{2}\left(\frac{1}{D_\ell} - \frac{1}{D_{\ell-1}}\right)} \tag{14}$$

With

$$\mu_\ell \equiv \left(\frac{K_\ell}{D_\ell}s + a_\ell\right), \quad a_\ell \equiv \left[\nu_\ell + \left(\frac{v}{2D_\ell}\right)^2\right], \quad \gamma(\ell) \equiv \frac{v}{2}\left(\frac{1}{D_\ell} - \frac{1}{D_{\ell-1}}\right), \tag{15}$$

equation (14) reduces to the compact form

$$\frac{d^2 n_\ell^{(j)}(z,s)}{dz^2} - \mu_\ell n_\ell^{(j)}(z,s) = -\nu_{\ell-1} n_{\ell-1}^{(j)}(z,s)\, e^{-\gamma(\ell)z}, \quad j \leq \ell \tag{16a}$$

This differential-difference equations system with variable coefficients is the

governing equation of our problems. Equation (10) transforms to

$$n_{\ell-1}^{(j)}(z,s) \equiv 0 \text{ for } \ell \leq j \tag{16b}$$

The general solution to these equations is a matter of some complexity and will be treated later. Here we consider two special cases of (16) which describe a number of physically important models.

Case 1. We assume the dispersion coefficients of the radioactive species in the medium are equal

$$D_\ell = D, \text{ for all } \ell \ . \tag{17}$$

Then γ vanishes, removing the complicating exponential term from (16). The corresponding equation system (1) together with (2) and (3) describes the far field migration problem in the presence of advection and dispersion. For a concentration boundary condition of form of (9), the general (non-recursive) analytical solution for radioactive chains of arbitrary length i has so far not been available to us. The most extensive model to date has been the recursive three member chain in a semi-infinite domain $\mathcal{D}_\infty$ on which the computer code UCB NE 10.2 is based. In the following we shall consider two distinct far field migration problems. One of these is the nuclide migration in a (semi) infinite domain $\mathcal{D}_\infty$, the other the migration in a finite domain $\mathcal{D}_f$. Thus we need to consider appropriate boundary conditions at the second boundary joint of $\mathcal{D}$.

For $\mathcal{D}_\infty$, $0 \leq z < \infty$, $N_i(\infty,t)$ and hence $N_\ell^{(j)}(\infty,t)$ together with their derivatives must vanish sufficiently strongly

$$\frac{d^r}{dz^r}\, n_\ell^{(j)}(z,s) = O(e^{-kz}) \text{ as } z \to \infty,\ k>0,\ r=0,1,2\ldots,\ z\varepsilon\mathcal{D}_\infty \tag{18}$$

For the problem in $\mathcal{D}_f$, $0 \leq z \leq L$, a general boundary condition of Type III is specified

$$D\varepsilon \frac{\partial N_i(L,t)}{\partial z} + h\left[N_i(L,t) - N_i^J(t)\right] = 0,\ t>0\ , \tag{19}$$

h may be a velocity dependent parameter which describes the surface coefficient of specie transport at z=L, into a medium z>L in which the i^{th} specie concentration is a prescribed function $N_i^J(t)$. The boundary position z=L can, for example, be interpreted to represent the biosphere boundary. As h is varied from 0 to ∞, the flux through the boundary at z=L varies from zero to an infinite value causing the specie concentration to decrease there. To express (19) in terms of the $N_\ell^{(j)}(z,t)$ functions, substitute the equation (6) so that

$$D\varepsilon \frac{\partial N_\ell^{(j)}(L,t)}{\partial z} + h\left[N_\ell^{(j)}(L,t) - \delta_{\ell j} N_\ell^J(t)\right] = 0,\ j\leqslant\ell,\ t>0 \tag{20}$$

Hence the $N_\ell^{(j)}(z,t)$ satisfy homogeneous boundary conditions for $j<\ell$, while $N_\ell^{(\ell)}(z,t)$ satisfies the inhomogeneous condition at z=L. On taking the Laplace transform of (20) and using the transformation (13) results finally in

$$D\varepsilon \frac{\partial n_\ell^{(j)}(L,s)}{\partial z} + h_2 n_\ell^{(j)}(L,s) = \delta_{\ell j} h e^{-\frac{vL}{2D}} N_\ell^J(s),\ j\leqslant\ell \tag{21}$$

where

$$h_2 \equiv \left(h + \frac{\varepsilon v}{2}\right)$$

Summarizing, we have for the problem with advection in either $\mathcal{D}_f$ or $\mathcal{D}_\infty$ the governing equations (16), the Laplace transformed boundary condition at z=0, i.e. equation (9),

$$-D\varepsilon \frac{\partial n_\ell^{(j)}(0,s)}{\partial z} + h_1 n_\ell^{(j)}(0,s) = \delta_{\ell j} \overset{\circ}{N}_\ell v\phi_\ell(s),\ j\leqslant\ell \text{ where } h_1 = v - \frac{\varepsilon v}{2} \tag{22}$$

The second boundary condition is given by (18) for $\mathcal{D}_\infty$ and by (21) for $\mathcal{D}_f$.

Case 2. Consider again the governing (16) but now without advection, i.e. v=0. By (15) γ vanishes, thus removing again the variable coefficient term from the differential difference equation. For this case, the specie diffusion coefficients D_ℓ need not be identical in order to obtain an analytical solution. The advection free formulation is applicable to the rock fracture

problem [1] where one wishes to account for the diffusion of radioactive species into the rock from water filled fissures. Another possible application can be found in the analysis of the diffusive migration of radionuclide chains with small half-lives in a water saturated backfill region which surrounds a waste form [2]. Backfill materials, such as Bentonite, possess low permeability to water flow so that the principal mechanism of transport through the layer may occur by diffusion. In case of the rock fracture problem the domain can be either $\mathcal{D}_\infty$ or $\mathcal{D}_f$ while in the backfill problem it is $\mathcal{D}_f$.

At the present time there appear to be insufficient data to apply the formulation to the diffusion of specie with unequal diffusion coefficients. For this reason we conduct the analysis, assuming the radionuclides to satisfy equation (17). The solution given below can however be readily generalized to include unequal D_ℓ's if desired.

Since the boundary conditions remain of the same mathematical form as quoted in (18), (20), (21) and (22) it is seen that Case 2 is merely a special case of Case 1 obtained by setting v=0 in the governing eq. (16) and assigning special values to h_1 and h_2 in equations (21) and (22) as well as to their right hand side functions. In the following we shall concentrate on the solution of Case 1. Although the solution procedures of this problem in $\mathcal{D}_\infty$ and $\mathcal{D}_f$ have certain common features, it is best to present their solutions separately.

III. The Solution of the Problem in $\mathcal{D}_f$.

The solution of the system of equations (16) in $\mathcal{D}_f$ is constructed with help of a finite Fourier transform with respect to the variable z. We define

$$n_\ell^{(j)}(\beta_m, s) = \int_0^L K(\beta_m, z)\, n_\ell^{(j)}(z,s)\, dz \ . \tag{23}$$

The Fourier kernel $K(\beta_m,z)$ satisfies the Sturm-Liouville system

$$\frac{d^2K(\beta_m,z)}{dz^2} + \beta_m{}^2K(\beta_m,z) = 0 \tag{24}$$

$$-D\varepsilon \frac{dk(\beta_m,0)}{dz} + h_1K(\beta_m,0) = 0 \tag{25}$$

$$D\varepsilon \frac{dK(\beta_m,L)}{dz} + h_2K(\beta_m,L) = 0 \tag{26}$$

The β_m's are the positive eigenvalues of this system. The kernel has the form [3]

$$K(\beta_m,z) = \sqrt{2}\ \frac{\beta_m\cos(\beta_m z) + \alpha_1\sin(\beta_m z)}{\left\{\left(\beta_m{}^2+\alpha_1{}^2\right)\left(L+\frac{\alpha_2}{\beta_m{}^2+\alpha_2{}^2}\right)+\alpha_1\right\}^{1/2}} \tag{27}$$

where

$$\alpha_1 = \frac{h_1}{D\varepsilon}\ ,\ \alpha_2 = \frac{h_2}{D\varepsilon} \tag{28}$$

The eigenvalues form a discrete, countable spectrum which is given by the solutions of the transcendental equation

$$\tan(\beta_m L) = \frac{\beta_m\left(\alpha_1+\alpha_2\right)}{\beta_m{}^2 - \alpha_1\alpha_2}\ ,\ m = 1,2\ldots\ . \tag{29}$$

If one applies the kernel to every term of equation (16) and integrates with respect to z over the interval (0,L) there results in view of (23), since γ=0,

$$\int_0^L \frac{d^2n_\ell{}^{(j)}(z,s)}{dz^2}\ K(\beta_m,z)\ dz - \mu_\ell n_\ell^{(j)}(\beta_m,s) = -\nu_{\ell-1}\ n_{\ell-1}{}^{(j)}(\beta_m,s) \tag{30}$$

The integral term J yields, with integration by parts,

$$J \equiv \int_0^L \frac{d^2 n_\ell^{(j)}(z,s)}{dz^2} K(\beta_m,z)\, dz = \left\{ K(\beta_m,z) \frac{dn_\ell^{(j)}(z,s)}{dz} - n_\ell^{(j)}(z,s) \frac{dK(\beta_m,z)}{dz} \right\} \Bigg|_{z=0}^{z=L} - \beta_m^2 \, n_\ell^{(j)}(\beta_m,s) \tag{31}$$

By (25), (26) and (28)

$$\frac{dK(\beta_m,0)}{dz} = \alpha_1 K(\beta_m,0) \; ; \; \frac{dK(\beta_m,L)}{dz} = -\alpha_2 K(\beta_m,L) \tag{32}$$

so that

$$J = K(\beta_m,L)\left\{ \frac{dn_\ell^{(j)}(L,s)}{dz} + \alpha_2 n_\ell^{(j)}(L,s) \right\} - K(\beta_m,0) \left\{ \frac{dn_\ell^{(j)}(o,s)}{dz} - \alpha_1 n_\ell^{(j)}(0,s) \right\} - \beta_m^2 n_\ell^{(j)}(\beta_m,s) \tag{33}$$

On applying equations (21) and (22) together with (28) results in

$$J = K(\beta_m,L)\, \delta_{\ell j} \frac{h}{D\varepsilon} e^{-\frac{vL}{2D}} N_\ell^{]}(s) + K(\beta_m,0)\, \delta_{\ell j} N_\ell^{\circ} \frac{v}{D\varepsilon} \phi_\ell(s) - \beta_m^2 n_\ell^{(j)}(\beta_m,s) \; . \tag{34}$$

When this is substituted into (30), one obtains the difference equation

$$n_\ell^{(j)}(\beta_m,s) = \left\{ \nu_{\ell-1}\, n_{\ell-1}^{(j)}(\beta_m,s) + \delta_{\ell j} g_\ell(\beta_m,s) \right\} \frac{1}{\beta_m^2 + \mu_\ell} \quad , \; j \leqslant \ell \tag{35}$$

where

$$g_\ell(\beta_m,s) \equiv \frac{K(\beta_m,L)}{D\varepsilon} h e^{-\frac{vL}{2D}} N_\ell^{]}(s) + \frac{K(\beta_m,0)}{D\varepsilon} N_\ell^{\circ} v\phi_\ell(s) \; . \tag{36}$$

Equation (16b) transforms to

$$n_{\ell-1}^{(j)}(\beta_m,s) = 0 \; , \; \ell \leqslant j \tag{37}$$

Equation (35) is solved in a recursive manner by setting j = 1 and letting ℓ run from $\ell = 1$ to $\ell = i$. This process is repeated for j = 2,3,...i in order to obtain the solution for the i nuclides of the chain.

Starting with j=1, and letting ℓ run through the values 1,2,...i, one takes from (37) $n_0^{(1)}(\beta_m,s) = 0$, so that (35) yields

$$n_1^{(1)}(\beta_m,s) = \frac{g_1(\beta_m,s)}{\beta_m^2 + \mu_1}$$

$$n_2^{(1)}(\beta_m,s) = \frac{\nu_1 n_1^{(1)}(\beta_m,s)}{\beta_m^2 + \mu_2} = \frac{\nu_1 g_1(\beta_m,s)}{(\beta_m^2 + \mu_1)(\beta_m^2 + \mu_2)}$$

- -

$$n_i^{(1)}(\beta_m,s) = \frac{\nu_1\nu_2 \cdots \nu_{i-1}\, g_1(\beta_m,s)}{(\beta_m^2 + \mu_1)(\beta_m^2 + \mu_2)\cdots(\beta_m^2 + \mu_i)} \qquad (38)$$

Next one takes j=2 and lets ℓ run through the values 1,2,3,--,i . From (37) one has $n_1^{(2)}(\beta_m,s) = 0$. Hence (35) yields

$$n_2^{(2)}(\beta_m,s) = \frac{g_2(\beta_m,s)}{\beta_m^2 + \mu_2}$$

$$n_3^{(2)}(\beta_m,s) = \frac{\nu_2 n_2^{(2)}(\beta_m,s)}{\beta_m^2 + \mu_3} = \frac{\nu_2 g_2(\beta_m,s)}{(\beta_m^2 + \mu_2)(\beta_m^2 + \mu_3)}$$

- -

$$n_i^{(2)}(\beta_m,s) = \frac{\nu_2\nu_3 \cdots \nu_{i-1}\, g_2(\beta_m,s)}{(\beta_m^2 + \mu_2\ (\beta_m^2 + \mu_3)\cdots(\beta_m^2 + \mu_i)} \qquad (39)$$

Continuing in this manner one shows that in general,

$$n_i^{(j)}(\beta_m,s) = \frac{A_i^{(j)} g_j(\beta_m,s)}{\prod_{n=j}^{i} (\beta_m^2 + \mu_n)} \quad , \ i>j \qquad (40)$$

where

$$A_i^{(j)} = \prod_{r=j}^{i-1} \nu_r, \tag{41}$$

while for j=i one has

$$n_i^{(i)}(\beta_m, s) = \frac{g_i(\beta_m, s)}{\beta_m^2 + \mu_i} \tag{42}$$

Equations (40)-(42) represent the solution of the difference equation (35)-(37). We turn next to the Laplace inversion process with respect to the t variable.

By (15), with $D_n = D$,

$$\beta_m^2 + \mu_n = \frac{K_n}{D}(s + \alpha_n) \tag{43}$$

where

$$\alpha_n = \frac{D}{K_n}(\beta_m^2 + a_n). \tag{44}$$

Hence (40) becomes

$$n_i^{(j)}(\beta_m, s) = \frac{D}{K_i} C_i^{(j)} \frac{g_j(\beta_m, s)}{\prod_{n=j}^{i} (s + \alpha_n)}, \tag{45}$$

with

$$C_i^{(j)} = \frac{A_i^{(j)}}{\prod_{n=j}^{i-1} \left(\frac{K_n}{D}\right)} = \prod_{n=j}^{i-1} \lambda_n \tag{46}$$

Now the inverse of $\left(\prod_{n=j}^{i} (s + \alpha_n)\right)^{-1}$ is

$$L^{-1}\left\{\frac{1}{\prod_{n=j}^{i} (s + \alpha_n)}\right\} = \sum_{n=j}^{i} \frac{e^{-\alpha_n t}}{\prod_{\substack{r=j \\ r \neq n}}^{i} (\alpha_r - \alpha_n)} \tag{47}$$

If one applies the convolution theorem to $g_j(\beta_m,t)$ and $e^{-\alpha_n t}$, equations (40) and (41) yield, with the * symbol denoting the convolution integral,

$$n_i^{(j)}(\beta_m,t) = \frac{D}{K_i} C_i^{(j)} \sum_{n=j}^{i} \frac{g_j(\beta_m,t)*e^{-\alpha_n t}}{\prod_{\substack{r=j \\ r\neq n}}^{i} (\alpha_r-\alpha_n)} \quad , \; i>j \tag{48}$$

$$n_i^{(i)}(\beta_m,t) = \frac{D}{K_i} g_i(\beta_m,t)*e^{-\alpha_i t} \; . \tag{49}$$

This is followed by the Fourier inversion with respect to the z variable. The inverse transform of (23) is given by (with ℓ now replaced by i in $n_\ell^{(j)}$),

$$n_i^{(j)}(z,t) = \sum_{m=1}^{\infty} K(\beta_m,z)\, n_i^{(j)}(\beta_m,t), \; i\geq j \tag{50}$$

The $n_i^{(j)}(\beta_m,t)$ in the summation are taken from equations (48) and (49). The inversion can be shown to be valid if $n_i^{(j)}(z,t)$ is continuous and satisfies Dirichlet conditions on $0 \leq z \leq L$ with t in the domain $t > 0$. From (44) one separates the β_m^2 dependence as follows

$$\alpha_n-\alpha_r = \Gamma_{rn}\beta_m^2 + \gamma_{rn} \tag{51}$$

where

$$\Gamma_{rn} = D\left(\frac{1}{K_n} - \frac{1}{K_r}\right) \; , \; \gamma_{rn} = \left[(\gamma_n - \gamma_r) - \left(\frac{v}{2D}\right)^2 \Gamma_{rn}\right] \tag{52}$$

There results with (48), (51), on substitution into (50), the inverse function

$$n_i^{(j)}(z,t) = \frac{D}{K_i} C_i^{(j)} \sum_{n=j}^{i} \sum_{m=1}^{\infty} \frac{K(\beta_m,z)g_i(\beta_m,t)*e^{-\alpha_n t}}{\prod_{\substack{r=j \\ r\neq n}}^{i} \left(\Gamma_{nr}\beta_m^2 + \gamma_{nr}\right)} \quad , \; i>j \tag{53}$$

and for $n_i^{(i)}(z,t)$ from (49) and (50),

$$n_i^{(i)}(z,t) = \frac{D}{K_i} \sum_{m=1}^{\infty} K(\beta_m,z)g_i(\beta_m,t)*e^{-\alpha_i t} \tag{54}$$

On re-introducing the exponential multiplier of (13) into the last two equations, one obtains all component parts of the solution for the chain member $N_i(z,t)$. Their substitution into (6b) yields the general (non-recursive) solution in $\mathcal{D}_f$,

$$N_i(z,t) = e^{\left(\frac{v}{2D}\right)z} \frac{D}{K_i} \left\{ \sum_{m=1}^{\infty} K(\beta_m,z) g_i(\beta_m,t) * e^{-\alpha_i t} + \sum_{j=1}^{i-1} c_1(j) \sum_{n=1}^{i} \sum_{m=1}^{\infty} \frac{K(\beta_m,z) g_j(\beta_m,t) * e^{-\alpha_n t}}{\prod_{\substack{r=j \\ r\neq h}}^{i} \left(\Gamma_{nr}\beta_m^2 + \gamma_{nr}\right)} \right. \tag{55}$$

It is readily verified that the dimensional terms in these equations have the following units (cgs)

$$K_1(\beta_m,z) = \left[cm^{-1/2}\right],\ g_j(\beta_m,t) = \left[\frac{gm}{(cm)^{9/2}}\right],\ * = [sec],\ \alpha_j = \left[\frac{1}{sec}\right]$$

$$c_i(j) = \left[(sec)^{j-i}\right],\ \Gamma_{rn} = \left[\frac{cm^2}{sec}\right],\ \beta_m^2 = \left[\frac{1}{cm^2}\right],\ \gamma_m = \left[\frac{1}{sec}\right],\ D = \left[\frac{cm^2}{sec}\right]$$

It follows from this that $N_i(z,t) = \left[\frac{gm}{cm^3}\right]$, as required.

The form of the solution (55) does not explicitly exhibit the steady state form of the solution $N_i(z,\infty)$. This limiting form is contained in the convolution time integrals and it results on letting $t \to \infty$. Alternately if one sets $s = 0$ in (45) (for $i > j$) and proceeds with the Fourier inversion with respect to z, following the indicated steps, one is led to $N_i(z,\infty)$. The resulting series can in some instances be summed in terms of elementary functions.

IV. The Solution of the Problem in $\mathcal{D}_\infty$.

The solution of the system of equations (16) in $\mathcal{D}_\infty$ follows along similar steps to that given in section III. In order to exhibit the correspondence of the solution method with the previous work we indicate corresponding equations by a dash mark.

We introduce an (infinite) Fourier transform with respect to the z variable

$$n_\ell^{(j)}(p,s) = \int_0^\infty K(p,z)\, n_\ell^{(j)}(z,s)dz \tag{23'}$$

The Fourier kernel K(p,z) satisfies

$$\frac{d^2K(p,z)}{dz^2} + p^2 K(p,z) = 0 \quad 0 \leq z < \infty \tag{24'}$$

$$-D\varepsilon \frac{dK(p,0)}{dz} + h_1 K(p,0) = 0 \tag{25'}$$

and instead of (26), K(p,z) satsfies a boundedness condition as $z \to \infty$. The solution to this problem is given by [3]

$$K(p,z) = \sqrt{\frac{2}{\pi}} \frac{p\cos(pz) + \alpha_1 \sin(pz)}{\left\{p^2 + \alpha_1^2\right\}^{1/2}} \tag{27'}$$

p replaces the eigenvalues β_m in (24), and it represents a continuous spectrum of range $0 \leq p < \infty$. One now transforms (16) with help of (23'). This leads to a set of equation steps comparable to (30)-(35), except that L is replaced by (∞). On account of the boundedness of K(p,z) and its derivative and in view of (18) the contribution to J at $z = \infty$ vanishes leaving us with

$$n_\ell^{(j)}(p,s) = \left\{\nu_{\ell-1} n_{\ell-1}^{(j)}(p,s) + \delta_{\ell j} g_\ell(p,s)\right\} \frac{1}{p^2 + \mu_\ell}, \quad j \leq \ell \tag{35'}$$

where

$$g_\ell(p,s) = \frac{K(p,o)}{D\varepsilon} N_\ell^\circ h_1 \phi_\ell(s) \tag{36'}$$

and

$$n_{\ell-1}^{(j)}(p,s) = 0, \quad \ell \leq j \tag{37'}$$

The steps of the solution of the difference equation (35') are identical to those in section III leading, on inverting with respect to t, to equations (48), (49) with β_m replaced by p. However, the Fourier inversion with respect to z is in place of (50) given by

$$n_i^{(j)}(z,t) = \int_0^\infty K(p,z) n_i^{(j)}(p,t)\,dp, \quad i \leq j \tag{50'}$$

Hence all steps between equations (51) to (55) remain unchanged except for the replacement of β_m by p and that of the summation $\sum_{m=1}^{\infty}$ by $\int_o^{\infty}(\ )\,dp$.

The result is the general (non-recursive) solution in $\mathcal{D}_\infty$,

$$N_i(z,t) = e^{\frac{v}{2D}z}\left\{\frac{D}{K_i}\int_o^{\infty} K(p,z)g_i(p,t)^* e^{-\alpha_i t}\,dp + \sum_{j=1}^{i-1} C_i(j) \sum_{n=1}^{i}\int_o^{\infty} \frac{K(p,z)g_j(p,t)^* e^{-\alpha_n t}}{\prod_{\substack{r=j \\ r\neq n}}^{i}\left(\Gamma_{nr}p^2 + \gamma_{nr}\right)}\,dp\right\}$$

$$0\leq z<\infty,\ t>0,\ i=1,2,.. \qquad (55')$$

with $g_i(p,t)$ prescribed by (36'). One verifies by dimensional arguments of the right hand side of (55') that $N_i(z,t) = \left[\frac{gm}{cm^3}\right]$.

V. The Advective-Dispersive Far Field Migration of Radionuclide Chains in $\mathcal{D}_f$

We illustrate the theory with an application of the diffusive and advective transport of radionuclide chains in the finite span $\mathcal{D}_f$: $0<z<L$. It is assumed that the chains orginate at the repository boundary z = 0. Subject to a release rate, which is a particular form of (3) i.e.

$$N_i(0,t) = N_i^o\,\phi_i(t),\ t>0 \quad i = 1,2,... \qquad (56)$$

At the biosphere boundary

$$N_i(L,t) = 0,\ t>0\ ,\ i = 1,2... \qquad (57)$$

These boundary conditions are special cases of (3) and (19) for which the original problem was solved. By specializing the parameters in the previous section III, the solution to the present problem is obtained by a limiting procedure.

First the Kernel function $K(\beta_m, z)$ is constructed from the equation system (24) to (26) with homogeneous boundary conditions of Type I. The comparison shows that in the present case D=0 in (25), (26), so that $\alpha_1 = \alpha_2 = \infty$ in (28).

With this (27) yields in the limit the kernel function

$$K(\beta_m,z) = \sqrt{\frac{2}{L}}\ \sin(\beta_m z) \tag{58}$$

The eigenvalues β_m are determined from (29) which reduces to

$$\sin\beta_m L = 0 \tag{59}$$

with the positive solutions

$$\beta_m = \frac{m\pi}{L}\ ,\ m = 0,1,2,\ldots\ . \tag{60}$$

Now the theory developed in Section III, and specifically the set of equation (31) to (35), assumes that the boundary condition for $K(\beta_m,z)$ at z=0 and z=L are of Type III, i.e. of the form of (25), (26)

$$\begin{aligned} -D\varepsilon\ \frac{dK(\beta_m,o)}{dz} + h_1 K(\beta_m,0) &= 0 \\ D\varepsilon\ \frac{dK(\beta_m,L)}{dz} + h_2 K(\beta_m,L) &= 0 \end{aligned} \tag{61}$$

Since in the present case the boundary conditions are of Type I and thus do not involve the derivative term, one must formally make the following limiting replacements in (36)

$$\frac{K(\beta_m,L)}{D\varepsilon} = -\frac{1}{h_2}\ \frac{dK(\beta_m,L)}{dz}\ ;\ \frac{K(\beta_m,0)}{D\varepsilon} = \frac{1}{h_1}\ \frac{dK(\beta_m,0)}{dz} \tag{62}$$

Further, a comparison of (57) with (19) shows that $N_i^{]}(t) \equiv 0$ so that $N_\ell^{]}(s) \equiv 0$. This leaves only the second term in (36) which reduces with the above to

$$\begin{aligned} g_\ell(\beta_m,s) &= \frac{dK(\beta_m,0)}{dz}\ \overset{\circ}{N_\ell}\ \phi_\ell(s) \\ &= \sqrt{\frac{2}{L}}\ \beta_m \overset{\circ}{N_\ell}\phi_\ell(s) \end{aligned} \tag{63}$$

With $K(\beta_m,z)$ and $g_i(\beta_m,t)$ determined the solution of the problem is given by (55).

The quantity of principal interest is the specie transport through the biosphere boundary at z=L which in view of (57) reduces to

$$\dot{m}_i(t) = -D\varepsilon \frac{\partial N_i(L,t)}{\partial z} \tag{64}$$

which will be investigated in the future.

As a second application consider the transport of the radionuclide chains by diffusion only, so that v=0 in (55). Aside from the term $e^{\frac{vL}{2D}}$ being replaced by unity, one must delete the term $\left(\frac{v}{2D}\right)^2$ in the expression for a_ℓ in (15). Recall that $\gamma(\ell) \equiv 0$. For the present boundary condition (56) a comparison with (22) shows that v can formally be set to unity so that no further changes are needed in (55) other than those mentioned.

References

1. Neretnieks, I., "Diffusion in the Rock Matrix, an Important Factor in Radionuclide Migration," **J. Geophy. Res., 85B**, 4379, 1980.

2. Lung, H. C. and P. L. Chambre', "Mass Transport of a Radioactive Decay Chain Through a Backfill," To be published.

3. Chambre', P. L., "Mathematics 220 Class Notes," University of California.

This report was done with support from the Department of Energy. Any conclusions or opinions expressed in this report represent solely those of the author(s) and not necessarily those of The Regents of the University of California, the Lawrence Berkeley Laboratory or the Department of Energy.

Reference to a company or product name does not imply approval or recommendation of the product by the University of California or the U.S. Department of Energy to the exclusion of others that may be suitable.

LAWRENCE BERKELEY LABORATORY
TECHNICAL INFORMATION DEPARTMENT
UNIVERSITY OF CALIFORNIA
BERKELEY, CALIFORNIA 94720